Hermann Janeschitz-Kriegl

Crystallization Modalities in Polymer Melt Processing

Fundamental Aspects of Structure Formation

SpringerWienNewYork

Hermann Janeschitz-Kriegl

Crystallization Modalities in Polymer Melt Processing

Fundamental Aspects of Structure Formation

SpringerWienNewYork

Prof. Dr. Hermann Janeschitz-Kriegl
Universität Linz
Inst. Polymerwissenschaften
Altenbergerstr. 69
4040 Linz
Austria
g.janeschitz@aon.at

Dedicated to Prof. Wilhelm Schneider, Technical University Vienna, on the occasion of his 70th birthday, and also for his essential contribution to the correct description of the course of crystallization under processing conditions

Acknowledgments

Preface

Structure formation in crystallizing polymers, as occurring during processing, has not been treated so far in a coherent form. This fact explains, why this monograph is written as the first book devoted to this subject. A quarter of a century ago the underdevelopment of this subject was obvious. Trial and error dominated. In fact, other apposite subjects as polymer melt rheology or heat transfer, had reached high levels. A great number of books has been devoted to them. Mold filling of amorphous polymers and the solidification of these polymers by vitrification can nowadays be simulated numerically with a high degree of accuracy. In the solidified sample even residual stresses and corresponding birefringence effects can accurately be calculated[1].

However, semicrystalline polymers, which form the majority of industrial polymers, have been excluded from these considerations for good reasons. In fact, great uncertainties existed about the formation of quality determining crystalline structures. In particular, polyolefins suffered from this shortcoming. In 1983 this fact instigated the polymer research group at the Johannes Kepler University in Linz to start with pertinent activities. The urgency of this kind of studies becomes evident, if advantages and hitches of these polymers are considered.

1. Versatility of processing: Injection molding into a great variety of shapes and sizes, from thin walled beakers to garden chairs, not to forget pipe and profile extrusion, cable coating, fiber spinning, film blowing.
2. Product qualities: Ductility, low density, good electric insulation, corrosion resistance, surface quality.
3. Processing parameters: No molding process is thinkable without pressurization, flow and quenching. But fast flow has an unavoidable influence on the anisotropy of the products. The grain size is influenced by deformation rate, pressure and speed of cooling.
4. Effects on end-use properties: Unfortunately, so far there are mostly only qualitative insights into the consequences of undesired structures. One knows

---

[1]Baaijens FTP (1991) Calculation of residual stresses in injection molded products. Rheol Acta 30:284–299.

of the anisotropy of shrinkage, warping, insufficient dimensional stability, oriented craze and crack development (a side-effect is split fiber formation), anisotropy of strength and elasticity.

5. Remedies: First of all the origins of all kinds of structure elements must be explored. Of course, a solid theoretical foundation for the connection between those crystalline structures and end-use properties would be desirable. For the moment, however, this book is devoted to an elucidation of the back-ground. The reader must not be disappointed, if only a partial goal is envisaged. Instead, he should be content with the fascinations, which nature provides even in such a prosaic subject as polymer processing.

In fact, some of the fundamental processes had not even been recognized. Striking examples are the enormous increase of the number density of stable nuclei (by many decades) as a result of fast cooling, of fast flow or of pressurization, and the role of local alignments in this matter (how to explain self-seeding!). Also, nobody has ever expected great differences in the stability of nuclei of varying origin, or the absence of sporadic nucleation in quiescent melts of flexible polymers.

As to the application of new techniques the short term shearing or stretching should be mentioned in first instance. This technique can be successful only because of the delayed relaxation of the point-like or thread-like nuclei activated during this flow. The surprisingly slow relaxation of these nuclei had not been observed previously. Other authors have later adopted this technique for shearing experiments under the name "shear pulse." Some of these authors found this technique so evident that they forgot to quote us. In an elegant way this technique separates nucleation during flow and subsequent growth.

In fact, only strategic experimentation could lead to those remarkable results. This meant that from the beginning our creativeness was directed on the construction of equipment, which could not be on the market. In fact, experimental conditions had to be chosen close enough to those prevailing in practical processing. Otherwise the obtained results could not be relevant enough. For the evaluation of the results, however, we could easily live with conventional techniques as birefringence, optical and electron microscopy and, occasionally, IR and X-ray techniques. In addition, our Viennese friends started with a mathematical technique for the correct description of the process of crystallization[2]. It goes without saying that this process occurs on the surfaces of already formed crystalline areas, a fact which has not been taken into account so far.

In some respect this monograph has the character of a detective story. This means that this book should not be considered as an ordinary review. In first instance it should be seen as a means to promote a new train of thoughts. As a consequence, papers from supportive authors have preferentially been quoted and discussed. The author wants to thank Prof. J.M. Dealy (Montreal) for drawing

---

[2]Schneider W, Köppl A, Berger J (1988) Non-isothermal crystallization of polymers. Int Polym Proc 2:151–154.

attention to a serious flaw in the manuscript. It is also written in memoriam of D.W. van Krevelen and P.J. Flory for their early encouragement.

It goes without saying that the usefulness of numerical simulations, as far as crystallization is concerned, can only be questionable at present. Admittedly, there are some hopeful exceptions. In fact, the similarity of the shear pulse technique with the injection molding process cannot be overlooked, even if the latter technique is not isothermal. So one can hope that old experiences with mold filling can be of some help in future interpretations (Can flow during mold filling be considered as nearly undisturbed by incipient crystallization?).

Finally the hope is uttered that this monograph will find a sufficient number of benevolent readers. It should serve as a justification for all the energy put into the subject by a small group of people at Linz University during the last 25 years, where work orders of the industry brought satisfaction but also considerable delay.

Linz, August 2009   Hermann Janeschitz-Kriegl

Contents

Chapter 1
Required Basic Achievements

1.1 Interaction of Three Transport Phenomena: Heat Transfer, Flow and Crystallization Kinetics

It is evident that the three transport phenomena, which are mentioned in the title of this section, are involved in structure formation during processing. In particular, flow is always engaged in mold filling. In one respect flow causes macroscopic heat and momentum transport. But it has also an enormous influence on the crystallization kinetics. In fact, crystallization is the consequence of transport on a microscale. It is rendered possible by rearrangements of molecules. However, these rearrangements are favored by flow. This seems obvious. But nobody would have expected that the influence of flow should be so tremendous. In fact, the biggest surprise for us was that the number density of (apparently athermal) nuclei could be enhanced by many decades, if shear or extensional flows were applied for short time spans to melts of industrial polypropylenes [1–3], which were undercooled to temperatures below the melting temperature of their spherulites (see Fig. 1.3 below). A similar big effect could be attained by rapid quenches of quiescent melts to a series of much lower temperatures. The details of these experiments will be described later in Sect. 2.1.1. However, a demonstration of the overwhelming effects seems important. For the purpose, Fig. 1.1 is introduced.

This figure is a three dimensional plot in perspective. The left horizontal axis gives the temperatures, to which the samples have been rapidly quenched from a temperature well above the equilibrium melting point. The right horizontal axis gives the specific mechanical works applied to the samples during shear and extensional flows at some not too low temperatures. On the vertical axis the obtained number densities of (athermal) nuclei are plotted. Because of the enormous influences of temperature or mechanical work, a logarithmic scale had to be chosen. With respect to the temperature axis one should not forget that the
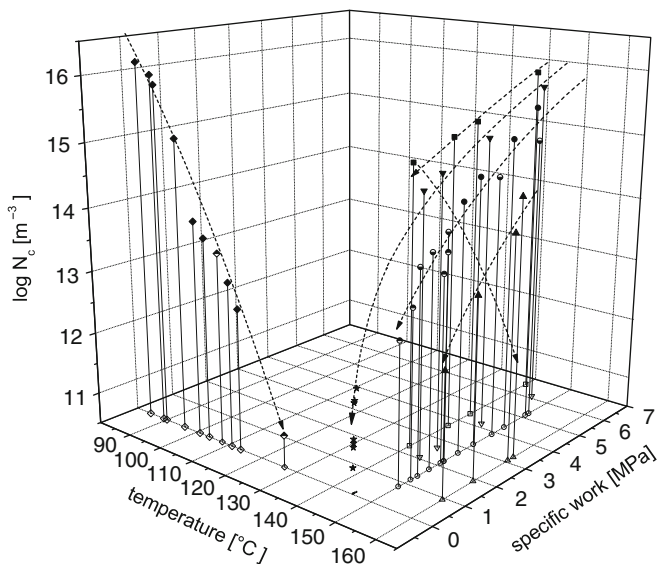
Fig. 1.1 A three-dimensional plot of the (logarithm) of the number density of nuclei against the temperatures of fast quenches (*left horizontal axis*) and against the applied specific mechanical works (*right horizontal axis*) for an industrial PP according to [2] and [3]. Courtesy of Springer

equilibrium melting point of PP is at $212°C$ [4]. But this means that the temperature axis must be doubled in length to get this point on the line. One could guess, how low the number density of these type of nuclei would be near this temperature. But also the work axis should be extended to 25 MPa for including the transition to thread-like nuclei. These remarks are made in promoting a feeling for the enormous range of relevant variables. The nature of the nuclei (sporadic, thermal or athermal) will be discussed later. The same holds for the use of specific work instead of flow time and external stress. Here one can suffice by noticing that the rate of specific work is the product of the external stress, which causes the orientation of the molecules (see the stress optical rule [5]), and the rate of deformation, which is proportional to the probability of an encounter of oriented molecules [6].

Figure 1.1 teaches us that there must be a tremendous interaction between the said variables. In particular, the crystallization kinetics, as expressed in Fig. 1.1 by the appearance of nuclei, is strongly dependent on flow and temperature. The second parameter of interest is the growth speed of crystalline domains. Unfortunately, it has not been possible so far to develop a method for a determination of the influence of flow on the growth speed. For quiescent melts of a series of poly-propylenes the growth speed of spherulites is plotted as a function of temperature in
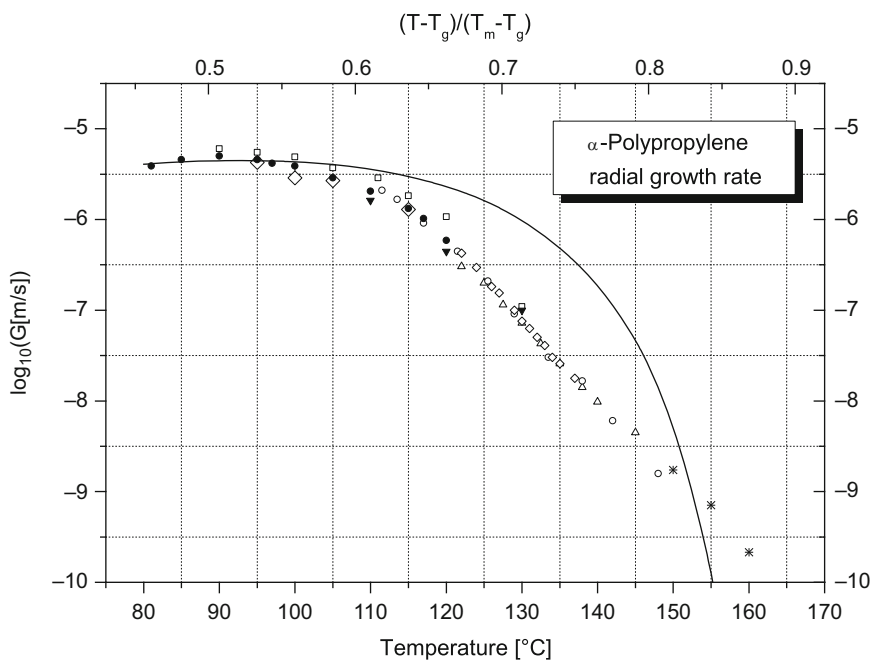
Fig. 1.2 The growth speed of spherulites, as observed in quiescent melts, is given as a function of the temperature of crystallization for a series of polypropylenes according to various sources given in [7]. The low temperature values were exclusively obtained in our laboratory [7]. Courtesy of Springer

Fig. 1.2 [7]. A description of the pertinent experiments is given in Sect. 2.1.2. Many external sources, however, have been used for the upper range of temperatures.

As in many slower crystallizing polymers, a maximum is observed half-way down to the glass transition temperature [8]. The full line refers to a theory by Van Krevelen, which is grafted on results of [8] (see Sect. 2.1.2). However, in this connection it must be admitted that for flow, which is not interrupted, the speed of lateral growth on lengthy crystalline entities (the so-called shish-kebabs) has not yet received a proper treatment. The reason for this omission lies in large experimental difficulties. In fact, spherulites do not grow during continued flow. In contrast, those spherical entities can grow slowly after cessation of short term flow. The pertinent number densities of spherulites correspond with the number densities of (oblong) nuclei created by this short term flow. Apparently the mutual distances between the said nuclei was still large compared with their lengths, when flow was stopped. See the right side of Fig. 1.1.

At this point it seems important, however, to discern between the effects of nucleation and growth on the process and its consequences. On one side the number and shape of nuclei has a large influence on the morphology, which can be observed in the cross-sections of the final product. On the other side, growth speeds have a
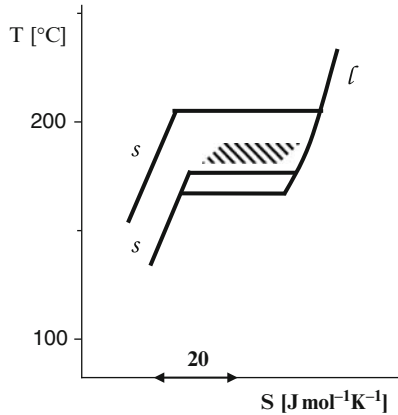
large influence on the course of the overall crystallization. In fact, as will be shown
below, only the first power of the number density of nuclei shows up in the relevant
equations, whereas a higher power, mostly the third power, characterizes the
influence of the growth speed. One should not overlook the importance of an
inherent proneness of some polymers (see HDPE) to fast crystallization. In fact, a
fast evolution of latent heat can be quite obstructive to the cooling process and will
level up inside the sample the crystallization temperature, which otherwise is
lowest near the cooled surface and increases with the distance from this surface.
However, the pertinent expectations must be quelled at this stage. To some extent,
all these problems will pass the review in later sections.

At the end of this section the *T,S*-diagram of polypropylene is given in Fig. 1.3
(*T* . . . absolute temperature, *S* . . . specific entropy, see [9]).

The advantage of this uncommon diagram is that one can directly read the
relevant temperatures from the graph. The entropy as the independent variable
can easily be calculated for a great number of polymers from well-known thermo-
dynamic tables (see, e.g., [10]). The figure describes two types of transitions from
the fluid to the solid. On the right side one has the common liquidus line "*l*." On the
left side one has two solidus lines "*s*," dependent on the type of the transition. The
level of the upper horizontal line is that of the equilibrium melting point of ideal
crystals [4], containing macromolecules in their stretched conformation. As is well-
known there is no way to realize this transition directly. For this purpose one would
have to start with sporadic nuclei, in which the molecules were already stretched.
But the probability for those nuclei is practically zero in view of the coiled
conformations of the melt. Ideal crystals can only be obtained in a slow recrystalli-
zation process, preferably under high pressure and at temperatures close to the
equilibrium melting point [11,12].

The lower level of transition, as indicated in Fig. 1.3 by two parallel horizontal
lines, corresponds to the melting or formation of spherulites. These spherulites
contain lamellae of finite thickness. In such a lamella the macromolecules are

arranged in a direction perpendicular to the extension of the lamella [13]. A double horizontal line is drawn because the melting temperature of the spherulites is not so well defined. The origin of these lamellae will be discussed in more detail in Sect. 2.2.3. In this section the role of local alignments as prestages of athermal nuclei will be brought in. With a not too low average molar mass the length of any molecule will surpass the length of any alignment by far. As a consequence, macromolecules will protrude from the body of the lamella on both sides or will be bent back into the lamella [14]. Also in this case no sporadic nucleation can be expected.

Looking at Fig. 1.3 one recognizes two temperature ranges, one between the two transitions and the other below the lower transition. It will turn out that in the upper range of temperatures sporadic nucleation can indeed be initiated by the action of flow, apparently because of the uncoiling of the molecules. In the range of temperatures below the melting range of spherulites (below the double line) athermal nuclei dominate and cause very different mechanisms for crystallization and, in particular, for flow induced crystallization. In this connection the stability of flow induced thread-like nuclei is remarkable. In fact, if those thread-like nuclei are formed in fast flows at temperatures close to the equilibrium melting point [15], they show a pronounced relaxation phenomenon. However, the length of the relaxation times increases so fast with decreasing temperature that close to the melting temperature of the spherulites these thread-like nuclei can be considered as practically stable, certainly with respect to the time scale of polymer processing. The temperature range of those stabilized nuclei is indicated by the shaded area in Fig. 1.3 (see also [16]). A similar kind of stability holds for nuclei, which are formed in the process of self-nucleation, as occurring in quiescent situations at temperatures around the melting temperature of spherulites [17]. These facts permit us to believe in the predominance of athermal nuclei in the temperature range below the melting temperature of spherulites, i.e., below the horizontal double line in Fig. 1.3.

1.2   Available Theories Describing the Crystallization Process

1.2.1   The Kolmogoroff–Avrami–Evans Theory

Kolmogoroff was the first to describe the consequences of nucleation and growth for the space covering by the formation of spherulites [18]. Later Avrami [19] and Evans [20] independently developed their theories, which meanwhile turned out to be essentially identical with Kolmogoroff's theory. Also Tobin [21] developed a theory, which he considered as an improvement of Avrami's theory. However, the results of this latter theory only deviate from those of the previous theories as a consequence of an unnecessary simplification introduced into the course of the calculation.

The goal of the present monograph is to deliver an introduction, which does not deter the reader by the use of advanced mathematics. Friends of such an approach are relegated to our review of 1997 [22] and to a later section of this book on confined samples. To start with, an equation is given, which relates the real space covering ξ_g to the virtual space covering ξ_g^*, which is obtained, if the impingement of the spherulites is disregarded. Subscript g stands for geometric. Both coverings are per unit volume. One has for the respective changes of these space coverings:

$$d\xi_g = \left(1 - \xi_g\right) d\xi_g^* \tag{1.1}$$

In fact, for the increase of the real space covering only the fraction $(1 - \xi_g)$ is available. This equation can easily be integrated. One obtains:

$$\xi_g = 1 - \exp(-\xi_g^*). \tag{1.2}$$

But this means that one has to calculate only the virtual space covering ξ_g^*. If spherulites are growing, one obviously has:

$$\xi_g^*(t) = \frac{4\pi}{3} \int\limits_{-\infty}^{t} du\, \alpha(u) \left[\int\limits_{u}^{t} dv\, G(v)\right]^3, \tag{1.3}$$

where α is the rate of formation of nuclei per unit volume and G is the growth speed of the spherulites. The expression between square brackets is the radius of a spherulite, which is born at time u, as observed at time t after unimpeded growth. If the expression of (1.3) is introduced into the exponent of (1.2), one obtains the famous equation, which has been given for the first time by Kolmogoroff. One has:

$$\xi_g(t) = 1 - \exp\left\{-\frac{4\pi}{3} \int\limits_{-\infty}^{t} du\, \alpha(u) \left[\int\limits_{u}^{t} dv\, G(v)\right]^3\right\}. \tag{1.4}$$

The number density of nuclei at time t is then:

$$N_c(t) = \int\limits_{-\infty}^{t} du\, \alpha(u) \left[1 - \xi_g(u)\right], \tag{1.5}$$

where ξ_g is here the real space covering of (1.4). If there is a prescribed relation between temperature T and time t, namely $T(t)$, one can use the just given equations also outside the regime of isothermal processes. If the time dependence of α and G are only via the time dependent temperature, one has

$$\alpha(t) = \tilde{\alpha}(T(t) \quad \text{and} \quad G(t)) = \widetilde{G}(T(t)). \tag{1.6}$$

However, if the course of the (local) temperature is a consequence of heat transfer, there is no prescribed relation between temperature and time. As a consequence, the above equations are not directly useful under those conditions. It will be clear to the reader that the change of specific volume, which occurs with the crystallization, is disregarded in these equations. This fact is expressed by the choice of the name geometric space covering.

For isothermal crystallization only two cases are of importance, namely the case, where the nuclei are there from the beginning, and the case, where the nucleation rate is constant and finite. In the first case one has a fixed number density of athermal nuclei or of heterogeneous nuclei, the latter being introduced by nucleation agents or impurities. In the second case the melt is clean, and sporadic nucleation of thermal nuclei is occurring. The critical point in both cases is the choice of time zero. In fact, the melt, which is originally kept at a temperature well above the equilibrium melting point, must be quenched fast enough to the temperature, where the crystallization is intended to happen. The time interval needed for the quench must be very short compared with the time required for the crystallization process proper. Only under this condition time zero can readily be chosen within the time interval needed for the quench. In the case of sporadic nucleation the rate of formation of nuclei can be kept constant as long as the temperature is constant. In fact, this nucleation process occurs in the still uncovered volume of the sample.

For practical reasons it has been assumed [18] that originally there is a constant number density N_v of points, where nuclei can be born. If for these points an activation mechanism is assumed, one has for the number density $N(t)$ of already activated nuclei:

$$N(t) = N_v \left[1 - \exp\left(-\frac{t}{\tau}\right)\right],$$

where τ is an activation time. If this equation is differentiated, one obtains for the rate of formation of nuclei per unit volume:

$$\alpha(t) = \frac{N_v}{\tau} \exp\left(-\frac{t}{\tau}\right). \tag{1.7}$$

The two important cases, as mentioned above, are obtained for t much longer than τ and for t much shorter than τ. With $\alpha(t)$ according to (1.7) one can obtain single integrated versions of (1.4) and (1.5), i.e.:

$$\xi_g(t) = 1 - \exp\left[-8\pi N_v \, G^3 \, \tau^3 \, e_4\left(-\frac{t}{\tau}\right)\right] \tag{1.8}$$

and

$$N(t) = N_v \int_0^{\frac{t}{\tau}} du \, \exp\left[-u - 8\pi N_v \, G^3 \, \tau^3 \, e_4(-u)\right], \tag{1.9}$$

where $e_4(z) = \sum_{i=4}^{\infty} \frac{z^i}{i!}$ is an exponential rest series.

For the important cases mentioned above, the direct integration of (1.4) is the easiest way. One obtains for $\alpha(t) = N_v\, \delta_0(t)$, where δ_0 is the Dirac function concentrated on $t = 0$ $(\tau \to 0)$:

$$\xi_g(t) = 1 - \exp\left[-\frac{4\pi}{3} N_v\, G^3\, t^3\right] \tag{1.10}$$

with $N = N_v$. The exponent of time is called the Avrami index, which is 3 for spherulitic growth, if the nuclei have been there from the beginning.

For $\alpha = \alpha_c = $ const. one finds:

$$\xi_g(t) = 1 - \exp\left[-\frac{\pi}{3}\, \alpha_c\, G^3\, t^4\right]. \tag{1.11}$$

In this case the Avrami index is equal to 4. The general form of these equations is:

$$\xi_g(t) = 1 - \exp(-k\, t^n), \tag{1.12}$$

with

$$k = \frac{4\pi}{3} N_V G^3 z; \quad n = 3$$

and,

$$k = \frac{\pi}{3}\alpha_c G^3; \quad n = 4. \tag{1.13}$$

As is well known, there are also two dimensional and one dimensional growth mechanisms. From a point of view of structure formation one has to consider only two cases: The growth from a thread-like precursor, which is created during a short period of heavy shearing or stretching and the growth from a flat surface, which is the wall of a container. If temperature is low enough, one has in the first case:

$$\xi_g(t) = 1 - \exp\left\{-2\pi L\left[\int_0^t dv\, G(v)\right]^2\right\}$$
$$= 1 - \exp\left[-2\pi L G^2 t^2\right] \tag{1.14}$$

where L is the total length of thread-like nuclei per unit volume. This length can be estimated experimentally like the total length of wooden logs of thickness D and of $1\,\mathrm{m}$ length in a stack of $1\,\mathrm{m}^3$. One has:

$$L = \frac{2}{\sqrt{3}\, D^2}. \tag{1.15}$$

For this purpose one has to estimate the average distance D between the threads from a microscopic picture. The reader may ask, why the growth mechanism of L is not introduced. The answer consists of two parts. First of all, the pertinent growth mechanism, which holds for the period of flow, has been a subject of discussion for many years. This subject can only be treated in Chap. 3, where the influence of flow is examined. Second, it has not yet been possible to determine the growth speed G of cylindrites during the period of flow. For the melt, which is quieted down after the period of flow, one can assume that this growth speed is equal to the relatively slow growth speed characteristic for spherulites in a quiescent melt. Equation (1.14) is valuable, because many useful experiments have been carried out so far, obeying the conditions, under which this equation can be used. In many industrial processes short term flow is applied (see injection molding). Our experiences have shown that the typical structures grow quite slowly only after the cessation of the flow, not withstanding the fact that they differ remarkably from those, which grow in permanently quiescent melts. Very often so-called shish-kebabs are formed. From the shish-kebabs, however, one learns that not the whole length of the shish (thread-like nucleus) is active. In fact, disk-like kebabs of a certain thickness are formed by lateral growth. So, only about half the length L must be used in (1.14).

The mentioned one-dimensional growth occurs with transcrystallization [23]. It also influences the result of differential scanning calorimetry (DSC) at temperatures not too far from the equilibrium melting point, where the number of nuclei in the melt is extremely low and, as a consequence, nucleation by the wall dominates. One has:

$$\xi_g(t) = A \int_0^t dv\, G(v) \;=\; AGt, \tag{1.16}$$

where A is the surface area in front of the unit volume. One can clearly see from (1.14) and (1.16) that the Avrami index is 2 in the two dimensional case and 1 in the one dimensional case. The equations, which contain an integral over the time, are also valid for a growth speed depending uniquely on the temperature. The equations containing G as such, hold only for the isothermal cases. For these latter cases the so-called Avrami plot has been invented. It reads:

$$\log(-\ln(1 - \xi_g)) = n\,\log(t) + \log(k). \tag{1.17}$$

This equation gives a linear plot with respect to $\log(t)$ with n as the slope. This plot became very popular in the past. However, the points of this plot have very different weights depending on their location. This fact makes the position of a straight line, as drawn through the experimental points, very unsecured. The position of this line is extremely sensitive to errors in small values of ξ_g, for which no secure determination is thinkable, and for the moment of zero time. In fact, the value of ξ_g depends on the specific volume, which deviates only little from that of a melt containing still

no crystalline domains. Light scattering increases in the beginning only with the sixth power of time. Small values of latent heat cannot easily be detected. And also log(t) is uncertain. What is the moment, when a melt, which must be cooled down from a temperature well above the equilibrium melting point, reaches the intended crystallization time? For all these doubts the reader is referred to a critical paper by Eder [24]. So, it does not surprise, if all kinds of Avrami indices, which do not agree with reasonable expectations, have been reported. And also, if DSC is used, the trans-crystallization effect can reduce the effective Avrami index, which otherwise will, for instance, be equal to 3.

An ingenious idea for coping with the influence of temperature, if the course of this temperature cannot be prescribed, has been published by Nakamura, Watanabe, Katayama and Amano almost thirty years ago [25]. For the purpose these authors introduced a dimensionless time replacing the quotient t/τ in (1.6) and (1.7). The latter equation reads now:

$$\alpha(t) = \frac{N_v}{\tau(t)} \exp\left[-\int_0^t \frac{du}{\tau(u)}\right]. \tag{1.18}$$

The extra condition, which is introduced here, is the so-called isokinetic assumption, which means that the growth speed and the activation frequency of primary nuclei $1/\tau(t)$ have the same temperature dependence. Obviously, for this assumption the activation process of nuclei, as has been sketched by (1.6), is of importance. It means that one has:

$$G(t)\,\tau(t) = \text{const.} = \lambda. \tag{1.19}$$

In this equation λ is a characteristic length, which cannot have a completely arbitrary value. In fact, the progress in growth is restricted by the time, which elapses up to the birth of the next nucleus. If the product $G^3\tau^3$ in (1.8) and (1.9) is simply replaced by λ^3, one obtains the corresponding equations for the case of isokinetics. In these equations the ratio t/τ must be replaced by

$$w(t) = \int_0^t \frac{du}{\tau(u)}. \tag{1.20}$$

The lower bound zero of the integral means that time zero is at the moment, when during cooling the sample passes the equilibrium melting point. In fact, τ can be assumed to be infinite above this temperature. One has:

$$\xi_g(t) = 1 - \exp\left[-8\pi\,N_v\,\lambda^3\,e_4\,(-w(t))\right] \tag{1.21}$$

and

$$N_c(t) = N_v \int_0^{w(t)} dw \ \exp\left[-w - 8\pi N_v \lambda^3 \ e_4(-w)\right].\qquad(1.22)$$

In these equations the thermal history of the cooling process, which normally varies in the sample from place to place, is represented by the value of $w(t)$. In particular, this function shows up as the upper bound of the integral of (1.22).

A criterion for the quality of the description is the number density of spherulites at infinite time, as this density is characteristic for the obtained structure of the sample. Since also $w(t)$ goes to infinity with t, one has:

$$N_c(\infty) = N_v \int_0^\infty dw \ \exp\left[-w - 8\pi N_v \lambda^3 \ e_4(-w)\right].\qquad(1.23)$$

Unfortunately it must be said that, obviously, this integral is a constant independent of the thermal history. But this means that the isokinetic approach is unable to predict a real structure. The structure, as obtained according to this approach, is predetermined by the chosen values of N_v and λ [22]. The general experience that the number density of spherulites increases strongly with the cooling speed, is not reflected by (1.23). As a consequence, also local variations of the structure, as found in every sample, cannot be described. It can also happen that $w(t)$ does not go to infinity because of the fact that the glass transition temperature is passed before crystallization is complete. In this case only a number density of spherulites lower than the one predicted by (1.23), can be expected according to this approach.

It also remains questionable, whether the evolved heat of crystallization is correctly described, if these equations are applied. In fact, this heat of crystallization interferes, dependent on the location in the sample, with the solution of the heat transfer problem. Because of the fact that, apparently, the isokinetic approach is not realistic, an almost thirty years' history of success, which has been booked for the equations of Nakamura et al., must be ended. Meanwhile, there is also direct evidence for the inadequacy of the isokinetic approach. In fact, if one looks at the experimental results shown in Sect. 1.1, one notices that the number density of nuclei increases continuously with decreasing temperature, whereas the growth speed goes through a maximum halfway down to the glass transition temperature. As will be shown later in this monograph, these experiences hold for a great number of polymers.

The conclusion must be that for a correct treatment of nonisothermal processes a more powerful method must be found. Such a method will be described in the next section.

1.2.2   The Rate Equations of Schneider, Köppl and Berger

A combination of Kolmogoroff's integral, as given in (1.3), with the equation of heat conduction, which is a differential equation, does not seem an easy task. As a consequence, Schneider et al. [26] decided to transform this integral into a more suitable configuration. For the purpose they differentiated this integral several times with respect to time. It appeared that with every step a useful auxiliary function was obtained. In this way a system of differential equations was created. The authors called these differential equations the rate equations. If the integral in (1.3) is denoted as φ_0, this system of equations reads in a slightly modified version:

$$\frac{d\varphi_i(t)}{dt} = \frac{1}{G(t)} \, \varphi_{i-1}(t) \tag{1.24}$$

for $i = 1, 2, 3$ and $\varphi_i(-\infty) = 0$. The latter condition just means that the history of the crystallization process is considered from a moment long before crystallization started. In (1.20) the begin was set at time zero for the same purpose. To start with one has:

$$\varphi_0(t) = \frac{4\pi}{3} \int\limits_{-\infty}^{t} du \, \alpha(u) \left[\int\limits_{u}^{t} dv \, G(v) \right]^3 , \tag{1.25}$$

where φ_0 is identical with ξ_g^* of (1.3). It is the total volume of spherulites per unit volume of the sample, if the impingement (space filling effect) is disregarded. In fact, this so-called undisturbed volume can formally become larger than the unit of volume of the sample. But this does not matter, as the necessary correction, which is given by (1.2), can always be carried out. The next auxiliary function is:

$$\varphi_1(t) = 4\pi \int\limits_{-\infty}^{t} du \, \alpha(u) \left[\int\limits_{u}^{t} dv \, G(v) \right]^2 . \tag{1.26}$$

This φ_1 is the total surface area of the undisturbed spherulites per unit volume of the sample. This function is of particular interest because the growth occurs on this surface. In continuation one has:

$$\varphi_2(t) = 8\pi \int\limits_{-\infty}^{t} du \, \alpha(u) \left[\int\limits_{u}^{t} dv \, G(v) \right] , \tag{1.27}$$

which is 8π times the sum of the radii of the undisturbed spherulites per unit volume, and

$$\varphi_3(t) = 8\pi \int\limits_{-\infty}^{t} du\ \alpha(u), \tag{1.28}$$

which is 8π times the number of these spherulites per unit volume. If one is interested in the rate $\alpha(t)$ of nucleation, one also can differentiate (1.28). One obtains:

$$\frac{d\varphi_3(t)}{dt} = 8\pi\ \alpha(t). \tag{1.29}$$

For reasons already mentioned, the first of the equations (1.24) is of particular interest. After a rearrangement it reads:

$$\frac{d\varphi_0(t)}{dt} = G(t)\ \varphi_1(t). \tag{1.30}$$

This equation expresses the fact that growth occurs at the surface of the spherulites. If impingement is taken into account, one has:

$$\frac{d\xi_g(t)}{dt} = G(t)\ \varphi_1(t)\ \exp(-\ \varphi_0(t)). \tag{1.31}$$

This equation is directly obtained by a differentiation of (1.4). If secondary crystallization is disregarded in a fast cooling process, the real degree of crystallinity ξ becomes:

$$\xi = p\ \xi_g, \tag{1.32}$$

where p (<1) is the fraction of crystallinity shortly after the manufacture.

For the moment only the one dimensional case of heat transfer will be mentioned. For this case the equation of heat conduction can be written as follows:

$$\frac{\partial T}{\partial t} = a\ \frac{\partial^2 T}{\partial x^2} + \frac{h}{c}\ \frac{\partial \xi}{\partial t}. \tag{1.33}$$

In this equation a is the heat diffusivity of the melt, h is the specific heat of crystallization and c the specific heat capacity per unit mass. It is now evident, how the equations are coupled by the evolved heat of crystallization.

The rate equations form the basis for the pertinent calculations. However, without knowledge of the time dependence of the kinetic parameters G and α these equations cannot become operative. As already mentioned in Sect. 1.1, G can be considered as not directly dependent on time. The situation with α is, in principle, a little more complicated. However, as the experimental results of Fig. 1.1 suggest, a unique

function of temperature can be assumed for the number density N of the nuclei after isothermal crystallization. But this means that α can be expressed as:

$$\alpha(t) = \frac{dN(T(t))}{dt} = \frac{dN(T(t))}{dT} \frac{dT(t)}{dt}.$$ (1.34)

It should be observed that both differential quotients on the right side of this equation carry a negative sign for α being positive with cooling.

The number density of nuclei as a unique function of temperature has previously been proposed by Van Krevelen [27] as the most practical approximation. However, it will be shown in Chap. 2 of this monograph that the overwhelming majority of nuclei in polymer melts is actually of the athermal type. For those nuclei the unique function of temperature is realistic.

It turns also out that (1.34) must be modified for the case that, as a consequence of the evolution of latent heat, local reheating occurs in the sample. But it is evident that nuclei, which come up during cooling, immediately experience some stabilization, so that they survive a modest reheating. In taking account of this effect, the course of the real local temperatures T must be modified for the time span, where the local reheating occurs. During this time span the real temperature must be replaced by the lowest temperature $T_{min}(x,t)$. This temperature is the temperature of the minimum, where the upturn sets in. Until with further outside cooling the real temperature returns to the value, which it had at the upturn, this T_{min} will be kept constant. During this time span no new nuclei should come up.

For the development of the morphology (1.34) can be used, if for the term between brackets $\exp(-\varphi_0)$ is inserted (cf. (1.4), (1.5) and (1.25)):

$$\frac{dN_c}{dt}(t) = \frac{dN}{dT}(T(t)) \frac{dT}{dt}(t) \exp(-\varphi_0(t)).$$ (1.35)

This equation can be integrated simultaneously with the (1.24), (1.28) and (1.33). This integration starts, before the temperature at the surface of the sample passes the equilibrium melting point during the process of cooling.

However, in principle there is still a problem of a different nature. A straight forward use of (1.33) is only possible, if the temperature gradients in the sample remain small enough for the assumption that every newly formed spherulite can simply grow at the calculated temperature of its nucleus. In fact, if the temperature shows a noticeable gradient already within the domain of the growing spherulite, this spherulite will show a faster growth on the side of the lower temperature. A description of this more complicated situation must be postponed to a later section. For the fine grained structures, which are desirable from the point of view of technology, such an improvement will probably not be necessary.

Another point is, that in practical processing one can certainly not disregard the influence of flow. But this means that in first instance one has to add a convection term to (1.33). In this way (1.33) is transformed into the so-called energy equation. Fortunately, one does not need the general case of this equation. In all relevant

cases the fluid flows with high speed along a sufficiently flat wall of lower temperature. For those cases one has:

$$\frac{\partial T}{\partial t} = a\,\frac{\partial^2 T}{\partial x^2} + \frac{h}{c}\,\frac{\partial \xi}{\partial t} + v_y(x)\,\frac{\partial T}{\partial y},\qquad(1.36)$$

where v_y is the fluid velocity in the y-direction as a function of distance x from the wall. For this equation it is assumed that heat conduction can be neglected with respect to heat convection in the y-direction. Only in the x-direction, which is perpendicular to the wall, conduction is of great importance. Nevertheless, a direct use of this equation cannot achieve its object. In this respect it is not the problem of an accurate calculation of the convection term, even if the rheology of the fluid is modified by incipient crystallization. The difficulty lies mainly in the second term on the right side. In fact, proper experiments have shown that the kinetics of crystallization are extremely sensitive to velocity gradients. And for continued flow this problem has not yet be settled. This fact will be discussed in Chap. 3 of this monograph.

Interestingly, for a number of practical situations there is an escape from this dilemma. In fact, it turned out that in short term experiments, when flow was applied only for rather short periods, number and character of the nuclei changed tremendously. But growth on these nuclei seemed to be delayed. In fact, after cessation of flow it took considerable time spans, before growth became noticeable. Apparently, the surface area of the newly formed nuclei, in particular of those, which are very thin threads, is extremely small in the beginning. In the quieted down melts it took waiting times, which were a hundred or even a thousandfold longer than the flow times. Only after these waiting times crystallization became noticeable by light scattering or depolarization of polarized light. The increased number densities of nuclei, as given on the right side of Fig. 1.1, were obtained from the number densities of spherulites finally found.

For the use of (1.36), however, this means that the convection term remains unchanged with respect to a melt, which did not undergo a crystallization process. And also, no latent heat h had been evolved during the period of flow. In particular, the interpretation of structures in injection molded parts can be favored by these facts.

1.3 Examples for Special Cases

1.3.1 Minimum Cooling Speed for by-Passing Crystallization, Eder [28]

If the cooling speed is prescribed, one has a case, where Kolmogoroff's equation (1.4) can directly be applied without a recurrence to the troubles caused by the solution of a heat transfer problem. In fact, the heat of fusion h does not play a role,

if the cooling speed is so fast that crystallization does not get a chance (see the title
of this section). However, a constant cooling speed can be obtained for the interior
of a sample, which remains amorphous, only if the coolant has a temperature, which
decreases linearly with time and if the sample itself is sufficiently thin. A rule of
thumb says that the Fourier number must be smaller than 0.5 for the achievement of
steady cooling. For a cylindrical sample this means:

$$Fo = \frac{a\,t}{D^2} < 0.5, \tag{1.37}$$

where D is the sample diameter and t is the running time, which is required for an
achievement of steady cooling. This equation shows that the said running time
t decreases with the square of the sample diameter. The fact that a finite running
time is unavoidable means that the temperature, at which the sample is exposed for
the first to the coolant, must be higher than the temperature, where crystallization
can be expected to start with slower cooling. One has for the pertinent temperature
difference:

$$\Delta T \approx q\,t, \tag{1.38}$$

where q is the constant cooling speed of the coolant, as governed by the following
equation:

$$T(t) = T_{\max} - q\,t. \tag{1.39}$$

For convenience the reference temperature $T_{\max}$ is chosen as the temperature,
where the growth speed $G(T)$ of the spherulites shows its maximum (cf. Fig. 1.2).

For the following calculations quite realistic approximate equations are chosen
for $G(T)$ and $N(T)$. These equations read:

$$G(T) = G_{\max}\,\exp\!\left(-\,(k_G(T - T_{\max}))^2\right) \tag{1.40}$$

and

$$N(T) = N_{\max}\,\exp\left(-k_N(T\ -\ T_{\max})\right). \tag{1.41}$$

In fact, the temperature dependencies of these parameters must be known, if their
influences are to be minimized. One can observe that the equation for the number
density does not show a maximum. The symbol $N_{\max}$ stands for the number density
at the temperature $T_{\max}$, where the growth speed has its maximum. For the calcula-
tions one needs the rate of nucleation. For N as a unique function of temperature one
obtains this rate from (1.34), where the term between brackets is omitted for the
present purpose. In the present case the rate of nucleation, which is undisturbed by
the impingement effect, is needed, as the degree of crystallinity remains negligible.

The function φ_0, as occurring in the exponent of Kolmogoroff's equation, is required. If (1.41) is differentiated with respect to T, and since dT/dt is equal to $-q$, one has:

$$\alpha(t) = N_{\max}\, k_N\, q\, \exp(k_N\, qt). \tag{1.42}$$

Equation (1.25) can now be integrated, if in (1.40) $k_G(T - T_{\max})$ is replaced by $-k_G\, qt$ (according to (1.39)) and (1.42) is used as it stands. One obtains in this way:

$$\varphi_0(t) = K f(k_G qt\,;\, k_N/k_G). \tag{1.43}$$

Explicitly function f reads:

$$f(v\,;\,\kappa) = \frac{\kappa}{8} \int\limits_{-\infty}^{v} ds\, [\mathrm{erf}(v) - \mathrm{erf}(s)]^3\, \exp(\kappa s) \tag{1.43a}$$

with $v = k_G qt$ and $\kappa = k_N/k_G$. The constant K reads:

$$K = \frac{4\,\pi^{5/2}}{3}\, \frac{N_{\max}\, G_{\max}^3}{k_G^3}\, \frac{1}{q^3} \tag{1.43b}$$

The critical cooling speed for by-passing crystallization is defined here as that cooling rate q_{crit}, giving at the end of the cooling ($t = \infty$) a degree of space covering of ξ_g of 0.01, as a space covering of zero would require an infinitely fast cooling speed. At this low space covering ξ_g and φ_0 are identical. So one has:

$$q_{\mathrm{crit}} = \sqrt[3]{\frac{400}{3}}\, \pi^{5/6}\, \frac{G_{\max} \sqrt[3]{N_{\max}}}{k_G}\, \sqrt[3]{f(\infty\,;\, k_N/k_G)} \tag{1.44}$$

It turns out that the numerical value of $f(\infty;\kappa)$ varies between 1 and 0.6 in the relevant range of κ between zero and five with its minimum of ≈ 0.6 at $\kappa \approx 3$. As the third root of f occurs in (1.44), the last term in (1.44) deviates at most by 0.15 from 1. Ignoring this maximum deviation one obtains:

$$q_{\mathrm{crit}} = 13.24\, \frac{G_{\max} \sqrt[3]{N_{\max}}}{k_G} \tag{1.45}$$

At this point one would like to find a table, which contains the critical cooling speeds q_{crit} for a series of industrially important polymers, as an illustration of the importance of (1.45). Notwithstanding the fact that the required kinetic data $G_{\max}$, $N_{\max}$ and k_G can only be scrutinized later in the context of their determination (see Chap. 2 of this monograph), such a table will be given here as Table 1.1.

Table 1.1 Minimum cooling speeds for bypassing crystallization in a series of industrial polymers, with required kinetic data

Polymer	G_{max} (ms^{-1})	k_G (K^{-1})	N_{max} (m^{-3})	q_{crit} (Ks^{-1})	Grade
HDPE	$>8 \times 10^{-4}$	~0.05	$>10^{17}$	>10,000	Borealis
PK	9.7×10^{-6}	0.036	3×10^{14}	620	RDP-211 Shell
	5.4×10^{-6}	0.045	6×10^{13}	240	Carillon Shell
iPP	5.0×10^{-6}	0.051	10^{14}	60	KS10 Borealis
PB	1.6×10^{-6}	0.072	6×10^{14}	25	0110 Shell
PET	2.5×10^{-7}	0.033	1.5×10^{15}	11.5	MPET Sinco
	4.0×10^{-7}	0.034	1.5×10^{14}	8.3	DMT Sinco
	2.0×10^{-8}	0.030	10^{13}	0.9	v. Antwerpen
iPS	2.5×10^{-9}	0.035		~0.02	v. Krevelen

From this table one can learn that critical cooling speeds vary by six decades from HDPE to i-PS. It will be seen later that the behavior of crystallizing polymers fills the gap between the behavior of metals and of glass forming minerals.

Probably, a few words must be said about the character of the approximate equation (1.40). In principle, the growth speeds go to zero at the melting point T_m and at the glass transition temperature T_g. In fact, at temperatures above the equilibrium melting point there are no (secondary) nuclei promoting growth and below the glass transition temperature the extremely high viscosity is prohibitive of any transport mechanism. However, these facts are not reflected by (1.40). This equation does not contain the parameters T_m and T_g. However, in this equation the growth speeds seem to become low enough on both sides of T_{max} for being of no considerable influence on the integration. Also the fact that with polymers of decreasing crystallization speed the distance between the melting point and the glass transition temperature decreases continuously, is practically taken into account by this equation. In fact, if G_{max} is low, one quickly arrives on both sides of T_{max} at sufficiently low values of the growth speed.

1.3.2   A Dimensionless Process Classification Number

The idea for the definition of such a number goes back to 1984 [29]. This number can be defined as:

$$Jk = \frac{\tau_{th}}{\tau_{cr}}, \tag{1.46}$$

where τ_{th} is the time needed for thermal equilibration (termination of the cooling process) and τ_{cr} is the time needed by the crystallization process. The symbol Jk has its origin in a paper by Astarita and Kenny [30]. These authors became fond of the idea and called the number the Janeschitz-Kriegl number. It turns out that it is not difficult to find a classical expression for τ_{th}. It reads:

$$\tau_{th} = \frac{(1 + Ste)\, d^2}{a} \qquad \text{with} \qquad Ste = \frac{\Delta h}{c_p (T_f - T_s)} \tag{1.47}$$

In this equation d is the thickness of the sample (a slab), a is the heat diffusivity of the sample, as averaged over the states of aggregation and Ste is the Stefan number with Δh being the specific latent heat corresponding with the final degree of crystallinity, c_p the averaged specific heat, T_f the starting temperature of the fluid and T_s the final temperature of the solid.

Unfortunately, we were not so successful in the formulation of the time τ_{cr}, which is required for the crystallization process. As a consequence it took quite a time, until Jk could be made operational. In fact, in the beginning we did not have the required kinetic data at our disposal. Nevertheless we were able to show that the metals were on one side of the spectrum and the glass forming minerals on the other side of the spectrum with the polymers in between. This comprehension was not so difficult to achieve, because of the enormous differences in the crystallization speeds.
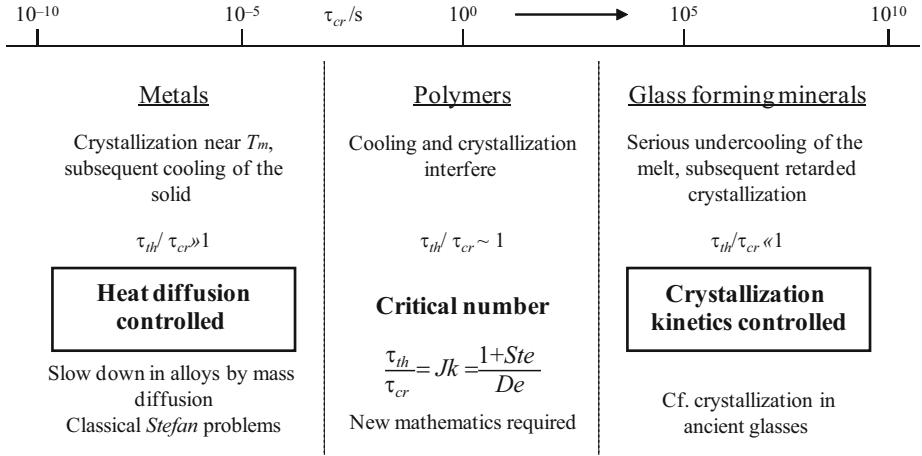
These speeds cover about 16 decades, whereas the heat diffusivities of the diverse materials cover only about four decades. As a consequence, manufacturing processes of metals with their enormous heat conductivities nevertheless are of the heat diffusion type. In fact, it is always the slower partial process, which determines the character of the whole process. But crystallization is so fast with metals that it always wins against cooling. Only with extremely thin samples one can find solidification processes, which are crystallization kinetics controlled, where crystallization becomes the slower process. The situation is completely different with glass forming minerals. With these minerals crystallization is extremely sluggish. As a consequence, even very thick samples still show crystallization kinetics controlled crystallization. The cooling speed is always too large for a heat diffusion controlled process. The outcome of this consideration is depicted in Fig. 1.4. It gives a viable classification of materials [31].

On top of this compilation one finds the scale of the crystallization times τ_{cr}. A time scale for the heat diffusivity is not shown. Its influence is secondary. In the middle one finds the Jk number. In this equation one finds the Deborah number $De = a\tau_{cr}/d^2$. But for polymers this presentation is too coarse. For these materials one needs an explicit expression for the time τ_{cr}.

From the consideration in the previous section we take over the suggestion that the product of $G_{\max} N_{\max}^{1/3}$ will be representative. If a sample is quenched fast enough to – say – $T_{\max}$, all spherulites start growing simultaneously on the number of nuclei representative for this temperature.

In this case one obtains the following form of Kolmogoroff's equation (see (1.10)):

$$\xi_g(t) = 1 - \exp\left(-\frac{4\pi}{3} N_{\max} G_{\max}^3 t^3 \right). \tag{1.48}$$

10^{-10}		10^{-5}	τ_{cr}/s	10^0	$\longrightarrow$	10^5	10^{10}

Metals	Polymers	Glass forming minerals
Crystallization near T_m, subsequent cooling of the solid	Cooling and crystallization interfere	Serious undercooling of the melt, subsequent retarded crystallization
$\tau_{th}/\tau_{cr} \gg 1$	$\tau_{th}/\tau_{cr} \sim 1$	$\tau_{th}/\tau_{cr} \ll 1$
Heat diffusion controlled	**Critical number**	**Crystallization kinetics controlled**
Slow down in alloys by mass diffusion Classical *Stefan* problems	$\dfrac{\tau_{th}}{\tau_{cr}} = Jk \dfrac{1+Ste}{De}$ New mathematics required	Cf. crystallization in ancient glasses

Fig. 1.4 A viable classification of materials on the basis of their processing conditions

According to this equation space covering is sufficient, if the argument of the exponential is −1. In this way the crystallization time can be calculated for this situation. One has:

$$\tau_{cr} = \frac{1}{1.63\ G_{max}N_{max}^{1/3}}. \qquad (1.49)$$

If this expression is used together with (1.47) in (1.46), one has:

$$Jk = \frac{(1 + Ste)\,d^2}{a}\ 1.63\ G_{max}N_{max}^{1/3}. \qquad (1.50)$$

This equation seems very acceptable. Nevertheless, some discussion seems necessary.

For the purpose the following train of thoughts is proposed: As a first step the fluid sample is cooled to T_{max} with the minimum speed, which prevents crystallization. In a second step the temperature is kept at T_{max}, until the sample has completely crystallized according to the criterion of (1.49).

With the said cooling step only about half the distance between T_m and T_g is covered. This means that one needs only half the time, which is calculated from (1.45). In this way one has $t_{cool} = (T_m - T_g)/(2q_{crit})$.

According to the Gaussian curve for $G(T)$ one has $k_g = 2/(T_m - T_g)$. A combination of these expressions with (1.45) yields:

$$t_{cool} = \frac{1}{13.24\ G_{max}N_{max}^{1/3}}. \qquad (1.51)$$

Table 1.2 Thermodynamic and kinetic data leading to a calculation of the Jk number. Courtesy of Hanser Verlag [31]

	ΔH (kJ mol^{-1})	T_m (K)	Ste (l)	C_p (J mol^{-1}K^{-1})	a (10^{-7}m^{2}s^{-1})	τ_{th} (s) (d = 1mm)	$1/\tau_{cr}$ (s^{-1})	Jk (l) (d = 1mm)
HDPE	8.22	415	1.12	63	1.3	16.3	561	9120
PK						$\approx$20	1.04	20.8
							0.34	6.50
iPP	8.70	483 (α–mod)	0.39	93	0.95	14.6	0.374	5.45
PB-1	7.00	411 (form I)	0.52	120	0.90	16.9	0.218	3.69
PET	26.9	550	3.58	298	1.43	32.0	4.76×10^{-2}	1.52
							3.51×10^{-2}	1.12
							0.32×10^{-2}	0.103
i-PS	10.0	516	2.58	178	1.0	35.8	8.71×10^{-5}	0.0031

As this time is only about one eighth of the time needed for the crystallization according to (1.49), this time t_{cool} can be disregarded in the rough estimate. But this means that for the polymers of medium speed of crystallization (1.50) seems quite useful. As a consequence, this equation is used for the calculation of the Jk numbers of the polymers, which were quoted already in Table 1.1. In this way Table 1.2 is prepared.

Table 1.2 also gives the required thermodynamic and statistical parameters. A sample thickness of 1 mm is assumed. With PK (polycarbonate) two copolymers were investigated. As no physical data were available, the value of τ_{th} was just estimated. There were three samples of PET of different molar masses. For this polymer the growth speeds depend on the molar mass, as the chain lengths are rather short in general. This fact has been documented by Van Antwerpen and Van Krevelen [32].

One notices that for the investigated polymers the values of Jk spread over many decades like the values of the critical cooling speeds (see Table 1.1). The difference is only that in Table 1.2 also the sample thickness plays a role. If instead of 1 mm a thickness of 0.33 mm is introduced, all values of Jk are reduced by a factor ten.

If one now looks at the edges of the spectrum, one can gain further insights. With fast crystallizing polymers like HDPE cooling of the samples cannot be fast enough for avoiding premature crystallization. The sample starts to crystallize much too early. The evolved latent heat causes a reheating, so that the samples crystallize close to the melting point. The time of crystallization is increased in this way with respect to the value calculated with (1.49). But this means that the Jk number is reduced. If a thinner sample is used, this effect becomes less pronounced.

If one now looks on the other edge of the spectrum, one can give the following analysis: With i-PS the minimum cooling speed for preventing crystallization is very low. So it takes hours, before T_{max} is reached, if the said concept is respected. Everyone tends to use too high a cooling speed. But in such a case, the glass transition temperature is reached before the onset of a one percent crystallization, as

is required by the concept of Eder [28]. One obtains a sample with a much lower degree of crystallinity as an end product.

1.3.3 Scanning Calorimetry

Differential scanning calorimetry is a well-known technique for the evaluation of thermal properties of materials. As a consequence it is not surprising that this technique has also been applied to polymers in order to get an impression of their crystallization kinetics [33]. However, polymers are materials with very low heat conductivities, a fact which has not been taken to heart sufficiently. As a consequence, machines were usually calibrated only with respect to temperature with a number of suitable metals. A calibration with respect to heat transfer had not been carried out up to the moment when we started our critical investigations [34,35]. In fact, metals have heat conductivities, which are factors of more than hundred larger than those of polymers. This means that the speed of cooling must have a tremendous effect with polymers, when compared with metals.

1.3.3.1 Unabridged Simulation

C.H. Wu successfully calculated the behavior of an industrial PP, of which except for the thermal data (heat conductivity, heat of fusion, final degree of crystallinity, specific heat and density) also crystallization kinetics data (number densities and growth speeds of spherulites as functions of temperature) were available to a sufficient extent [35]. Admittedly, at that time reliable growth speeds for the relevant α-modification of this polymer were known only for temperatures higher than 110°C. An extrapolation to lower temperatures was carried out on the logarithmic scale of G with the aid of a tangent drawn to the part of Fig. 1.2, which existed already at that time (see [36], Fig. 1.7, open symbols, closed symbols holding for the β-modification). A similar, less critical extrapolation was carried out also for the number density of nuclei. In fact, this number density shows up as a first power in the equations, in contrast to the third power of the growth speed. Also a heat transfer coefficient, as determined for the transfer between pan and furnace with the aid of metallic samples [34] was at our disposition. As we are convinced that the general character of the results is not seriously influenced by the provisional kinetic low temperature data, characteristic results of these calculations are reproduced here. In these calculations the rate equations by Schneider et al. [26] were successfully used for the first time. Mrs. Wu, as a post doctorate fellow in mathematics, was just the right person for these involved calculations.

Reality lies between two limiting cases: The sample as a tablet is sandwiched between two metal walls (symmetric case) of equal temperature or the sample is in contact only with one metal surface. Its other surface is a free adiabatic surface (asymmetric case). In the DSC-machine a situation prevails, which just lies

between the said limiting cases. The sample is in contact with the bottom of the pan which, on its part, is in touch with the furnace. On the upper side heat transfer is not directly zero but much less than at the bottom. The said limiting cases have the advantage that they can be treated together. In fact, at the midplane of the symmetric case the temperature gradient is zero. But the same holds for the adiabatic free surface of the asymmetric case. But this means that the solution for the asymmetric case is the same as for the symmetric case with doubled sample thickness. If in the latter case the sample formally has twice the thickness, one also must use twice the heat transfer coefficient on the contact surface.

The boundary value problem for the symmetric case can now be formulated. For the sample one has:

$$
\begin{aligned}
\frac{\partial T_s}{\partial t} &= a_s \frac{\partial^2 T_s}{\partial x^2} + \frac{h_s}{c_s} \frac{\partial \xi}{\partial t} && \text{for all } (x,t) \in (D_p, D_p + D_s/2) \times (0, \infty) \\
T_s|_{t=0} &= T_i(x) = T_{rf} && \text{for all } x \in [D_p, D_p + D_s/2] \\
\lambda_s \frac{\partial T_s}{\partial x}\bigg|_{x=D_p} &= \lambda_p \frac{\partial T_p}{\partial x}\bigg|_{x=D_p} && \text{for all } t > 0 \\
\frac{\partial T_s}{\partial x}\bigg|_{x=D_p+\frac{D_s}{2}} &= 0 && \text{for all } t > 0.
\end{aligned}
\tag{1.52}
$$

The symbols are T for temperature, D for thickness, a for heat diffusivity, λ for heat conductivity, h for the latent heat (corresponding to the attainable degree of crystallinity), c for specific heat, ξ for fraction of crystallized material, t for time and x for the distance from the surface of the furnace. Subscripts are p for pan, s for sample, i for initial and rf for reference. One finds the symbol T_{rf} in the equation describing the course of the furnace temperature T_f with time:

$$
T_f(t) = T_{rf} - qt \quad \text{with} \quad q = -\frac{dT_f}{dt} = \text{const.,}
\tag{1.53}
$$

which is the nominal constant rate of temperature change, as programmed for the furnace. The furnace is assumed to follow this temperature course exactly. For the interior of the wall of the pan one has:

$$
\begin{aligned}
\frac{\partial T_p}{\partial t} &= a_p \frac{\partial^2 T_p}{\partial x^2} && \text{for all } (x,t) \in (0, D_p) \times (0, \infty) \\
T_p|_{t=0} &= T_i(x) = T_{rf} && \text{for all } x \in [0, D_p] \\
\lambda_p S_1 \frac{\partial T_p}{\partial x}\bigg|_{x=0} &= \frac{\gamma}{2}\left(T_p|_{x=0} - T_f(t)\right) && \text{for all } t > 0
\end{aligned}
\tag{1.54}
$$

A few additional symbols are S_1 for one of the contact surfaces on one side of the sandwich and γ for the heat transfer coefficient between pan and furnace. For the symmetric case the total contact surface is $S = 2\,S_1$. The heat transfer coefficient is subdivided into two equal parts $\gamma/2$ for each contact surface.

As one can see on (1.52), (1.53) and (1.54), the values of an enormous number of parameters are required. Most of them, in particular the thermal data, can be found in the usual tables for polymers. In the original paper [35] there is an extended table of all necessary data. Here we content ourselves with referring to Figs. 1.1 and 1.2 of this report, from where the kinetic data can be extracted in principle. In fact, these data were needed in the rate equations [26] of Sect. 1.2.2, which were integrated by Mrs. Wu together with (1.52) and (1.54). In addition a value for the heat transfer coefficient between furnace and pan was needed. This coefficient had been determined in [34] to $\gamma = 0.016\,\mathrm{W\,K^{-1}}$. The way, in which this coefficient has been obtained, will be described below in connection with the difference, which is made between metallic and polymer samples.

The results of the said calculations are given in Figs. 1.5 and 1.6. In these figures the apparent latent heat $l(T_f)$ is plotted for two samples of differing thickness (0.3 and 0.9 mm) against the furnace temperature for eight nominal cooling rates of 50, 40, 30, 20, 15, 10, 5 and $1\,\mathrm{K\,min^{-1}}$. The apparent latent heat $l(t)$, which is considered as the DSC-signal, is defined as:

$$l(t) = \frac{\gamma\left(T_p|_{x=0} - T_b(t)\right)}{m_s q}, \tag{1.55}$$

where T_b is the so-called "base line" (see later). Time t and furnace temperature T_f are related by (1.53).
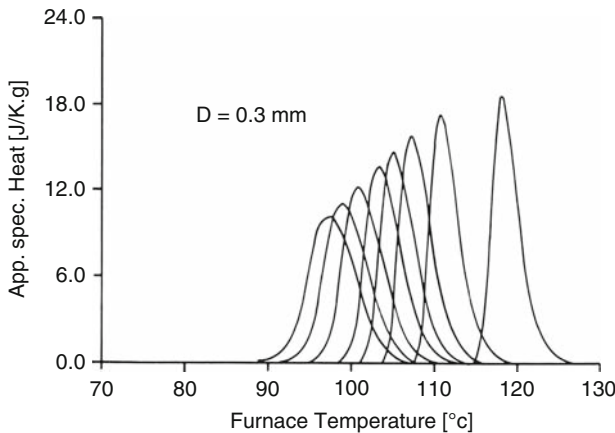
Fig. 1.5 Courses of apparent latent heats as functions of furnace temperature for the nominal cooling rates (*from left to right*) of 50, 40, 30, 20, 15, 10, 5 and $1\,\mathrm{K\,min^{-1}}$ and a sample of PP of a thickness of 0.3 mm, according to Wu's calculations [35]. Courtesy of Springer
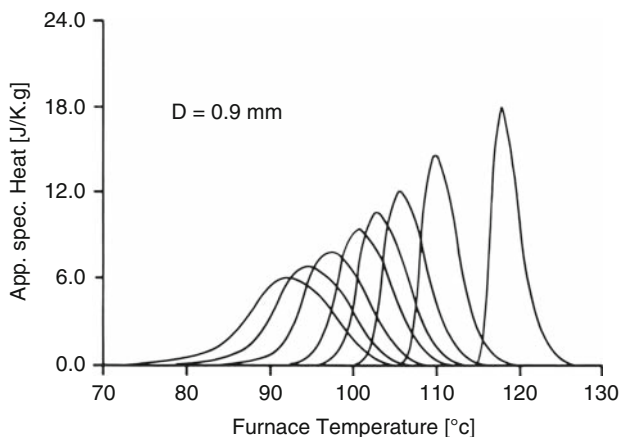
Fig. 1.6 Courses of apparent latent heats as in Fig. 1.5, but for a sample thickness of 0.9 mm [36]. Courtesy of Springer

Figures 1.5 and 1.6 show a similar tendency: With increasing cooling rate the peaks shift to lower temperatures and become lower and broader. For the thicker sample (Fig. 1.6) this effect is more pronounced.

The results of these calculations are compelling. In fact, if the heat transfer problem is ignored, the peaks have all the same height and shape. They are only shifted to lower temperatures with increasing cooling speeds [35,36]. There is also another important result, which cannot be seen on these figures: With increasing cooling speed the temperature difference between the midplane of the sample and the furnace increases considerably, up to more than 12°C even with the thinner sample. By the way, with the more realistic course of G as a function of temperature, as shown in Fig. 1.2, the peaks at the highest cooling rates will become lower and broader than in Figs. 1.5 and 1.6. This means that the approximation of the first paragraph leads to an underestimate of the effect.

In this connection we have to admit that the heat transfer coefficient γ is lowered in our experiments a little bit by the fact that three knobs were punched in the bottom of the pan in order to improve the reproducibility of the measurements. In fact, the bottoms of the pans are never completely flat. But the reader should accept that even with an optimum touch of the pan the corresponding heat transfer coefficient will not rise to infinity, as some optimists seem to believe. But this means that the general picture provided by Figs. 1.5 and 1.6 will remain unchanged. And a somewhat decreased heat transfer coefficient will be of advantage for a simplified treatment of the problem, as will be shown right away.

1.3.3.2   A Simplified Analytical Solution

As a first step a comparison is made with the results obtained for the asymmetric case. For the pertinent calculations the full value of γ was used on the contact side.

On the other side a zero heat transfer coefficient was assumed. It appeared that for a thickness $D_s = 0.3$ mm the results for the asymmetric case were practically identical with the results depicted for the symmetric case in Fig. 1.5 for that thickness. In particular this held for the highest, most critical cooling rate of 50 K min^{-1}. So, practically no difference was found for the two limiting cases, where the reality lies in between. But this means that the results are dominated by the relatively high resistance against heat transfer between furnace and pan. In fact, the internal heat transfer problems seemed to play only a minor role. However, for the larger sample thickness of $D_s = 0.9$ mm the situation was quite different. For this larger thickness of the sample the peaks became considerably broader for the asymmetric case. Apparently, with the larger distances for heat flow within the sample it became of importance, whether heat flew to both sides or only to one side. But this meant that a criterion had to be found for the license to believe that it does not matter, where exactly on the sample surface the heat transfer takes place.

For the purpose, the authors of [35] defined kind of a Nusselt number Nu^* as the ratio of the outer heat transfer coefficient γ and the sample intern heat transfer coefficient γ^*, i.e.:

$$Nu^* = \frac{\gamma}{\gamma^*}, \tag{1.56}$$

where γ^* is defined as

$$\gamma^* = \frac{4\,S\,\lambda_s}{D_s}. \tag{1.56a}$$

The authors observed that for a diameter of the tablet of 3 mm, a thickness of 0.3 mm, an outer heat transfer coefficient of 16 $\mathbf{W\,m^{-1}K^{-1}}$ and a heat conductivity of 0.193 $\mathbf{W\,m^{-1}K^{-1}}$ the said Nusselt number was:

$$Nu^* = 0.11. \tag{1.56b}$$

For the thicker sample of 0.9 mm a value of 0.33 was found. The conclusion is that Nu^* must not be larger than one tenth, if a simplified method, which will be explained right away, can be used. In fact, Nu^* can always be calculated with the aid of the available data. It should be clear that for metallic samples Nu^* is always extremely small because of the large values of λ_s. (For indium one has $\lambda_s = 76.2\ \mathbf{W\,m^{-1}K^{-1}}$, which is about 400-fold the value given above for PP).

In the simplified model one can content oneself with a simple balance equation, which reads:

$$-\left(m_s c_s + m_p c_p\right)\frac{dT_s}{dt}(t)\ +\ m_s h_s \frac{d\xi}{dt}(t) = \gamma\left(T_s(t)\ -\ T_f(t)\right) \tag{1.57}$$

with

$$T_s|_{t=0} = T_{rf}, \tag{1.57a}$$

where T_s is now "the" sample temperature. The "apparent latent heat" reads now:

$$l(t) = \frac{\gamma\,(T_s(t) - T_b(t))}{m_s q} \tag{1.58}$$

where the "base line" is

$$T_b(t) = T_f(t) + \frac{q}{\alpha}, \tag{1.59}$$

with T_f according to (1.53). In fact, the straight base line runs parallel to the straight line giving the furnace temperature, but is delayed in the present case of cooling by the second term on the right side of the equation (see [34]). For α see (1.61) below. This line shows the influence of the heat flow, which occurs without crystallization because of the cooling effect. It is evident that the heat capacities of sample and pan are not zero.

Using these equations one obtains DSC-curves which are almost indistinguishable from the curves shown in Figs. 1.5 and 1.6. For the thicker sample, for which Nu^* seems to be too large, this fact is a little surprising.

Now we arrive at the point, where the determination of the heat transfer coefficient becomes urgent. This determination is based on the fact that the DSC-signal returns to the base line according to an exponential function of time, as soon as the phase transition (crystallization) comes to an end. For the present purpose this moment is chosen as time $t = 0$. For this initial condition and for $d\xi/dt = 0$ the solution of (1.57) reads:

$$T_s(t) - T_b(t) = (T_s(0) - T_b(0))\, e^{-\alpha t} \tag{1.60}$$

with

$$\alpha = \frac{\gamma}{m_s c_s + m_p c_p}. \tag{1.61}$$

Aiming at a linear dependence on time the logarithm is taken on both sides of (1.60):

$$\ln(T_s(t) - T_b(t)) = \ln(T_s(0) - T_b(0)) - \alpha t. \tag{1.62}$$

At this point (1.53) must be reconsidered. Because of this linear relation one can consider T_f also as a time parameter. For the use of this parameter (1.62) must only

be multiplied by q on both sides. If (1.53) is rearranged into $-qt = T_f(t) - T_{rf}$ one obtains the following equation, where the logarithm of the apparent latent heat is involved.

$$q \ln(l(T_f)) = f(q) + \alpha T_f \qquad (1.63)$$

The recipe for the determination of α, to which the heat transfer coefficient γ is related by (1.61), is now obvious. The logarithm of the DSC-signal must be multiplied by the cooling rate q and plotted against the furnace temperature. The slope of the straight line, which is obtained, if the right temperature range is chosen, gives the value of α. In Fig. 1.7 this is demonstrated for an industrial PP.

   The cooling rates are indicated near the curves. The expected linearity and parallelism is clearly shown. The slight curvatures at the lower ends must be ascribed to small errors in the base line position. The value of γ, which is obtained with the aid of (1.63), is a little lower than the value of $\gamma = 16 \ mWK^{-1}$, as used in Wu´s calculations, i.e. $\gamma = 10 \ mWK^{-1}$. This fact can easily be explained: In [34] metals were used for the samples. As the heat conductivities of these samples is factors of about 400 higher than that of the polymer, the obtained heat transfer coefficient is higher and practically equal to the coefficient for the transfer between pan and furnace. In the case of the polymer the effective temperature in the sample is an average temperature. As a consequence, the heat transfer coefficient is also an effective one, which is influenced by the low conductivity of the sample.

   The balance equation (1.57) can be used for the derivation of an interesting equation, which relates the degree of crystallinity, which grows during the cooling
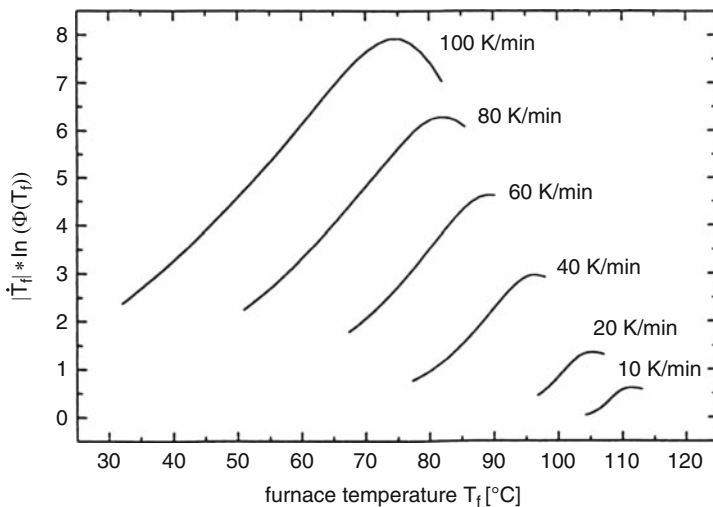
Fig. 1.7 Plot of the DSC-curves according to (1.63) for an industrial PP. The cooling rates are indicated near the curves [22], courtesy of VCH Wiley, Weinheim

cycle, to the development of the DSC-curve. For the purpose time t is replaced by T_f according to (1.53) and the integration is carried out with respect to the latter variable. For this procedure it is important to realize that the heat flow

$$\Phi(t) = \gamma \left(T_s(t) - T_f(t) \right) \tag{1.64}$$

which is found on the right side of (1.57), comprises not only the flow of the evolved latent heat $m_s h_s$ but also that of the stored heat $(m_s c_s + m_p c_p)$ of the system. So, one has

$$\Phi(t) = \Phi_{cr}(T_f(t)) + \Phi_{st} = \Phi_{cr}(T_f(t)) + q \left(m_s c_s + m_p c_p \right), \tag{1.65}$$

where subscript cr stands for crystallization and subscript st for stored heat, which is removed in creating the base line $T_b(T_f)$. The differential equation (1.57) is properly transformed into a differential equation with T_f as the independent variable. When this equation is integrated, (1.65) is substituted. In this way one arrives at:

$$\xi(T_f) = \frac{\Phi_{cr}(T_f)}{\alpha \, m_s h_s} + \frac{1}{m_s h_s q} \int_{T_f}^{T_{rf}} \Phi_{cr}(u) \, du. \tag{1.66}$$

This equation was derived by G. Eder in the course of the preparation for our review of 1997 [22]. One may observe that the upper temperature T_{rf} lies outside the peak area of the DSC-measurement. As a consequence only the lower temperature T_f of the integral is of importance. However, if the cooling is continued to the lower end, the well established integral over the whole peak is left over in the second term of (1.66). In fact, Φ_{cr} is zero again at that lower end. From this integral one obtains the degree of crystallinity of the just solidified sample. If on the other side an intermediate temperature T_f is considered, one has to bear in mind also the first term. It is now ten years from the publication of this result. So far, as we can take in the situation, nobody has ever cared of this fact. This first term depends on the heat transfer coefficient through α (1.61), which means that this coefficient has to be determined anyway.

Equation (1.66) enables the calculation of the progress of crystallization as a function of the time variable T_f. This is shown by the left curve of Fig. 1.8 for an industrial PP, which has also been used for the measurements leading to Fig. 1.7. For the purpose a high cooling rate of 100 Kmin^{-1} was applied. The furnace temperature T_f takes over the role of time in this curve.

The high cooling rate was achieved in a special DSC-apparatus at Philips Research in Eindhoven. This apparatus was cooled with liquid nitrogen. Nowadays there are already machines, which can be cooled much faster [33]. The present authors take the liberty to ask, whether the pertinent authors want to entangle
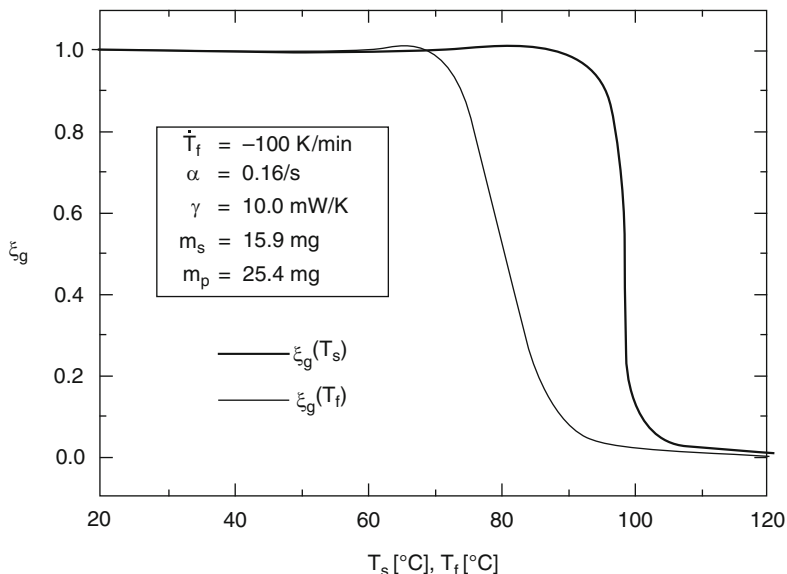
Fig. 1.8 The *left curve* gives the course of the crystallization of an industrial PP according to (1.66) for the high cooling rate of 100 $K min^{-1}$. For this curve the furnace temperature takes over the role of the time. The *right curve* gives the course of the crystallization as a function of the real sample temperature according to (1.67). See [22]. Courtesy of VCH-Wiley, Weinheim

themselves in insoluble heat transfer problems inherent to the architecture of the traditional machines.

The second curve in Fig. 1.8 invites us immediately for a discussion. It will turn out that with higher cooling rates a correction of the peak temperature becomes unavoidable, as also Eder has shown. As already announced, the temperature T_s in the sample becomes quite different from the furnace temperature T_f at the maximum of the DSC-curve. In fact, according to a combination of (1.59) with $\Phi_{cr} = \gamma$ $(T_s - T_b)$ one has:

$$T_s(t) = T_f(t) + \frac{q}{\alpha} + \frac{\Phi_{cr}(T_f(t))}{\gamma} \tag{1.67}$$

The sum of the second term and the third term of this equation can give quite a temperature rise above the furnace temperature. This becomes evident for the high cooling rate of 100 $K min^{-1}$. In fact, with the aid of this equation the transformation from T_f to T_s was carried out on the abscissa of Fig. 1.8. In this way the right curve of this figure is obtained. It shows that with a nominal cooling rate of 100 $K min^{-1}$ crystallization occurs with this polymer virtually at a constant internal temperature of about 99°C. At this point the reader is reminded of the considerations in Sect. 1.3.2, where the dimensionless classification number is defined. In this connection it has been assumed that crystallization occurs at a definite temperature above the
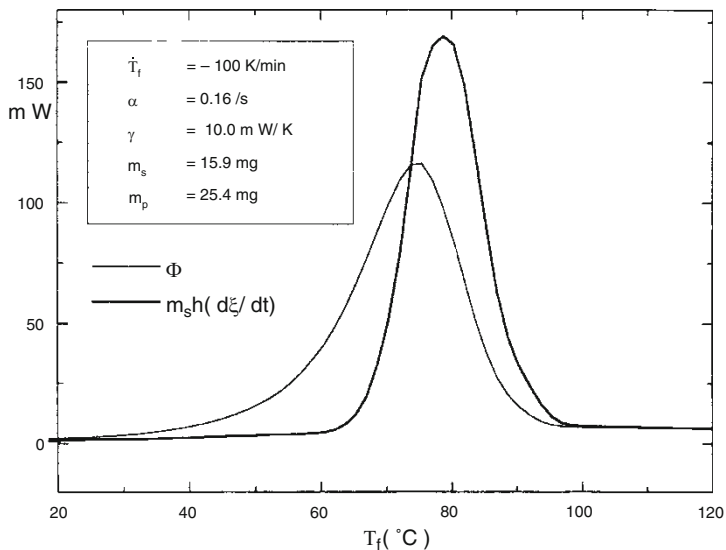
Fig. 1.9 *Left curve*: Exothermal peak of DSC-curve at a cooling rate of 100 K min^{-1} for the PP of the previous figures. *Right curve*: Heat evolved by the sample in the time span corresponding to the span of T_f. Both curves as functions of T_f. See [22]. Courtesy of VCH-Wiley, Weinheim

temperature, where the growth speed of spherulites shows its maximum. A look on Fig. 1.2 informs us that this maximum lies for PP at about 90°C.

If after a change of the scale of the abscissa (with the use of (1.53)) the left curve of Fig. 1.8 is differentiated with respect to time, one has only to multiply the result by $m_s h_s$, in order to obtain the real rate of crystallization $m_s h_s d\xi/dt$. This rate is plotted in Fig. 1.9 (right curve) against the furnace temperature T_f. For comparison Φ_{cr} is also plotted against T_f (left curve). One notices the difference. But the right curve is not a real DSC-curve: the internal rate of cooling is not constant because of the internal reheating effect.

1.3.3.3 Scanning Microcalorimeter for High Cooling Rates

The two previous sections were not formulated with the intention to advocate them for practical use. In fact, from the onset it was clear to us that cooling rates, as occurring in processing praxis, are much higher than those, which can be realized in DSC-machines of traditional architecture. The goal of the just mentioned sections was a more general one. These sections were considered to be very useful for a demonstration of the difficulties, which arise in principle with scanning calorimetry and other measuring techniques helpful for the evaluation of processing parameters. Our group has never been engaged seriously in those techniques before. But we became aware of the central role, which those measurements play in the understanding of polymer processing. Another point was a theoretical one. In fact, the

calculations by Mrs. Wu clearly demonstrate the usefulness of Schneider's rate equations, which cannot easily be replaced by other equations.

Recently, however, a research group at Rostock University has developed a microcalorimeter, which deserves a serious consideration in the present context [37–41]. In fact, this calorimeter enables extremely high cooling rates. One has to consider this development as a break-through in scanning calorimetry. For the purpose samples of about 100 ng are placed on the middle of a thin silicon nitride membrane, which has a thickness of a few μm and a diameter of about 2 mm. Below the sample there is a tiny electric heater surrounded by the hot junctions of six thermopiles, of which the cold junctions are on the frame supporting the whole, which is immersed in a closed gas atmosphere. The nature of the gas (nitrogen, helium), its pressure and its temperature can be varied for the purpose of more or less severe cooling. Such an apparatus can be used for a lot more applications than those, which are of interest in the present study, where the consequences of rapid cooling attract our attention.

In the first paper mentioned [37] one finds a graph of particular interest. In this graph the apparent heat capacity (latent heat) of a 120 ng sample of a special polyethylene of a narrow molar mass distribution is plotted against the temperature of the heater for various extremely high cooling rates indicated (Fig. 1.10). This apparent heat capacity is deduced from the power input of the heater, which is controlled for pertinent linear decreases of the heater temperature with time. As expected, the locations of the peak maxima shift to lower temperatures with increasing cooling rates. The big sensations are the high cooling rates. The location of the peak, which is obtained at a cooling rate of only 10 $K\,min^{-1}$ with an ordinary DSC-machine, is indicated at the abscissa by an arrow.

The fact that the peak for a cooling rate of 140 $K\,s^{-1}$ is lower than that for 450 $K\,s^{-1}$, cannot easily be explained. From kinetic data of HDPE Eder [28] estimated a minimum cooling rate of at least 10,000 $K\,s^{-1}$ (Table 1.1) for bypassing crystallization. This result seems to fit nicely into the picture delivered by Fig. 1.10. The fact that the peaks become broader and lower with decreasing temperature of the maximum, can have various reasons. There is the heat transfer problem which, however, cannot easily be solved because of the fact that the sample experiences two heat flows, one from the heater and the other to the gas of constant low temperature. But there is also a possible influence of changing crystallization kinetics with decreasing temperature. Mrs. Wu assumed for her calculations an undisturbed linear increase of the logarithm of the growth speed with decreasing temperature (tangent on the half logarithmic plot at higher temperatures). If sample and furnace have equal temperatures (no heat transfer problems), this assumption leads to equal peak heights [36]. However, with temperatures lower than 400 K one finds with HDPE a considerable deviation to lower values from the said tangent of the logarithmic growth speed. The temperature of the maximum of the growth speed of spherulites of HDPE must lie at about 300 K (half way between melting point and glass transition). Our measurements [9](see also [22,42]), which reach down to about 350 K, already indicate the approach of that maximum. So, the flattening of the peak in Fig. 1.10 can also be explained in this way.
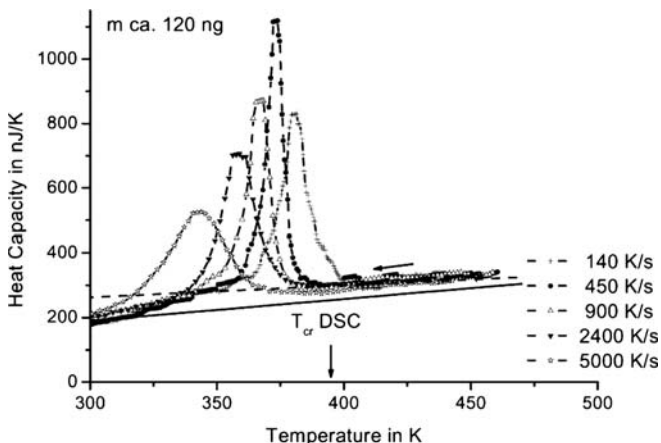
Fig. 1.10 Temperature dependence of the apparent heat capacity of a sample of a linear polyethylene of about 120 ng for various cooling rates according to [37] (*From left to right* 5,000, 2,400, 900, 450 and 140 Ks^{-1}). *Dashed* and *solid straight lines*: temperature dependence of heat capacities of permanently amorphous and crystalline samples of corresponding mass. Courtesy of Elsevier

Another very interesting result of the Rostock apparatus is shown in the fifth publication cited above (De Santis et al. [41], Figs. 5 and 6). In these figures the behavior of a sample of iPP is presented. The first of these figures is reproduced here as Fig. 1.11.

At the lower cooling rates, between 30 and 120 Ks^{-1}, one observes peaks, which can be ascribed to the α-modification. This fact was verified by the authors in heating experiments at 50 Ks^{-1}. The typical melting peak at 160°C was found. With further increasing cooling rates one observes the upcoming of a peak, for
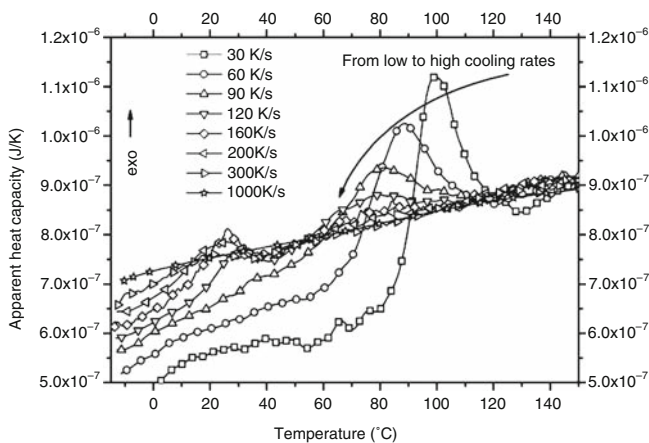
Fig. 1.11 Thermograms of a sample of iPP for various selected rates of 30, 60, 90, 120, 160, 200, 300 and 1,000 Ks^{-1} according to [41]. Courtesy of American Chemical Society

which the mesophase is responsible. With a cooling rate as high as $1{,}000\,\mathrm{Ks}^{-1}$ no crystallization at all could be registered. The obtained straight line depicts the decrease of the heat capacity of the amorphous material with decreasing temperature. Interestingly, after the formation of the α-peak the heat capacity submerges with farther decreasing temperature below the value of the amorphous material by about 30%. This dip seems to reflect the lower heat capacity of the crystalline material. For the first time this figure gives a complete analysis of the processes occurring during cooling of a sample of iPP. Also the mesophase could be identified by the typical thermogram, which was found with reheating.

Again, there seems an interesting comparison with the results of Table 1.1 of the present publication. In this table one finds for iPP a minimum cooling speed for bypassing crystallization of $60\,\mathrm{Ks}^{-1}$. From Fig. 1.11 one learns that $160\,\mathrm{Ks}^{-1}$ were needed for suppressing the α-peak. It appears that this value is higher than the value calculated by Eder from the kinetic data. However, we find this fact satisfying: Our results, as depicted in Figs. 1.1 and 1.2 of the present publication, seemed too exaggerated to some critics. However, in order to make the result of Eder's calculation agree with the above result of a thermal measurement, at least higher maximum values of the growth speed will have to be assumed.

For those interested in the heat transfer queries, Fig. 1.6 of the said paper seems to be informative. This figure is reproduced here as Fig. 1.12.

The authors of the paper think that the lower positions for the standard DSC are a consequence of a relatively smaller surface. An alternative idea, however, is that the positions from DSC are too low because of insufficient heat transfer. In this connection Fig. 1.9 should be considered. If this is true, one can conclude that the heat transfer problem is less urgent with the nanocalorimeter.
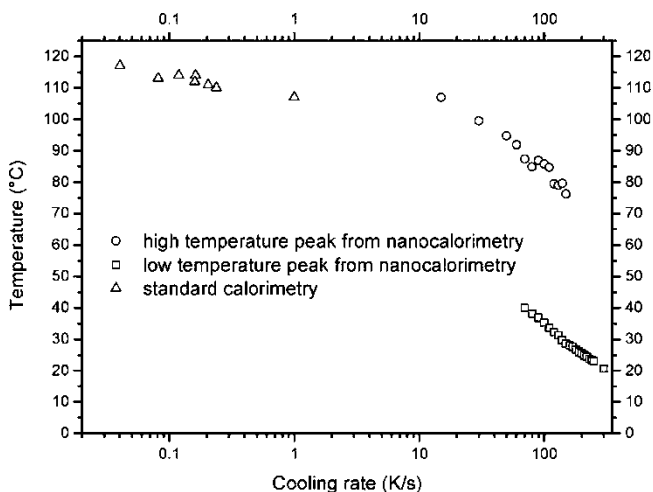

Fig. 1.12 Exothermal peak positions versus cooling rates, as obtained for an iPP [41]. *Circles*: α-modification, *squares*: mesomorphic phase, both according to nanocalorimetry, *triangles*: α-modification from standard DSC. Courtesy American Chemical Society

1.3.4   Phenomena of Propagation and Spreading

It will be clear to the reader that a situation, where crystallization starts simultaneously as a homogeneous process in a large volume, is a very unrealistic situation. Theoretically, such a process can happen only, if the temperature is everywhere the same. But such a homogeneous temperature can be obtained only after a thermal equilibration at a certain degree of undercooling, and the material is not permitted to start crystallization within the time span, which is needed for this equilibration. At the onset of every solidification process the molten material is still at a temperature above the melting point. But this means that crystallization starts in reality always at some boundary, where the cooling process sets in. A particularly drastic process is initiated by a quench of the wall of the vessel, in which the melt is contained. But every quench takes some time. Even if a thin metal wall of one to two millimeters thickness is quenched on its outside with the aid of a streaming heat transfer fluid, it can take some seconds until its inner surface has reached the desired constant temperature. The present section is devoted to all kinds of problems arising around these queries.

1.3.4.1   Fast Crystallizing Polymers

The propagation of the crystallization in HDPE, starting at a quenched wall, has been measured by Ewa Ratajski [43]. For the purpose two versions of an apparatus were developed. In both cases the polymer was inserted as a solid cylindrical piece of a diameter of 20 mm and a height of 10 mm. With one apparatus the cylindrical piece was cut into two pieces under a certain angle with the axis. Before the obtained two pieces were joined again, a strip of black paper was interposed. The sample, as prepared in this way, was shoved into a tube of glass or aramide. This tube could be heated with the aid of a stream of hot air and indirectly by heat conduction from metal tubes situated on both ends. On one side the glass tube was closed by a metal plate, which could be quenched with the aid of a heat transfer fluid. On the other side there was a glass plate, through which the sample could be inspected. The whole arrangement was heated to a temperature, where the polymer sample melted. After equilibration the metal plate was quenched to a previously chosen temperature and the hot air was adjusted to a temperature between the original temperature and the temperature of the heat transfer fluid. As a consequence crystallization started at the quenched wall and propagated in axial direction into the sample. On the black strip this propagation could be followed because of its inclined position with the aid of a cathetometer. An inspection from aside is impossible because of the strong temperature gradients in the sample, by which the light beam is deflected into the direction of the lower temperature, an effect which causes an overestimate of the thickness of the crystallized zone. In the second version of the apparatus an inspection from aside was permitted. But a microscale printed on a strip of white paper was inserted into
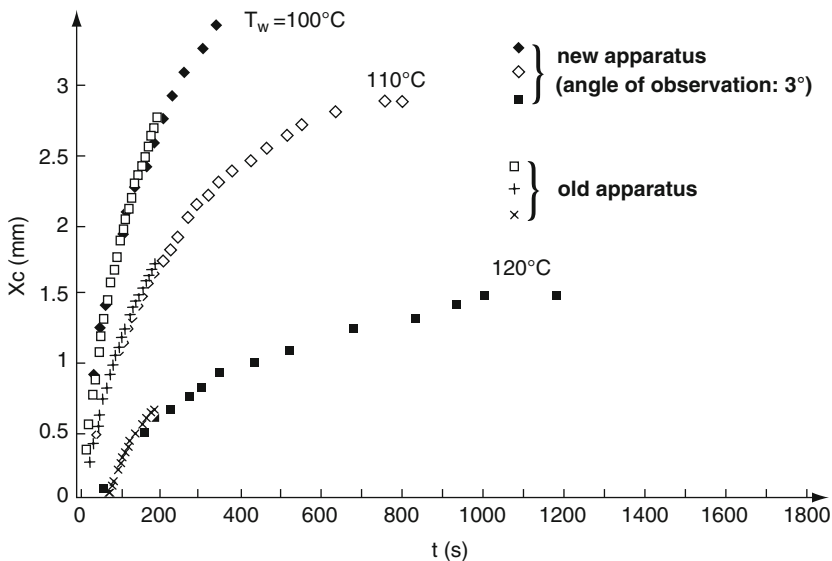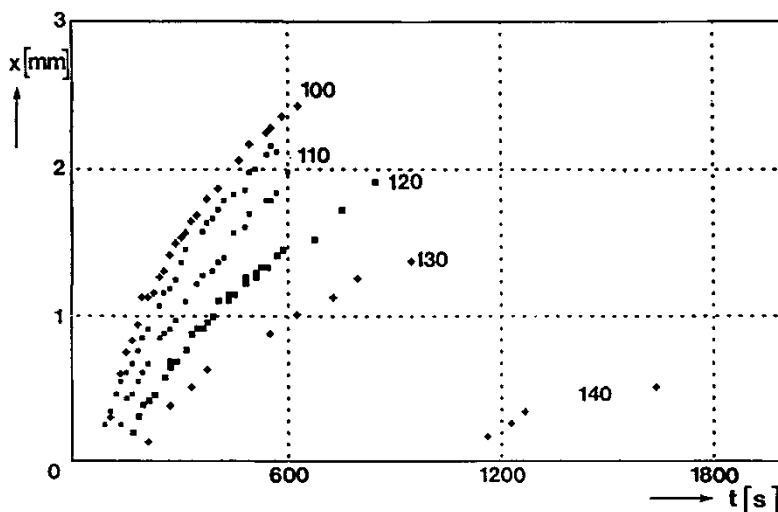
Fig. 1.13 Thickness of the crystallized layers as functions of time for a series of temperatures of the quenched wall for a sample of HDPE. Initial homogeneous melt temperature $T_i = 170°C$, wall temperatures 120, 110, 100°C *counter-clockwise*, according to E. Ratajski [43]. *Stars, diamonds and closed squares* were obtained with the newer apparatus, *open squares* and two types of crosses are from to the elder apparatus

the heart of the sample in axial direction or at an angle of 30° with the axis (for a better illumination only).

Results of measurements, which were obtained by E. Ratajski for a sample of HDPE, are reproduced in Fig. 1.13. With HDPE the transition from the transparent melt to the opaque solid is quite sharp. Nevertheless, this transition occurs in a diffuse crystallization zone, which is relatively narrow for HDPE. The contrast with a real crystallization front will be discussed below.

It turns out that the agreement between the elder and the newer measurements is excellent (see the caption to the figure). One notices that the curves do not go through the origin. However, at the lowest applied wall temperature of 100°C it becomes difficult to recognize this fact. The shape of this curve becomes quite similar to curves, which are obtained with the classical square root law (see below). In an early paper Berger and Schneider [44] have shown that one can indeed expect curves of a shape similar to the curve obtained with the square root law. Only, these curves are shifted down parallel to the ordinate axis. The higher the wall temperature the larger the necessary shift. In this way they cut the time axis at finite values indicating the room for transcrystallization.

If a polymer is investigated, which shows a much lower crystallization speed like iPP, one obtains curves, for which the distances in time between the origin of the graph and the apparent intersections with the time axis are larger. Of course, for the purpose the said curves, as drawn through the experimental points, have to be

Fig. 1.14 Thickness of the crystallized layers as functions of time for various temperatures of the quenched wall for an industrial PP. Initial homogeneous temperature of the melt $T_i = 200°C$, wall temperatures 140, 130. 120, 110, 100°C *counter-clockwise*, according to E. Ratajski [43]

continued down to the abscissa. For instance, this effect is characteristic for an industrial PP, for which Fig. 1.14 is prepared. But for such a polymer also the transition from the clear melt to the solid is more gentle. The crystallization zone is broader and more diffuse and cannot be determined as accurately as with HDPE. On the other hand one can clearly see that at short times there must be a supplementation for the necessary connection with the origin. In fact, the curves have to start necessarily with a finite slope at time zero (By the way, this is also the crux with the square root law, which starts with an infinite slope. No real process can start in this way. For a proper discussion see below).

In fact, if the temperature of the quenched wall is not too low, and the said distance to the origin is still large enough, one finds the so-called "transcrystallization" within the corresponding time span. This term has been introduced by Wunderlich [23] some time ago. This name has to do with the fact that with a very thin sample this type of crystallization propagates without hindrance from one to the other surface of the sample, if a proper, not too low temperature is chosen. In our case this propagation is hindered after some time by the diffuse crystallization in the bulk of the sample.

The transcrystallization has its origin at nuclei located in the wall surface, whereas the diffuse crystallization is initiated by nuclei located in the melt itself. If the influence of the released latent heat is to be taken into account, a correct theoretical description of this situation can be carried out only with the aid of Schneider's rate equations [26] and the kinetic data presented in Sect. 1.1. Ratajski and Eder [43] assumed that the influence of the latent heat is not too strong. So, the time dependent spatial temperature distribution (error function solution) was used
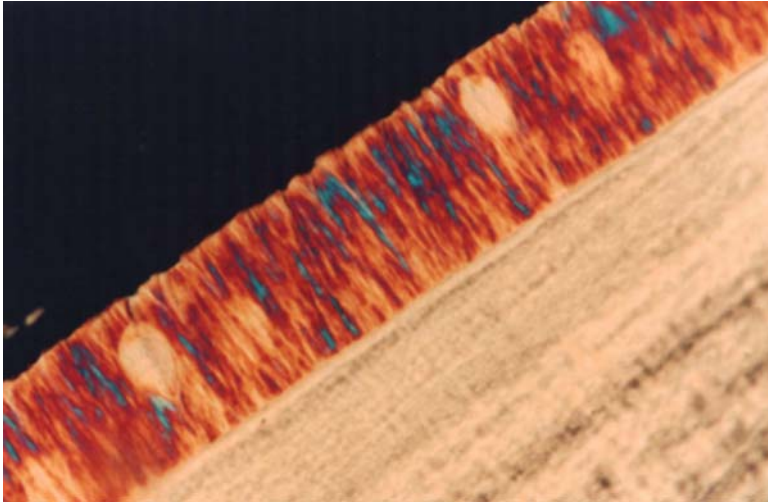
Fig. 1.15 Undisturbed transcrystallization for an industrial PP at an initial temperature in the bulk of 200°C, a quenched wall temperature of 110°C and a contact time of 49 s, if the β-modification is initiated at the wall [43]

for an amorphous fluid and the crystallization kinetics were engrafted on this distribution by local integration over the time. The result was quite realistic. Some justification will be tried in the next section. However, for a complete description, including the upcoming hindrance by the crystallization in the bulk, only the complete theory for samples of restricted size will be helpful. A later section will be devoted to this difficult subject.

As an illustration a photograph is taken over, on which the effect of transcrystallization is shown for an industrial PP. In this case the wall was rubbed in with Cinquasia Gold as an agent for β-nucleation. As a consequence of this preparation of the wall the transcrystalline layer contains only the β-modification. Such a layer grows faster than a layer of the α-modification and gives a more pronounced effect. By the way, in Wu's calculations, aiming at a presentation of the heat transfer effect in differential scanning calorimetry, any influence of transcrystallization was disregarded. However, for the lower peak temperatures, which are reached with higher cooling rates, this simplification cannot be of a larger thermal influence. In fact, those transcrystallized layers could be observed in cross-sections taken from samples, which were removed from the pan of the DSC-apparatus. The higher the cooling speed was the thinner were the transcrystallized layers [22].

Interestingly, within the transcrystallized zone one finds some enclosed spherulites of the α-modification. Apparently, these spherulites were nucleated at temperatures higher than the temperature of the quenched wall, where only a few α-nuclei were present (see Fig. 1.1) (In fact, the melt itself was not nucleated for the β-modification). During the growth of the said α-spherulites the crystallization front of the β-modification arrived from the wall. Nuclei of the α-type of a larger

number, as characteristic for the lowered temperature, were certainly covered by the front growth, before they could reach a noticeable size. There are still two remarks to be made: The birefringence of the β-crystals is much higher than that of the α-crystals, because of epitaxial growth of the latter crystals. This was pointed out by Turner-Jones et al. [45]. This fact may also be the reason for the slower growth.

The enclosed α-spherulites have the shape of pears. One can see that their growth was hampered by the β-growth, particularly on the apex turned towards the wall. On the tail there was a running match, which was finally won by the faster β-growth. These phenomena were discussed first by Lovinger et al. [46].

1.3.4.2   Theory of the Front Growth

The theory of front growth is quite instructive, even if front growth is always restricted with polymers to a short time span, as the previous section has demonstrated. In fact, the zone moves faster comparable with a well performed relay race, where with every handling over of the baton one arm length (spherulite radius) is won. The classical theory for the front growth yields the famous square root law. As a first step one needs the heat balance at the moving boundary. For the progress of crystallization starting at a cold wall one has:

$$\lambda_c \left(\frac{\partial T}{\partial x} \right)_c = \rho\, h\, \frac{dx_c}{dt} + \lambda_l \left(\frac{\partial T}{\partial x} \right)_l. \tag{1.68}$$

In this equation subscripts stand for liquid ("l") and crystalline ("c"). For the heat conductivities λ is used, h is the latent heat, taken positive for the crystallization, ρ is the density, averaged over the two phases, x is the distance from the wall, T is the temperature and t is the time. The term on the left side gives the amount of heat removed by conduction from the moving boundary through the solid, the first term on the right gives the latent heat accompanied with the speed of the moving boundary, and the second term on the right gives the amount of heat conducted into the boundary from the still hotter melt. This equation must always be fulfilled.

However, Neumann [47] assumed that the temperature at the boundary is constant and equal to the temperature T_m at the equilibrium thermodynamic melting point. In this way it was easy to fit the two well-known similarity solutions of the equation of heat conduction.

$$T_w + A\, \mathrm{erf} \left(\frac{x_c}{2\sqrt{a_c t}} \right) = T_\infty + B\, \mathrm{erf\, c} \left(\frac{x_c}{2\sqrt{a_l t}} \right) = \mathrm{const.} = T_m \tag{1.69}$$

In this equation A and B are still undetermined constants, and a_l and a_c are heat diffusivities of melt and solid. Equation (1.69) consists of two equations. The

function erfc(u) is the complementary error function $(1-\mathrm{erf}(u))$. Because (1.69) must be valid for all values of time, x_c must obey the following equation:

$$x_c(t) = 2\,\kappa\sqrt{a_c\,t}. \tag{1.70}$$

As (1.69) and (1.70) are three equations for the three unknown factors A, B and κ, one can now calculate the values of these factors. Of particular interest is factor κ showing up in (1.70). However, the analytical solution is quite complicated [47] and will not be reproduced here. The only important fact is that κ decreases with increasing latent heat. The more heat is released in the boundary, the lower is the speed, with which the boundary can move.

As already mentioned, this square root law cannot be valid for short times. There is no real process, which can start with infinite speed. As a consequence, one has to look for a better solution. In fact, the condition of a constant temperature T_m at the moving boundary means that crystallization must occur without delay, when this temperature is reached during the cooling process. In reality, however, one has always some degree of undercooling, before the process can start with finite speed.

In the modified model, as developed by Eder and Janeschitz-Kriegl [48] (see also [36]), the temperature T_c at the moving boundary is no longer invariant. It becomes part of the solution. The speed of the movement of the boundary is determined by this temperature. The assumption is made that this speed is equal to the growth speed of spherulites at that temperature. Remarkably, at T_m this speed is equal to zero. As the growth speed of spherulites can be determined experimentally (see Fig. 1.2), also dx_c/dt can be considered as a known function of T. Eder calculated the temperature T_c at the boundary for a sandwich confined between two parallel plates. Before the experiment is started, both plates are at T_i above the equilibrium melting point. At time $t = 0$ one of the plates is quenched to temperature T_w below the melting point. No calculations are known for the semiinfinite space. However, at low Fourier numbers $Fo = ta_l/D^2$, where D is the thickness of the slab, there will be no noticeable difference between the result for the slab and for the semiinfinite space. An iterative numerical procedure was necessary, because of the fact that for every chosen T_c the influence of the corresponding dx_c/dt had to be checked, until (1.68) was satisfied.

The following data where used for the calculation: $T_i = 245°C$, $T_w = 90°C$, $T_m = 160°C$, $T_g = 60°C$, $a_l/a_c = 0.54$, $\lambda_l/\lambda_c = 0.60$ and $D = 1$ mm. A parabolic temperature dependence of the growth speed as a function of temperature was assumed, which went through zero at T_m and at the glass transition temperature T_g. At its maximum, halfway between T_g and T_m, a maximum growth speed of 5.2 mm s^{-1} was assumed. Later it was realized that this maximum growth speed was chosen much too high. For the fastest crystallizing polymers, namely HDPE or polyketones (see Table 1.1) this maximum growth speed was found to be at least a decade lower. However, the calculations keep their value because not only the speed of the layer propagation but also the development of the diffuse crystallization, which finally hampers the propagation of the growth front, obeys the same temperature dependence, which has been exaggerated for the said calculation.
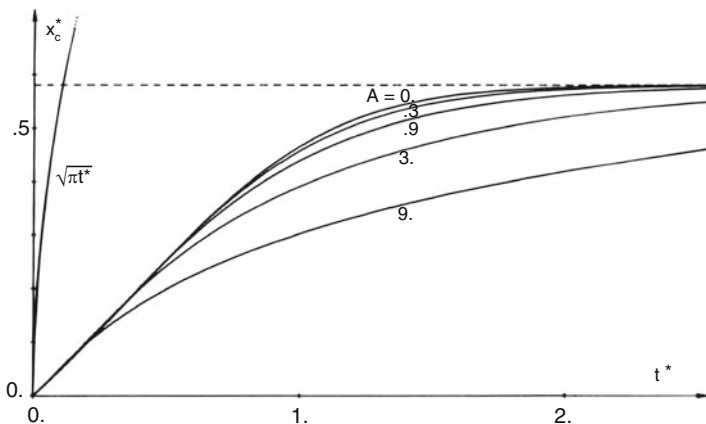
Fig. 1.16 Reduced distance x_c^* of the crystallization front from the quenched wall against the Fourier number t^* for various values of the Stefan number Λ for a slab of finite thickness according to [48], courtesy of Springer

Dimensionless parameters have been used for the presentation of the results, namely $x^* = x/D$, $t^* (= Fo) = ta_l/D^2$, $\Lambda (= St) = h/c_l(T_i - T_w)$ and $\Theta_c = (T_c - T_w)/(T_i - T_w)$. From Fig. 1.16 one learns that all values of x^* *start with a linear part at low values of the Fourier number* t^*. At large Fourier numbers the value of x^* is approached, which holds for the stationary state, as obtained between the hot and the cold walls of constant temperatures. The Stefan number Λ is of great influence only at high values. With polymers one can assume that the Stefan number is always of the order of one. Also the result of the square root law is indicated in Fig. 1.16 by the not very accurate course of $(at)^{1/2}$. This law, which is drawn up for the semiinfinite space, certainly holds as long as x_c^* remains small compared with unity. At this point it must be emphasized, however, that with the use of a realistic growth speed of only one tenth (see above) the discrepancy with $(at)^{1/2}$ will be many times larger.

In Fig. 1.17 the reduced temperature Θ_c, as obtained at the moving boundary, is shown as a function of the Fourier number t^*. For relevant Stefan numbers Λ this temperature remains close to the wall temperature for small values of the Fourier number. According to the classical theory Θ_c should be constant and equal to Θ_m. The results are according to [48].

In conclusion one can say that at short contact times, where the diffuse crystallization does not yet hinder the front growth, the speed of this front growth is determined by the growth speed of spherulites at the temperature of the quenched wall. The prerequisite is that the average distance between nuclei on the surface of the wall is much smaller than the average distance between the nuclei in the melt. In fact, with a dense population of nuclei on the wall the spherical growth fronts, which are formed in the beginning around each nucleus, quickly unite to a flat growth front, which moves into the melt. This fact will be used for the determination of growth speeds in a later section of this monograph.
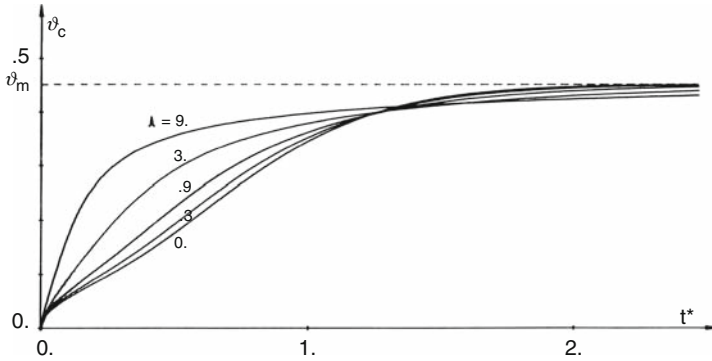
Fig. 1.17 Reduced temperature Θ_c at the crystallization front against the Fourier number t^* for various Stefan numbers Λ. According to the classical treatment for all Fourier numbers Θ_c is at the constant value of Θ_m, Courtesy of Springer

1.3.4.3 Correctly Quenching a Polymer at a Metal Wall [49]

So far it was always assumed in Sect. 1.3.4 that a quench of the wall could occur fast enough, so that the wall reached the desired temperature within a time span short compared with the characteristic time of the crystallization process at that temperature. However, for fast crystallizing polymers this is a questionable assumption. In coping with this difficulty the hot polymer sample was suddenly brought into contact with a preheated metal wall of established temperature. This method was used in some critical experiments (see [7]). In this way the temperature dependence of growth speeds could be determined by an optical method, which will be described in a later section (Light scattering arising at the surface). However, with extremely fast crystallizing polymers like HDPE an improvement of this method appeared necessary nevertheless for temperatures below 90°C. One has to look at Fig. 2.15, as given in Sect. 2.1.2, for the growth speeds of spherulites. In this figure a kink is found at 90°C, where the full squares (for HDPE) abruptly fall off with further decreasing temperature. But such an abrupt deviation from a curve, which should be smooth, cannot be explained easily. The suspicion arose that there could be a heat transfer problem (reheating by latent heat).

For an elucidation of this problem a machine was used, which originally was designed as a dilatometer. This dilatometer should permit an extremely fast quench of a thin slab of the polymer, so that a further decrease of the volume could be assigned to the crystallization kinetics. However, with preliminary temperature measurements in one of the metal walls we learnt that our goal could not be reached along this path. We called our machine a negative baking oven. Not the cold dough was pushed into the hot oven, but a thin layer of the hot polymer sample, as preheated on an aluminum foil in a special oven, was quickly shoved between two relatively cold parallel metal plates and sandwiched between these plates at time zero. The temperature at the newly formed contact surfaces between polymer and metal wall obeyed the following well-known equation:

Table 1.3 Physical Properties of relevant materials. For polymers see [54], for metals see [55]

Material	$\lambda(\text{Wm}^{-1}\text{K}^{-1})$	$\rho(\text{kg m}^{-3})$	$c_p(\text{J kg}^{-1}\text{K}^{-1})$
Polyethylene	0.17	770	2,100
Steel	50	7,900	500
Copper	390	8,900	390

$$\frac{T_{0,\text{melt}} - T_{\text{interface}}}{T_{\text{interface}} - T_{0,\text{wall}}} = \frac{\sqrt{(\rho \cdot c \cdot \lambda)_{\text{wall}}}}{\sqrt{(\rho \cdot c \cdot \lambda)_{\text{melt}}}} \qquad (1.71)$$

In this equation ρ, c and λ stand for density, specific heat capacity and heat conductivity. The subscripts indicate the respective structure elements. As in particular density and heat conductivity of the metal are much larger than those of the polymer, only a slight increase of $T_{\text{interface}}$ above $T_{0,\text{wall}}$ was expected. For convenience, the relevant data for polyethylene, steel and copper are given in Table 1.3.

For the combination of HDPE and steel one obtains a temperature increase above the original wall temperature of 3.9 K, if the following temperatures are chosen for the materials in their state before the contact. For the wall of the machine: 40.5°C (313.7 K), for the original temperature of the polymer: 150°C (423.2 K).

However, for a sample thickness of 1.7 mm a quite curious course of the temperature was measured in one of the metal walls at a distance as close as possible to the contact surface. This course is shown in Fig. 1.18.

The whole procedure was repeated three times. A quite good reproducibility was obtained. During about three seconds the temperature close to the contact surface rose by almost ten degrees. As the temperature profile in the wall must show a continuous decrease from the contact surface to the outer surface, one can judge that the temperature at the contact surface arose by more than ten degrees. If a thinner polymer sample was used, the temperature rise was a little lower and the return to the temperature of the cooling water was a little earlier. If a measurement would be possible in the contact surface itself, one would find that in this surface the said temperature difference would start not at 0°C but at 3.9°C. This was confirmed by a numerical simulation. The wish-dream would be that the temperature difference in the contact surface would stay at those 3.9°C instead of going up and down in an interval of ten degrees. But ten degrees is quite a lot for such a fast crystallizing polymer as HDPE. This fact becomes obvious also from a look at Fig. 1.13.

Interestingly enough, it is possible to achieve such a constant surface temperature, but not with a water cooled relatively thin steel wall [49]. As one of the authors (G.E.) has observed, the contact between two semiinfinite media is instructive in this respect. If the x-axis starts at the plane of the contact surface and both media are infinitely extended, one has the well-known solution of the equation of heat conduction in terms of the error function. With a constant interface temperature $T_{\text{interface}}$ such a solution reads for the metal on the positive side:

$$T(x,t) = T_{\text{interface}} - (T_{\text{interface}} - T_{0,\text{wall}}) \; \text{erf}\left(\frac{x}{2\sqrt{a_{\text{wall}}t}}\right) \qquad (1.72)$$
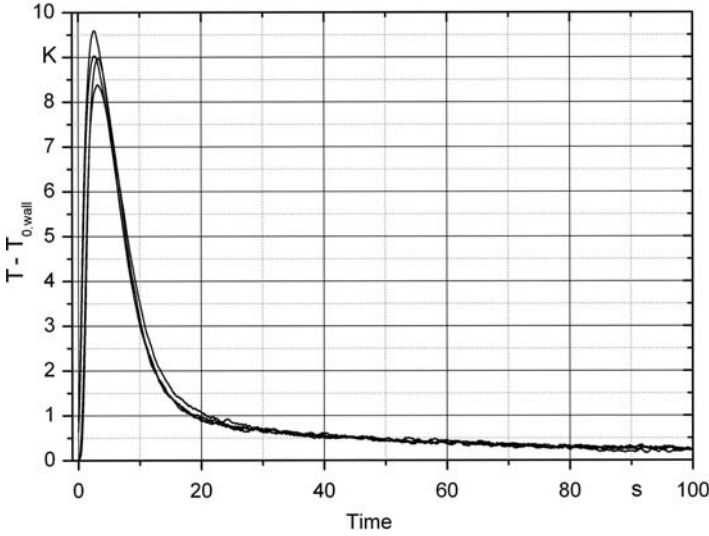
Fig. 1.18 Water cooled steel wall of 2 mm against sample of HDPE of 1.7 mm. Course of temperature versus time at a distance of about 0.4 mm from the contact surface. Original temperatures of wall and polymer were: 40.5°C and 150°C [49]. Courtesy of Hanser-Verlag

For the polymer on the negative side one has under this condition:

$$T(x,t) = T_{\text{interface}} + (T_{0,\text{melt}} - T_{\text{interface}}) \operatorname{erf}\left(\frac{-x}{2\sqrt{a_{\text{melt}}t}}\right) \tag{1.73}$$

If the derivatives with respect to x are formed of both equations for $x = 0$ and multiplied by the corresponding values of the heat conductivities, one obtains the heat flows at $x = 0$. These heat flows must be equal. In this way one obtains (1.71). As the time dependent terms cancel on both sides, the correctness of the assumption of a constant interface temperature, as calculated by (1.71), is proved for semiinfinite media. Admittedly. however, this proof only holds, if no crystallization occurs. The latent heat evolved would interfere with the chosen solution.

There is also another point: None of the media extends to infinity. As a consequence the condition $T_{\text{interface}} = \text{const.}$ only holds until the cooling effect (in the melt) reaches the midplane of the sample slab or the warming effect (in the wall) reaches the outer surfaces of the confinement. The events happening at such a moment will be discussed below.

For us it is of importance that one can imagine also a situation, where with finite distances to outer surfaces the constant contact temperature can be retained – at least, if no crystallization occurs. For the purpose the following train of thoughts is followed. A periodic sandwich construction, containing polymer and metal slabs alternatively, is envisaged. The corresponding values for the thickness of the layers must properly be adjusted. In order to keep the heat content in the polymer layer

continuously equal to the heat content in – say – the slab of steel, one must find the right proportion. This proportion is given by:

$$D_{\text{metal}} = D_{\text{polym}} \sqrt{\frac{a_{\text{metal}}}{a_{\text{polym}}}}. \tag{1.74}$$

In this way one obtains the well-known periodic solutions for the cooling of a slab (of the polymer) or the heating of a slab (of the metal) at constant equal surface temperatures (see apposite text books). If one now imagines only a single polymer layer enclosed between two metal walls, one must assume that these walls are thermally insulated at their outside (with zero temperature gradient) and possess each one half of the thickness calculated with (1.74).With a thickness of the polymer layer of 1.7 mm one needs a thickness of 9.33 mm for two confining steel walls, which are insulated at their outer surfaces.

The next question is: What happens if the wall thickness is inadequate, in particular, if it is too small, and if cooling occurs by streaming water at the outside. There is a well-known equation for the penetration depth, if a temperature change occurs at the surface. This penetration depth means the depth, where the said change at the surface is felt for the first time. One has:

$$x_{\text{pen}}(t) = \sqrt{\pi a_{\text{wall}} t} \tag{1.75}$$

If the wall thickness is 2 mm, as in our case, the time, at which the penetration depth reaches this value, is 0.1 s. Looking at Fig. 1.18 one observes that the temperature maximum is reached at a much later time. With (1.72) one obtains for the difference $(T(x,t) - T_{0,\text{wall}})$ at the point (2 mm, 0.1 s) a value of 0.8°C. If, however, at this distance of 2 mm there is no discontinuity in the metal wall, it makes sense to look at the differential quotient of (1.72) for the point (2 mm, 0.1 s). After a multiplication of this differential coefficient by the heat conductivity of steel one obtains a heat flux of 44.800 Wm^{-2}. This should be the heat, which would be taken up per unit of time by a steel mantle much thicker than 2 mm. For a comparison the heat flux is estimated, which can be taken up by a fast stream of water at that distance of 2 mm. A heat transfer coefficient of 3.000 Wm^{-2}K has been reported [50]. With $\Delta T = 0.8$ K one obtains with this heat transfer coefficient only a heat flux of 2.400 Wm^{-2}. But this means that with this configuration most of the heat, which can be conducted through a steel wall of a larger thickness, can no longer be drained off. But this means that there must be a temperature rise in the wall, as shown in Fig. 1.18. Actually, such a temperature rise can be found in a numerical simulation, as will be shown in the next paragraph. Such a numerical simulation will be unavoidable, if latent heat is evolved during a crystallization process.

The just described situation has been simulated for the initial temperatures for wall and polymer melt, which are given above. No latent heat was incorporated in the calculations. The pertinent results are shown in Fig. 1.19 [49]. In this figure the

Fig. 1.19 Simulated courses of temperature in the steel wall for increasing distances from the contact surface (0, 0.23, 0.55, 0.97, 1.48 and 2.00 mm). The initial temperatures of melt and wall were 150°C and 40.5°C [49], conform with Fig. 1.18. No latent heat was taken into account. The curve for the temperature, which holds directly for the contact surface, is included as the *uppermost curve*. It starts at 317.6 K, as calculated according to (1.71), and shows a horizontal initial part, which ends at about 0.1 s. For a discussion see the text. Courtesy of Hanser-Verlag
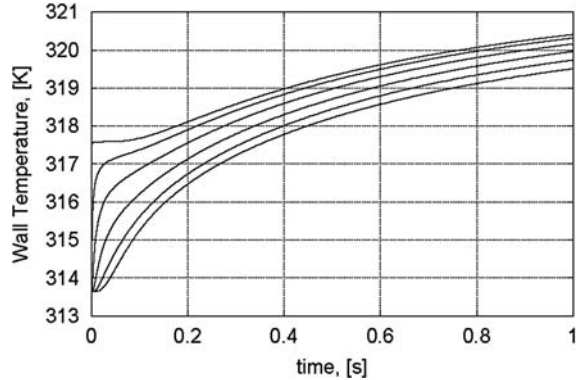
time axis stretches over only one second, in contrast to Fig. 1.18, where the time axis extends over 100 s. As a consequence the curves look much flatter.

First of all it must be mentioned that all curves go through a maximum at about two seconds, practically conform with Fig. 1.18. The pertinent figure is omitted here in saving space. The height of this maximum is at about 321 K for the uppermost curves, which corresponds with an increase of 7°C above the initial wall temperature. The bigger height in Fig. 1.18 can be a consequence of latent heat produced in the real sample of HDPE. The extended time scale is chosen in order to show the initial horizontal part of the curve for the temperature in the contact surface. This horizontal part ends at about 0.1 s, in accordance with the simple result deduced from (1.75). At this point a temperature increase above the original wall temperature of 1.5°C is obtained in these calculations. This increase is of the same order as the estimated increase of 0.8°C, as mentioned above. If the thicknesses of the steel wall and the polymer sample are extended from 2 mm and 1.7 mm to infinity, the level of the short horizontal part is retained up to infinite times and the curves for increasing distances from the contact surface, which change for times longer than 0.1 s, snuggle adequately (see the original paper).

An important point, of course, is the influence of the latent heat. As is obvious from the just presented results, a thin walled steel wall can be excluded from a further consideration. If a massive wall is preferred, the discussion remains about the most proper material. A numerical simulation was carried out for steel and for copper. HDPE was chosen as the polymer. A layer thickness of 1.7 mm was chosen as before. The thermal data of this polymer are contained in Table 1.3 of this section. For the calculation it is assumed that this polymer crystallizes quickly at 127°C. The melting point is at about 145°C. But crystallization kinetics are extremely sluggish at temperature close to 145°C. Even at 127°C there is no abrupt
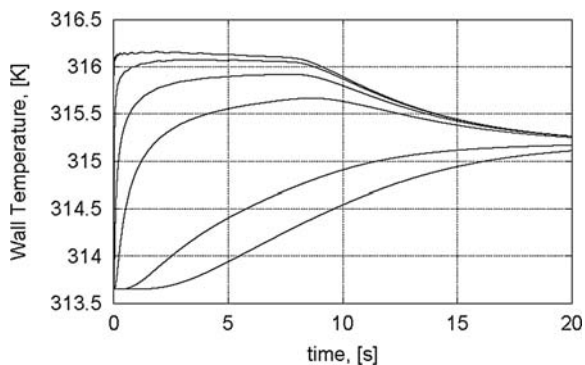
Fig. 1.20 Courses of the temperatures in an externally insulated copper wall of 63.6 mm thickness at increasing distances from the contact surface of 0, 1.0, 4.0, 10.0, 35.0 and 63.6 mm. Initial temperatures for a 1.7 mm layer of HDPE and for the massive copper wall are 150° and 40.5°C

change to infinite speed of crystallization. So, one will still get an overestimate of the influence of crystallization. In Fig. 1.20 the result of the pertinent calculation is given for a copper plate of 63.6 mm thickness, being insulated at the outer surface.

In absorbing also the latent heat of the HDPE layer of 1.7 mm the thickness of an externally insulated copper wall must be 63.6 mm, in contrast to steel, where this thickness must be 21.6 mm. For copper the contact temperature according to (1.71) is 315.2 K, in contrast to steel, where this temperature is 317.6 K. From Fig. 1.20 one learns that for copper the crystallization process enhances the contact temperature very quickly to 316.2 K. From the accurate numerical data an increase of 0.95 K is obtained. For a steel wall a corresponding increase by 2.4 K is found, which means that copper is preferable. After about 7.5 s the plateau of Fig. 1.20 falls of. Finally the level of 315.2 K is reached, which holds according to (1.71) in the absence of latent heat. From the calculated course of the crystallization inside the sample of HDPE one learns that at this time of 7.5 s the crystallization is finished in the heart of the sample. However, as close to the surface crystallization can occur only earlier, the interesting processes will happen at times shorter than 7.5 s. So one can use the plateau temperature for the interpretation of data like those for transcrystallization.

Remains only the interpretation of the practical use of these informations. If one assumes that within these 7.5 s the interesting measurements can be done, one asks (1.75), how far the penetration has proceeded in this time. One obtains 18.3 mm. This is short compared with 63.3 mm. But this means that a thickness of 20 mm will be enough and no insulation will be necessary at the outer surface. However, laterally infinitely extended plates are also not operable. At best one can think of cylindrical pieces of a diameter of 20 mm and a length of 20 mm. Such cylinders can be insulated at their mantle to make them behave more like infinite plates. The biggest advantage is that one can insert thermocouples into the body of one of these cylinders. The required holes can be drilled into the body in a direction parallel with the axis, ending at various distances from the contact surface. As the couples have a

lower conductivity than the body, the readings are not influenced by the conduction
through the electrical leads, as is the case, if those couples are inserted into a
cylinder of the low heat conductivity of a polymer. As already mentioned, the
temperature profiles parallel to the axis are always showing a monotonic increase
towards the contact surface. This means that an extrapolation to the surface will not
be difficult and can be realized by a simple computer program, so that one can
check the contact temperature every moment during the measurement. Unfortu-
nately, such measurements have not yet been carried out. As a consequence, the
present Sect. 1.3.4.3 can serve for the moment only as an enrichment of our
insights.

1.4   Crystallization in Confined Spaces

So far this text has ignored or silently accepted the fact that every volume of
a material is necessarily enclosed in a vessel or, at least, confined on some sides
by walls. But walls are not ineffective with respect to the crystallization kinetics. In
general they furnish extra nucleation centers. For instance, it has been assumed in
Sect. 1.3.4.2 without much ado, that the wall can nucleate a growth front, which
moves into the sample. In contrast, with the simulation of the processes occurring in
differential scanning calorimetry (see Sect. 1.3.3.1) any wall effect has been
ignored. So it will be clear to the reader that the corresponding backgrounds still
have to be elucidated and the errors evaluated.

1.4.1   A Derivation of Kolmogoroff's Equation According to G. Eder, Enabling a Generalization

In a fundamental paper [51] G. Eder was able to describe a promising route for this
endeavor. The reader should also consult [22] for a somewhat more elaborate
version. The author started with an equation taken from the theory of point
processes [52]. For an illustration the author presented three point configurations.
These configurations are shown in Fig. 1.21. for two dimensions.
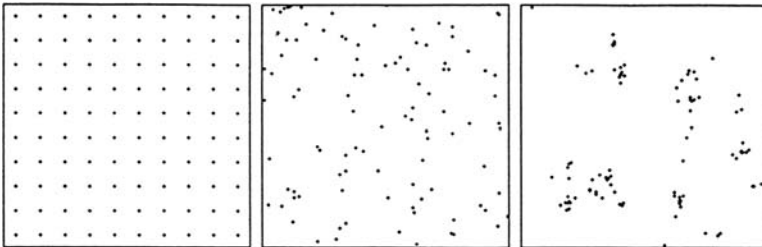
Fig. 1.21 Examples of point configurations on a square: regular, Poissonian, cluster type [51].
Courtesy of Marcel Dekker, Inc

Fig. 1.22 Schematic space-time diagram [51]. The diameters of growing spherulites are given by the stretches on the *x*-axis against time *t*. For an explanation see the text. Courtesy of Marcel Dekker, Inc
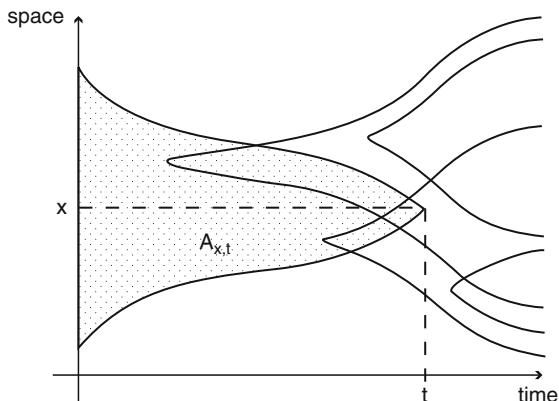
The first configuration shows a regular pattern, the second one is generated with the aid of uniformly distributed random numbers and the third one shows clusters. Admittedly, the third configuration is often found in connection with poorly distributed nucleation agents. For the present purpose, however, the second configuration is preferred. It is connected with the simplest point process, the Poisson process, which is based on the lowest degree of information.

As a first step another picture is shown from the original publication. It is introduced here as Fig. 1.22. This picture explains the underlying train of thoughts.

The figure shows five tapered points. From each of these points two curves extend, which are mirrored with respect to a virtual horizontal line drawn through their point of origin x',t'. Let us first consider one pair of curves, which is completely outside the shaded area. The time t' corresponding to the point of departure is the time, when the special spherulite starts growing at x'. Its diameter, which increases with time, is indicated by the increasing stretch in the *x*-direction between the two curves. In a next step we take point x,t (without accents!). It is maintained that no spherulite can start at this point. This fact can be explained as follows: Two of the spherulites, which started at earlier times, had their starting points within the shaded area. But this means that the growing spherulites cover the point x,t. The reader may observe that at every moment all curves have a slope of equal value accept for the sign. These slopes are equal to $\pm G$, if G is the growth speed of all radii at that time (temperature). In emphasizing that this derivation holds for the general case that temperature changes during the growth process, the curves are not drawn as straight lines. In fact, straight lines would be characteristic for the isothermal case with constant G (G is assumed to be a unique function of temperature, as has been explained earlier in this text). The shaded area $A_{x,t}$ seems to present kind of an inverse growth area. Apparently, a purely geometric description is given. This means that the density change, which is accompanied by the crystallization, is ignored.

But there is still another point: In reality spherulites extend in three dimensions, in contrast to the one dimension shown in the figure. One can still imagine

a presentation in two dimensions. For the purpose, the flat areas between the curves of Fig. 1.22 must be replaced by rotational bodies around the horizontal lines going through the points of departure. Admittedly, three dimensional spherulites cannot be envisaged easily. One has to assume a spherical symmetry in space around the point x,t , where the time axis is replaced by a series of snapshots. Anyway, one can give a mathematical description for this realistic case.

One looks for a set $A_{x,t}$ of points (x',t') in a four-dimensional space containing time as the fourth variable, where $x(= x,y,z)$ is a vector. For all points of this space the distance between x' and x must be

$$|x - x'| < r(t,t') \quad \text{with} \quad r(t,t') = \int_{t'}^{t} G(u) \ du \qquad (1.76)$$

for remaining inside the contour of the mentioned inverse growth area. A point outside this contour cannot give rise to a spherulite covering point x,t.

In other words, the following set must be found:

$$A_{x,t} = \{(x',t')|t' < t \wedge |x - x'| < \int_{t'}^{t} G(u) \ du\}. \qquad (1.76a)$$

In a next question it is asked, how large the probability will be that all points of this set are unoccupied by nuclei, which can grow out into spherulites. If no dependence on the location exists, the expectation value for the occupation of each point (volume element) is:

$$d\Lambda = \alpha(t) \ dx \ dy \ dz \ dt, \qquad (1.77)$$

where $\alpha(t)$ is the homogeneous rate of nucleation per unit volume of the sample. At this point the distribution function of Poisson has to be consulted. This distribution function has the peculiarity that the probability of the occurrence of an unoccupied point can be given, if the volume element dV is occupied in the average by $d\Lambda$. As is well know, the Poisson distribution reads:

$$\Pi(k) = \frac{\langle n \rangle^k}{k!} \exp\left(- \langle n \rangle\right), \qquad (1.78)$$

where $\Pi(k)$ is the probability for k-fold occupation and $\langle n \rangle$ is the average degree of occupation. If one asks for the probability that $k = 0$, only the exponential is left. In fact, one has $\langle n \rangle^0 = 1$ and $0! = 1$. In our case one obtains:

$$\pi(x, t) = \exp\left[-\Lambda\left(A_{x,t}\right)\right], \qquad (1.79)$$

where Λ is the integral over all $d\Lambda$ of (1.77). In fact, a sum in the exponent means a product of all individual probabilities of events, which must occur simultaneously. If no restriction by a wall is within reach, i.e., if $r(t,t')$ is not obstructed in its growth by an extra condition, this integral reads:

$$\Lambda(A_{x,t}) = \frac{4\pi}{3} \int_{-\infty}^{t} ds\, \alpha(s) \left[\int_{s}^{t} du\, G(u) \right]^{3} \tag{1.80}$$

Actually, the subscript x can be omitted because of the fact that the integral does not depend on any location of the volume elements.

If the lower bound of the first integral is chosen as $-\infty$, this means that the whole crystallization process is included, which starts at a temperature well above the melting point, from where the temperature is continuously lowered to a temperature, where the crystallization proper takes place. If (1.79) gives the probability that all points of $A_{x,t}$ are unoccupied, the degree of space covering is given by:

$$\xi_g(x, t) = 1 - \pi(x, t) = 1 - \exp\left[-\Lambda(A_{x,t})\right] \tag{1.81}$$

If $\Lambda(A_{x,t})$ is taken from (1.80) and the subscript x is omitted, one obtains the well-known equation of Kolmogoroff:

$$\xi_g(t) = 1 - \exp\left(-\frac{4\pi}{3} \int_{-\infty}^{t} ds\, \alpha(s) \left[\int_{s}^{t} du\, G(u) \right]^{3} \right) \tag{1.82}$$

For a later discussion it is mentioned that

$$\frac{4\pi}{3} \left[\int_{s}^{t} du\, G(u) \right]^{3}$$

is the volume $v(t,s)$ of a sphere, which grows from any location during a time span between s and t.

1.4.2   *Behavior of Confined Samples*

The question is now, what happens, if one does not look back on hopefully unoccupied sites (volume elements) in a sea of liquid but also on unoccupied sites on the surfaces of walls, which confine the sample. For the purpose an

infinitely extended slab M of constant thickness D was considered by Eder: $M = [-D/2, +D/2] \times R \times R$. Except for the intensity measure in the fluid, as given by (1.77). There is now also an intensity measure at the wall surface $\partial M = \{-D/2, +D/2\} \times R \times R$. One has:

$$d\Lambda_3 = \alpha_3(t) \, dx \, dy \, dz \, dt$$

and

$$d\Lambda_2 = \alpha_2(t) \, dy \, dz \, dt, \tag{1.83}$$

where the subscripts indicate the dimensions (volume and surface). Also for these equations the condition holds that there is no dependence on the location of the volume or surface elements. With $\alpha_3(t)$ one has the nucleation rate per unit volume of the fluid according to (1.34) and (1.35). This means that according to our points of view it is assumed that new nuclei only show up, if the temperature decreases as a function of time. A similar assumption is also made with respect to $\alpha_2(t)$, which is the rate of nucleation per unit surface of the wall.

Instead of (1.81) one has:

$$\begin{aligned}\xi_g(x,t) &= 1 - \exp\left[-\left(\Lambda_2(A_{x,t}) + \Lambda_3(A_{x,t})\right)\right] \\ &= 1 - \exp\left[-\varphi_0(x,t) - \psi_0(x,t)\right].\end{aligned} \tag{1.84}$$

Here the x-coordinate cannot be disregarded. In fact, the x-axis is perpendicular to the wall surfaces. One has:

$$\varphi_0(x,t) = \int_{-\infty}^{t} ds \, \alpha_3(s) \, v(t,s,x)$$

and

$$\psi_0(x,t) = \int_{-\infty}^{t} ds \, \alpha_2(s) \, a(t,s,x). \tag{1.85}$$

The function $v(t,s,x)$ is the volume of a body, which a sphere with its center at x and a radius $r(t,x)$ cuts out of the sample M. This body may be a full sphere or a sphere truncated on one or on both sides by its intersection with one or both walls. The function $a(t,s,x)$ is the area, which a sphere with its center at x and a radius $r(t,x)$ cuts out of the sample surface ∂M. This area can be zero. But it can also consist of one or two disks cut from one surface or from both surfaces. Table 1.4 gives the pertinent classification.

Table 1.4 Classification of the variables (t,x)

Class	Condition
1	$|x| < D/2 - R(t)$
2+	$|D/2 - R(t)| < x < D/2$
2−	$-D/2 < x < -|D/2 - R(t)|$
3	$|x| < R(t) - D/2$

In this table $R(t) = r(t,-\infty)$ is the radius of a sphere, which in principle starts growing at $t' = -\infty$. This means that, again, the assumption is made that the count of the time starts at a temperature well above the melting point. The temperature is then lowered to a value, where the crystallization proper can occur. But this also means that $G(t)$ is not a constant. It increases continuously from zero to some finite value.

The content of Table 1.4 is illustrated by Fig. 1.23.

In this figure the locations of the classes are shown. The distance between the horizontal lines at $x = \pm D/2$ and the curved lines is $R(t)$. This distance does not increase linearly with time for the reason just explained: Continuous cooling is assumed to be started above the melting point. In class 1 one finds complete spheres and zero areas on the walls. For the use in the other classes two auxiliary functions $\tau_+(t,x)$ and $\tau_-(t,x)$ are required. These functions are defined by the following integrals:

$$\int_{\tau_+(t,x)}^{t} du \, G(u) = \frac{D}{2} - x$$

and

$$\int_{\tau_-(t,x)}^{t} du \, G(u) = \frac{D}{2} + x. \tag{1.86}$$

The first function gives the time $s = \tau_+$, at which a spherulite, which is nucleated at $+x$, reaches the upper wall at time t. The second function gives the time $s = \tau_-$, at which a spherulite, which is nucleated at $-x$, reaches the same upper wall at time t. If s is an earlier time than $\tau_+(t,x)$, $v(t,s,x)$ is the volume of a sphere truncated on the upper side and $a(t,s,x)$ is the area of a disk, which is cut from the upper surface. This means that (t,x) is in class 2+. If s is later than $\tau_+(t,x)$, (t,x) is in class 1. However, if s is earlier than $\tau_-(t,x)$, (t,x) is in class 3. As the symmetric case with respect to $x = 0$ is of major interest, class 2 − will not be mentioned any more, even if also the asymmetric case with two different surface nucleation rates is within reach.

For the evaluation of these principles straightforward but cumbersome calculations are required. In the review of 1997 [22] the results of these calculations, which have been carried out by G. Eder, are reproduced. Even, if $G(t)$ and $\alpha(t)$, the latter

Fig. 1.23 Classification of the variables t and x according to [22]. Courtesy of Verlag Chemie – John Wiley
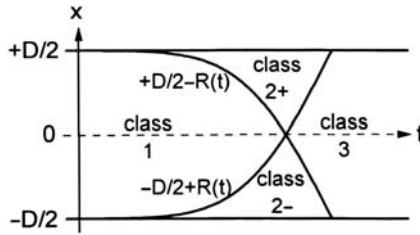
according to (1.34), allow for a description in terms of a changing temperature, the practical effect is zero. In fact, the function $T(t)$ is not known a priori. It is part of the solution of a heat transfer problem.

For the purpose, a system of rate equations according to the ideas of Schneider et al. [26] would be required. Eder managed to derive those equations for the case of confined samples [22]. He arrived at seven rate equations and two extra differential equations with respect to time for τ_+ and τ_-. Four of the rate equations hold for nucleation in the melt and three for nucleation on the wall surfaces. The structures of these equations strongly depend on the classification given in Table 1.4. So, it does not surprise, if the general case of heat transfer has not yet been put into practice. The merit of Wu's treatment [35] of heat transfer in DSC will be discussed below. In this treatment Schneider's original rate equations were used without taking into account the influence of the surface of the pan. First we need a simplified treatment, as given in the next section.

1.4.2.1 Isothermal Case for a Slab of Constant Thickness

For a constant temperature after a sharp quench it is assumed that:

$$\alpha_3(t) = N_V\, \delta_0(t) \quad \text{and} \quad \alpha_2(t) = N_A\, \delta_0(t)$$

together with

$$G = \text{const.} \tag{1.87}$$

In the first pair of equations δ_0 is the Dirac-function concentrated around $t = 0$. At time $t = 0$ a number of N_V nuclei per unit volume comes up suddenly in the bulk and N_A nuclei per unit surface show up suddenly at the surfaces of both walls. Also, the growth speed is constant from the first moment. With respect to the occurrence in the bulk one can say that the validity of the first (1.87) is not only welcome as a simplification. There are also serious physical reasons for this validity, which will be explained in Chap. 2 of this monograph. A sharp quench, however, is a theoretical assumption.

The results of the pertinent calculations were given in dimensionless coordinates

$$t' = 2\frac{Gt}{D} \quad \text{and} \quad x' = 2\frac{x}{D}. \tag{1.88}$$

Two dimensionless parameters were introduced:

$$d_V = \frac{1}{D\sqrt[3]{N_V}} \quad \text{and} \quad d_A = \frac{1}{D\sqrt{N_A}}. \tag{1.89}$$

In Fig. 1.24 the results of Eder's calculations are collected.

Various combinations of the parameters d_V and d_A were used. On the vertical axes of the square shaped diagrams the degree of crystallinity is plotted. On the horizontal axes the reduced distance from the midplane is drawn. On the right sides one finds the surface of the slab. The reduced times are indicated at the contour lines. Small values of both parameters indicate high number densities of nuclei in the bulk and on the walls. Most interesting are the diagrams at the lower left and at the upper right corners. At the lower left one has a combination of a high number density of nuclei in the bulk and of a low number density of nuclei at the surfaces.
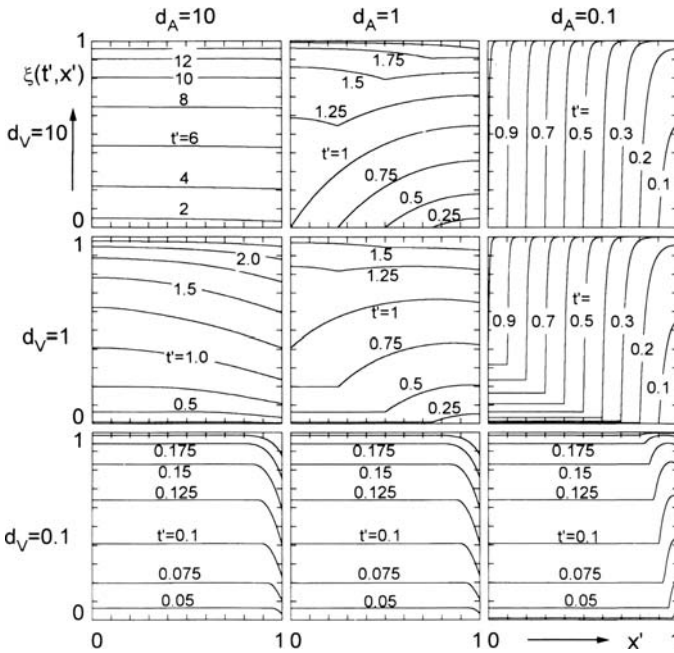
Fig. 1.24 Crystallinity profiles under isothermal conditions for a slab of constant thickness [22]. Results are shown for various combinations of the parameters d_V and d_A. Courtesy of VCH-Wiley

Except for the vicinity of the wall one finds a homogeneous increase of the degree of crystallinity with time. Only close to the wall the crystallinity falls off at short times to one half of the value far from the wall. In fact, if the centers of spherulites are at the wall, only half spheres start growing. Initially, these half spheres cover only half the available space. At the upper right one has an opposite situation: a low number density in the bulk and a high number density at the surfaces. In this case a more or less perfect growth front moves from the surface into the sample. With increasing time the distance from the wall increases, where the crystallinity falls off from one to zero. Nevertheless, one has a dominant effect of transcrystallization. The diagram at the lower right shows the lot of transcrystallization, if there is a high number density of nuclei also in the bulk. Transcrystallization is restricted in this case to a narrow range close to the surface.

1.4.2.2 Significance of the Avrami Index

For an evaluation of the Avrami index one needs the degree of crystallinity averaged over the sample thickness. One has:

$$\langle \xi_g \rangle(t) = \frac{1}{D} \int\limits_{-D/2}^{+D/2} dx \, \xi_g(x,t). \tag{1.90}$$

For the limiting cases with no nuclei at the surfaces ($N_A = 0$) or in the bulk ($N_V = 0$), corresponding Avrami plots are shown in Fig. 1.25.

The local slopes are given as encircled numbers. The second case is most interesting. One finds a continuous transition from an apparent Avrami index of 2 over an index 3 to an index 1. In fact, at extremely low number densities at the surface one starts with disk-like growth (index 2), passes the number densities, where half spheres are formed (index 3), and ends up with front growth (index 1) at very high number densities on the surface. Both cases, see also the upper figure, show that there is a variety of possible Avrami indices, which can be traced back to the fact that the sample is confined. In an unconfined sample index 3 should be expected with spherulitic growth.

However, confinement does not form the only reason for varying Avrami indices. As mentioned already at an earlier occasion, also the insufficient effectiveness of quenches has its influence. One does not exactly know, when crystallization starts. Eder formulated this problem in a simple way [51]. He defined a dimensionless time with the aid of the time of half conversion $t_{1/2}$. This dimensionless time reads:

$$t^* = \frac{t}{t_{1/2}}. \tag{1.91}$$
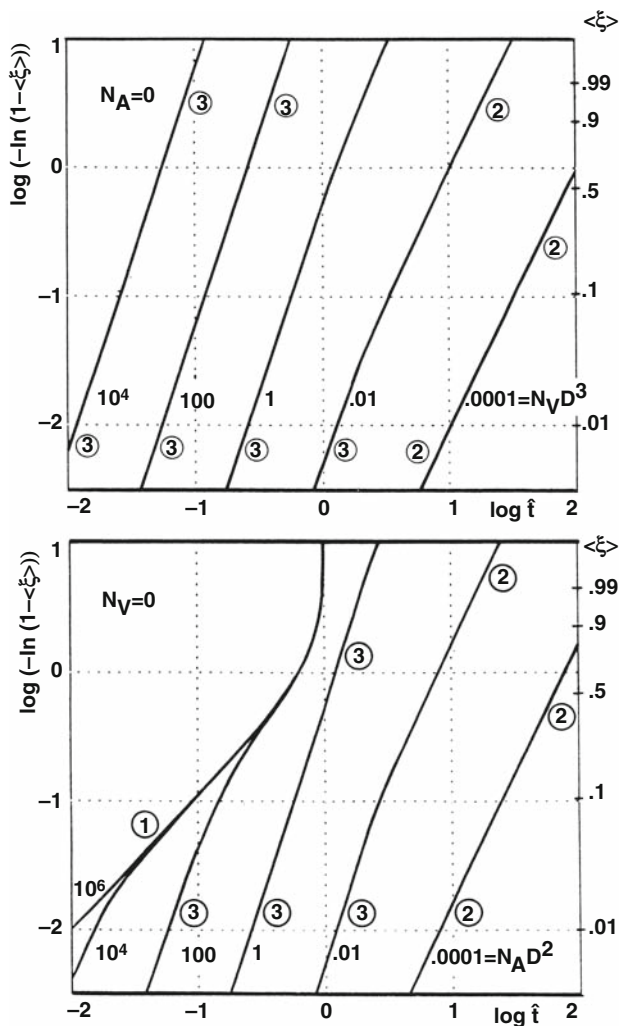
Fig. 1.25 Avrami plots on the basis of the mean degrees of crystallinity for the limiting cases $N_A = 0$ and $N_V = 0$ [51]. The dimensionless parameters $N_V D^3$ and $N_A D^2$, as indicated near the curves from *left to right*, correspond to the previous parameters of (1.89) $d_V = 0.0464, 0.216, 1.0, 4.64, 21.6$ and $d_A = 0.01, 0.1, 1.0, 10, 100$, providing a comparison with Fig. 1.24. Courtesy of Marcel Dekker, Inc

It can easily be shown that the Avrami equation reads with this definition of the time:

$$\xi(t^*) = 1 \; - \; 2^{-(t^*)^n}. \tag{1.92}$$

Now it is assumed that crystallization does not start exactly at $t^* = 0$ but a little later or earlier, because of the uncertainty caused by the badly defined quench. This
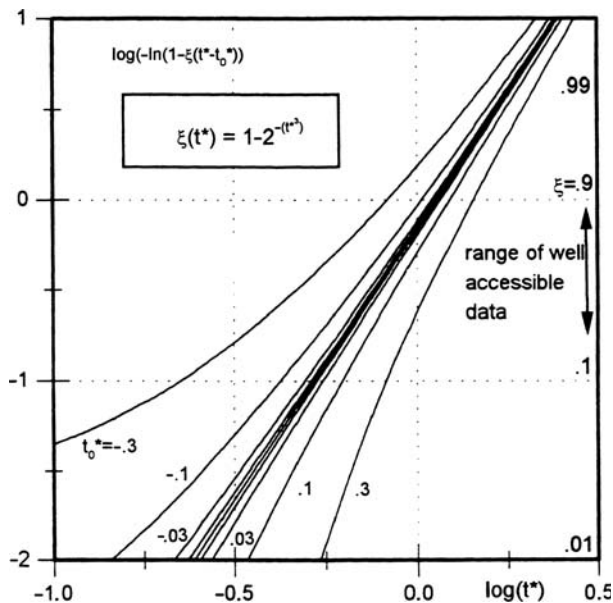
Fig. 1.26 Avrami plots for crystallization processes with different shifted time scales for an expected Avrami index of three [24]. Courtesy of American Soc. Mech. Engng

means that t^* has to be replaced in the above equation by $t^* - t_0^*$ with t_0^* being larger or smaller than zero. In Fig. 1.26 a plot is given of $\log[-\ln(1-\xi(t^* - t_0^*))]$ vs. $\log(t^*)$ for values of t_0^* between -0.3 and $+0.3$, if theoretically an Avrami index of three is expected. On the right ordinate axis also the range of degrees of crystallinity is shown, for which crystallinities can possibly be determined. In this range all curves can easily be approximated by straight lines. With increasing values of t_0^* the slopes of these lines clearly deviate from three. Apparently, ignoring the influence of confinement, one still can obtain deviations from the expected value of the Avrami index.

However, in Chap. 2 of this monograph an extraordinary situation will be described, where the Avrami plot can be applied with success.

In this case crystallization is initiated by the application of pressure at a rather high crystallization temperature, where normal crystallization kinetics are still extremely sluggish. The moment, when the pressure is applied, is well defined. And also, one can use rather large samples, so that the confinement is practically of no influence. These conditions form the basis for a successful dilatometry in a special case.

1.4.2.3   Some Final Remarks

After having recognized the importance of the confinement on the kinetics of crystallization one wonders, whether calculations, as carried out at the time by Wu (see Sect. 1.3.3.1), are still of importance. In fact, Wu used the original rate equations by Schneider et al. (see Sect. 1.2.2), which only hold for unconfined media. With these equation she calculated the progress of crystallization under the influence of heat transfer in the pan of a DSC apparatus. Without any doubt, such a pan forms a serious confinement. In assuaging this situation cross-sections through two samples are shown in Figs. 1.27 and 1.28. These samples come from DSC runs at 5 and 50 $Kmin^{-1}$. These pictures have been published before [22]. But they are extremely instructive. They show that with iPP the zone, where transcrystallization occurs near the surface, becomes smaller with increasing cooling rate. If a picture is taken, which is obtained after extremely slow crystallization at – say – 130°C, one finds only the footprints of transcrystallization. A look on Fig. 1.1 shows that the number density of nuclei, as found in the bulk of iPP, increases tremendously with decreasing crystallization temperature. (The technique applied avoids surface effects, as will be explained in Chap. 2!) If the number density on the surfaces does not increase as much with decreasing temperature, the thickness of the transcrystallized layer must decrease with increasing cooling speed, as the figures actually show. One moves down the diagrams on the right side of Fig. 1.24. Wu's results gain importance with increasing cooling speeds. If the greater
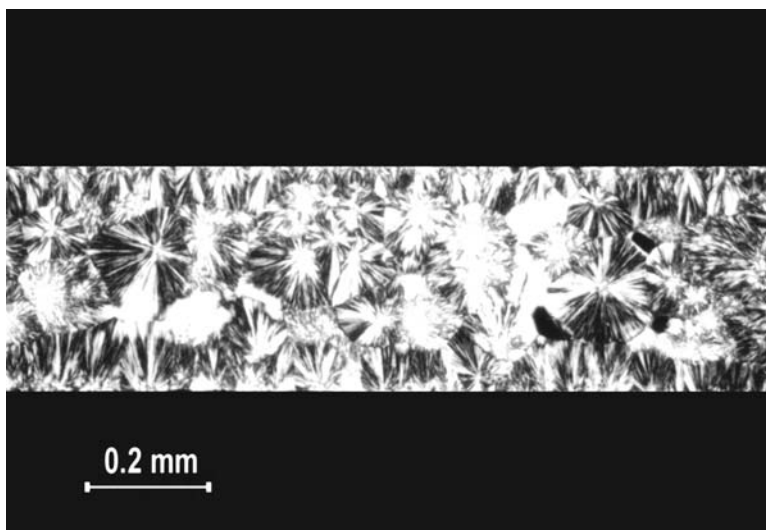
Fig. 1.27 Cross-section from a sample of iPP, as obtained from the DSC pan after a cooling run of 5 $Kmin^{-1}$ [22]. Courtesy of VCH-Wiley
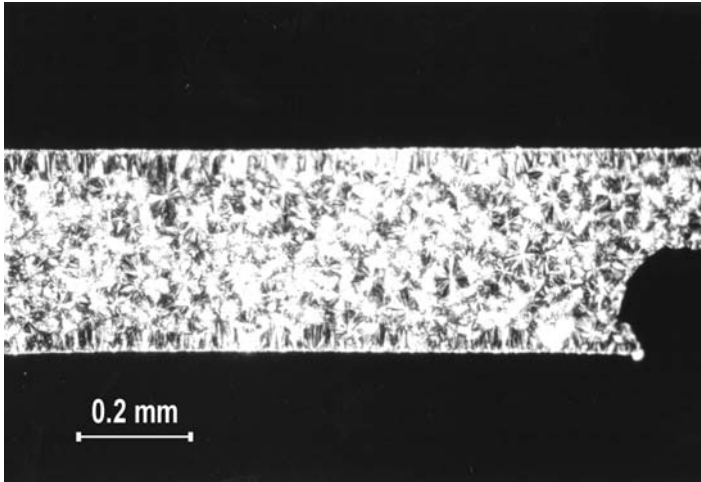
Fig. 1.28 Cross-section from a sample of iPP, as obtained from the DSC pan after a cooling run of 50 Kmin^{-1} [22]. Courtesy of VCH-Wiley

part of the sample crystallized, as if there were no surface influence, one could take the results of Wu´s calculation as significant for the thermal effects envisaged.

Another point of discussion is the unavoidable influence of flow. Actually, there is almost no way to form a material without applying flow. But the influence of flow is particularly effective near the sample surface. And this means that transcrystallization, as occurring at the surface of a quiescent sample, looses its importance. In fact, as already shown in Fig. 1.1, the number density of nuclei increases so much in the sheared melt (more than fast cooling), that the nuclei on the wall loose their importance anyway (cf. Fig. 1.28).

1.5   Influence of Strong Temperature Gradients

So far, it has always been assumed silently in this report that a spherulite, which starts growing at a certain nucleus, grows in all directions with the same speed, which is determined by the local temperature at the spot, where the nucleus is found. However, if in the vicinity of the nucleus the temperature gradient is strong, this concept fails. The spherulite must grow faster in the direction of decreasing temperature and more slowly in the inverse direction of increasing temperature. If a very fine grained structure is obtained, this effect may be unimportant. In such a case the density of nuclei is high, so that the spherulites impinge before they can grow out into objects of noticeable size. However, not only the temperature dependence of the growth speed must be taken into account. An opposite effect is caused by the fact that the number density of nuclei is not constant but increases

with decreasing temperature. In the direction of decreasing temperature one finds an increased speed of growth. At the same time, however, there will be less space for the growth because of the increased density of nuclei. The question is only, which of these two effects will dominate for the final structure in the solidified sample.

   If crystallization is stopped by a final quench, before impingement of the growing spherulites occurs, one can expect that, as a first approximation, spherulites remain spherical with unchanged diameter but with an envelope slightly shifted to the side of lower temperatures. It will be difficult to observe such an effect. However, with a sufficiently strong temperature gradient the envelope will become an ellipsoid and its volume will increase. The present section is devoted at least partly to such an effect.

1.5.1   Growth of Spherulites in Temperature Gradient

G.E.W. Schulze and T.R. Naujeck [53] observed a two-dimensional spherulite in a stationary linear temperature field. In such a field the growth speed can be described by $G(x) = G(0)(1 + px)$, where $G(0)$ is the growth speed at the place of the nucleus ($x = 0$). The envelope of a spherulite, which starts growing at $t = 0$ and $x = 0$, has the following shape:

$$(x - x_m(t))^2 + y^2 = r(t)^2 \tag{1.93}$$

with

$$x_m(t) = R(t)g(pR(t)), \quad r(t) = R(t)f(pR(t)) \quad \text{and} \quad R(t) = G(0)t \tag{1.94}$$

The functions $g(u)$ and $f(u)$ read:

$$g(u) = \frac{\cos h(u) - 1}{u} = \frac{u}{2} + \frac{u^3}{24} + \dots$$

and

$$f(u) = \frac{\sin h(u)}{u} = 1 + \frac{u^2}{6} + \frac{u^4}{120} + \dots \tag{1.95}$$

As already mentioned, the radius of the spherulite does not change to a first approximation because of the behavior of $f(u)$. If $pR(t)$ is very small compared with 1, concentric circles will grow with speed $G(0)$.

   Eder generalized these equations for the case that the temperature field is time dependent. He proposed:

$$G(t,x) = G^*(T(t,x)) = G^*(T(t,0)) \, (1 + p(t)x) \tag{1.96}$$

with

$$p(t) = \frac{\partial \ln G^*}{\partial T}(T(t,0)) \, \frac{\partial T}{\partial x}(t,0). \tag{1.97}$$

If for some reason the local temperature gradients $\partial T/\partial x$ do not change with the overall temperature (see Sect. 1.3.1, constant cooling rate in slab), $p(t)$ becomes practically constant for any location and for the temperature range, where also $\partial \ln G/\partial T$ is constant (tangent to the right side of Fig. 1.2). Only in the third equation (1.94) $R(t) = G(0)t$ has to be replaced by the integral:

$$R(t) = \int_0^t du \, G^*(T(u,0)). \tag{1.98}$$

For the calculation of the degree of crystallinity as a function of time at the position, where the special $\partial T/\partial x$ is envisaged (our x is counted from the place, where the nucleus is located), one can use (1.81). For the purpose one has only to calculate the proper set $A_{x,t}$. This set consists of all nucleation points (x',t') leading to (deformed) spherulites covering the point of observation (x,t). Instead of the first (1.76) one has:

$$(x' - x_m(t',t,x))^2 + (y' - y)^2 \le r(t',t,x)^2, \tag{1.99}$$

where

$$x_m(t',t,x) = x + (1+px)R(t',t)g(pR(t',t))$$

and

$$r(t',t,x) = (1+px)R(t',t)f(pR(t',t)) \tag{1.100}$$

with

$$R(t',t) = \int_{t'}^t du \, G^*(T(u,0)). \tag{1.101}$$

For the validity of (1.100) it is necessary that x is not too large. One should remain in the vicinity of the origin of the nucleus, so that p does not change too much.

So far, everything is o.k., but for a further calculation some additional assumptions seem necessary. The next simplifying assumption was that the rate of nucleation $\alpha(t',x')$ should be independent of x'. For a calculation of the degree of crystallinity this assumption is reasonable. In fact, the crystallinity depends in first

instance on the third power of the growth speed. Only the first power of the number of nuclei is involved. With this simplification the degree of space covering is:

$$\xi_g(t,x) = 1 - \exp\left[- \int_{-\infty}^{t} du\, \alpha(u)\, v(u,t,x)\right]$$

with

$$v(t',t,x) = \frac{4\pi}{3}\, r(t',t,x)^3. \tag{1.102}$$

This radius r can only be bigger than $R(t)$ because of the behavior of function $f(u)$ according to (1.95). A next assumption was that the rate of nucleation should be concentrated around $t = 0$ ($\alpha(t) = N_V \delta_0(t)$). With this assumption one has:

$$\xi_g(t,x) = 1 - \exp\left[- \frac{4\pi}{3}\, N_v\, r(0,t,x)^3\right]. \tag{1.103}$$

Finally this equation is capable of the necessary series developments enabling a determination of the tolerable maximum temperature gradient, at which still no observable deviation is found from the derivations of previous sections. With the use of (1.97) one has (see Eder [22]):

$$\left|\frac{\partial T}{\partial x}\right| \leq 3.09 \frac{\sqrt[3]{N_v}}{\left|\frac{\partial \ln G}{\partial T}\right|} \sqrt{\varepsilon}. \tag{1.104}$$

In this equation ε is the permitted relative error for the temperature gradient. If $\varepsilon = 0.05$, one has for iPP with $(1/G)\partial G/\partial T = 0.2\ \mathrm{K}^{-1}$ values for the tolerable temperature gradient, which still depend on the number density of nuclei. For $N_V = 10^{12}\,\mathrm{m}^{-3}$ and for $N_V = 10^{15}\,\mathrm{m}^{-3}$ (see Fig. 1.1) one obtains $3 \times 10^4\,\mathrm{Km}^{-1}$ and $3 \times 10^5\,\mathrm{Km}^{-1}$, respectively. In practical processing, however, those gradients are often exceeded.

In this connection one should not forget, however, that with respect to the morphology of the end-product the ideas that the rate of nucleation or the number density of nuclei are independent of the x-coordinate, seem incorrect. In fact, with high temperature gradients the number density of nuclei increases tremendously with decreasing temperature, so that the space for growth in that direction is reduced. This effect counterbalances the just described effect. Unfortunately, a pertinent theory does not yet exist. It will also be difficult to carry out a decisive experimental study. But the existence of such a counter-balancing effect can be demonstrated at the other end of the "spectrum."

1.5.2   Counter-Balance by a Gradient in the Number Density of Nuclei

In connection with this problem the reader is reminded of Fig. 1.13. In this figure the progress of the diffuse crystallization zone is followed as a function of time for a high density polyethylene up to a distance of about 3 mm from the quenched wall. In the apparatus, which is used for the purpose, a cylindrical polymer sample of a diameter of 2 cm has been quenched on one end surface to the temperatures indicated in the graph. The temperature of the other end surface was kept at the original temperature of the sample of 170°C. The distance between the end surfaces is 10 mm in this apparatus. A similar experiment was also carried out with a sample of iPP (See Fig. 1.14). In principle, the temperature of the diffuse zone increases with its distance from the quenched wall. But from Fig. 1.2 we know that above 140°C the number density of nuclei is immeasurably small in iPP. (An explanation of this fact will be given in Chap. 2).

In the present Fig. 1.29 a special morphology of a sample of iPP is shown at a distance of 2.6 mm from the other end surface, which was kept at 180°C (after a preheating of the whole machine to 240°C). The quenched surface stayed at 120°C. It took days, before the diffuse crystallization zone reached this distance of 7.4 mm from the quenched wall. The sample as a whole was quenched after that long time to a lower temperature for a fixation of the obtained morphology. As one can see on the figure, an almost sharp growth front was found at the moment of the quench. This growth front was possible because of a lack of nuclei on the side of the

Fig. 1.29 Morphology at the crystallization zone of an iPP, if this zone has proceeded over a considerable distance into the sample. The fine grained structure on the *right* is caused by the final quench. For conclusions see the text. Ewa Ratajski, unpublished

higher temperatures. There was enough space for an undisturbed though slowed down growth. One can see also that at lower crystallization temperatures, which prevailed a little earlier, i.e., on the lee side of the growth front, a lot more nuclei influenced the picture. This pronounced increase of the number density with decreasing temperature is in accord with Fig. 1.1. Looking at this figure we also have asked the legitimate question, how low the number density must be at temperatures above – say – 140°C – in a quiescent melt of iPP. These figures fit together in a convincing way.

Remains now a discussion of the vicinity of the growth front. One does not need much fantasy to imagine the completed shapes of the big outgrowths. One probably would have found big ellipsoids with their focuses near the colder side. One of these focuses can even be sensed. But there is no doubt that the growth speed is higher at the colder side. However, growth is apparently hampered much more at that side by the larger number of nuclei. On the warmer side the growth speed is certainly lower, but this drawback is outweighed by the reduced number of nuclei. These conclusions remain valid even if the faster growing β-crystal-modification is involved, as may be suggested by the bigger birefringence of the outgrows [45]. In this connection also the experiences of Lovinger et al. [46] with enclosures of the other modification should not be overlooked.

References

1. Tribout C, Monasse B, Haudin JM (1996) Experimental study of shear-induced crystallization of an impact polypropylene copolymer. Colloid Polym Sci 274:197–208
2. Janeschitz-Kriegl H, Ratajski E, Stadlbauer M (2003) Flow as an effective promotor of nucleation in polymer melts: a quantitative evaluation. Rheol Acta 42:355–364
3. Stadlbauer M, Janeschitz-Kriegl H, Eder G, Ratajski E (2004) New extensional rheometer for creep flow at high tensile stress, part II. Flow induced nucleation for the crystallization of iPP. J Rheol 48:631–639
4. Marand H, Xu J, Srinivas S (1998) Determination of the equilibrium melting temperature of polymer crystals: linear and non-linear Hoffman-Weeks extrapolation. Macromolecules 31:8219–8229
5. Janeschitz-Kriegl H (1983) Polymer melt rheology and flow birefringence. Springer, Berlin, Heidelberg, New York, pp 181–187, 424
6. Smoluchowsky M (1916) An attempt of a mathematical theory of the kinetics of coagulation in colloidal solutions (in German).
7. Ratajski E, Janeschitz-Kriegl H (1996) How to determine high growth speeds in polymer crystallization. Colloid Polym Sci 274:938–951
8. Gandica A, Magill JH (1972) A universal relationship for the crystallization kinetics of polymeric materials. Polymer 13:595–596
9. Janeschitz-Kriegl H, Eder G, Stadlbauer M, Ratajski E (2005) A thermodynamic frame for the kinetics of polymer crystallization under process conditions. Monatshefte für Chemie (in English) 136:1119–1137
10. Van Krevelen DW (1990) Properties of polymers, 3rd edn. Elsevier, Amsterdam, p 120
11. Woodward AE (1989) Atlas of polymer morphology. Hanser, Munich, Vienna, New York, pp 106–109

12. Prime RB, Wunderlich B, Melillo L (1969) Extended chain crystals V. Thermal analysis and electron microscopy of the melting process in polyethylene. J Polym Sci A-2 7:2091–2097
13. Keller A (1957) Single crystals in polymers: evidence of folded-chain configuration. Philos Mag 2:1171–1175
14. Hoffman JD, Miller RL (1997) Kinetics of crystallization from the melt and chain folding in polyethylene fractions revisited: theory and experiment. Polymer 38:3151–3212
15. Eder G, Janeschitz-Kriegl H, Krobath G (1989) Shear induced crystallization, a relaxation phenomenon in polymer melts. Progr Colloid Polym Sci 80:1–7
16. Azzurri F, Alfonso GC (2005) Lifetime of shear-induced crystal nucleation precursors. Macromolecules 38:1723–1728
17. Blundell DJ, Keller A, Kovacs AJ (1966) A new self-nucleation phenomenon and its application to the growing of polymer crystals from solution. Polym Lett 4:481–486
18. Kolmogoroff AN (1937) On the statistical theory of the crystallization of metals (in Russian). Bull Acad Nauk SSSR Math Ser 1:355–359
19. Avrami M (1939–1941) Kinetics of phase change I, II, III. J Chem Phys 6:1103–1112; 8:212–224; 9:177–184
20. Evans VB (1945) The laws of expanding circles and spheres in relation to the lateral growth rate of surface films and grain size of metals. Trans Faraday Soc 41:365–374
21. Tobin MC (1974–1976) Theory of phase transition with growth site impingement I, II. J Polym Sci Phys Ed 12:399–406; 14:2253–2257
22. Eder G, Janeschitz-Kriegl H (1997) Processing of polymers: crystallization. Mater Sci Technol 18:269–342
23. Wunderlich B (1973) Macromolecular Physics, vol 1. Academic, New York, London, p 282
24. Eder G (1997) The role of heat transfer problems in standard crystallization experiments. ASME Int HTD 351:131–137
25. Nakamura K, Watanabe T, Katayama K, Amano T (1972) Some aspects of non-isothermal crystallization of polymers. I Relationship between crystallization temperature, crystallinity and cooling conditions. J Appl Polym Sci 16:1077–1091
26. Schneider W, Köppl A, Berger J (1988) Non-isothermal crystallization of polymers. Int Polym Proc 2:151–154
27. Van Krevelen DW (1978) Crystallinity of polymers and the means to influence the crystallization process. Chimia 32:279–294
28. Eder G (1998) Crystallization in polymer processing: modelling and experimentation. In: Leif Alkeryd et al. (eds) Progress of Industrial Mathematics at ECMI 98. Teubner, Stuttgart, Leipzig, p 138
29. Janeschitz-Kriegl H, Eder G (1984) A less familiar feature of crystalline layer growth on a cold surface. Plastics Rubber Process Appl 4:145–148
30. Astarita G, Kenny JM (1987) The Stefan and Deborah numbers in polymer crystallization. Chem Eng Commun 53:69–110
31. Janeschitz-Kriegl H, Eder G, Ratajski E (2006) A process classification number for the solidification of crystallizing materials. Int Polym Proc 21:521–526
32. Van Antwerpen F, Van Krevelen DW (1972) Influence of crystallization temperature, molecular weight and additives on the crystallization kinetics of poly(ethylene terephthalate). J Polym Sci Polym Phys Ed 10:2423–2435
33. Pijpers TFJ, Mathot VBF, Goderis B, Scherrenberg RI, Van der Vegte EW (2002) High-speed calorimetry for the study of the kinetics of (de)vitrification, crystallization and melting of macromolecules. Macromolecules 35:3601–3613
34. Janeschitz-Kriegl H, Wippel H, Ch P, Eder G (1993) Polymer crystallization dynamics, as reflected by differential scanning calorimetry. Part I: On the calibration of the apparatus. Colloid Polym Sci 271:1107–1115
35. Wu CH, Eder G, Janeschitz-Kriegl H (1993) Polymer crystallization dynamics, as reflected by differential scanning calorimetry. Part II: Numerical simulations. Colloid Polym Sci 271:1116–1126

36. Eder G, Janeschitz-Kriegl H, Liedauer S (1990) Crystallization processes in quiescent and moving polymer melts under heat transfer conditions. Progr Polym Sci 15:629–714
37. Adamovsky SA, Minakov AA, Schick C (2003) Scanning microcalorimetry at high cooling rates. Thermochim Acta 403:55–63
38. Adamovsky S, Schick C (2004) Ultra-fast isothermal calorimeter using thin film sensors. Thermochim Acta 415:1–7
39. Minakov AA, Mordvintsev DA, Schick C (2004) Melting and reorganization of poly(ethylene terephthalate) on fast heating (1000 K/s). Polymer 45:3755–3763
40. Minakov A, Morikawa J, Hashimoto T, Huth H, Schick C (2006) Temperature distribution in thin-film chip utilized for advanced nanocalorimetry. Meas Sci Technol 17:199–207
41. De Santis F, Adamovsky S, Titomanlio G, Schick C (2006) Scanning nanocalorimetry at high cooling rate of isotactic polypropylene. Macromolecules 39:2562–2567
42. Janeschitz-Kriegl H (1996) The role of transport phenomena in polymer science. J. Macromol Sci Pure Appl Chem A 33:841–858
43. Ratajski Ewa (1993) Doctoral Thesis, Linz University
44. Berger J, Schneider W (1986) A zone model of rate controlled solidification. Plastics Rubber Process Appl 6:127–133
45. Turner-Jones A, Aizlewood JM, Beckett DR (1964) Crystalline forms of isotactic polypropylenes. Makromol Chem 74:134–158
46. Lovinger AJ, Chua JO, Gryte CC (1977) Studies of the α and β forms of isotactic polypropylene by crystallization in a temperature gradient. J Polym Sci Polym Phys Ed 15:641–656
47. Carslaw HS, Jaeger JC (1959) Conduction of heat in solids, 2nd edn. Clarendon, Oxford, p 285
48. Eder G, Janeschitz-Kriegl H (1984) Stefan problem and polymer processing. Polym Bull 11:93–98
49. Janeschitz-Kriegl M, Janeschitz-Kriegl H, Eder G, Forstner R (2006) Heat transfer through metal walls of finite thiskness. Int Polym Proc 21:41–48
50. Dittus FW, Boelter LMK (1930) Heat transfer in automobile radiators of tubular type. Publications on Engineering, Berkley
51. Eder G (1997) Fundamentals of structure formation in crystallizing polymers. In: Koichi Natada, Tatsuki Kitayama, Otto Vogl (eds) Macromolecular design of polymeric materials. Marcel Dekker, Basel, pp 761–782
52. Daley DJ, Vere-Jones D (1988) An introduction to the theory of point processes. Springer, New York
53. Schulze GEW, Naujeck TR (1991) A growing 2D spherulite and calculus of variation. Colloid Polym Sci 269:689–695
54. Bundrup J, Immergut H (1990) Polymer handbook. Wiley, New York
55. Ullmann F (1990) Enzyklopaedie der techn. Elsevier, Chemie

Chapter 2
Kinetics and Structure Formation in Unloaded Quiescent Melts

2.1 Introductory Remarks

It goes without saying that structure formation in a permanently quiescent unloaded melt does almost never occur in practical polymer processing. In fact, flow and pressurization can almost never be avoided. Nevertheless, the present chapter will appear of great importance, as flow or pressure induced crystallization cannot be understood without a profound basic knowledge of the processes occurring in a permanently quiescent melt, which has not been put under pressure. Such a melt must be cooled down in its quiescent state from a temperature well above the equilibrium melting point, where the residues of previous crystallization processes are erased.

2.2 Empirical Techniques

2.2.1 Number Density of Nuclei

The number density of nuclei is of particular interest for the structure formation. This quantity determines the number density of spherulites, which is finally obtained and which determines various properties of the product. In fact, a fine grained structure is preferable in many cases because of the good ductility obtained with such a structure. On the other hand, as has been pointed out in Sect. 1.2.1, the growth speed of the spherulites mainly determines the speed of the solidification process and, as a consequence, the heat transfer problems.

From the early times up to now there has been a discussion, whether the assumption of sporadic nucleation with a temperature dependent rate of nucleation

or just the assumption of a predetermined number density of nuclei as a unique function of temperature will be most appropriate for a description of the solidification process in quiescent polymer melts (see the alternative use of (1.11) or (1.12)). The use of the latter assumption and equation has been advocated by Van Krevelen in an early paper [1] just because of the easier handling. However, fortunately it has turned out meanwhile that there are strong physical reasons for the latter assumption. One can be quite sure that below the melting temperature of the spherulites (see Fig. 1.3) all nuclei are of the athermal type [2,3], which means that they have their specific temperature of activation. As a consequence they become effective immediately, when this temperature is reached during the cooling process. A theoretical discussion will be given below. In the present section just the experimental methods will be described, which lead to the determination of the said number densities as functions of temperature.

Janeschitz-Kriegl, Ratajski and Wippel [3] described a successful method for the determination of the number density of an industrial PP as a function of temperature. For the purpose a cylindrical sample of a diameter of 4 mm was prepared in the solid state. In the heart of this sample a thin hole was drilled from one end down to half the length of the sample. In this hole a thin thermocouple with a diameter of 0.3 mm was placed, so that its junction was at the end of the hole. This sample was wrapped into a metal foil and suspended in a horizontal position in the coil of a wire. The whole was placed into a glass cylinder, which could be closed at both ends. A heating wire was wound around its outer surface. This glass tube had two inlets near its ends and an outlet in the middle. In the beginning there was no fluid in the tube. The sample was heated by radiation to a temperature well above the equilibrium melting point. In this way remnants of previous crystallization were erased. After the moment, when the radiation heater was switched off, a fast stream of a fluid of a temperature much lower than the intended crystallization temperature, was let in through one of the inlets. In this way the sample was cooled much faster than in the case that from the beginning a fluid of the intended temperature would have been admitted. However, at the moment, when the thermocouple in the heart of the sample passed the intended temperature, a fluid of this temperature was introduced through the second inlet. It replaced the colder fluid in a counter-current. In this way the cooling was quite abruptly stopped. The number density of nuclei is assumed to be equal to the number density of spherulites, which is found after the final solidification of the sample. It goes without saying that this solidification has to occur at the temperature, for which the determination of the number of nuclei is intended. A good measure for this density is the number of spherulites sectioned per unit surface of the cross-section, after being raised to the power 3/2. For this procedure part of the cross-section is used, which is obtained close to the heart of the sample, sufficiently remote from the sample surface. The difference in bulk density of the melt and the solidified sample is ignored in this method. In view of the large effects of temperature changes on the number density of nuclei, however, this ignorance has no serious consequences.

Cooling curves, as obtained with this type of experiments, are shown in Fig. 2.1. Average cooling rates are given near the curves. Always a certain undershoot is
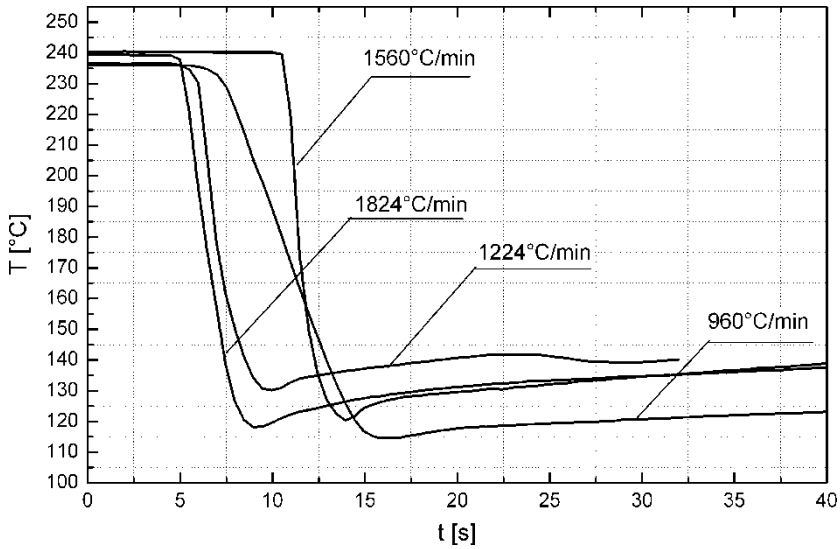
Fig. 2.1 Sample temperatures as functions of time for samples of an industrial PP, according to the described method. Average cooling rates are indicated near the curves [3]. Courtesy of Springer

found for the temperature. For the evaluation the lowest temperature was used. One of the reasons for this choice is that nuclei, which show up at a certain temperature, will quickly be stabilized so that a mild reheating will not change their number. But such a reheating, if it should be of influence, could only reduce the number of nuclei. Also, if cooling is not fast enough, some nuclei will start growing already during the cooling cycle. The rising spherulites will cover some space, where otherwise further nuclei can come up. But this means that, in principle, the said method can give only an underestimate of the number density. The scope of such an underestimate can only increase with decreasing crystallization temperature.

This statement is of particular interest in view of the enormous increase of the measured number density of nuclei, as found with decreasing temperature. This means that, in reality, this increase, which is shown in Fig. 2.2, can only be more pronounced. For the microscope it requires a remarkable selection of magnification optics.

The curve of Fig. 2.2 has been transferred to the left side of Fig. 1.1. As already mentioned, when this latter figure was introduced, a logarithmic scale had to be used for the number density because of its enormous increase with decreasing temperature. For i-PP a range of temperatures from about 110 down to 85°C was covered. Previously, a range of similar scope has never been envisaged.

A similar result was obtained according to Braun et al. [4] with a sample of PB-1, which did not contain a nucleation agent (PB0300). Another sample, which was nucleated (PB0110), showed a larger number density over the whole range of temperatures from about 110 to 50°C. This difference was particularly pronounced at the higher temperatures. This is in accord with the intended influence of a nucleation agent. In Fig. 2.3 the pertinent results are shown.
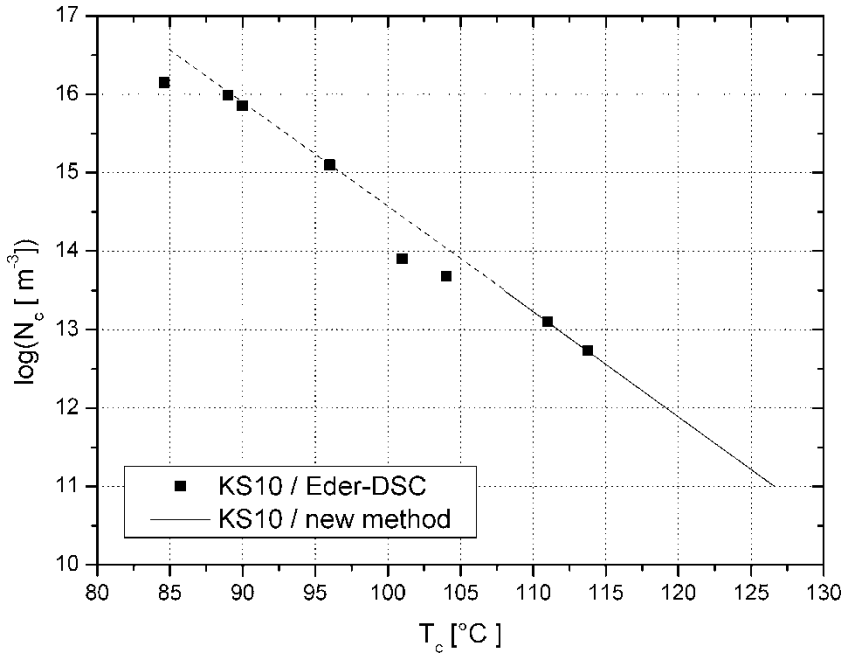
Fig. 2.2 Number density of nuclei as a function of crystallization temperature for a sample of industrial PP according to [3]. *Full line* obtained on samples from the DSC-machine (see Figs. 1.27

Two polyketones of different degrees of copolymerization were investigated by Stadlbauer et al. [5]. Accept for the just described counter-current method also a thin layer technique was applied. In the latter method a very thin sample of a thickness of a few micrometers is prepared by evaporating the droplet of a dilute solution on a cover glass. The obtained layer is then covered by a second cover glass and reheated under slight pressure to a temperature well above the equilibrium melting point for obvious reasons. The application of a thin layer has the advantage that the number of spherulites, which is finally found, is tremendously reduced and can easily be counted. This fact has been advocated by Chew, Griffiths and Stachurski [6]. In fact. only those spherulites can grow in such a layer, which have their nuclei within the volume of this layer. And the surface of the glasses has no influence on the number of nuclei, because glass is an undercooled fluid. If one takes a thin slice, as cut from the bulk of an already solidified sample, this slice contains also parts of spherulites, which have their nuclei outside the volume of this slice.

In Fig. 2.4 the said thin slice apparatus is shown [5]. The two chambers of this apparatus are separated by the sandwich of the sample. Two heating blocks, which are located above and below the chambers, serve for the initial heating erasing remnants of previous crystallization. When the experiment proper is started, two streams of a heat transfer fluid, which are at the intended crystallization temperature
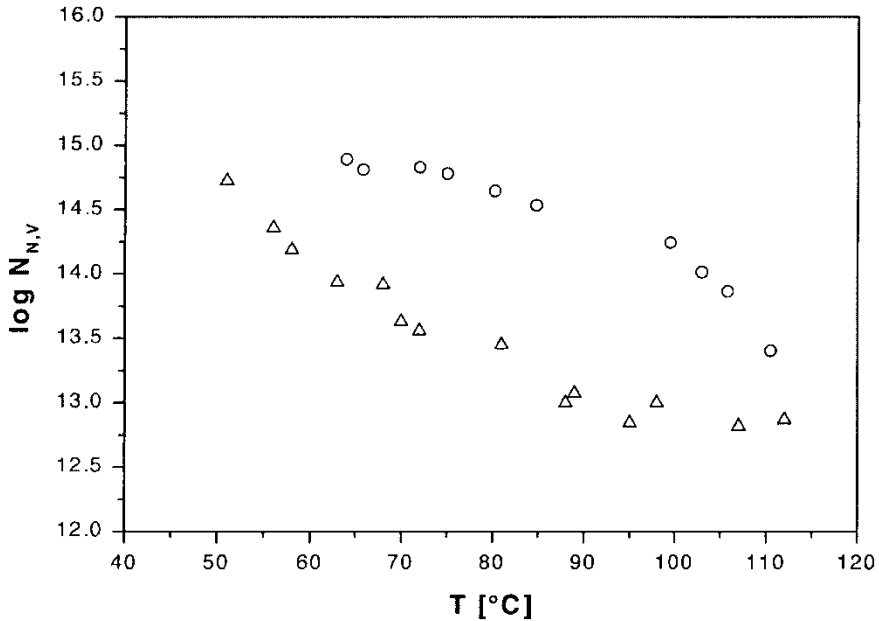
Fig. 2.3 Number densities (per m^3) against crystallization temperatures for PB0110 (*circles*) and PB0300 (*triangles*) [4]. PB0110 was nucleated. Courtesy of the Society of Plastics Engineers

T_c, enter the chambers. Because of the fact that the sample is extremely thin, there is no possibility to measure the sample temperature itself. But a thermocouple is located as close as possible to the sample. One has to trust that the sample temperature adjusts quickly enough to the fluid temperature as the thermocouple does. The course of the temperature of the thermocouple is shown in the lower part of the figure. After some time, which may be called the crystallization time t_c, streams of lower temperature can replace the original streams. These streams cause an almost abrupt decline of the temperature. This trick is of particular importance, if the growth speed of the spherulites is to be determined. This will be explained below.

For the present purpose an early interruption of the crystallization will keep the formed spherulites separated from each other. In fact, with the polyketones the samples can be quenched into the glassy state at 15°C, so that the surroundings of the spherulites can be kept clear. (With i-PP one obtains a fine grain phase, which can easily be discerned from the spherulites). A separation of the spherulites is important, if fast growing spherulites must be counted in a system of high nucleation density. In fact, those spherulites are still small, when impinging, and their boundaries are not well developed. This will be shown to be the case with polyethylenes.

The number of spherulites, which are counted per unit surface under the microscope, must not be raised to the power 3/2 in this case. One must just divide this number by the thickness of the sample, in order to obtain the number density of nuclei per unit volume. The accuracy of this method depends in first instance on the accuracy of the thickness measurement. Nevertheless, for the polyketones a

a

b
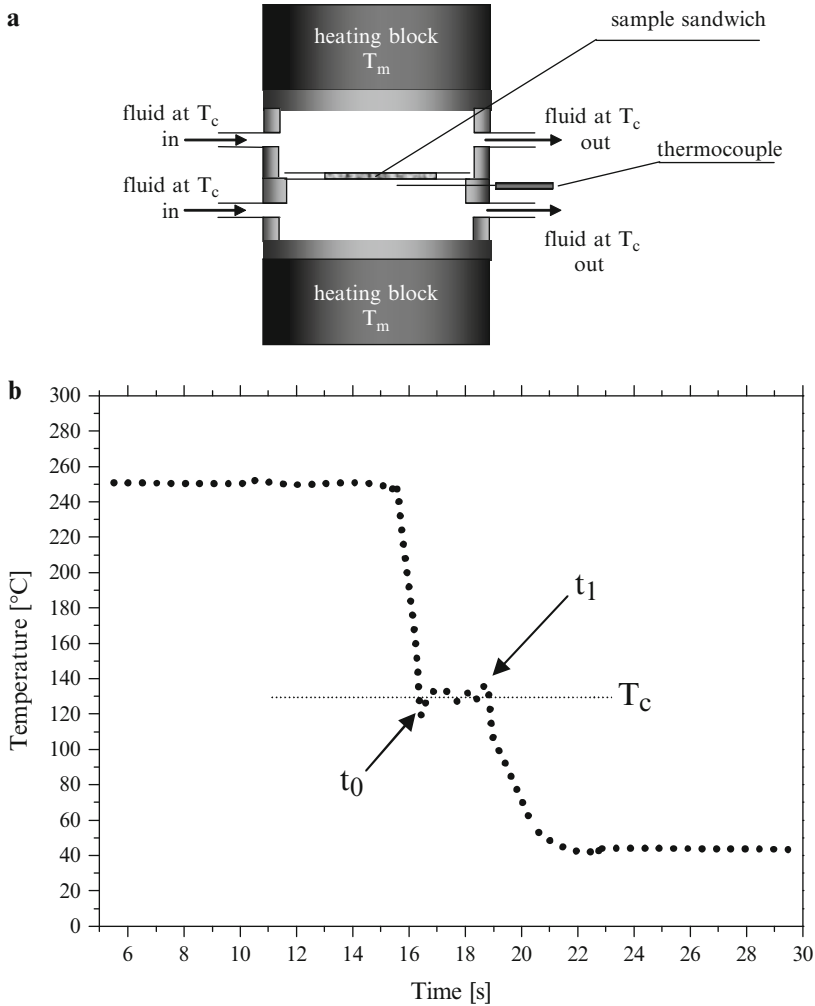
Fig. 2.4 The thin slice machine according to Stadlbauer et al. [5]. In the lower part the temperature profile is shown for $T_c = 130°C$ and $t_c = 2$ s. Courtesy of Elsevier

comparison with the results of the counter-current method turns out to be quite satisfying. This is shown in Fig. 2.5.

The number densities of PK220 are a factor four larger than those for PK230. Interestingly, the melting points of the spherulites show an inverse trend: For PK220 one has $T_m = 220°C$ and for KP230 one has $T_m = 230°C$. The polymer, which does not contain a fraction of propylene, has a melting point of 257°C, which is too high for convenient processing.

Finally, the problems with polyethylene will be discussed. The thin slice method has just been described. In Fig. 2.6 a photograph is shown of a sample of HDPE of a thickness of $0.85\,\mu$m, as obtained by M. Stadlbauer. This sample was quenched
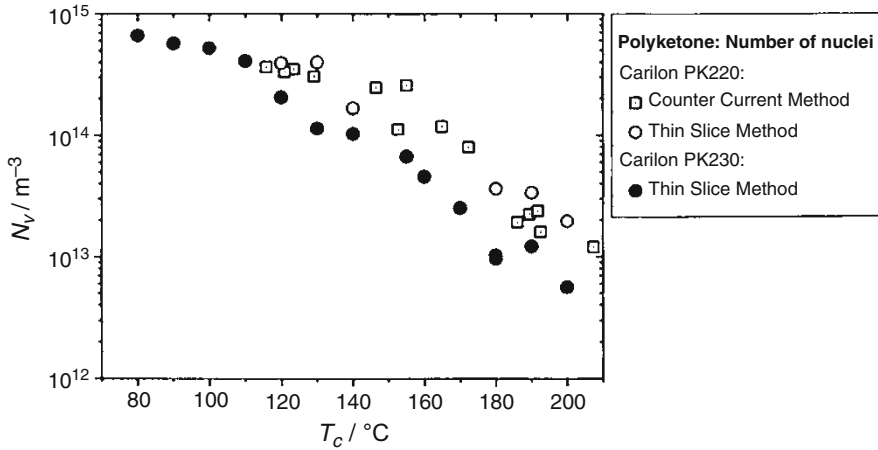
Fig. 2.5 Number density of nuclei versus crystallization temperature for two polyketones of Basell with 6% propylene (PK230) and with 3% propylene (PK220) as replacements for ethylene in the copolymer of carbon monoxide and ethylene. *Full circles* for PK230 as obtained in thin slice measurements. *Open circles* for PK220 from thin slice measurements. *Open squares* for PK220 from counter-current measurements [5]. Courtesy of Elsevier
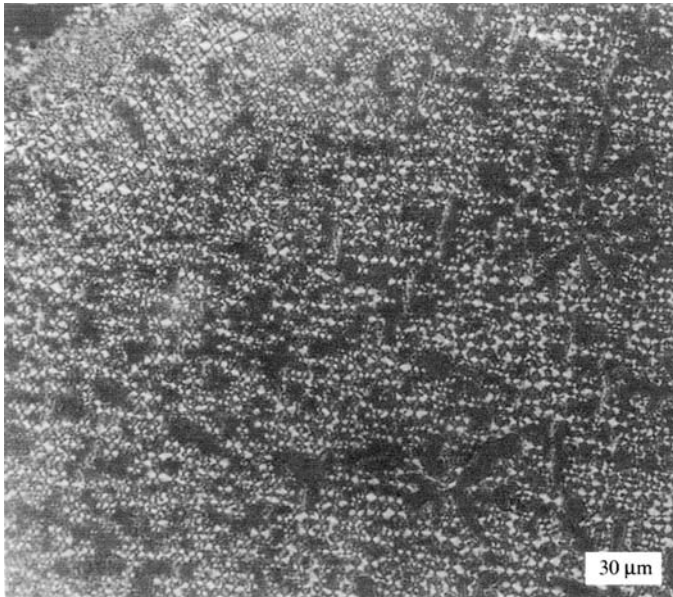
Fig. 2.6 Micrograph of a layer of HDPE of a thickness of $0.85\,\mu\text{m}$ after a quench from 180 to 100°C and a second quench with ice water just before the spherulites could coalesce. Obtained by M. Stadlbauer [9]. Courtesy Springer Wien
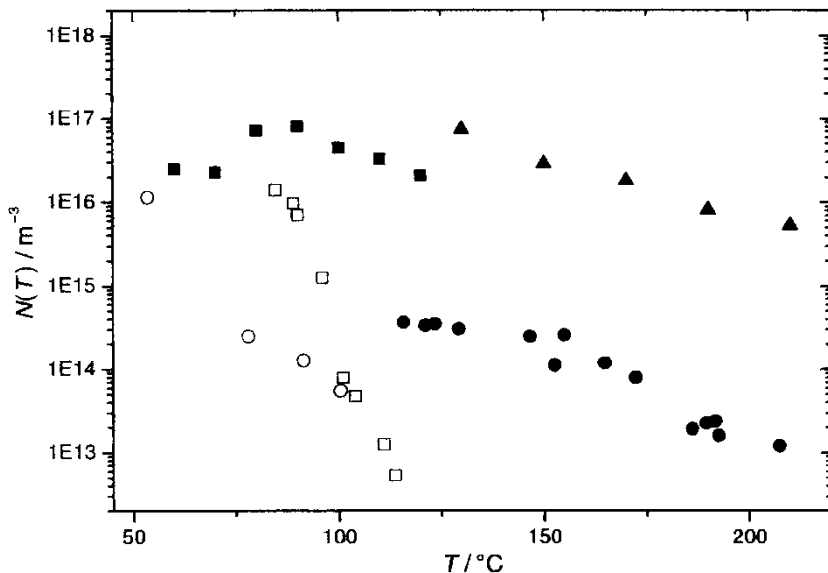
Fig. 2.7 Number densities of nuclei for several industrial polymers as functions of temperature: *full squares* HDPE, *open squares* i-PP, *open circles* PB-1, *closed circles* polyketones, *closed triangles* PET, according to [9]. Courtesy of Springer Wien

from 180 to 100°C. The growth of the spherulite was stopped by a second quench with ice water, before coalescence of the (disk-like) "spherulites" occurred. A number of 300 spherulites was counted on an area of 7.13×10^{-8} m². Knowing the thickness of the sample one arrives at 4.5×10^{16} nuclei per cubic meter.

The result of the count is given in Fig. 2.7, where also the number densities of nuclei of other industrial polymers, as investigated in our group, are shown for comparison. For the investigated HDPE the number densities of nuclei increase with decreasing temperature down to a temperature of about 80°C. With lower temperatures smaller values were found, which cannot easily be explained. In fact, with all the other polymers the number densities of nuclei continuously increase with decreasing temperature, in accordance with (1.41), as must be expected for athermal nuclei (see the consideration given below). Remarkably, the steepness of the increase is particularly high with i-PP. For HDPE and the polyketones the numbers are particularly high over the whole range of temperatures.

As just mentioned, the kink in the curve for HDPE cannot easily be explained. But in this respect one should not forget the difficulties experienced with these measurements, when the temperature is further lowered. Apparently, the 100°C of Fig. 2.6 were still high enough for avoiding those difficulties. Anyway, E. Ratajski investigated a series of copolymers of polyethylene with increasing amounts of propylene. With these polymers the number densities of nuclei decreased. But below 70°C she was not able to count the spherulites. It is not only that the number of rising spherulites increases. Also their contours become less sharp.

The results presented in this section will serve as a basis for the understanding of the nature of athermal nuclei in polymers and for the influence, which flow can exert on the number density of effective nuclei and on the formation of thread-like precursors ("shishs") leading to highly oriented structures. These facts explain, why the determination of the number densities of nuclei is treated here so extensively. So far there are no investigations of other laboratories, which have been extended over such large ranges of temperature. In this connection the reliability of our measurements has been questioned. However, the fact that two quite different types of measurements (raising the number of the sectioned spherulites to the power 3/2 and counting spherulites in a thin slice) led to comparable results (see Fig. 2.5), should convince the reader.

2.2.2 Growth Speeds of Spherulites

This subject has tradition in the famous work by Magill and his coworkers, of which the paper by Gandica and Magill is quoted here [7] as a representative contribution. These authors investigated the growth speeds of spherulites of a great number of polymers, which were prepared in the laboratory. All these polymers showed growth speeds, which were not too high, so that the growing spherulites could be observed under the microscope. The growth speeds of all polymers showed a maximum halfway between the melting point and the glass transition temperature. This fact is in contrast to the temperature dependence of the number densities. As we have seen, these densities increase continuously with decreasing temperatures. The authors arrived at the conclusion that a universal curve could be constructed, if the ratio $G/G_{\max}$ is plotted against a dimensionless temperature Θ, where $G_{\max}$ is the growth speed at the maximum and the definition of Θ reads as follows:

$$\Theta = \frac{T - T_\infty}{T_m - T_\infty},$$
(2.1)

where $T_\infty = (T_g - 50 \text{ K})$, with T_m being the melting point and T_g the glass transition temperature. In this connection the reader should be reminded of the remarks made, when (1.40) was introduced for an approximate description of the temperature dependence of the growth speed with respect to the roles of T_m and T_g as limiting parameters for the growth range.

2.2.2.1 Growth Speeds of Fast Growing Spherulites

In general the growth speeds of industrial polymers are too high for an observation under the microscope, if the interesting temperature ranges are envisaged. The microscope can be used only at temperatures rather close to the melting point. But at those temperatures solidification occurs at a slow pace, which is of no interest
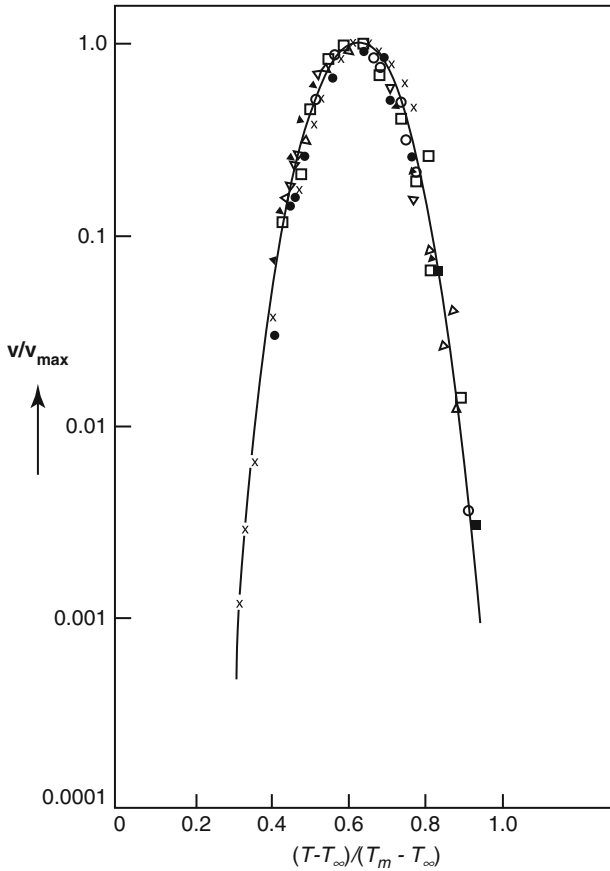
Fig. 2.8 Dimensionless master curve for the growth rates ($v = G$) of a variety of synthetic polymers according to Gandica and Magill [7]. Courtesy of Elsevier

for practical processing. In order to cover the whole range of the dimensionless temperatures of Fig. 2.8, samples must be rigorously quenched. In fact, as will be shown below, with polymers of increasing growth speed also the distance between the melting point and the glass transition temperature increases. A special paper has been devoted to the methods of determining high growth speeds by Ratajski and Janeschitz-Kriegl [8].

The most direct method is the quench of ultra thin slices. For the purpose slices of $5\,\mu$m are cut with a microtome from a solid sample, embedded between cover glasses (of 0.15 mm thickness), and heated in a first stage to a temperature well above the equilibrium melting point in order to destroy residues of previous crystallization. These samples are then quenched with a heat transfer fluid to proper temperatures of crystallization. At those crystallization temperatures the samples are kept for various time spans (crystallization times), before being quenched to

a much lower temperature, where crystallization is arrested. With some polymers this can be a temperature below the glass transition temperature, for others only a temperature, where fast crystallization leads to a fine grained matter separating the spherulites formed at the said crystallization temperature. For the first quench diethylene glycol has been used in most cases. The second quench occurred with ice water, in which the ethylene glycol dissolves. The solidified samples were put under the microscope, where the radii of the spherulites, which actually are disk-like because of the low thickness of the samples, are measured. If these radii are plotted for the same crystallization temperature against the crystallization times, one always obtains straight lines. The slope of such a line gives the speed of growth at the chosen temperature. For i-PP the results of this investigation are shown in Fig. 2.9.

Some remarks have to be made with respect to Fig. 2.9. First of all it is remarkable that the radii of the obtained spherulites do not differ very much from each other. This fact is explicitly shown in Fig. 2.10. This uniformity points to the fact that the bulk of the spherulites starts growing practically at the same time. Probably only few of them started a little earlier before the temperature, at which the quench aimed, had exactly been reached. This fact underlines our assumption of the occurrence of athermal nuclei, which have their exact temperature of sudden activation. But the uniformity is also of practical use.

In fact, after each quench one finds other spherulites in contrast to the micro-scope, where the growth of the same spherulite can be followed. From Fig. 2.9 one also learns that there is practically no incubation time. Within the accuracy of the
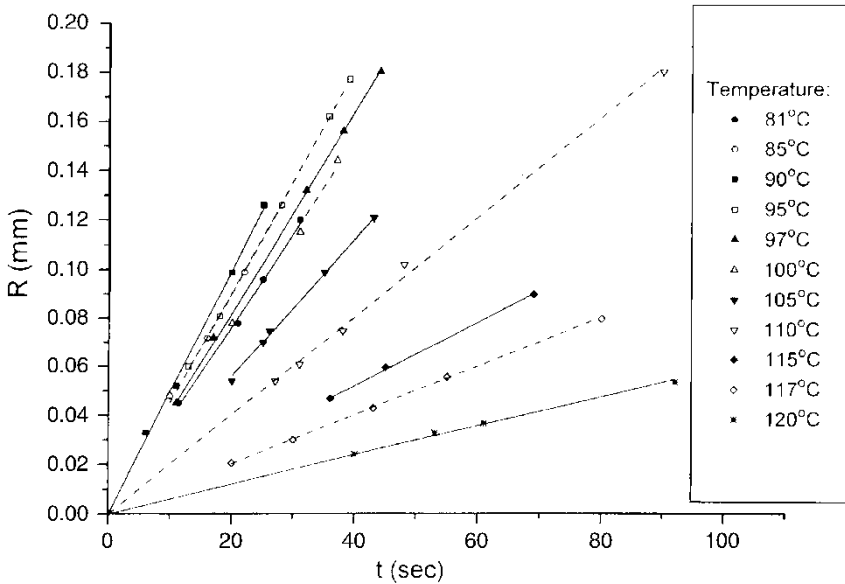
Fig. 2.9 Radii of the biggest spherulites of an industrial PP against the temper times for a series of bath temperatures [8]. Courtesy of Springer
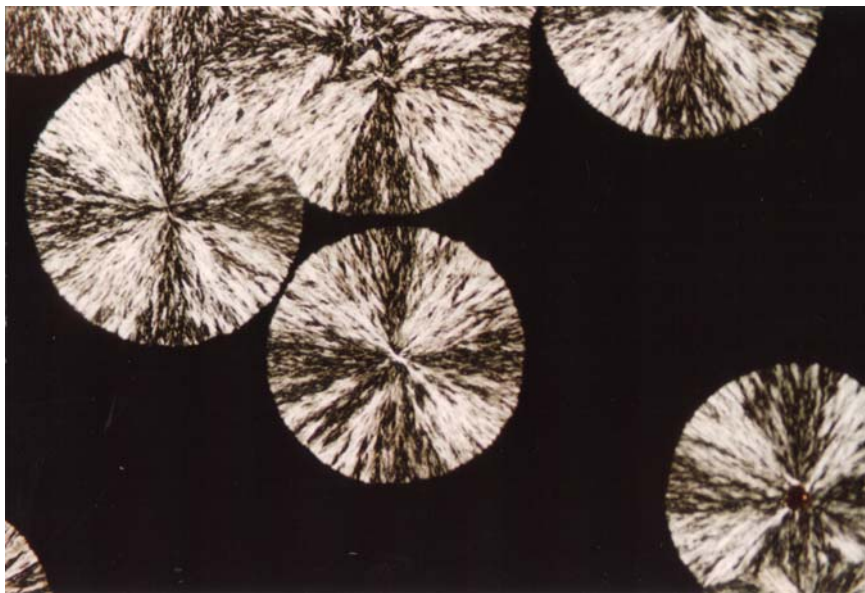
Fig. 2.10 Micrograph of two-dimensional "spherulites" of an industrial PP, as obtained in a bath of 95°C after a temper time of 39 s [8]. The diameter of the biggest spherulite (*upper left corner*) is 0.177 mm. Courtesy of Springer

measurements all lines start at the origin. By the way, with PB-1 a retarded start was found at a temperature closer to the melting point (at 100°C), when growth of spherulites was investigated under the microscope [4]. At the lower temperature of 71°C, where the above technique was applied, the line started at the origin, as in Fig. 2.9 [5]. There are also examples, where the straight line started at a positive intercept with the ordinate axis. This happens with fast growing spherulites, if the quench is not fast enough but sufficiently reproducible. This happened for HDPE at temperatures below 85°C [9].

Another point is that the observed spherulites are actually disk-like. If the contact angle between the spherulite, the melt and the glass is finite, which must be assumed, the growth speed can only be reduced with respect to the growth speed of a free spherulite in the melt. However, the effect cannot be very large, as the consistency of the spherulite, which contains still a lot of amorphous material, cannot differ very much from that of the pure melt. Also, PP shows polymorphism [10]. Interestingly enough, however, only spherulites of the α-modification were observed in this investigation. These spherulites show a low birefringence in contrast to the spherulites of the β-modification. This contrast will be subject of discussion in one of the next paragraphs. Apparently, the β-modification is nucleated only at metal walls or by the addition of a proper nucleation agent (Fortunately, glass walls do not nucleate any modification. In fact, glass is an undercooled fluid).

In our laboratory also other methods were applied in order to determine growth speeds. It goes without saying that the application of various techniques is

important for a check of the reliability of determinations. Short descriptions will be given of two techniques: Transcrystallization against a temperature gradient and onset of turbidity after touch with a thermostated wall.

As already pointed out at earlier occasions in this monograph, transcrystallization [11] is hampered regularly by the occurrence of spherulites at some distance from the wall. This happens particularly, if the initial temperature of the melt is not too high and is still uniform at some distance from the quenched wall. This effect can be avoided, if the sample thickness is chosen small enough, so that the second confining wall, which is kept at the original high temperature, keeps its influence on the temperature distribution in the sample. In such a case transcrystallization occurs against a steep temperature gradient. Admittedly, such a gradient causes a retardation of the front movement, but reduces the probability for the occurrence of spherulites. The pertinent experiment occurs in two steps. In the first step one wall is quenched to the desired crystallization temperature. After a chosen time both walls are quenched to a much lower temperature, where a fine grained structure is obtained during continued crystallization. Finally, the solidified sample is removed from the confinement and a cross-section is made in a plane perpendicular to the plane of the confining walls. In this cross-section the location of the undisturbed crystallization front can easily be observed.

For i-PP, however, which has been our appropriate experimental object, such experiments cannot be carried out directly because of the polymorphism of this polymer. The consequences of this polymorphism are shown in Fig. 2.11. This figure shows large parts of an undisturbed growth front of the α-modification, as observed under the polarizing microscope. Unfortunately, there are places at the wall, where the β-modification is nucleated. As this modification grows faster, one obtains a bright cone with its apex at the point at the wall, where this modification is nucleated. (The cross-section does not go exactly through this point). The brightness of this cone is due to the high birefringence of the β-crystallites. Those phenomena were observed first by Lovinger et al. [12]. On Fig. 2.11 it can be seen easily that at a certain distance from the wall the growth front becomes one of the β-modification. (In the beginning of our investigations we overlooked this fact. It led to an overestimate of the growth speed of the α-modification in a temperature range between 90 and 110°C [13], see Fig. 2.6 of this paper, or [14], Fig. 2.3).

In avoiding this uncertainty a rigorous choice was made. The wall was rubbed in with Cinquasia Gold (Permanent Red E3B), a nucleation agent for the β-modification. In this way an undisturbed crystallization front of the β-modification was obtained. Such a front is already shown in Fig. 1.15 of the first chapter. In the present Fig. 2.12 the propagation of this type of fronts is shown for a series of quenched wall temperatures at a temperature of the opposite wall of 200°C. The initial slopes of these curves should give the growth speeds of β-spherulites at the indicated temperatures of the quenched wall. However, the determination of those initial slopes is extremely inaccurate. At this point a method, as proposed by G. Eder [15], has been introduced.

Eder's method analyzes the shape of the curves over a bigger distance from the wall. To start with, it was shown that the critical Fourier number was passed over in
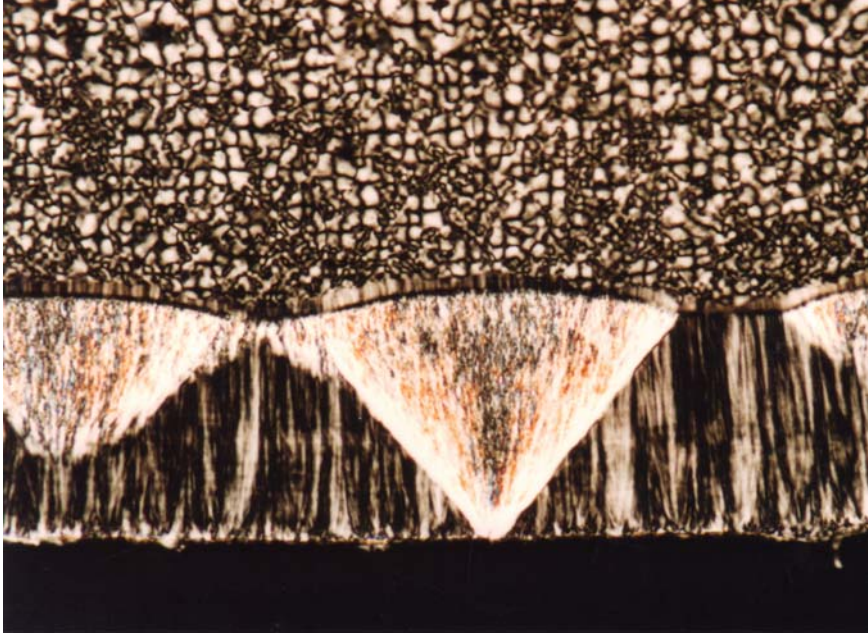
Fig. 2.11 Transcrystalline layer of the α-modification of i-PP at a wall temperature of 110°C and a contact time of 103 s. A single β-nucleus at the wall produces a conical body, which becomes dominant after a distance of 0.153 mm from the wall [8]. Courtesy of Springer

all experiments. This means that the temperature profile should be linear, if the production of latent heat was ignored. The Fourier number reads:

$$Fo = \frac{at}{D^2},\tag{2.2}$$

where a is the heat diffusivity of the melt, t is the time and D is the distance between the walls. For $a = 10^{-7}\,\text{m}^2\text{s}^{-1}$ and $D = 1$ mm one obtains from (2.1) a critical time $t = 5$ s. A look at Fig. 2.12 shows that all points were found at larger times. Two assumptions were made for the required calculations (see also [15]):

(a) For a sufficiently steep temperature gradient the kink, as caused by the latent heat, can be ignored. So one has for the temperature profile:

$$T(x) = T_w + (T_i - T_w)\frac{x}{D},\tag{2.3}$$

where x is the distance from the quenched wall and T_i is the initial temperature of both walls (i.e., the temperature of the opposite wall) and T_w is the temperature of the quenched wall after the quench.
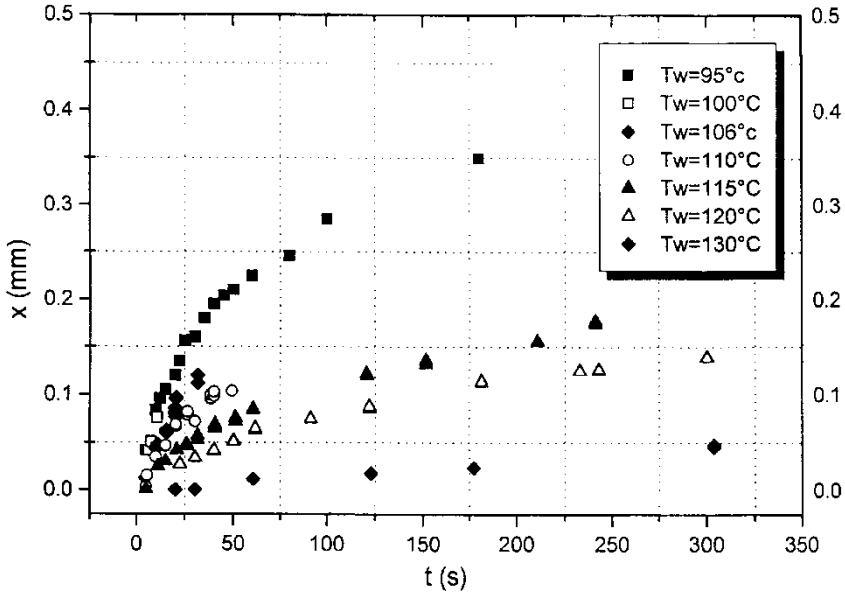
Fig. 2.12 Front positions of the transcrystalline β-layers as functions of time for various temperatures of the quenched wall. The temperature of the opposite wall at a distance of 1 mm was 200°C [8]. Courtesy of Springer

(b) For the growth speed as a function of temperature the following equation has been used:

$$G(T) = G_w \exp\left(-\beta(T - T_w)\right) \text{ with } G_w = G(T_w). \qquad (2.4)$$

The reader will notice a contrast between this equation and (1.40), where a quadratic dependence on temperature is proposed. However, T_w is not $T_{\max}$ and (2.4) describes a tangent to $\log(G)$ vs. T at some temperature T_w along this curve. With these assumptions the differential equation for the progress of the growth front reads:

$$\frac{dx}{dt} = G(T(x,t)) = G_w \exp\left(-\beta \frac{T_i - T_w}{D} x(t)\right). \qquad (2.5)$$

This equation can easily be integrated. One obtains:

$$\log(x(t)) = \log(G_w) + \log\left[\tau \ln\left(1 + \frac{t}{\tau}\right)\right] \qquad (2.6)$$

$$\text{with } \tau = \frac{D}{\beta\,(T_i - T_w)\,G_w}. \qquad (2.7)$$

It may be recognized that τ depends on the location along the curve $\log(G)$ vs. T, i.e., on T_w – also through β, T_w and G_w. If for a series of assumed values of τ a pattern of curves $\log[\tau \ln (1 + t/\tau)]$ vs. $\log(t)$ is prepared, this pattern covers all combinations of the parameters of (2.7) within the mashes of this pattern. Such a pattern has been drawn on a transparent sheet and put on the experimental curve $\log (x(t))$ vs $\log(t)$ and shifted along the log x-axis until the shape of one of the curves of the pattern fitted the shape of the experimental curve. In this way the ordinate of the corresponding $\log(G_w)$ was obtained with reasonable accuracy. In Fig. 2.13 the result of this procedure is given for a large number of wall temperatures between 80 and 120°C for the growth speed of β-spherulites of i-PP. Only at higher temperatures growth speeds of these spherulites were known from the work of Lovinger et al. [12].

In a next step Lovinger's cone angle K was used in order to obtain the growth speeds of the α-spherulites in the same range of temperatures (see Fig. 2.11). In fact, one has:

$$\frac{G_\alpha}{G_\beta} = \cos\left(\frac{K}{2}\right). \tag{2.8}$$
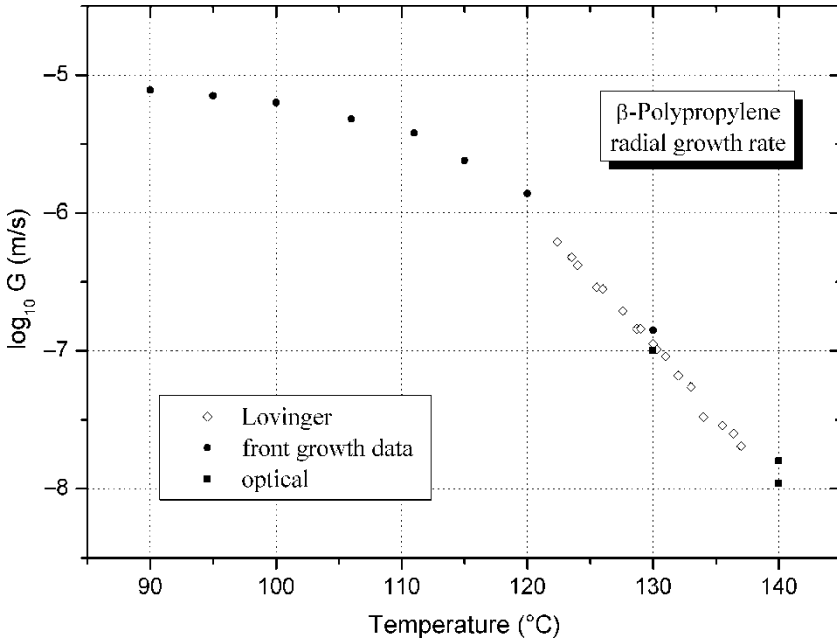
Fig. 2.13 Growth speeds of β-spherulites of i-PP as functions of temperature according to Eder's method for temperatures between 80 and 120°C [8]. At higher temperatures growth speeds, as obtained by Lovinger et al. [12], are taken over. Courtesy of Springer

The points, which were obtained in this way, fitted nicely into the picture repro-
duced in Fig. 1.2 together with points, which were obtained in the thin slice
experiments. Only at higher temperatures many points of other authors could be
included. So far in the present section results were reported, which were obtained
with transcrystallization against a steep temperature gradient.

Interestingly enough, the second method announced above, i.e., onset of turbid-
ity after touch with a thermostated wall, is based on a quite different physics. It is
based on the time needed for a crystallization process starting at time zero until it
becomes apparent with the aid of light scattering. In this respect the reader is
reminded of interesting work by Berger and Schneider [16].For the case that no
nucleation takes place at the quenched wall, the said authors showed that a zone of
diffuse crystallization must move into the melt of originally uniform temperature.

If one considers the line of half conversion, this line has a shape very similar to
the line of the square root law. The only grave difference is that it does not start at
$x = 0$ but is shifted downwards the x-axis, so that it cuts a positive section from the
time axis. Of course, negative distances x are only formal. The zone starts at the said
positive value of the time, a fact which creates the impression of an incubation time.
However, no incubation time is in the basic assumptions of the model. A look on
Fig. 1.14 of Chap. 1 conveys the experimental situation. In fact, also the experi-
mental curves start at positive values of time. So, there must be another reason than
incubation for the delay in response. And there is only one way to explain this
phenomenon: light scattering becomes intensive enough only after some time.
Initially spherulites or their precursors have a scattering power proportional to the
square of their volume. They are Rayleigh scatterers. As the volume of a ball shaped
scatterer is proportional to $(Gt)^3$, one obtains for the development of the scattering
power S of the unit of volume of the sample:

$$S = CN (Gt)^6, \tag{2.9}$$

where C is an optical constant, N is the number of nuclei per unit volume, G is the
growth speed of the spherulites and t is the time elapsed from the moment of the
quench of the wall. Equation (2.9) presents a parabola of the sixth order, which
shows an upswing only after a considerable time. During this time span the
crystallization process remains unobservable. In reality a more complex scattering
mechanism can be developed. However, such a scattering will not occur earlier than
the one predicted by (2.9). If now also the assumption is made that the development
of structure follows the same route, independent of the speed of formation, one
obtains the following equation for the growth speed:

$$G = \left(\frac{S}{C}\right)^{1/6} \frac{1}{N^{1/6}t} . \tag{2.10}$$

Anyway, one can conclude from this equation that the time elapsing until the
moment, when the light scattering becomes observable, must be inversely

proportional to the growth speed, whereas the number density of nuclei can only play a minor role. In fact, the sixth root of this quantity cannot change very much within the range of temperatures, where this equation will be of use. Obviously, (2.10) must be calibrated at a higher temperature, where the parameters G and N can be determined along other routes. Preferably, a comparison over a larger range of temperatures should be accomplished. This was no problem with the quite slowly crystallizing PP.

An excuse for the application of this equation is that it can be used, if the time span becomes so short that other techniques can no longer be applied. For many years this was the case for HDPE at temperatures remote from the melting point. At time zero sample melts were brought into contact with a metal wall, which was thermostated at the required crystallization temperature. Shortly after this moment the contact surface was abruptly clad by a film of opaque material. This process could even be followed with the aid of a stop watch. In a more accurate method the moment was determined, when the reflection of a light beam was interrupted. This light beam was directed through the still transparent melt on the polished contact surface. Fractions of a second could be determined in this way. Only more recently, M. Stadlbauer [9] improved the thin slice technique, so that a comparison with his more direct measurements was possible.

As an example Fig. 2.14 is introduced. It shows the growth speed of spherulites of HDPE as a function of temperature. Down to 123°C the results of Chew et al. [6] are reproduced. These results were obtained by direct measurement of spherulite radii (black squares). Our (2.10) was calibrated at 120°C with the result of these authors. In this way the range of measurements could be extended by more than 40°C to lower temperatures. Down-pointed triangles stand for the results obtained with interrupted reflection. Upright triangles are obtained with the stop watch. Open circles give results obtained from the intercept of the diffuse crystallization zone with the time axis. (With HDPE the zone of transition from the clear melt to the homogeneously opaque material is very narrow in contrast to the zone obtained with i-PP, which is much broader, cf. Figs. 1.13 and 1.14).

The theoretical line, which is shown in Fig. 2.14, will be explained in Sect. 2.3.1.

Recently Stadlbauer was able to extend the range of measurements with the improved thin slice method on both sides of the range of Chew et al., namely to lower and also to higher temperatures. These results are given in Fig. 2.15, which shows a survey of all growth speed measurements, which were carried out in our laboratory. With HDPE one notices that at about 80°C there is a downwards kink in the curve. We suspect that measurements below this temperature are no longer reliable. Above this temperature Stadlbauer's points exactly fall on the line of Fig. 2.14. This fact endorses the usefulness of (2.10). In the graphs, where radii of spherulites are plotted against temper time for temperatures below the kink, the straight lines, as drawn through the points, do not go through the origin. (Cf. Fig. 2.9). Positive intercepts with the ordinate axis are found. This shows that the quenches were not fast enough for preventing premature spherulite growth. In this connection one should not forget that the cover glasses are rather thick compared with the slices.
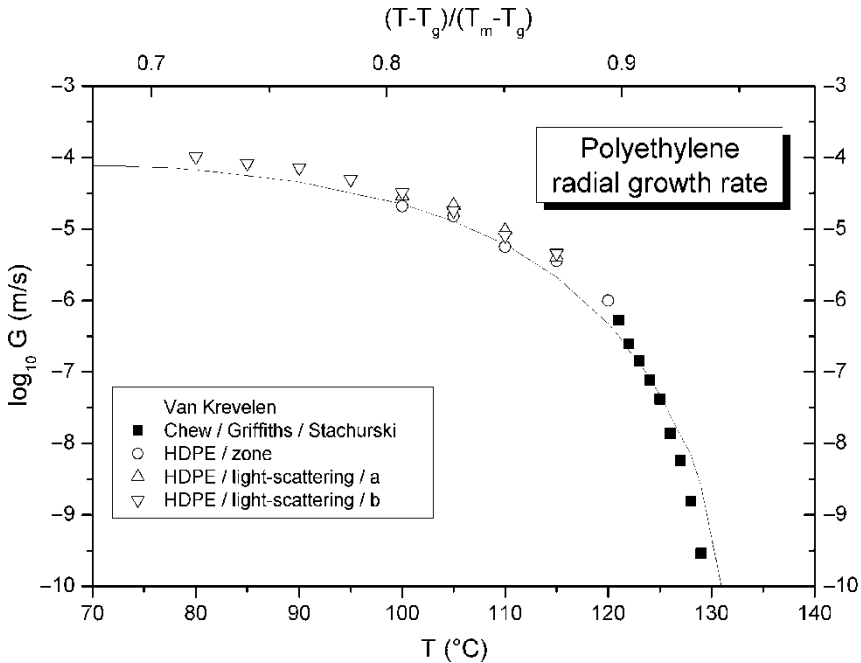
Fig. 2.14 Growth speeds of spherulites of HDPE over a wide range of temperatures. *Black squares* stand for measurements in a thin slice equipment [6]. Other points were obtained with the use of (2.10) [8]. Courtesy of Springer

On Fig. 2.15 one can see the enormous differences in the growth speeds of diverse industrial polymers. In fact, similar differences are shown in Fig. 2.7 for the number densities of nuclei. In particular, the number density of nuclei shows a particularly strong increase with decreasing temperature for i-PP. For HDPE the level of the number density of nuclei is much higher, but less dependent on temperature. But this is in favor for the application of (2.10). $N^{1/6}$ will be practically independent of temperature.

Finally it must be emphasized that the value of (2.10) is more in the field of general insights. The usefulness of this equation shows that there are no incubation times. Also the simultaneity of the start of the growth for all nuclei is of importance for our insight into the physics. At temperatures below the melting temperature of the spherulites one finds only nuclei, which are "prefabricated" by the so-called "local alignments". This will be explained in Sect. 2.3.2.

2.2.2.2   Growth Speed and Small Angle Light Scattering

The intention to determine the growth speed of spherulites with the aid of small angle light scattering (SALS) dates back to the sixties. At that time Stein and Rhodes [17] published a trend setting paper, in which they showed that a scattering
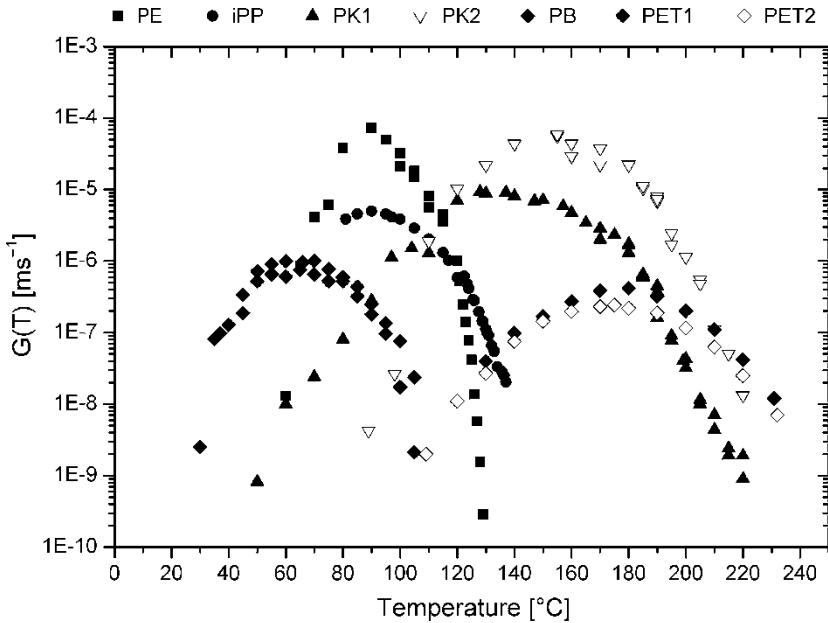
Fig. 2.15 Growth speeds of several industrial polymers as functions of temperature: *full squares* HDPE, *full circles* i-PP, *full diamonds* PB-1, *full and open triangles* two polyketones of different comonomer content, *open diamonds* PET of two molar masses, according to [9]. Courtesy of Springer Wien

pattern of the shape of a four-leafed clover is obtained, if crossed polars (H_V) are used. In this pattern the distance of the center of light intensity in the leafs from the point of impact of the primary beam is inverse proportional to the spherulite radius. The pertinent theory was improved step by step, until Keijzers [18] found a quite simple equation for this relation. This equation reads:

$$R = \frac{4.1\ \lambda}{4\pi\ \sin(\Theta_m/2)}\ , \qquad (2.11)$$

where R is the radius of an ideal spherulite, λ is the wave length of the light and Θ_m is the scattering angle, both in the medium. An ideal spherulite is a spherulite, in which the polarizable elements are in an exactly radial position (polarization only radial and tangential). An underground scattering is added for the imperfections. Keijzers published this equation only in his thesis [18] and not in the pertinent paper with Van Aartsen and Prins [19]. But Van Antwerpen and Van Krevelen used this equation for their investigation of the growth speeds of spherulites of PET [20,21]. These authors also checked the equation with nylon, which forms beautiful spherulites. Unfortunately, one needs a light scattering photometer in order to follow the development of the pattern during the growth process. Van Antwerpen monitored the light intensity along a line under 45° with respect to the polarizer.

| Scattering angle (rad): | 0 | $\pi/6$ | 0 | $\pi/6$ | 0 | $\pi/6$ |
| t_{cryst}(s): | | 16 | | 25 | | 58 |
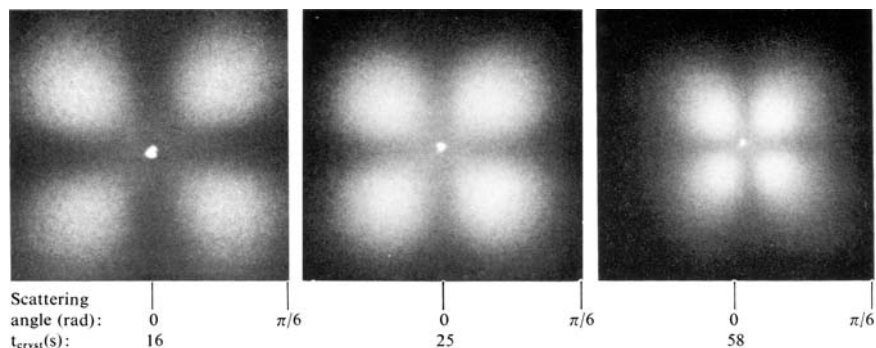
Fig. 2.16 H_V scattering patterns for a PET sample of a number average molar mass of 35,400 Da. Crystallization temperature is 175°C. Crystallization times 16, 25 and 58 s. The polarization directions are vertical and horizontal. These results are from [20] and [21], courtesy of the American Chemical Society

Some representative results of Van Antwerpen and Van Krevelen are shown in Fig. 2.16. In this figure the four-leafed clover is shown for three stages in the development of the crystallization of a PET sample.

It goes without saying that also some explicit results must be presented. For the purpose Fig. 2.17 is introduced. In this figure results are combined, which were obtained by heating the sample from the glassy state and by cooling the sample from the melt to the required crystallization temperature. No significant differences were found between the results of both methods. A regression was applied for the calculation of the drawn lines. Only for three samples the measurement points were inserted. In contrast to the experience with samples of sufficiently high molar masses a strong dependence on the molar mass was obtained for these low molar mass samples. A discussion of this contrast will be given in the next section.

A continuation of the discussion on the usefulness of SALS will be given in Chapter 4 in connection with flow induced crystallization. A reason for the better chances of this method in flow experiments is the fact that flow induced crystallization can be investigated at much higher temperatures, where practically nothing happens in unloaded quiescent melts. A consequence of this fact is that the samples can be cooled without much troubles to the experimental temperatures, before flow is started. Also pressurization, which enhances crystallization, can be activated after such a relatively slow cooling process. In an unloaded quiescent melt, however, the sample must be cooled to much lower temperatures for the initiation of interesting phenomena. For rather slowly crystallizing materials like i-PS or PET there is still no big problem with cooling. However, for fast crystallizing polymers the situation changes drastically. As an example the behavior of HDPE is quoted. When using (2.10), which certainly is loathed by scattering specialists, one encounters times below 1 s with quiescent HDPE. I do not think that the above technique can be applied under those extreme conditions.

Fig. 2.17 Spherulite growth rates versus crystallization temperatures for PET samples of different molar masses M_n in Daltons. 1: 19,000, 2: 22,300, 3: 24,000, 4: 27,000, 5: 30,100, 6: 34,500, 7: 39,100, according to [21], courtesy of Wiley
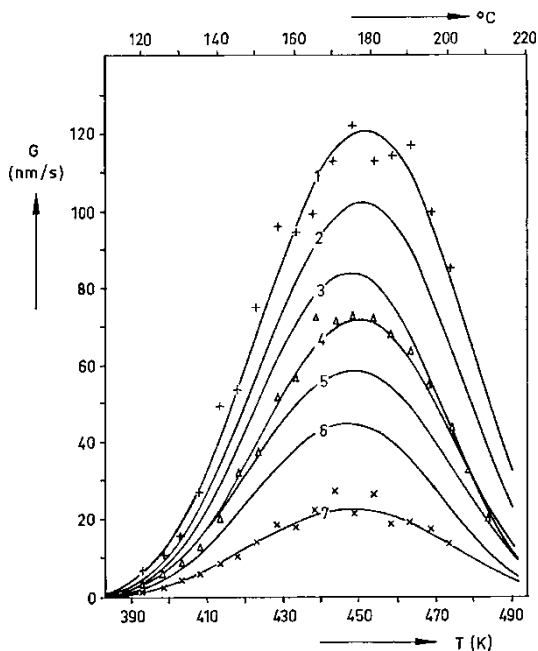
2.3 Theoretical Considerations

2.3.1 Theory of the Growth Speed of Spherulites

In this section the work of Van Krevelen [1,22] will provide the guideline. The results of this work are of high practical value, and there is no reason to believe that these results have become obsolete. However, as will be shown in the next section, there are good reasons, why the classical approach, as applied by Van Krevelen, is valid only for the growth speed, but not for the primary nucleation. In fact, the growth of lamellae, of which spherulites are built, just requires local rearrangements of parts of neighboring macromolecules. (See the independence of the growth speed of the molar mass, except for very short molecules [23]). In contrast, major rearrangements should be required for the formation of primary nuclei, if the surrounding would be at random (see Fig. 1.3). But the topology of long molecules with their surroundings prohibits those undertakings effectively. We were forced to accept this hitherto uncommon vision because of the results of our experiments. This fact will make Sect. 2.3.2 particularly thrilling. However, the local mobility, which can be proved even for some materials in the glassy state (see, e.g., Heijboer [24]), seems to preserve the classical theory of the growth speed.

After this introduction it will be clear, why only the equation for secondary nucleation, which is responsible for the growth mechanism, is quoted here. One has for the rate of growth:

$$G = G_0 e^{-\frac{E_D}{RT}} e^{-\frac{\Delta G_2}{kT}}. \tag{2.12}$$

In this equation G_0 is a constant of the order of kT/h, E_D is an activation energy for the transport per mol of a designated part of a molecule and ΔG_2 is the free energy of a local nucleus for two-dimensional growth. Interestingly, the last term of this equation gives a Boltzmann distribution for the occurrence of this state of energy. Actually, such a Boltzmann term only holds for an equilibrium situation, which is not given here. The first exponential term serves as a substitute for this omission. Interestingly enough, Ziabicki and Alfonso [25] have shown quite recently that a correct description of the "growth diffusion" against the slope of the barrier ascending to ΔG_2 can be given in terms of a suitable Fokker–Planck equation. An absorbing wall at the top serves as the adequate boundary condition. Unfortunately, the authors were not able to give the resulting flux over the barrier in terms of measurable parameters.

Van Krevelen [1] derived a semiempirical equation for the activation energy occurring in the first exponential (the transport factor). For the purpose he evaluated elder results by Mandelkern et al [26]. In terms of the characteristic temperatures (T_m and T_g) of a variety of "normal" polymers Van Krevelen's equation reads:

$$\frac{E_D}{R} = C_D \frac{T_m^2}{T_m - T_g} \tag{2.13}$$

with $C_D \approx 5$.

A little earlier Hoffman [27] proposed the use of the WLF-equation [28] for a calculation of the transport factor for lower temperatures (more close to the glass transition), where a temperature independent activation energy no longer holds. This equation reads:

$$\frac{E_D}{RT} = \frac{C_1}{R(C_2 + T - T_g)} \tag{2.14}$$

with the "universal" constants $C_1 = 17.2$ kJ mol^{-1} and $C_2 = 51.6$ K.

In this way one arrives at a rather simple semiempirical expression for the growth rate of spherulites:

$$\ln(G) = \ln(G_0) - \frac{E_D}{RT} - \frac{265\text{K}}{T} \frac{T_m}{\Delta T} \tag{2.15}$$

with $G_0 = 10^{12}$nm s^{-1}.

One can now introduce (2.13) or (2.14) into (2.15). In carrying out this substitution two dimensionless variables $\xi = T_m/T_x$, with T_x being the crystallization temperature, and $\delta = T_g/T_m$ are introduced. Also a certain temperature T_k is defined,

which lies between T_g and T_m and will be scrutinized a little later. One obtains for $T_x \geq T_k$:

$$\log G = \log G_0 \; - \; 2.3 \, \frac{\xi}{1 - \delta} \; - \; \frac{115\text{K}}{T_m} \, \frac{\xi^2}{\xi - 1} \,. \tag{2.16}$$

For $T_x < T_k$ one has:

$$\log G = \log G_0 \; - \; \frac{895K \; \xi}{51.6K \; \xi \; + \; T_m(1 \; - \; \delta \xi)} \; - \; \frac{115K}{T_m} \, \frac{\xi^2}{\xi - 1} \,. \tag{2.17}$$

In Fig. 2.18 both equations have been used. For the right side (2.16) is responsible. The corresponding curve has been calculated up to the highest point, which defines the said temperature T_k. In a next step (2.17) has been used for a calculation of the lower part on the left side. As the temperature range for the validity of this equation is restricted, this curve has been connected by hand with the apex of the right curve. In this way a most interesting result is obtained. Dependent on the value of the parameter $\delta = T_g/T_m$ one obtains curves with their maxima at the specific value of T_k. But the heights of these maxima differ enormously, i.e., from almost 10^6 nm s^{-1} to about 10^{-16} nm s^{-1}, if δ varies between 0.45 and 0.90. Admittedly, these curves only hold for so-called normal polymers. However, the general behavior of polymers follows the trend reflected in this picture: the closer the glass transition temperature is to the melting point, the lower is the growth speed. Also, the picture of Fig. 2.18 holds for a melting point of 473 K. For every 10°C, that T_m is higher or lower than 473 K, log(G) (G is replaced by v in the graph) will be about 0.1 higher or lower than given in the graph.

By the way, most satisfactory is the observation that, apparently, HDPE belongs to the "normal" polymers. In fact, in Fig. 2.14 a theoretical line is shown, which agrees rather well with the experimental points. This line is obtained with the aid of (2.16), if the following values are inserted for the characteristic temperatures: $T_m = 144°C$ (=417 K) and $T_g = -84°C$ (=189 K). As was pointed out, when Fig. 2.15 was discussed, the kink in the curve for HDPE should be ascribed to the uncertainties of the thin slice measurements below 80°C. Above this temperature, there is a very good agreement with the values shown in Fig. 2.14. But this means that the theoretical curve can replace the experimental points below 80°C. So, it seems clear that the kink is an artifact.

Quite different is the behavior of i-PP. Van Krevelen's curve does not fit the experimental points for the α-modification (see Fig. 1.2). Between 100 and 150°C it lies above the experimental points with the biggest distance of one decade at about 130°C. Only the maximum growth speed is correctly predicted. Within the range of usual tacticities these tacticities do not seem to play a predominant role. And the spherulites of the β-modification play their own game: Over the whole range of temperatures the growth speeds of the β-spherulites are higher than those of the α-spherulites. This happens not withstanding the fact that the temperature, where the spherulites of the α-modification are melting, is higher than the corresponding temperature for the β-modification. Details can be found in [8], where also the references are given.
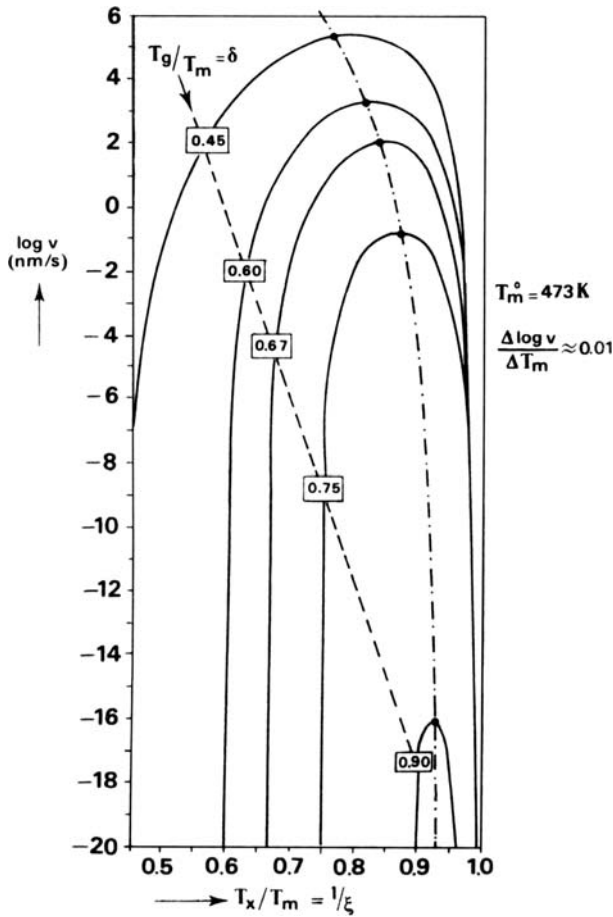
Fig. 2.18 Master curves for the linear growth speeds of spherulites (v instead of G) versus dimensionless crystallization temperature T/T_m (=1/ξ), with $T_g/T_m = δ$ as parameter, according to Van Krevelen [1,22]. Courtesy of Brunner, Zürich, and of Elsevier

The described deviations of the growth speed of the α-modification of PP from the so-called "normal" behavior have certainly to do with the fact that the α-modification of PP shows several growth regimes, as has been described by Hoffman et al. (See [29,30]).

Finally, it should be mentioned that Van Antwerpen [31] has investigated more closely the molar mass dependence of the growth speed, as it has been found for low molar mass samples. According to this author this dependence is contained in the second term. One has:

$$G_{0,M} = G_0 + \frac{const.}{M_n}, \tag{2.18}$$

where M_n is the number average molar mass. Obviously, $G_{0,M}$ goes to the constant parameter G_0, if M_n becomes large enough, as it should be according to the general experience. The present author is permitted to say that he has difficulties with this interpretation. Apparently, the higher growth speeds of those low molar mass samples are due to enhanced transport mechanisms. Probably, this discrepancy has to do with the problem addressed by Ziabicki and Alfonso [25].

For more recent developments in the field one can consult the second edition of Mandelkern's book [32] or a paper by Hoffman and Miller [33]. For our purpose, however, the results of Van Krevelen's school must be preferred, because of their greater practical relevance. In the book by Mandelkern a host of results is given, which surpasses the scope of the present treatise, which aims at structure formation. Unfortunately it must be said that with respect to the development of the theory Mandelkern's presentation is not completely up to date. For instance, Tobin's theory is treated to the full extent. But in Sect. 1.2.1 of the present treatise it is shown that this theory is a theoretical artifact. Its deviation from Kolmogoroff is caused only by an unnecessary fictitious simplification. In fact, the same model is used. A similar criticism holds for the theory by Nakamura et al. Mandelkern apparently overlooked that Nakamura's treatment only holds, if the number density of nuclei is independent of temperature and predetermined. Nakamura's theory cannot hold for the general case. Amongst others this becomes evident from Fig. 1.1 of the present treatise, a figure which unfortunately was only published about the same time as Mandelkern's second edition. The criticism on the said theories was stressed already in our review from 1997 [15], 7 years before Mandelkern's second edition appeared. A valid alternative to Nakamura's theory was already published in 1988 by Schneider et al. (see Sect. 1.2.2 of the present treatise). This theory is not mentioned by Mandelkern.

2.3.2   On the Nature of Primary Nuclei in Polymer Melts

2.3.2.1   Some Comments on the Theory by Hoffman and Lauritzen

In two pioneering papers [34,35] these authors opened the discussion of the nucleation in polymer crystallization. In their theoretical approach they obtained lengthy nuclei. In fact, this type of nuclei must be expected, if long molecules are associated. But the assumption, which was made by the authors in order to obtain those nuclei, was not directly the presence of long molecules but the occurrence of an increased surface tension at the end surfaces with respect to the side surfaces. Actually, it took us quite a time before we realized this fact. Apparently, the authors exchanged cause and consequence. Our biggest riddle was in this respect the self-nucleation effect, as discovered by Blundell, Keller and Kovacs [36].

Many people have tried meanwhile to reproduce the self-nucleation effect, which had been found for the first time by the just mentioned authors. In fact, if a carefully grown spherulite is slowly heated under the microscope up to a

temperature, where it just melts, one can find quite a lot of new nuclei within the domain of the old spherulite, when the temperature is lowered again. This is the self-nucleation. If the spherulite is heated a little less carefully, one can get back at least the old spherulite at the same place. But what does this effect mean? In the latter case it meant that the nucleus, on which the spherulite had grown for the first time, survived the melting of the spherulite. In the case of self-nucleation it is even shown that many new nuclei, which came into existence in the previous crystallization process, survived at a temperature, where the spherulite melted. So far, nobody dared to explain this self-nucleation. A big crystalline body melts, but tiny remainders survive. By accident the author of this monograph met a person from the sugar industry, who provided the priming.

2.3.2.2   The Theory by Larson and Garside

Studying the behavior of saturated sugar solutions Larson and Garside [37,38] discovered a serious shortcoming of the classical theory of nucleation, a theory which goes back to Becker and Döring [39]. In this classical theory the assumption is made that the barrier ΔG in the free energy between small enclaves of the new phase and the continuum of the fluid mother phase is a consequence of the surface tension existing between the phases. And the additional assumption was made that this surface tension is independent of the size of the enclave of the new phase. Along this route the mechanism of sporadic primary nucleation has been derived. One obtains for the free energy difference ΔG_r of a spherical enclave:

$$\Delta G_r = \frac{4\pi}{3} r^3 \frac{\rho}{M} \Delta\mu + 4\pi r^2 \sigma. \tag{2.19}$$

In this equation r is the radius of the new phase, ρ is its density, M is the molar mass, $\Delta\mu$ is the difference in the chemical potential of the new and the old phase and σ is the surface tension.

The first derivative with respect to r is zero at $r = 0$ and at the critical value:

$$r_m = \frac{2\sigma M}{|\Delta\mu|\rho}, \tag{2.20}$$

where ΔG_r has its maximum

$$\Delta G_{r,m} = \frac{16\pi}{3} \frac{\sigma^3 M^2}{(\Delta\mu)^2 \rho^2}. \tag{2.21}$$

Only, if r is larger than r_m, such a nucleus can grow, because only then ΔG_r decreases with increasing r. It is important to realize that particles of the new

phase are formed sporadically. And if $r < r_m$, they disappear again as a consequence of the thermal motion. But (2.21) only works if

$$\Delta G_{r,m} \geq kT .\tag{2.22}$$

In fact, if $\Delta G_{r,m}$ is smaller than kT, such a barrier becomes ineffectual. For $\Delta\mu$ the well-known first order approximation in terms of the undercooling ΔT can be introduced. It reads:

$$\Delta\mu = \frac{\Delta H_{tr}}{T_{tr}}\,\Delta T ,\tag{2.23}$$

where ΔH_{tr} is the latent heat of the phase transition and T_{tr} is the equilibrium temperature of this transition. If (2.23) is introduced into (2.21), one obtains:

$$\Delta G_{r,m} = \frac{16\pi}{3}\,\frac{\sigma^3 M^2 T_{tr}^2}{\rho^2\,\Delta H_{tr}^2}\,\frac{1}{(\Delta T)^2} .\tag{2.24}$$

This equation reminds us of (2.15) except for the fact that the square of ΔT shows up in the teller, because of the three-dimensional case represented here.

In Fig. 2.19 the shape of the curve, as described by (2.19), is reproduced as a full line of ΔG vs. r. It is characterized by a slope zero at $r = 0$. However, Larson and Garside pointed to the fact that the said surface tension is not a constant, but decreases with decreasing size of the newly formed particle. This fact has been stressed already quite early by Tolman [40]. Tolman showed that the transition zone of thickness δ between the two phases is responsible. As a consequence, in the second term of (2.19) σ must be multiplied by $f(\delta/r)$, a function, which goes to zero, if the ratio between brackets goes to infinity, i.e., if r goes to zero. Rusli and Larson [41] chose an approximate function.
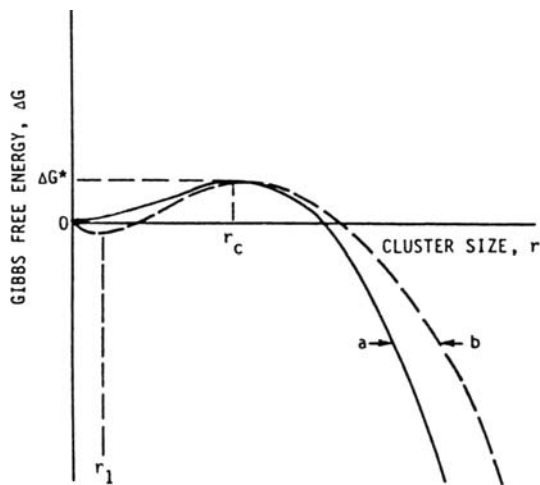
Fig. 2.19 Gibbs free energy of a spherical phase against its radius according to [41]. Courtesy of Pergamon Press

Unfortunately, the parameters of such a function are not known. Nevertheless, qualitatively one obtains the result, which is shown by the dashed line in Fig. 2.19. The conclusion must be that small enough associates should be stable, a fact which could not be explained by the classical theory. Colloid chemists may be grateful for this conclusion. Larson and his collaborators could show that clusters of sugar molecules, but also of ionic substances, are stable in still clear super-saturated solutions.

The implications of this result for an explanation of self-nucleation will be treated in the next section. In prevision of its importance the work of Larson et al. was already quoted in our early review article from 1990 [14].

By the way: From the upper transition in Fig. 1.3 one can estimate an equation for the maximum tolerable undercooling ΔT [42]. One obtains:

$$\Delta T = \frac{1}{3} \frac{\Delta H_{tr}}{C_{p,l}}, \qquad (2.25)$$

where $C_{p,l}$ is the specific heat of the fluid. One can show that this equation is not unrealistic. For the purpose one has to put $\Delta G_{r,m}$ on the left side of (2.24) equal to kT and fill in the value for ΔT from (2.25) together with the known thermodynamic parameters. In this way one obtains an equation for σ, which yields a realistic value. And also: Applying this ΔT one remains above the shaded area of Fig. 1.3.

2.3.2.3   The Role of Local Alignments

There is still another point, which did not get any attention in the discussion, which had been carried on so far on nucleation. This point concerns the local alignment of macromolecules. In rheology Pechhold et al. [43] realized the importance of this phenomenon. However, as the three-dimensional description was impossible, these authors proposed a two-dimensional model. They called it the meander model. However, two dimensions are by far too restrictive. In fact, if a random flight path is drawn in two dimensions on a sheet of paper, a neighboring molecule has to follow a path of almost the same shape, if a high density of lines is required. In this way the authors arrived at their meanders. But also a qualitative consideration of the three-dimensional case can be conclusive. In fact, if one selects an arbitrary macromolecule in a quiescent melt, this macromolecule has a statistical shape. But if one now considers a neighboring molecule, one finds that this molecule cannot have an independent arbitrary shape. At least over some part of its contour it must snuggle to the first mentioned molecule. At other parts of its contour it will snuggle to a third and a forth molecule. In fact, if one prepares a series of stiff wire models of statistical shapes and throws them on a heap, one will never get the high density of a melt. The achieved density will be more that of a gas. The conclusion can only be that the molecules must show a sufficient flexibility, so that they can adjust their shapes like cooked spaghetti. And it will also be clear that there will be alignments of widely differing qualities.

In Chap. 1 (Sect. 1.1) a T,S-diagram has been introduced. In this diagram two transitions are shown (Fig. 1.3). The upper horizontal line indicates the melting temperature of ideal crystals. The level of this line gives the equilibrium melting point. The lower double line gives the range of melting temperatures of spherulitic structures. Above this latter range of temperatures one finds a shaded area, where still stable nuclei have been found. One type of those nuclei are the mentioned nuclei, which are obtained by self-nucleation. However, these nuclei are not the only ones, which are found to be stable above the melting temperature of the spherulites. In stressing this fact, a picture is introduced here in Fig. 2.20, which actually must be discussed in Chap. 3, where the flow induced crystallization will be treated. However, for a valid argumentation this picture is transferred to the present section. It shows the relaxation times of shear induced thread-like precursors, which were obtained in a melt of PP at the temperatures quoted at the abscissa. The applied shear rates (in duct flow) were of the order of 1,200 s^{-1}, with shearing times of ≈0.5 s. The data, which are used in this graph, have a long history. Already in 1989 a pertinent paper was published by Eder, Janeschitz-Kriegl and Krobath [44]. In our first review [14] the quantitative data, as obtained by H. Wippel in his engineer's thesis, were published. Finally, a recollective paper was recently
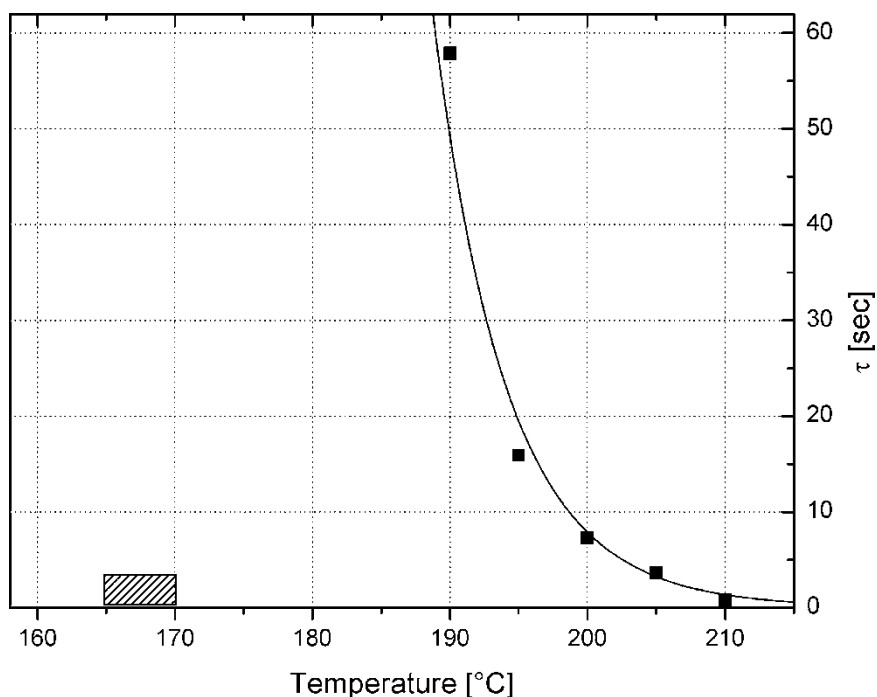
Fig. 2.20 Relaxation times of thread-like precursors versus temperature of shearing and subsequent tempering, as valid for an industrial PP [45]. *Shaded block* on the temperature axis: range of temperatures, where spherulites melt. Courtesy of Taylor and Francis

published by Janeschitz-Kriegl and Eder [45], where the above figure was presented. One notices that the relaxation times tend to go to infinity at temperatures much higher than the temperature, where the spherulites melt. An important point was that the precursors, which apparently were thread-like and produced striped oriented structures after quenching, were so tiny that they had no measurable influence on the flow birefringence, which prevailed during the flow. For the determination of the relaxation times various waiting times were introduced between the cessation of the flow and the quench. With increasing waiting times the oriented structures faded according to a single relaxation time. These facts were already shown in the first paper mentioned. The conclusion is that also these nuclei are stable at temperatures well above the melting temperature of the spherulites.

Interestingly enough, the stability of nuclei does not necessarily mean that they are automatically active centers for growth. Starting with the basic idea of local alignments one must conclude that these nuclei look like fringe micelles. In fact, local alignments cannot be longer than the participating molecules. They will mostly be much shorter. As a consequence one will find so-called tangling ends of molecules on both ends of the regular body of the micelle. Length and thickness of the body of the micelle will be a formal criterion for its orderliness.

If a micelle is very thin, the surface tensions at its side surfaces and, in particular, also on its ends will be very small (according to Tolman and Larson). The latter fact is the consequence of the fact that the tangling ends of molecules have a great freedom in conformation. However, if the conditions for the growth of a lamella are given (see below), this conformational freedom is reduced during the lateral association of other molecules. As the space, which the tangling ends of molecules need in a direction parallel with the growing lamella, is larger than the space required by those parts of the molecules, which are in the body, an effective surface tension is built up during such a growth. The tangling ends get into a squeeze. But this process hampers the growth and will bring it to a halt, if the announced conditions for growth are not sufficiently fulfilled. This is shown schematically in Fig. 2.21.

Because of the apparent importance of this conclusion, also a schematic picture of the dependence of the effective surface tension on the number of associated macromolecules is given in Fig. 2.22.

As a next point the condition for growth must be formulated. As already announced, growth can only happen, when the finally obtained lamella is stable. For this purpose the surface tension in its rough surfaces, where also back-folding can occur in reducing the tension [46], must be borne in mind. In fact, the positive free energy per unit surface at the end of a growing fringe micelle must be in balance with the negative free energy (difference with the fluid), as counted per unit surface at an internal cross-section of the micelle. But, the negative value of the latter free energy depends on the length of the body of the micelle, i.e., on its orderliness. But this means that for a longer micelle the barrier is lower than for a shorter micelle. And there is also the influence of temperature. Whereas the surface tension is not very sensitive to temperature (see the role of kT in rubber elasticity), the internal free energy difference is very sensitive to temperature. (At the equilibrium melting point the latter is zero, whereas the surface tension remains finite!
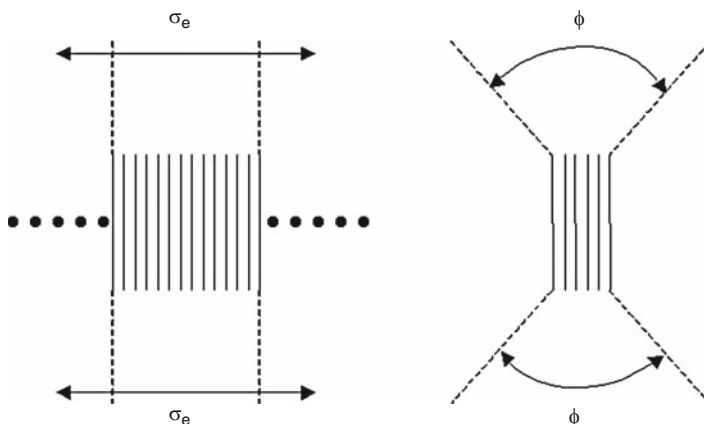
Fig. 2.21 A schematic presentation of the structure (**a**) of a lamella of considerable lateral dimension and (**b**) of a bundle of strands of a lateral dimension insufficient for an effective surface tension σ_e. The freedom of the tangling ends is symbolized for the latter configuration by the cone angle ϕ, according to Janeschitz-Kriegl [57]. Courtesy of Springer
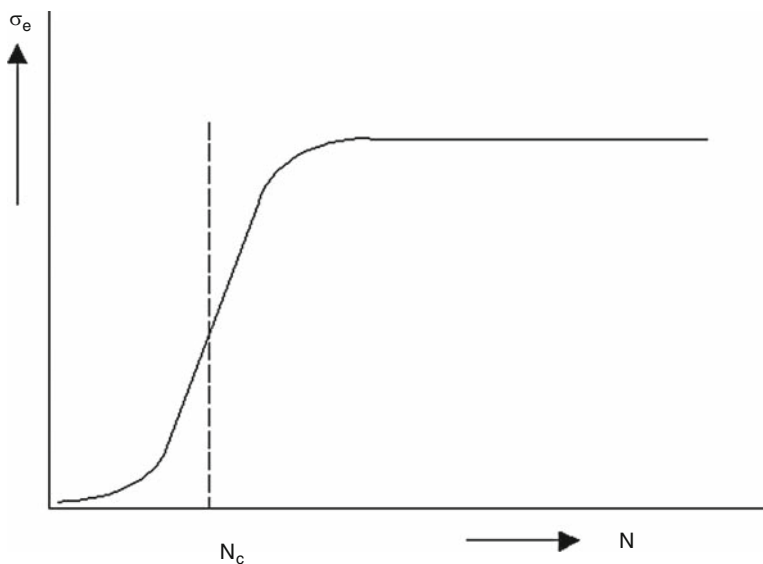
Fig. 2.22 The course of the effective surface tension σ_e, characteristic for the (rough) surface of a lamella, as a function of the number N of laterally associated macromolecules. At a critical number N_c the increase of σ_e will be most conspicuous [57]. Courtesy of Springer

See Janeschitz-Kriegl [42]). But this means that the negative value of the body free energy difference increases seriously with decreasing temperature, so that the barrier decreases rapidly also for those micelles, which are not so well structured. This fact is reflected for PP by the left side of Fig. 1.1, where the number density of

activated nuclei increases by about five decades, if the temperature is lowered from about 130 to 85°C. We are confident that this result also shows the statistical nature of the local alignments. Certainly there must be many more badly structured alignments than well structured ones.

These results lead us to the conviction that the local alignments, which are described above, are transformed into stable athermal nuclei, when the melt is cooled to a temperature below the temperature range, where the spherulites melt. In this connection it is also instructive to follow the succession of events happening during the melting of a spherulite. During this process not only single molecules will be detached. Certainly also whole bundles of molecules will be separated from each other. If these bundles become slim enough, they will be stabilized according to the principles outlined above. In our opinion this is a valid explanation for the self-nucleation effect.

Unexpectedly we received a very well-come support for our ideas by Kornfield and collaborators [47] quite recently. These authors used an ingenious novel technique of levitating a small electrically charged particle of about 1 ng in an electric field. If such a particle changes its weight by – say – absorption of the vapor of a fluid, the increased weight can accurately be determined by adjusting the electric field in order to keep the particle at its original height. The method is called "scanning activity gravimetric analysis SAGA." For the above mentioned purpose the authors exposed a tiny particle of poly(ethylene oxide) PEO to a humidity cyclically varying with time. As PEO is water soluble, the humidity (the activity of water) can take over the role of the temperature. It appeared that at a humidity somewhat higher than the humidity, at which the particle dissolved and formed a clear spherical droplet, nuclei survived in the droplet for hours. The formation of the clear droplet was documented with the aid of the proper light scattering (Mie scattering) and by the increased weight. In fact, when the applied maximum humidity was reduced again, crystallization started at a considerably higher humidity than in a droplet, which had been exposed to a much higher maximum humidity, where the nuclei apparently could not survive. Crystallization was detected by the upcoming turbidity. A survival of hours indicated that there was no kinetic effect at stake. A theoretical interpretation was given in terms of the behavior of a special disk-like lamella.

It remains to be emphasized that the tremendous difference between the equilibrium melting point and the melting temperature of the spherulites, as shown in Fig. 1.3, must be a consequence of the melting point depression caused by the surface tension on the lamellae. And Strobl [48] gave a nice description of the pertinent process. It must also be pointed to the fact that ideal crystals cannot be obtained in a direct way. They have always been obtained in a recrystallization process under high pressure and at temperatures close to the equilibrium melting point, as Wunderlich and also Bassett have shown [49–51]. And this equilibrium melting point has always been obtained in keen extrapolation processes by Hoffman and Weeks and by Marand et al [52,53]. These facts are not surprising. In the temperature interval between the melting temperature of the spherulites and the equilibrium melting point sporadic nuclei must have a stretched conformation

for the formation of ideal crystals, in which the molecules are also stretched. However, in the melt one will not find any molecules, which are completely stretched in a spontaneous conformation. This also explains, why in this temperature range crystallization kinetics are not observable. Only flow can change this situation, as will be shown in Chap. 3.

2.3.3   Winter's Gel Point

Some time ago Winter and Chambon [54] published a fundamental paper on the exact determination of the gel point (of the time elapsing until gelation) of a cross-linking polymer. For their experiments the authors used a polydimethylsiloxane (PDMS). This polymer could be cross-linked in its fluid state at the ends of the molecules with the aid of tetrasilane. In dynamic mechanical measurements the authors found that at a certain stage of the process storage and loss moduli became congruent over a wide range of frequencies. At too early a stage the loss modulus was larger than the storage modulus. After gelation the storage modulus was the larger one. The criterion for the gel point was:

$$\tan(\delta_c) = \frac{G_c''}{G_c'} = \tan\frac{n\pi}{2} = const., \tag{2.26}$$

where δ_c is the loss angle at the gel point and the shear loss and storage moduli, as obtained at this point, are given in the usual notation. And n is a positive constant equal or larger than one half. In order to exploit this criterion, a frequency sweep over at least five decades is required. Of particular interest is the time t_c, which elapses until this gel point is reached. However, for a practical execution this time must be much longer than the time required for the frequency sweep, which largely depends on the lowest frequency required. In fact, within this sweep the properties of the sample should not change to any extent. Later Pogodina and Winter [55] used this criterion also for the gelation of i-PP, as caused by incipient crystallization. The authors found that this time decreased remarkably with decreasing temperature, i.e., with increasing undercooling. However, only low degrees of undercooling were permitted. At larger undercoolings the crystallization process became too fast. Acierno and Grizzuti [56] extended these type of measurements on i-PP down to 135°C. In order to cope with a faster process, they invented the "inverse" quench. For the purpose the sample was kept for some time at the low temperature. The obtained crystallinity was then stabilized by a quick increase of the temperature to 158°C, where kinetics were so slow that an accelerated frequency sweep, making use of the spectrum of harmonics, could be carried out. If the right time was chosen at the lower temperature, the criterion of (2.26) was met at 158°C. The obtained results are shown in Fig. 2.23. One notices that the gel times are extremely large for our terms. Even at the lowest temperature of 135°C ($\Delta T = 56$ K) t_c was almost 1 h (3,500 s).
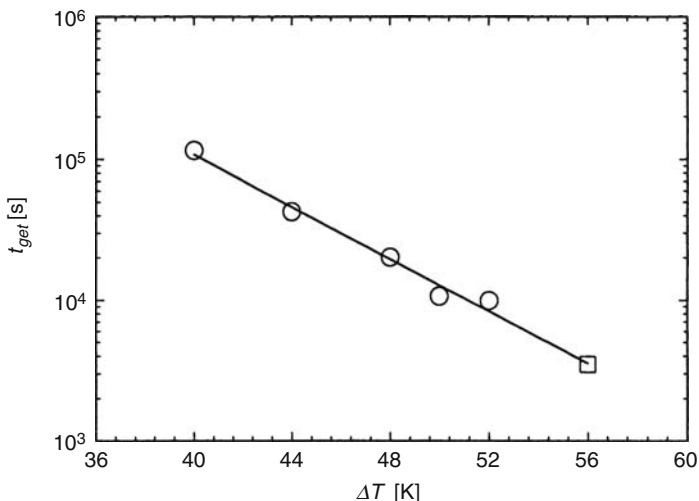
Fig. 2.23 Gel time of i-PP as a function of the degree of undercooling according to [56]. The square symbol was used for the point, which was obtained with the inverse quenching technique. Courtesy of the Society of Rheology

(ΔT is surprisingly large for 135°C, because a relatively high value of 191°C was chosen for the melting temperature of the spherulites). Also, at the gel point the degree of crystallinity is still very low, of the order of a few percent. So far we are not able to lay a connection to our results except for the fact that the cross-links are practically stable at 158°C, a temperature not too far below the melting temperature of the spherulites. This fact is in accord with our vision on the stability of nuclei.

References

1. Van Krevelen DW (1978) Crystallinity of polymers and the means to influence the crystallization process. Chimia 32:279–294
2. Fisher JC, Hollomon JH, Turnbull D (1948) Nucleation. J Appl Phys 19:775–784
3. Janeschitz-Kriegl H, Ratajski E, Wippel H (1999) The physics of athermal nuclei in polymer crystallization. Colloid Polym Sci 277:217–226
4. Braun J, Pillichshammer D, Eder G, Janeschitz-Kriegl H (2003) Industrial solidification processes in polybutene-1. Part I – Quiescent melts. Polym Eng Sci 43:180–187
5. Stadlbauer M, Eder G, Janeschitz-Kriegl H (2001) Crystallization kinetics of two aliphatic polyketones. Polymer 42:3809–3816
6. Chew S, Griffiths JR, Stachurski JH (1989) The crystallization kinetics of polyethylene under isothermal and non-isothermal conditions. Polymer 30:874–881
7. Gandica A, Magill JH (1972) A universal relationship for the crystallization kinetics of polymer materials. Polymer 13:595–596
8. Ratajski E, Janeschitz-Kriegl H (1996) How to determine high growth speeds in polymer crystallization. Colloid Polym Sci 274:938–951

9. Janeschitz-Kriegl H, Eder G, Stadlbauer M, Ratajski E (2005) A thermodynamic frame for the kinetics of polymer crystallization under processing conditions. Monatshefte für Chemie (Chemical Monthly) 136:1119–1137

10. Turner-Jones A, Aizlewood JM, Beckett DR (1964) Crystalline forms of isotactic polypropylene. Makromol Chem 74:134–158

11. Wunderlich B (1973) Macromolecular Physics, vol 1. Academic, London, p 282

12. Lovinger AJ, Chua JO, Gryte CC (1977) Studies of the α and β forms of isotactic polypropylene by crystallization in a temperature gradient. J Polym Sci Polym Phys Ed 15:641–656

13. Janeschitz-Kriegl H, Wimberger-Friedl R, Krobath G, Liedauer S (1987) On the development of layer structures in injected plastic parts (in German). Kautschuk + Gummi, Kunststoffe 40:301–307

14. Eder G, Janeschitz-Kriegl H, Liedauer S (1990) Crystallization processes in quiescent and moving polymer melts under heat transfer conditions. Prog Polym Sci 15:627–714

15. Eder G, Janeschitz-Kriegl H (1997) Processing of polymers: crystallization. Mater Sci Technol 18:269–342

16. Berger J, Schneider W (1986) A zone model of rate controlled solidification. Plastics Rubber Process Appl 6:127–133

17. Stein RS, Rhodes MB (1960) Photographic light scattering by polyethylene films. J Appl Polym Sci 31:1873–1884

18. Keijzers AEM (1967) Light scattering by crystalline polystyrene and polypropylene. Doctoral thesis. Delft, The Netherlands, p 23

19. Keijzers AEM, Van Aartsen JJ, Prins W (1968) Light scattering by crystalline polystyrene and polypropylene. J Am Chem Soc 90:3107–3113

20. Van Antwerpen F (1971) Kinetics of crystallization phenomena of spherulites in poly(ethylene terephthalate). Doctoral thesis Delft, The Netherlands

21. Van Antwerpen F, Van Krevelen DW (1972) Light scattering method for investigation of the kinetics of crystallization of spherulites. J Polym Sci Polym Phys Ed 10:2409–2421

22. Van Krevelen DW (1990) Properties of polymers, 3rd edn. Elsevier, Amsterdam, pp 594–603

23. Magill JH (1967) Crystallization of poly(tetra methyl-p-silphenylene)siloxane. J Polym Sci A2 5:89–99

24. Heijboer J (1968) Study of the movements of cycloalkyl side groups in polymethacrylates by dynamic mechanical measurements. J Polym Sci C 16:3413–3422

25. Ziabicki A, Alfonso GC (1994) Memory effects in isothermal crystallization I. Colloid Polym Sci 272:1027–1042

26. Mandelkern L, Kim H (1968) Temperature dependence of the bulk crystallization rate of polymers. J Polym Sci A-2 6:965–706

27. Hoffman JD (1964) Theoretical aspects of polymer crystallization with chain folding: bulk polymers. SPE Trans 4:315–362

28. Williams ML, Landel RF, Ferry JD (1955) Temperature dependence of relaxation mechanisms in amorphous polymers and other glass forming liquids. J Am Chem Soc 77:3701–3707

29. Hoffman JD, Davis GT, Lauritzen JI Jr (1976) In: Hannay NB (ed) Treatise on solid state chemistry, vol 3, chap. 7. Plenum, New York

30. Clark EJ, Hoffman JD (1984) Regime III crystallization in polypropylene. Macromolecules 17:878–885

31. Van Antwerpen F, Van Krevelen DW (1972) Influence of crystallization temperature, molar weight and additives on the crystallization kinetics of poly (ethylene terephthalate). J Polym Sci Polym Phys Ed 10:2423–2435

32. Mandelkern L (2004) Crystallization of polmyers, vol 2, Kinetics and mechanisms, 2nd edn. Cambridge university Press, Cambridge, pp 1–204

33. Hoffman JD, Miller RL (1997) Kinetics of crystallization from the melt and chain folding in polyethylene fractions revisited: theory and experiment. Polymer 38:3151–3212

34. Lauritzen JI Jr, Hoffman JD (1960) Theory of formation of polymer crystals with folded chains in dilute solution. J Res Nat Bur Stand 64A:73–102

35. Hoffman JD, Lauritzen JI Jr (1961) Crystallization of bulk polymers with chain folding: theory of growth of lamellar spherulites. J Res Nat Bur Stand 65A:297–336
36. Blundell DJ, Keller A, Kovacs AJ (1966) A new self-nucleation phenomenon and its application to the growing of polymer crystals from solution. Polym Lett 4:481–486
37. Larson MA, Garside J (1986) Solute clustering in supersaturated solutions. Chem Eng Sci 41:1285–1289
38. Larson MA, Garside J (1986) Solute clustering and surface tension. J Cryst Growth 76:88–92
39. Becker R, Döring W (1935) Kinetic treatment of nucleation in supersaturated vapour (in German). Ann Phys 5(24):719–752
40. Tolman RC (1949) The effect of droplet size on the surface tension. J Chem Phys 17:331–337
41. Rusli IT, Larson MA (1987) Solute cluster formation in saturated solutions. In: Stratman, Klein, Melis (eds) Cryst Precip Proc Int Symp. Pergamon, Oxford, p 71
42. Janeschitz-Kriegl H (1997) Conditions of nucleation in crystallizable polymers, a reconnaisance of positions. Colloid Polym Sci 275:1121–1135
43. Pechhold W, Hauber MET, Liska E (1973) Meander model of amorphous polymers. Kolloid Z, Z Polym 251:818–828
44. Eder G, Janeschitz-Kriegl H, Krobath G (1989) Shear induced crystallization, a relaxation phenomenon in polymer melts. Progr Colloid Polym Sci 80:1–7
45. Janeschitz-Kriegl H, Eder G (2007) Shear induced crystallization, a relaxation phenomenon in polymer melts: a recollection. J Macromol Sci B Phys 46:1–11
46. Keller A (1957) Single crystals in polymers: evidence of folded chain configuration. Philos Mag 2:1171–1175
47. Olsen AP, Flagan RC, Kornfield JA (2006) Manipulation of athermal nuclei in aqueous poly (ethylene oxide) by scanning activity gravimetric analysis. Macromolecules 39:8419–8427
48. Strobl G (1996) The physics of polymers. Springer, Berlin, p 160
49. Prime RB, Wunderlich B, Melillo L (1969) Extended chain crystals V. Thermal analysis and electron microscopy of the melting process in polyethylene. J Polym Sci A-2 7:2091–2099
50. Bassett DC (1981) Principles of polymer morphology. Cambridge University Press, Cambridge, p 168
51. Woodward AE (1989) Atlas of polymer morphology. Hanser, Germany, pp 106–115
52. Hoffman JD, Weeks JJ (1962) Melting process and equilibrium melting temperature of poly (chloro trifluoro ethylene). J Res Nat Bur Stand A66:13–28
53. Marand H, Xu J, Srinivas S (1998) Determination of the equilibrium melting temperature of polymer crystals: linear and non-linear Hoffman-Weeks extrapolation. Macromolecules 31:8219–8229
54. Winter HH, Chambon F (1986) Analysis of linear viscoelasticity of a crosslinking polymer at the gel point. J Rheol 30:367–382
55. Pogodina NV, Winter HH (1998) Polypropylene crystallization as a physical gelation process. Macromolecules 31:8164–8172
56. Acierno S, Grizzuti N (2003) Measurement of the rheological behavior of a crystallizing polymer by the "inverse quenching" technique. J Rheol 47:569–576
57. Janeschitz-Kriegl H (2003) How to understand nucleation in crystallizing polymer melts under real processing conditions. Colloid Polym Sci 281:1157–1171

Chapter 3
Flow Induced Processes Causing Oriented Crystallization

3.1 Preamble

The investigations in this field started around the year 1970. From the beginning shear flow [1] and extensional flow [2] experiments were carried out. Another classification was with respect to experiments, where flow was continued until the viscosity of the melt started to increase rapidly [1], and those, where the progress of crystallization was followed during flow in a more subtle way by dilatometry [3], by scattering experiments [4] or by a count of upcoming nuclei [5]. In fact, flow can increase the speed of crystallization enormously. Last not least the pioneering work by Van der Vegt and Smit [6] should not be forgotten. With decreasing temperatures these authors observed an increasing obstruction at the entrance to a capillary, which was used for viscometry. The authors correctly interpreted this obstruction as the result of a crystallization starting under the influence of the extensional entrance flow.

Another classification has been with respect to the type of rheometers used. Parallel plate rotational rheometers were often used [3, 4], lately also in [7, 8] (using the apparatus of Linkam Scientific Instruments with glass plates). For high shear rates rectilinear flow is required. In rotational viscometers secondary flow can be very disturbing at high angular velocities. For a suitable rectilinear flow a sandwich construction has been used, where one glass plate moves at a constant distance with respect to another glass plate. [1, 9–11]. A rectilinear flow is also obtained, if a glass fiber is drawn through the undercooled melt [12]. Near the surface of the fiber rather high rates of shear can be obtained.

Also duct flow is of the type of rectilinear flow. Actually in injection molding one has such a situation, if the cavity is a duct of rectangular cross-section of large aspect ratio [13, 14]. However, with injection molding big complications are caused by two facts: the hot polymer melt is injected into a cold mold and, at the beginning, this mold is empty. So, one has a heat transfer problem and the complicated flow pattern at the flow front (the so-called "fountain flow" [15]).

Nevertheless, duct flow experiments can be very useful. A prerequisite is that one starts with an already filled duct, which is cooled down with its content (the sample) from a temperature well above the melting point to the desired crystallization temperature. When this temperature is reached, injection is resumed. No fountain flow occurs in a filled duct. No heat transfer problem exists for the period of flow. Short term shearing is desirable [16]. Of course, the duct must be open at its end. Close to this end windows are placed for an optical observation. It turns out that premature crystallization, which, in principle, seems possible in the still quiescent melt during cooling, is a minor problem. In fact, at not too low temperatures, where flow has already a large effect, kinetics are still extremely sluggish in quiescent melts. These experiments led to the first quantitative interpretation. For the purpose a research group at the CALTECH built a miniature equipment for small samples [17].

3.2   Some Comments of Considerable Reach

As is well-known, the entropy of a rubbery network structure is reduced, if the network is stretched, which means that its free energy is lowered. As a consequence its melting point must increase by stretching [18, 19]. The question is, how far such an effect will also be of importance for flowing polymer melts, in which the macromolecules are also stretched and oriented. However, any theory describing such an effect is necessarily based on a molecular model. Aware of this difficulty the present author discovered that one can actually measure the change of the free energy [20]. In fact, every experienced rheologist knows that the first normal stress difference N_1, as occurring in steady shear flow of a rubber-like liquid, represents twice the stored free energy. Being purely entropic according to all types of molecular theories, this normal stress leads to the equation:

$$N_1 = 2\Delta G = 2T\Delta S_0, \tag{3.1}$$

where subscript "0" stands for orientation. In fact, the said molecular theories always contain extra assumptions in addition to that of the entropic nature of the forces. If the equations

$$T_0 = \frac{\Delta H}{\Delta S - \Delta S_0} \quad \text{and} \quad T_m = \frac{\Delta H}{\Delta S}$$

are combined, one obtains:

$$T_0 = T_m \left(1 + \frac{N_1}{2\,\Delta H} \right). \tag{3.2}$$

Naturally, the free energy stored during shear flow is always much smaller than the heat of fusion ΔH of a phase transition. Moreover, N_1 can be measured. The most convenient way is the indirect way with the aid of the flow birefringence Δn. One has [21]:

$$N_1 = \frac{\Delta n}{C} \, \cos{(2\chi)} = \Delta\sigma \, \cos{(2\chi)}, \qquad (3.3)$$

where C is the stress optical coefficient (as known for many polymers [21]), χ is the extinction angle and $\Delta\sigma$ is the principle stress difference. The latter two parameters hold for the given shear rate. This equation holds for the (1,2)-plane, where direction "1" is the flow direction and direction "2" is the direction of the velocity gradient. The light beam is in the "3" direction in this case. A simpler equation is obtained, if the light beam is in the "2" direction, which means that the birefringence is observed through windows positioned in the large side walls of a rectangular duct (of large aspect ratio). One has in this case of a "slit rheometer":

$$\Delta n = n_{11} - n_{33} \approx C \, N_1. \qquad (3.4)$$

In this equation Δn is an average value (half the value at the duct surface) over the cross-section of the duct.

The use of the constant stress-optical coefficient C justifies also the use of (3.1). In fact, the stress-optical coefficient appears to be constant (at constant temperature) and independent of the molar mass for many polymer melts over three to four decades in the shear rate. In this range the non Newtonian viscosity decreases for some polymer samples by more than one decade (cf. [21], pp. 108–119). But this means that, surprisingly, stress in flow birefringence is clearly dominated by the orientation of chain segments as in rubber. In fact, there is no other reason for – say – stress induced birefringence because of the softness of the melt (see [21], p. 184). There is a simple proportionality factor between the stress and the refractive index tensors of any chain segment, independent of its temporal length (This length should not bee too short, of course). The only condition is that with change of the conformation of the segment its internal equilibration must be fast compared with the changes in contact points with the surrounding. The consequence is that (3.1), which primarily holds for rubber, also holds for flowing polymer melts. In this way, (3.1) is actually underpinned mainly by an experimental evidence. Probably, one can short-circuit this consideration just by assuming:

$$\frac{\Delta n}{C} \approx T\Delta S_0. \qquad (3.4a)$$

For our estimate, however, this does not matter. From measurements, as carried out at the time by Wales and Philippoff [22](see also p. 146 of [21]), one learnt that for the melt of a LDPE the birefringence was about 10^{-4} at a shear rate of one hundred

reciprocal seconds and a temperature of 190°C. From this result it followed with
(3.4) and $C = 2.1 \times 10^{-9}\,\text{Pa}^{-1}$ that N_1 was about $4.76 \times 10^{-2}\,\text{MPa}$. However, for ΔH
(per cubic meter!) of LDPE a much higher value of about 130 MPa is calculated
from the value of ΔH given in the Polymer Handbook [23]. It is now only necessary
to transform the first normal stress difference from 190°C to 110°C. For the purpose
the shift factor for this polymer is required. It is found on p. 37 of the said book [21],
as taken from the work of Münstedt and Laun [24]. From 190 to 110°C a shift over
about one decade is required. To illustrate this procedure, Fig. 3.1 is introduced.
This figure is from the said work of Wales and Philippoff (see also Wales [25]).
Of interest for the present purpose is only the upper line on the right side. It holds
for $n_{11} - n_{33}$ (filled triangles), as obtained with a slit rheometer. (Open squares are
from an extrapolation of cone and plate measurements). If this line is shifted by one
decade to the left, one obtains a vertical distance with the original line
corresponding to a factor three. So one obtains a N_1 of about 0.14 MPa for the
temperature of the flowing melt of the LDPE. This N_1 is less than one thousandth of
the heat of fusion. With a melting temperature of roughly 400 K this means an
increase of this melting temperature about 0.1 K. At decreasing rates of shear this
value decreases in accord with Fig. 3.1. With HDPE the heat of fusion is much
higher than with LDPE. But the elasticity of the melts of HDPE is not much larger.
The conclusion is that under usual experimental conditions an increase of the
melting point will not be of importance.

   This conclusion also holds for polymers with an extra broad distribution of molar
masses. It is true that in such a polymer the molecules of the highest molar mass
carry most of the load and contribute most strongly to the orientation and the
corresponding birefringence of the sample. As Brochard and De Gennes showed
[26], the longest molecules, if taken together, would form a new phase of lower free
energy, which should separate from the mother phase. However, the highly oriented
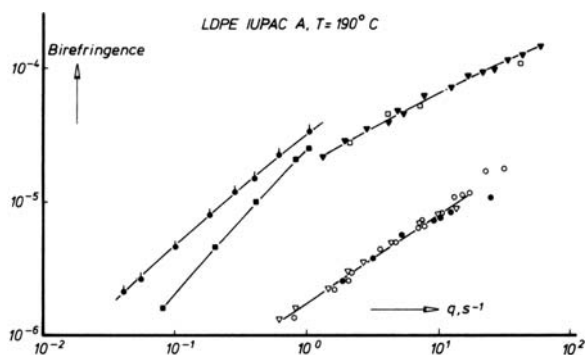
Fig. 3.1 Various types of flow birefringence of a sample of LDPE, as plotted against the shear rate
for a temperature of 190°C [21, 22], Courtesy of Dietrich Steinkopf Verlag. *Upper left curves*:
cone and plate measurements of Δn and $n_{11} - n_{22}$. *Upper right curve*: $n_{11} - n_{33}$ from measure-
ments in a slit rheometer. *Lower curve*: $n_{33} - n_{22}$ from axial capillary measurements, of no
relevance in the present case

molecules are dispersed amongst the large number of short molecules. In a relaxation experiment, the orientation of the short molecule will relax faster, but the still highly oriented long molecules will not get together within their prolonged relaxation because the required self diffusion in a direction perpendicular to the previous direction of the stretch will certainly take more time. In fact, only direct neighboring molecules can participate in the nucleation of a new phase.

This conclusion leads us to the next far reaching comment. As is well-known, with heavy shearing and with extensional flow thread-like precursors ("shishs") are created. After cessation of flow, overgrowths ("kebabs") are formed on these threads. During the period of flow these shishs can reach almost macroscopic lengths well hundredfold the length of a single macromolecule. But many authors make us belief that these threads can be formed by spontaneous association of macromolecules, which are in a state of orientation. However, such a process is unthinkable for reasons similar to those formulated in the last paragraph. There is only one possibility for the formation of these overlong threads. Obviously these threads are formed by a growth mechanism starting at some inhomogeneity (a local alignment?). In fact, if in the direct neighborhood a macromolecule is anchored to the thread, it is "ironed" under the conditions of flow and increases the length of the thread. At the same time the thickness of the thread is not increased very much because of the almost negligible cross-section of the molecule. In this respect longer molecules will be more effective than shorter ones. But these longer molecules do not arrive at the side of the thread by self-diffusion in a transverse direction over a greater distance. They are encountered only sporadically by the thread on its growth route. So to say, they are in its way. By this consideration the principle is upheld that only direct neighbors can be used for the formation of a nucleus.

But it is not only this principal consideration, which is in favor of the idea that long threads can be formed only by a growth mechanism. In a great number of duct flow experiments, as carried out in Linz and characterized in Graz [16, 27], it has been shown that such a growth mechanism offers the only possible explanation for the great total shish length per unit volume. This fact will be elucidated later in this chapter.

In this connection the a priori existence of local alignments is of particular interest. A proper growth mechanism can explain the transformation into more effective nuclei. In fact, at low temperatures one finds a very large number of badly structured alignments, which form only dormant nuclei at the higher temperatures of shearing (see Fig. 1.1). Apparently, these nuclei are improved by the shear treatment. It will also be evident that these nuclei must not necessarily be point-like. During short term flow their length is increased, but has not yet reached a length comparable with their mutual distance. This means that there will still be enough space for the growth of spherulites, which happens as soon as flow is stopped. As has been pointed out in Sect. 2.3.2.3, local alignments must have the shape of fringe micelles. Apparently, these fringe micelles are oriented by the action of the flow, before they grow in axial direction under this influence and become effective nuclei at the higher temperature of shearing. Figure 1.1 is suggestive in this respect. In fact, after flow at higher temperatures the number

Fig. 3.2 Number densities of
nuclei in melts of iPP against
pressure for various
temperatures, unpublished
work (see the text)
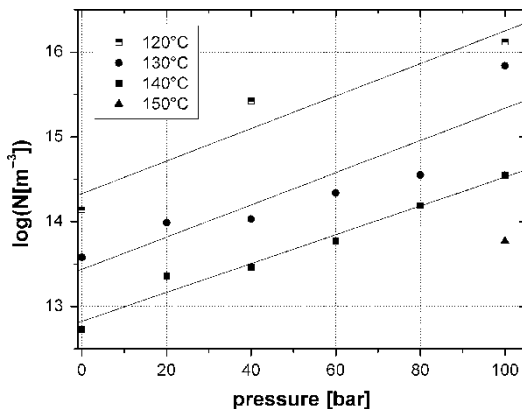
density reaches a level as in the quiescent melt at lower temperatures. Do the same
nuclei show up at the higher temperatures after their improvement?

A similar improvement of the fringe micelles is also suggested by the effect of
pressurization. By the application of about 100 bar the number density of effective
nuclei considerably increases in iPP, as two exchange students (E. Rexhepaj and
R. Vukicevic) have experienced during their (short) stays in Linz. These results are
reproduced in Fig. 3.2. One must assume that the fringes are ironed by the pressure
because of the lower density in their surroundings. Quite old work points to another
growth mechanism of fringe micelles. Boon, Challa and Van Krevelen [28–30]
reported of the following experiment with a melt of isotactic polystyrene: This melt
was first cooled down to the glass transition temperature, where it apparently did
not crystallize. Then it was reheated to various higher crystallization temperatures.
The authors found that the number densities of spherulites was increased in this way
by factors of one hundred thousand, when compared with number densities, which
were obtained, if the samples were directly cooled from the molten state to the said
crystallization temperatures. Apparently, the local alignments have grown by this
procedure so that they became effective at higher temperatures. This is shown in
Fig. 3.3. Also here no orientation effect was at stake. The large effect, as shown in
Fig. 3.3 for the described detour in cooling, should be compared with the large
effect of shearing, as shown on the right side of Fig. 1.1.

The author is tempted to ascribe another badly understood effect to the said
growth mechanism. As reported be Keller and Kolnaar [31], shish-kebabs are
found in stretched network structures. During stretching the shishs appear almost
immediately. The overgrowth (kebab formation), however, which occurs after the
stretching, takes time. Self-diffusion of oriented molecules can be excluded with
such a fast process. But the shishs, which are observable under the electron
microscope, are certainly not represented by single stretched molecules. Close
neighbors must have been aligned.

A further comment fits into this discussion. In one of the above paragraphs short
term shearing was already mentioned in passing. In fact, the technique of short term
shearing (or stretching) has been introduced by us in ref. [16]. It turned out that it
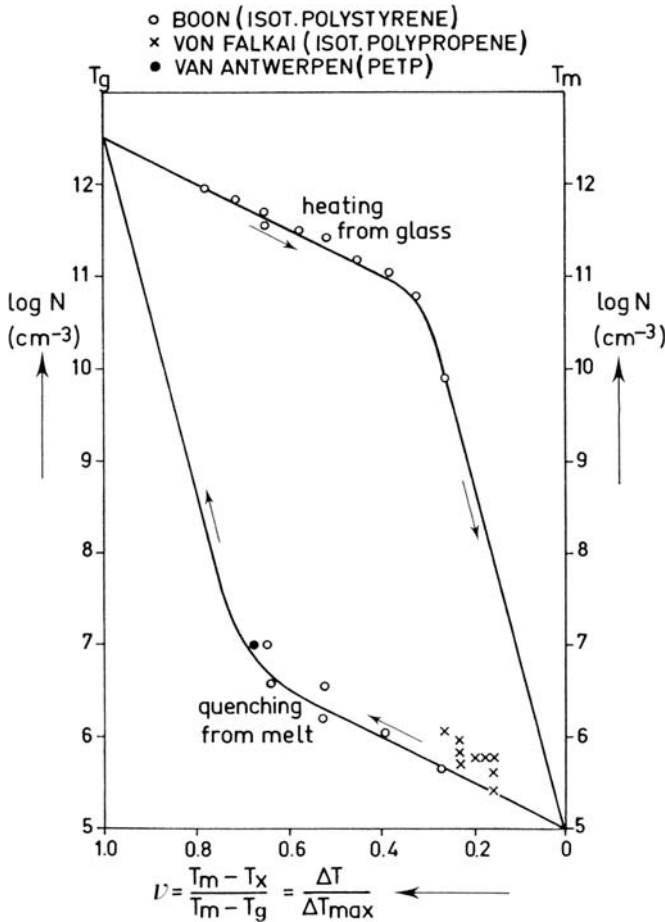
Fig. 3.3 Number densities versus reduced temperature in iPS. *Lower line* is found after a direct cooling to the temperature of crystallization, *upper line* stands for the effect of an intermediary quench to the glass transition temperature [29]. On the *lower curve* one also finds some points for iPP and PET. Courtesy of Brunner Verlag, Zürich

enables us to separate nucleation during flow in an elegant way from the growth process occurring afterwards. The criticism given in Mandelkern's book [32] is not to the point. Mandelkern claims that "chain relaxation dynamics will play an important role in crystallization under these conditions." It is interesting that quite a number of authors succumb to this misconception, as will be shown later. Apparently, none of these authors has ever carried out the necessary experiments. In fact, at Linz we were very early with those experiments. The title of our first paper on this subject of 1989 was: "Shear induced crystallization, a relaxation phenomenon in polymer melts" [33]. In our first review of 1990 this concept was worked out more precisely [20]. This relaxation phenomenon is characterized by a single relaxation time, which increases with decreasing temperature much faster

than the relaxation times of free or entangled molecules (zero shear viscosity). In this connection one should look at Fig. 2.20 of the previous chapter. From this figure one can learn that in the majority of experiments, which were carried out below the melting temperature of the spherulites, the shishs were stable immediately after their formation. We already knew this fact, when we started the experiments, which led us to the results reported in ref.[16]. But this means that "chain relaxation dynamics" do not play any role in these directive experiments. As has been indicated in previous sections of this monograph, also small ("short") nuclei can be considered as stable at temperatures below the melting temperature of the spherulites. There are also strong indications that after shearing the increased number of seemingly point-like nuclei remains constant over long times. In all these cases we apparently have to do with aggregates of a stability surpassing by far the stability of the state of orientation of loose macromolecules. Many details will be treated in the subsequent sections.

In particular, it will become evident that, so far, no valid molecular theory does exist for the said growth processes. In fact, as long as for the quiescent melt the topology of the local alignments remains unexplored, no useful insight can be expected into the much more complex processes occurring under the conditions of flow. Admittedly, a beginning has been made with a treatment of the interaction between neighboring molecules by the introduction of the reptation model [34, 35]. However, as only the average influence of the surroundings is treated in this model, one ends up with the behavior of the singled out molecule. And this result is insufficient for our purpose. This remark seems disillusionizing. However, it is better to face up to the reality than to trust some approaches, which are based on insufficient insight. In this connection it must be emphasized that the orientation of the molecules is a necessary but not a sufficient condition.

3.3 Survey of Activities in the Field of Flow Induced Crystallization

In recent years the number of publications in this field resembles almost an explosion. The early activities are sketched in the preamble. However, when the group at Linz University decided to start in this field in 1983, it seemed as if interest had dropped off. Nevertheless, local interest was pushed by the problems arising in injection molding. In this connection not only the mold filling problems were of importance. As is well-known, those problems arise when a mold of a more complicated shape has to be filled completely. In this respect untimely solidification in narrow passages can play a major role. Under those circumstances low filling rates can be preferable with respect to fast filling. This fact is in contrast to the requirements of heat transfer considerations. But we know that high shear rates and also local extensional flow can shift the temperature of solidification to much higher values. From these experiences it became evident that some quantitative experiments would be helpful any way.

As already mentioned, two main streams have been recognized so far. In Linz we concentrated on the structure development. In this connection not only duct flow experiments should be mentioned. A very simple experiment consists in drawing a glass fiber through the undercooled melt. The processes occurring on the surface of the moving glass fiber can be observed under the microscope, if confining glass plates are used. Other investigators used rotational viscometers containing transparent parallel plates of glass or plates with Beryllium windows for simultaneous X-ray measurements. In the second main stream the samples were kept flowing until the viscosity of the undercooled melts showed an upswing. At first sight one would be inclined to treat the main streams separately and compare the results in a final discussion.

However, many experiments were of a mixed nature. Also the understanding and the planning of the experiments depended strongly on the insights obtained up to those moments of decision. So, in the following the historic development will be followed, even if, as a consequence, sometimes complicated situations have to be unraveled. Being a little immodest we start with the duct flow experiments, as carried out in Linz in the late eighties and in the early nineties. We believe that results obtained with these measurements, namely the first successful phenomenological growth model and the extraordinary relaxation behavior of thread-like precursors, have been decisive for a further development of the field. Only those publications, which have meanwhile turned out to be of real importance, deserve to be quoted.

3.3.1   Duct Flow Experiments

3.3.1.1   Short Term Shearing ("step strain") experiments [16]

For these measurements an ordinary single screw extruder has been adapted. A schematic presentation of the pertinent arrangement is given in Fig. 3.4. There are two essential parts. One of them is the lengthy duct of rectangular cross-section of large aspect ratio. This duct furnishes a practically two dimensional flow pattern, as the influence of the small side walls can be disregarded in the middle of the flow field. Near the end of this duct a pair of glass windows is placed in the opposite large duct walls. Near the entrance a pressure gauge is mounted flush in one of the large side walls. At the entrance a valve is placed. The second essential part is the accumulator. It is mounted on a reservoir, which connects the extruder with the duct. This accumulator consists of a tube with a honed inner surface, in which a plunger fits slidingly. This plunger is loaded over a lever with an exchangeable weight. The choice of this weight determines the pressure in the melt. At the lower end of the accumulator there is a second valve, which serves as a bypass.

With the plunger in a low position the duct is filled in an ordinary extrusion process. During this process the machine is kept as a whole at a temperature well above the equilibrium melting point of the polymer. The required heating is achieved by electric heating bands. Such a heating band is also wound around the
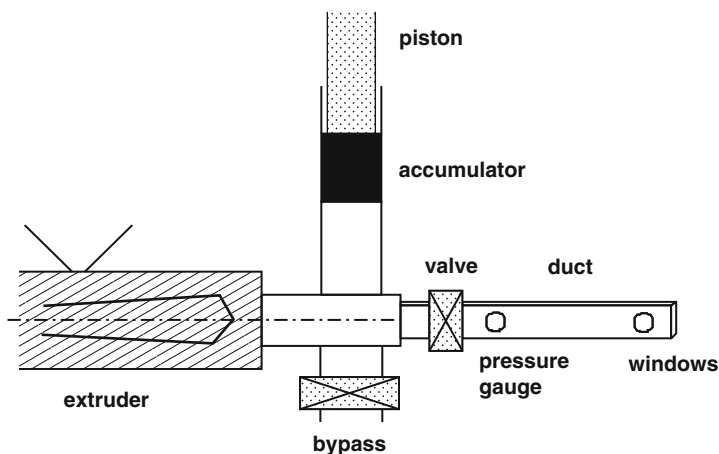
Fig. 3.4 Schematic presentation of the arrangement for the short term shearing experiment [16]. Courtesy of Hanser Verlag

cylindrical outer surface of the part containing the duct. This part consists of two halves enclosing the duct. In a second step the valve at the entrance to the duct is closed and, after a proper relaxation time, which is relatively short for the high processing temperature, the duct is cooled with the aid of a heat transfer fluid, which is pumped through the bodies of the said two halves. In this way the chosen lower temperature of the crystallization is reached with a melt, which does not remember previous maltreatment. At the same time the extruder is switched on again in order to push the plunger up in the accumulator. The experiment proper is started, when the valve at the duct entrance is opened. In this way hot melt of the original temperature is pushed into the cooler duct under the constant entrance pressure guaranteed by the weight on the lever. However, before this hotter fluid reaches the windows, flow must be stopped suddenly. This is accomplished by opening the bypass. Of course, also shorter periods of flow were possible. In these experiments only fluid of the proper crystallization temperature passes the windows. The pressure near the windows remains always low (no pressurization!). The high temperature at the entrance is required mainly in avoiding crystallization in the converging (extensional) entrance flow [6]. After a proper waiting time the duct was quenched to the temperature of tap water and the solidified sample was extracted from the duct. This was a very convenient method for iPP, as the solidified samples of this polymer did not stick to the walls.

Two types of measurements were carried out. One type of measurement, using the windows, was concerned with the course of the optical properties (birefringence, depolarization). The other measurements were carried out on cross-sections of the solidified sample (optical and electron microscopy). In Fig. 3.5 the said optical measurements are demonstrated for an industrial PP with a molar mass $M_w = 289,000$ [20]. The chosen parameters were: $T_c = 150°C$, shear rate at the wall: 84 s^{-1}, shearing time 4 s. Distance from the entrance to the center of the
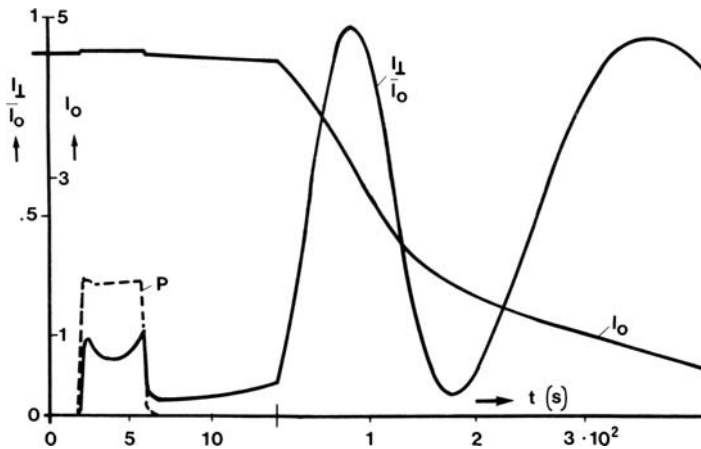
Fig. 3.5 Reduced light intensities versus time, as obtained with crossed polars for a short term shearing experiment on the undercooled melt of an industrial PP, as described in the text [20]. Courtesy of Pergamon Press

windows was 115 mm, cross-section of the duct was 10×1 mm. The box-like pressure profile is demonstrated by the dashed line. The flow birefringence is shown together with this pressure profile. It disappears quickly and almost completely at the end of the pressure treatment. The optical retardation, as caused apparently by the insetting crystallization, is given by the wavy curve. The total transmitted intensity, as normalized by its initial value, decreases continuously with time because of the upcoming turbidity. At 14 s there are kinks in both curves because of a change in the speed of the recorder. The time, when the first peak reaches its maximum, is taken as a measure for the progress of the crystallization. This time gives the moment, when a retardation of half a wave length is reached.

In Fig. 3.6 the continuously measured optical retardations are given as functions of time for a variety of flow conditions, as applied to an industrial PP. Temperature (150°C) and shear rate (108 s^{-1}) were kept constant in this series of experiments. Only the shearing times were varied. They are given in seconds at the ends of the curves. The optical retardations were determined with the aid of the well-known equation:

$$I = I_0 \sin^2\left(\frac{\pi \Gamma}{\lambda}\right), \tag{3.5}$$

where Γ is the retardation, λ is the wave length in the medium, I is the observed light intensity, as obtained with crossed polars, and I_0 is the transmitted total intensity, which is weakened by the turbidity. One notices that even the longest shearing time of 7 s is only 5% of the corresponding waiting times. For the other shearing times one obtains much lower percentages. The shearing times are of a much lower order than the waiting times.
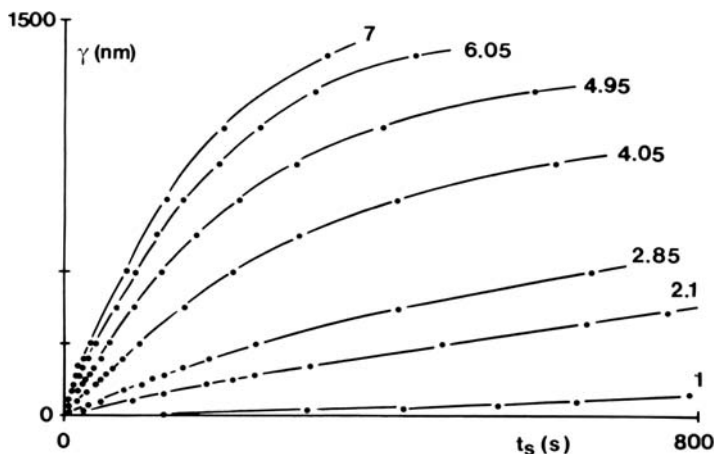
Fig. 3.6 continuously monitored optical retardations as functions of the monitoring time, as obtained with an industrial PP after shear treatments of $108 \, \text{s}^{-1}$ at the duct wall and a temperature of 150°C. Shearing times in seconds are indicated at the respective curves [16]. Courtesy of Hanser Verlag

For illustration a microphotograph, as taken with crossed polars from a cross-section of a solidified sample, is shown in Fig. 3.7. This cross-section was parallel to the previous flow direction and perpendicular to the large duct walls. The conditions of shearing were: a temperature of 150°C, a shearing time of 7 s and a shear rate of $72 \, \text{s}^{-1}$ at the wall. Near the wall a highly oriented zone is shown on this figure. The picture covers a distance of $350 \, \mu\text{m}$ from the duct wall. This picture resembles cross-sections taken from injection molded samples. However, the flow conditions were strictly isothermal and there were no influences of a flow front.

The times, at which a retardation of half the wave length (of $550 \, \mu\text{m}$) was reached, were plotted against the shearing times on double logarithmic scales for three temperatures: 143, 150 and 157°C. In Fig. 3.8 the results for 150°C are reproduced. The steep negative slopes are remarkable. A provisional theoretical consideration suggested the preparation of a set of straight lines on a transparent paper. The slope of these lines was minus two and the vertical distances between these lines were chosen to be four times the logarithm of the ratio of neighboring wall shear rates. This grid was put on the plot of the experimental points in a judgment by the eye. The pertinent wall shear rates are shown near the lines. If the adjustment is accepted, one arrives at the conclusion that the shear treatment is governed by the following surprising combination of variables:

$$q_w^4 \, t_s^2, \tag{3.6}$$

where q_w is the shear rate at the wall and t_s is the shearing time. But a look on the graph suggests that the distance between the lines should even be larger. The corresponding picture for a temperature of 138°C has been shown on several previous occasions. It resembles very much the picture shown in Fig. 3.8. In

Fig. 3.7 Cross-section through a solidified sample of an industrial PP, as obtained after shearing at 150°C for 7 s at a wall shear rate of 72 s^{-1} [16]. Courtesy of Hanser Verlag
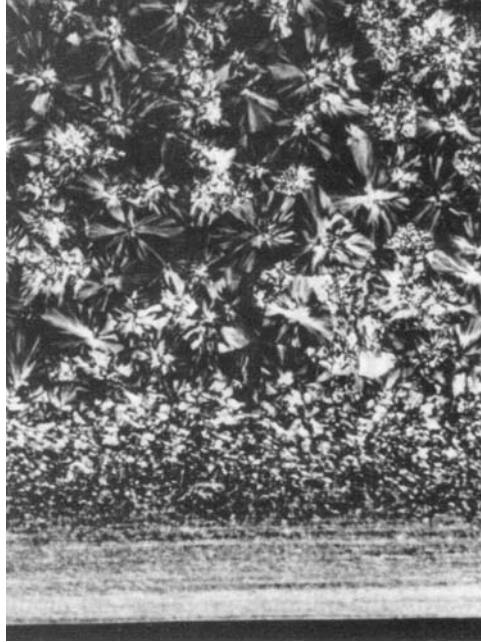
particular also for 138°C the vertical distance between the constructed lines is not big enough.

3.3.1.2   A Preliminary Interpretation of the Results of Section 3.3.1.1

One of the basic principles of such an interpretation is that the process cannot depend on the direction of shearing. But this means that the dependence on the shear rate q must be expressed by an even function of this shear rate. We decided for simplicity to use the square of the shear rate as the simplest even function. (In this connection it may be mentioned that q^2 can also be considered as the second invariant of the rate of deformation tensor). And the forth power of the shear rate, as suggested by the just mentioned experimental results, can only be obtained by the superposition of two processes, which both depend on the square of the shear rate. For the purpose we assumed that in the first process primary nuclei are created spontaneously, whereas in the second process thread-like precursors grow on those primary nuclei. As a consequence the first differential equation reads:

$$\frac{dN}{dt} = \left(\frac{q}{q_{a,n}}\right)^2 g_n - \frac{N}{\tau_n}, \qquad (3.7)$$

where N is a number of nuclei per unit volume, $q_{a,n}$ is a shear rate of activation, g_n is

Fig. 3.8 Double logarithmic
plot of the observation time,
at which half the wave length
of retardation is reached,
against the shearing time for
the mentioned industrial PP.
The belonging shear rates at
the duct walls are given near
the lines. The temperature of
experimentation was 150°C
[16]. Courtesy of Hanser
Verlag
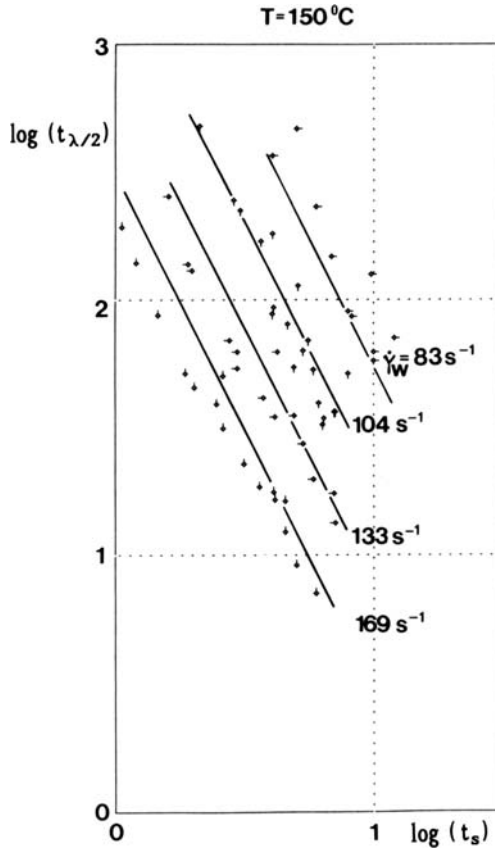
a factor with the dimension $s^{-1}m^{-3}$ and τ_n is a relaxation time. With an initial
condition of $N(0) = 0$ one obtains by an integration of (3.7):

$$N = \left(\frac{q}{q_{a,n}}\right)^2 g_n \tau_n \left[1 \; - \; \exp\left(-\frac{t_s}{\tau_n}\right)\right]. \tag{3.8}$$

If one assumes that the growth of thread-like precursors starts immediately, when
the primary nucleus is born, one can put τ_n equal to infinity and obtains:

$$N = g_n \left(\frac{q}{q_{a,n}}\right)^2 t_s. \tag{3.9}$$

The total length L_{tot} of thread-like precursors per unit volume becomes in this way:

$$L_{tot}(t_s) = 2 \int_0^{t_s} \frac{dN}{ds} L(t_s - s) \, ds. \tag{3.10}$$

The differential equation for the growth of the threads reads now:

$$\frac{dL}{dt} = \left(\frac{q}{q_l}\right)^2 g_l - \frac{L}{\tau_l},$$
(3.11)

where q_l again is characteristic shear rate and g_l is a constant with the dimension $s^{-1}m^{-2}$. As we already know from Fig. 2.20, for iPP the relaxation time τ_l will be of importance only close to the equilibrium melting point. At temperatures below 190°C it will be practically infinitely large. This certainly holds for measurements below 160°C. By integration of (3.10) and (3.11) and initial condition $L(0) = 0$ one obtains:

$$L_{\text{tot}}(t_s) = 2 \frac{q^4}{q_{a.n} q_l} g_n g_l \tau_l \left[(t_s - \tau_l) + \tau_l \exp\left(-\frac{t_s}{\tau_l}\right)\right].$$
(3.12)

Previously this equation was used by us for a more detailed consideration [36]. However, this approach turned out to be unrealistic. If the exponential function is developed in terms of t_s/τ_l, its first term cancels against the first term in square brackets and one obtains a dominating quadratic term:

$$L_{\text{tot}} = g_n g_l \frac{q^4}{q_{a,n}^2 q_l^2} t_s^2.$$
(3.13)

This equation furnishes exactly the product given in (3.6).

Meanwhile we decided that there should be a more adequate even function of the shear rate. We chose for the specific work applied to the sample during the period of the flow. In fact, in shearing experiments the rate of this work is equal to the product of shear stress and shear rate. And in a rubber-like liquid the external (shear) stress determines the degree of orientation, whereas the flow rate (shear rate) is a measure for the probability that oriented molecules meet each other. In our later and more extended experimental investigations on the formation of effective nuclei the specific work appeared to be a very useful parameter. It can replace also the shearing time. In fact, as long as the external stress is constant, this replacement is obvious because of the proportionality between work and time.

In first instance, however, it should be said that our mind was thrown into disorder by the fact that between the number density of primary nuclei and the shearing time no linear relation was found in this later work. But such a linear relation is required by (3.9). A parabola of third to forth grade has been obtained in reality.

At the time we argued as follows: If one of the factors of the product $q^2 = q \cdot q$ is transformed into the shear stress σ, it must be multiplied by the viscosity η, i.e., $\sigma = q\eta$. As long as this viscosity is a constant, which is independent of the shear rate, this viscosity can be concealed in the constant factors g_n and g_l. However, as soon as the non Newtonian behavior of the melt becomes important, this hide-out is no longer permitted. This fact makes the mentioned argumentation shaky.

Admittedly, our "law," as given by (3.13), was obtained by the measurement of the course of the birefringence, which was caused by the overgrowth. These doubts, however, are mitigated by the fact that there is a direct proof for the validity of (3.13). This proof will be given in the next section. In any case this equation corroborates that the total length of shishs per unit volume depends in an unexpectedly strong way on the shear rate.

Postponing further deliberations for later one can say that the given quite rough interpretation of the experimental results leads to a quite useful description of the facts. Within the frame of this description one can say that there is only one adjustable parameter, which is formed by

$$\frac{g_n\, g_l}{q_{a,n}^2\, q_l^2} = f(T, MWD).\tag{3.13a}$$

where MWD means molar mass distribution. And it can be said that the temperature dependence of this parameter appears to be rather small [16]. This fact becomes apparent, if the influence of the growth rate is eliminated from the results of Fig. 3.8 and other figures of this type. This growth rate, which – after cessation of flow – is taken equal to that of a quiescent melt, is well known to be strongly temperature dependent (see Fig. 2.15).

3.3.1.3   Optical and Electron Microscopy [16]

With respect to the optical measurements the first puzzle is the linear increase of the retardation at short waiting times (see Fig. 3.6). In fact, if one would assume the growth of cylindrical bodies around the shishs, one should expect a zero initial slope and a quadratic increase with time, because of the quadratic increase of the surface of cylindrical bodies. But this puzzle is solved by a look on cross-sections through a solidified sample, as cut in a direction perpendicular to the previous flow direction.

In Figs. 3.9 and 3.10 two pertinent pictures are shown, as obtained with the aid of an electron microscope after staining with RuO_4. The pertinent flow data, as applied to the used PP, were a wall shear rate of 72 s^{-1}, a shearing time of 7 s at a temperature of 150°C. Figure 3.9 shows a cross section taken close to the duct wall. This picture covers an 11 μm distance from this wall surface. Figure 3.10 covers an area between 55 and 66 μm from the duct wall.

First of all one notices on both pictures that lateral growth occurred in the quieted down melt along spokes starting at the points, where the shishs pierced through the surface of the cut. This fact can explain the mentioned linear growth of the retardations with time. Secondly, one observes that the average mutual distance between the shishs increases with the distance from the wall.

As in the above theoretical formulation the total length of shishs per unit volume is calculated, one needs a relation between this length and the observed mutual distance between the shishs. As a model for this purpose the unit volume of a stack

Fig. 3.9 Electron micrograph of a cross-section perpendicular to the previous flow direction, covering a distance of $11\,\mu$m from the large surface of the sample. Data for the sample of PP and conditions of flow are given in the text [16]. Courtesy of Hanser Verlag
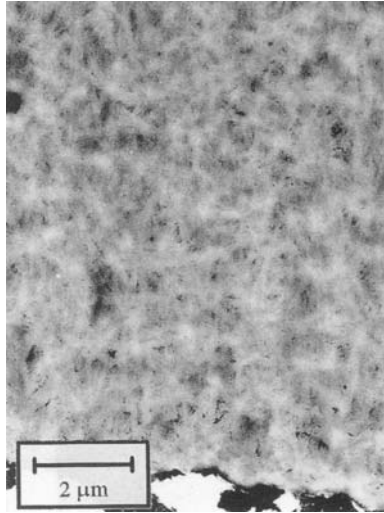
Fig. 3.10 Electron micrograph as in Fig. 3.9, but covering a distance between $55\,\mu$m and $66\,\mu$m from the surface [16]. Courtesy Hanser Verlag
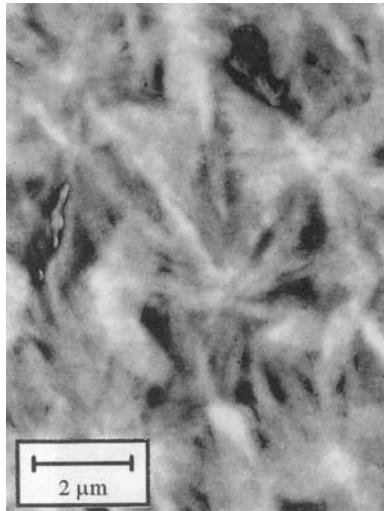
of wooden logs of equal thickness D and of a uniform length of one meter is considered. An easy calculation gives:

$$L_{\text{tot}} = \frac{2}{\sqrt{3}\,D^2} \tag{3.14}$$

(By the way: One should not forget that the dimension of L_{tot} in this equation is correct, because m/m^3 = 1/m^2). Counting is quite difficult on Fig. 3.9. But on

Fig. 3.10 one finds only about 15 points, where shishs pierced through the surface of the cut. The longer side of the picture corresponds with $11\,\mu$m and the shorter side with $8.5\,\mu$m. So one calculates an area of $91 \times 10^{-12}\,$m^2. If one divides this area by 15, one obtains per shish an area of $6.07 \times 10^{-11}\,$m^2. If this area is put into (3.14) instead of D^2, one obtains for L_{tot} an enormous value of $1.9 \times 10^{11}\,$m/m^3.

If for the shear rate profile in the duct the so-called power law is used with $n = 0.33$, one has:

$$q(x) = q_w \left(\frac{2x}{H}\right)^{1/n}, \tag{3.15}$$

where x is the distance from the central plain and H is the duct height. Half the duct height is $350\,\mu$m. If $55\,\mu$m are subtracted, one obtains for distance x from the center $295\,\mu$m. Inserting these values into (3.15), one obtains for the shear rate at $55\,\mu$m from the wall $q(x) = 44.8$ s^{-1}, if the shear rate q_w at the wall is 72 s^{-1}, as quoted above. The forth power of the ratio of these shear rates is 6.5. But this means that on the area of Fig. 3.9. a number of $15 \times 6.5 \cong 98$ points should be found. It is difficult, to carry out a count on this figure, but the order of magnitude of the number of points is certainly correct. A better idea is certainly, to make the two pictures coincide by enlarging Fig. 3.9 properly. The corresponding linear magnification of Fig. 3.9 would be $\sqrt{6.5} = 2.56$. Instead of carrying out this enlargement completely, we decided to reduce Fig. 3.10 by a factor 0.54 and enlarge Fig. 3.9 by a factor 1.4. In fact $(1.4/0.54) \cong 2.6$. This procedures were carried out on both figures. For comparison these figures were turned by ninety degrees. So Fig. 3.11 enables us to carry out a convenient comparison. The conclusion can only be a satisfactory one.

Finally one can say that a direct optical comparison confirms the indirect conclusion, which was drawn from the course of the optical retardations described in the previous section. The total length of shishs per unit volume is surprisingly high. It supports our idea that shishs are created by a systematic growth process and not by the sporadic association of a few perfectly stretched molecules [31], which are particularly long and loosely distributed in space.[1]

---

[1]*Note added at proof:* The present author regrets for having overlooked a decisive paper by a group of Japanese authors with Prof. Kornfield [79]. These authors applied small angle neutron scattering to three special samples of iPP. These samples were mixtures of three fractions of different molar masses. In each sample one of the fractions was Deuterium labeled. Of particular interest was the sample, in which the low molar mass fraction was labeled with Deuterium. After partial remelting the highly oriented surface layer, as obtained after duct flow, the authors found that the same amount of the said low molar mass fraction was present in the surface layer and in the bulk. This means that no selection of the high molar mass molecules has occurred during the crystallization process, which was caused by the flow treatment.

Fig. 3.11 Comparison of the pictures from Figs. 3.9 and 3.10 after proper change of magnifications [16]. Courtesy of Hanser Verlag
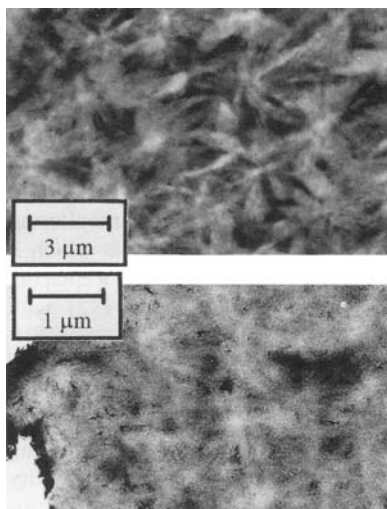
3.3.1.4   More About Structures and a Growth Mechanism

Some years ago the research group at the CALTECH developed a miniature apparatus for short term shearing in duct flow [17]. The purpose of this machine is that small quantities of specially prepared samples can be investigated. In Fig. 3.12 a cross-section through this machine is given. The left part gives a protocol of the working of the machine, if iPP is to be investigated. After what has been said so far, no comment is necessary. The right part is sometimes equipped with Beryllium windows situated near the end of the duct [37]. These windows are necessary for WAXD measurements. The same holds for the conical aperture at the exit of the beam. It enables the recording of a wide angle fiber diagram. The dimensions of the duct are: $63.5 \times 6.35 \times 0.5$ mm^3. The polymer melt is pushed into the duct by a plunger system driven by gas pressure. Maximum throughput is about 100 mg. The X-ray measurements were carried out at the chosen temperature of crystallization (see the left part of Fig. 3.12). As an X-ray source a synchrotron is used with a wave length of $\lambda = 130.7$ pm.

In the first paper of a series of papers [38] visible light intensities were measured through crossed and parallel polars. In this respect the reader is asked to look at the previous Fig. 3.5. On this figure one has to observe the course of the optical retardation, which is found during the period of 5 s, when the pressure was applied. In the beginning this retardation shows an overshoot, which relaxes soon. However, a renewed increase of the retardation is noticed, which does not completely relax, when the pressure is taken off. At the early times, no particular attention was paid to this phenomenon. But the research group of Prof. Kornfield made up for this omission. It was observed by this group that the formation of thread-like precursors ("shishs"), which apparently happened during the period of flow, was linked to this renewed upswing of the retardation.
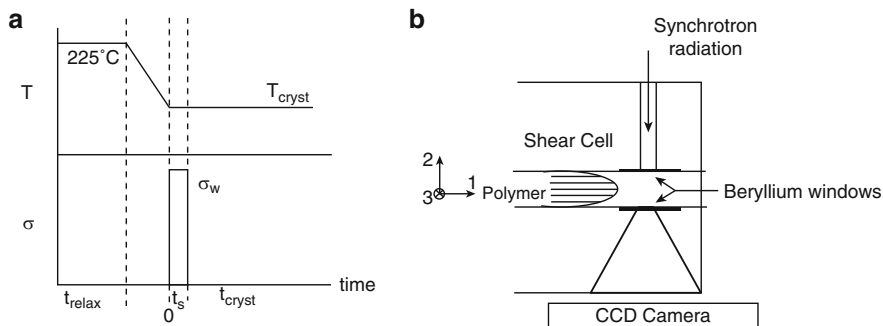
Fig. 3.12 Schematic presentation of the shear unit [37]. A description is given in the text. Courtesy of Elsevier
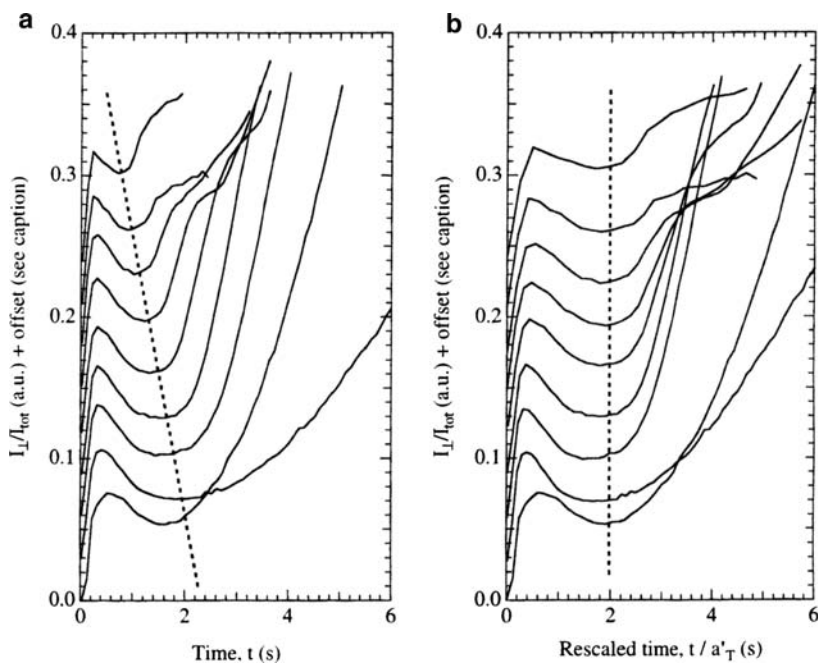
Fig. 3.13 Reduced light intensities through crossed polars, as obtained during shearing of an isotactic PP at a fixed shear stress of 0.06 MPa and a series of temperatures. These temperatures were 135–175°C in intervals of 5°C, starting at the bottom [38]. Courtesy of the American Chemical Society

The said authors produced an extremely interesting graph, which is shown in Fig. 3.13. It consists of two parts. On the abscissa of both parts only the time t_s, which elapses during shearing, is plotted. On the ordinate axes the reduced light intensities $I_\perp/I_{tot}$, as obtained through crossed polars, are plotted as in Fig. 3.5. All measurements were carried out at a shearing time of 5 s and at a fixed shear

stress of 0.06 MPa. For clarity the curves are vertically offset. Otherwise they would be too close to each other. The curves represent measurements taken at the following temperatures: 135, 140, 145, 150, 155, 160, 165, 170 and 175°C, starting from the bottom. Only at the highest temperature of 175°C the birefringence relaxed completely after cessation of the flow. The left figure shows a seemingly absurd result: The higher the temperature was, the faster occurred not only the relaxation of the overshoot but also the growth of the renewed retardation. In the right graph the time axis is rescaled according to the time–temperature superposition principle [39]. For the purpose the times t_u, at which the lowest points of the curves were reached, were divided by a temperature dependent shift factor a'_T, so that all minima occurred at the same reduced time t_u/a'_T (see the right part of Fig. 3.13). And the course of this shift factor agreed practically with the course of the shift factor a_T^{WLF} of iPP according to ref. [39]. This is shown in Fig. 3.14. This result rightly caused the authors to choose "Evidence of a kinetic pathway to nucleation" as a subtitle of their paper.

However, at this point the present author would like to add a comment. The shear rates at the duct wall, which are not mentioned in the papers from the CALTECH (because of the uncertainty in their determination), do nevertheless play a qualitative role. These shear rates certainly increase with the experimental temperature, if the shear stress is kept unchanged. The argumentation of the present author is elucidated in Fig. 3.15. For simplicity a two dimensional sketch is prepared. In this picture attention is paid to the behavior of a small fraction of particularly long molecules, which are strongly oriented and highly stretched during shearing. In fact, experience teaches us [31] that those long molecules play a prominent role in the formation of thread-like precursors. With three blobs
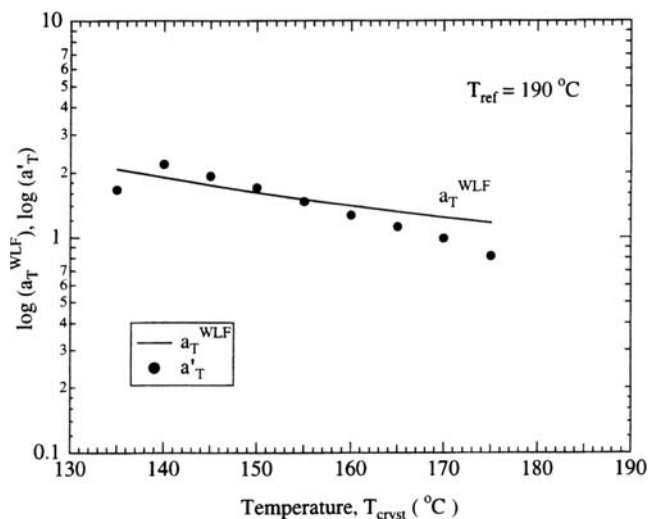
Fig. 3.14 Comparison of the shift factor a'_T for t_u (*filled circles*) with the shift factor a_T^{WLF} (*solid curve*) for iPP [38]. Courtesy of the American Chemical Society

Fig. 3.15 A sketch of the circumstances, which are relevant for association of macromolecules to aggregates in a shear field. For an explanation see the text
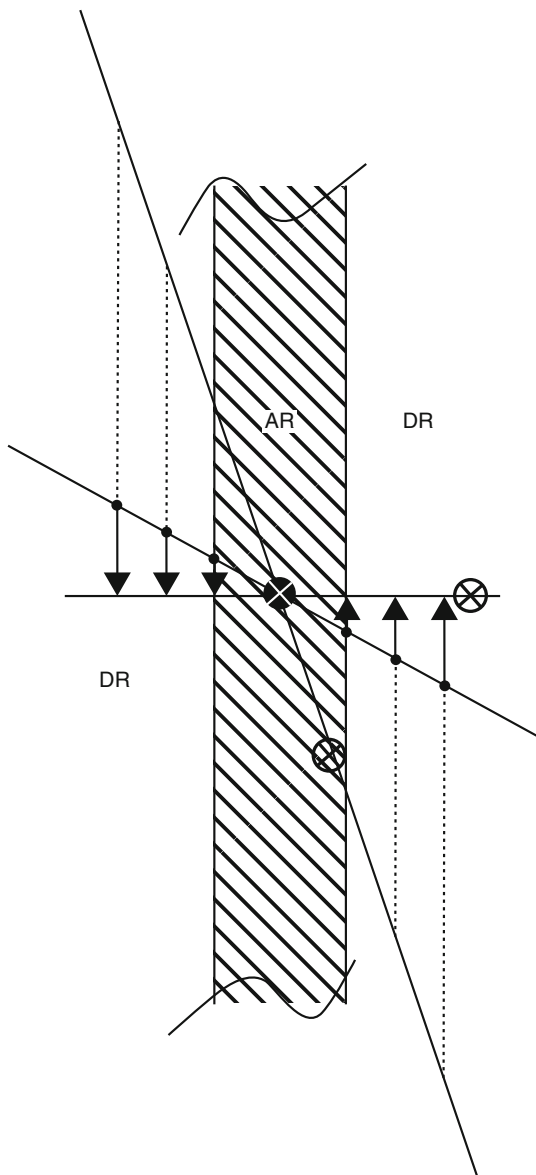
the centers of two long macromolecules and an aggregate (local alignment) are
given. At the center of the aggregate the relative flow profiles are sketched for two
shear rates, a smaller one and a larger one. The centers of the two long macro-
molecules are drawn at equal distances from the center of the aggregate. The
corresponding vectors, however, point into very different directions. With the
distance between two straight lines, which are drawn parallel to the flow direction

on either side of the aggregate, the transverse bounds are indicated of the critical contact region, within which a stretched macromolecule can touch the aggregate, when passing by in the flow direction. Obviously the contact region of the aggregate is most important. In Fig. 3.15 this region is indicated as the association region AR. The field outside this region AR may be called the disentanglement region DR. In fact, a macromolecule, which passes by with its center somewhere in DR, will never touch the central aggregate. If such a molecule reaches the upper right quadrant of Fig. 3.15, its distance to the said aggregate will increase without bounds to infinity. In fact, it seems quite realistic if one assumes that in the average all molecules continue to move parallel to the flow lines. Entanglements will tug on all sides, before they break. Complete disentanglement will be the consequence. The higher the shear rate is, the more partners will be brought up in AR during a certain time span.

The reader may now understand, why the rate of specific work has been introduce by the working group at Linz University. To say it again: the shear stress is a measure of the orientation and the shear rate is a measure for the frequency of encounters. And the product of both is the rate of applied specific work. So, the conclusion must be that the increase of the growth rate of shishs with increasing temperature, as observed in the left part of Fig. 3.13, is a consequence of an increase of the rate of specific work with temperature. Moreover, because of the relative stability of the formed aggregates the increments of total specific work, as applied during an arbitrary time span are simply additive. Only at temperatures well above the melting temperature of spherulites the stability of the aggregates seems to decrease. The relaxation times of aggregates will be discussed extensively in a later section (cf. Fig. 2.20). However, it must be recognized that at lower temperatures the role of the integral specific work can be considered as accepted. But this does not mean that the proper proportionality factors are also found. One should not think that the results of existing molecular theories, which are exclusively based on the orientation of singled out molecules, can solve these problems.

Returning to the experiments at the CALTECH further important results must be mentioned [40, 41]. The authors carefully prepared mixtures of two polypropylenes of extremely different molar mass distributions. For one case these distributions are shown in Fig. 3.16. The sample of the lower average molar mass formed the basic polymer. The high molar mass sample of particularly narrow molar mass distribution was added in small quantities. It was prepared by fractionation. The samples were first dissolved in xylene at $141°C$, where the mixing occurred. The mixtures were precipitated in methanol and dried. So, no mechanical degradation of the high molar mass molecules occurred during the mixing. Against oxidation the samples were protected by an antioxidant.

For the high molar mass fraction the overlap concentration of the coils was calculated according to De Gennes [42]. For this fraction an overlap concentration of 7×10^{-3} g cm^{-3} was calculated. In Fig. 3.17 the reduced light intensities $I_\perp/I_{tot}$, as obtained during flow and, in continuation, also after cessation of flow, are given as functions of time for various concentrations of the high molar mass fraction. These concentrations were in g cm$^{-3} \times 10^{-3}$: A: 0.00, B: 1.76, C: 3.51, D: 7.00,

Fig. 3.16 Molecular mass
distributions of the fraction of
iPP [41]. Courtesy of the
American Chemical Society
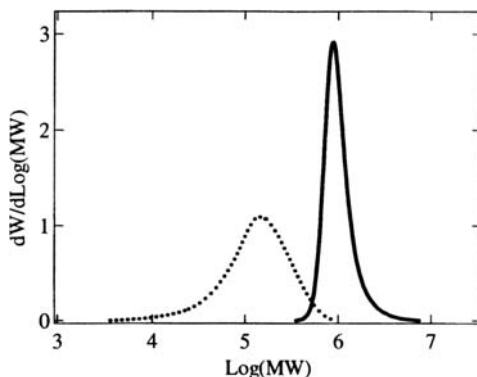
D: 13.9. The shear stress applied was always 0.14 MPa and the temperature of the experiments was 137°C. Near the curves one finds the shearing times in seconds and the throughputs in milligrams. In parts A, B and C one notices almost no influence of the increasing number of long molecules. In part D, however, at the critical concentration of the overlap, one notices a considerable shift of the maxima to shorter times. This is true at least, if the throughput is equal or higher than 0.75 mg. For twice the overlap concentration (part E) this effect is even more pronounced. The heights of the maxima were also greater, which should point to an increased transparency. The authors emphasize that a sharp increase of the crystallization speed, as found at the overlap concentration, points to a cooperative effect of the molecules: The orientation of singled out molecules does not explain this behavior. This statement is very satisfying for the point of view of the present author. The fact that the lowest throughputs do not follow this trend, may be explained by a too small specific work. This should point to the building up of a threshold, as the present author would see it in terms of the specific work.

The authors of [41] also found another very interesting fact: The undiluted high molar mass polymer did not produce a highly oriented zone near the duct surface. In this respect this high molar mass polymer behaved like the low molar mass polymer. The explanation was that, in contrast to the mixtures, the load was not concentrated on the few long molecules but homogeneously distributed over all molecules, so that the degree of orientation of single molecules remained low.

In [37] a WAXD study is presented. The result, which seems most impressive to the present author, is shown in Fig. 3.18. A sample of iPP with a weight average molar mass M_w of 300,000 gmol^{-1} and an M_w/M_n of 6–8 was investigated. The melt of this polymer was subjected to short term duct flow. As a high energy X-ray synchrotron source was used (of a wave length of 130.7 pm), a fiber diagram could already be obtained before the end of shearing. The details of this treatment are given in the caption to the figure. Interestingly enough already after a flow time of only 10 s (at a wall shear stress of 0.06 MPa and a temperature of 141°C) a complete fiber diagram for the α-crystal modification was obtained. After cessation of flow this diagram remained unchanged during a waiting time of as much as 1,200 s.
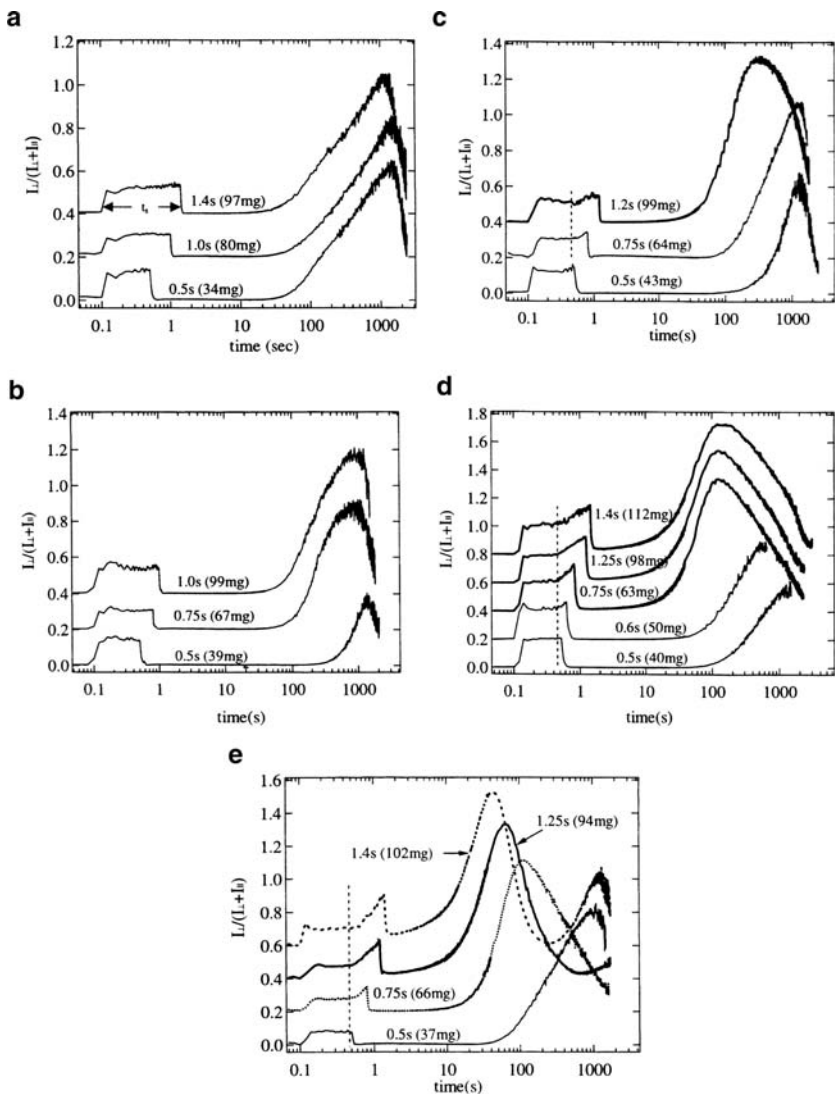
Fig. 3.17 Relative light intensities ($I_\perp/I_{tot}$) through crossed polars during and after short term shearing at a shear stress of 0.14 MPa and at a temperature of 137°C. These intensities are plotted against time for the samples A through E, which contain an increasing amount of the high molar mass fraction [41]. Observe the offsets in times and intensities. Courtesy of the American Chemical Society

As the interior of the sample experienced lower stresses (and much lower shear rates in a velocity profile approaching plug flow – because of the non Newtonian behavior of the melt!), the crystallization apparently did not progress very much in the interior during these 1,200 s at 140°C. Otherwise a diagram without any indication of orientation would prevail because of the overwhelming thickness of
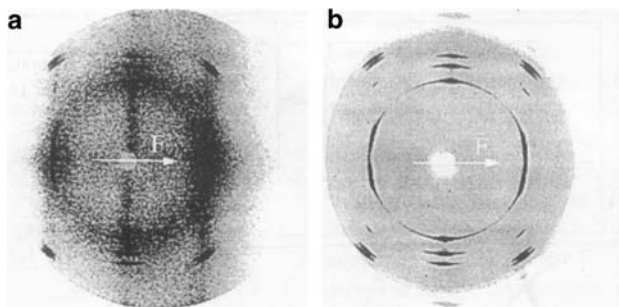
Fig. 3.18 In situ fiber diagrams, as obtained on a sample of iPP, when crystallized under shear ($T = 141°C$, $\sigma_w = 0.06$ MPa, $t_s = 12$ s). The flow direction is horizontal. (**a**) is obtained by acquiring data for 10 s during the period of shearing, (**b**) is the diffraction pattern obtained after 1,200 s during an acquisition time of 40 s. The data have been normalized for the acquisition time [37]. Courtesy of Elsevier

the bowel of the sample. In fact, the sample was quenched after a little more than 1,200 s. On a cross-section it was found that the highly oriented surface layer was only very thin. Apparently 1,200 s are much too short at 140°C for a space filling spherulitic crystallization in the practically quiescent part of the melt (see the extremely low nucleation densities and growth speeds, as shown in previous Figs. 1.1 and 1.2 for quiescent melts of iPP near 140°C).

The authors of [40] and [41] arrived at a series of important conclusions:

(a) The formation of thread-like precursors (shishs) is a cooperative process, in which several molecules take part.
(b) Long molecules greatly enhance the growth of thread-like precursors, but only mildly enhance the formation of nuclei, from which threads can grow.
(c) The total length of threads per unit volume increases up to a saturation value.
(d) For concentrations of the high molar mass fraction below the overlap concentration one can observe the finite lengths of single threads with the aid of TEM. Most threads were less than $20\,\mu m$ long.
(e) The abrupt transition between the skin layer and the spherulitic core provides a measure for the threshold stress of ≈ 0.12 MPa, which hardly varies with the concentration of long molecules.
(f) The highly oriented skin layer contains also many short molecules. In fact, the concentration of long molecules has been too small in the bulk for filling the space within the skin layer.
(g) Threads do not tumble because of growing continuously. And also, for slender particles the tumbling period increases strongly with their length, as Jeffrey has shown [43].

Probably, a few comments should be added to this list. The transition between the skin layer and the core has not always been so abrupt as in the work of the CALTECH group. Our experience with an industrial polypropylene was that at lower extrusion speeds only a fine grained layer was found near the wall, at medium

speeds a highly oriented layer existed close to the wall, more inwards taken over by a fine grained layer, on which the spherulitic core followed in the middle. At sufficiently high extrusion speeds there actually was only an abrupt transition from the highly oriented skin to the spherulitic core. It will not be easy to explain these facts. We tried hard [36], but we no longer believed in our theoretical approach. With respect to the addressed absence of the tumbling one may add that with short term shearing the region close to the wall undergoes something like a planar extension, during which tumbling hardly can be expected.

Duct flow experiments appeared to be particularly useful for the creation of highly oriented structures. As just mentioned, however, sometimes also fine grained structures were found. Our cooperator Liedauer was lucky to take some beautiful photographs. On one of them a clear boundary could be observed between a highly oriented skin layer and a fine grained layer underneath [36]. This picture is reproduced here as Fig. 3.19 for the following flow conditions: $T = 150°C$, $q_w = 68$ s^{-1}, $\sigma_w = 0.055$ MPa, $t_s = 15.6$ s. Interestingly enough, from the point of view of the shear stress there was only a small gap from $\sigma_w = 0.033$ MPa to $\sigma_w = 0.078$ MPa, within which the transition occurred from an exclusively fine grained surface layer to an exclusively highly oriented skin layer. (For these extreme situations the shear rates at the wall and the shearing times were 19.7 s^{-1}, 39.3 s and 169 s^{-1}, 2.45 s, respectively. In the CALTECH work a critical shear stress of about 0.12 MPa was obtained, which clearly lies above our bounds). The pity with all these experiments is that the applicable shearing time necessarily decreases with increasing shear stress and shear rate. As a consequence it becomes very difficult to discern between the exclusive influence of the shear stress and the influence of the integrated specific
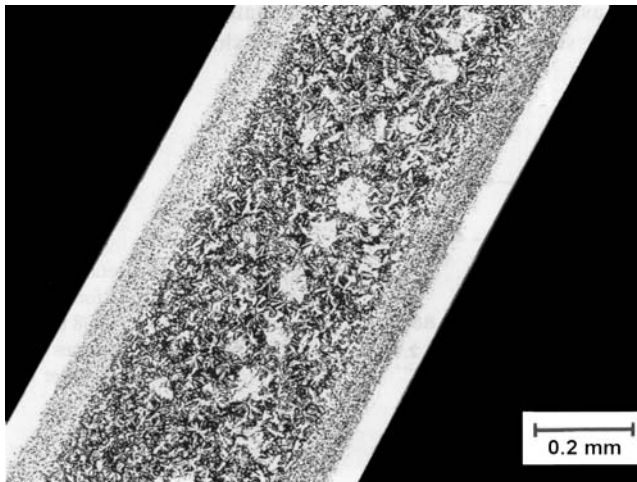
Fig. 3.19 Cross-section through a sample of PP ($M_w = 322,000$, $M_n = 47,000$) after short term shearing in a flat duct for 15.6 s at a temperature of 150°C with a shear rate of 68 s^{-1} and a shear stress of 0.0553 MPa, both at the large duct wall [36]. Courtesy of Hanser Verlag

mechanical work as a whole. In fact, this work increases linearly with the shearing time, which becomes shorter and shorter with increasing shear stress.

In the above paragraph shear stresses and shear rates, as occurring at the large duct wall, where quoted for the PP used in Linz. However, the reader, who wants to check these results, needs the rheological equation of state, which has been used for the purpose. Before giving this equation, which actually holds only for the steady state, one has to explain, why this equation is useful nevertheless. There is a rule of thumb. According to this rule steady state is reached in shear creep experiments after a total shear of about 5 units. But the total shears are much larger in the present case. The pertinent equation, which is ascribed to Carreau [44], reads:

$$\sigma_w = \frac{\eta_0 \, q}{\left[1 \; + \; (\lambda \, q)^m \right]^{\frac{1-n}{m}}}. \tag{3.16}$$

The data for 150°C are: $\eta_0 = 21{,}380$ Pa.s, $\lambda = 1.8$ s, $m = 0.537$ and $n = 0.34$.

3.3.2   Flow Induced Small-Sized ("point-like") Nuclei

3.3.2.1   Rectilinear Shearing Between Glass-Slides

One of the difficulties with duct flow is the marked change of the shear rate with increasing distance from the duct wall. The shear stress does not change so rapidly with this distance. This fact is due to its linear dependence on the distance from the central plane, which follows from the simple demand that forces must always be in balance. In contrast, the rheological behavior of the melt is reflected by the dependence of the shear rate on the distance from the central plane.

In order to escape this dilemma, the use of a sandwich construction was introduced at Linz University. For the purpose two glass slides are used as confining parallel plates. Both plates have a length of 15 cm and a thickness of 0.2 cm. The width of the lower plate is a little larger, namely 3 cm. A sheet of the polymer ($6 \times 1 \times 0.1$ in centimeters) is sandwiched between these plates and sheared after a proper heating cycle over maximal 5 cm. In this way a maximum shear of 50 units can be obtained. On both sides of the polymer sample Teflon strips of 0.1 cm thickness are inserted. A proper, slightly lubricated weight secures the contact between the polymer and the confining surfaces. The minimization of friction in the driving system is a delicate matter. With the application of high shear stresses one has no problems. The upper plate is set going by a piston, which moves in a pneumatic cylinder connected to an air pressure system. As the sheared surface decreases from 6 to 1 cm during the full movement of 5 cm, the force must be reduced for keeping the shear stress constant. In fact, the polymer melt behaves more like a fluid than like a rubber. A mechanical device serves for a proper counter force increasing with the distance, over which the upper plate is shifted. This device, which is loaded with a proper weight, actually keeps the shear stress practically constant. The sandwich is embedded in a chamber,
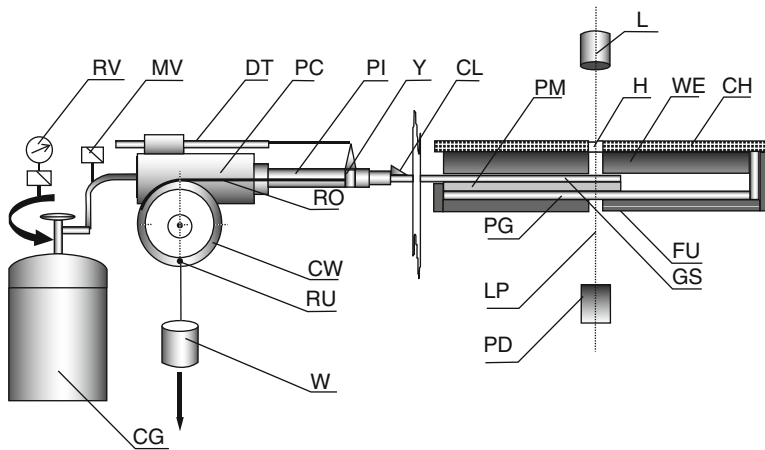
Fig. 3.20 Shear unit, as used in Linz. PM: polymer melt, PG: bottom plate of glass, GS: glass slide, FU: furnace, CH: cover with heating elements, WE: weight, H: holes, LP: light path, L: laser, PG: photo diode, CG: steel cylinder for pressurized gas (diminished graphic reproduction), RV: reduction valve, MV: magnetic valve, PI: piston, DT: Displacement transducer, CL: clamp, Y: yoke (perpendicular to the plane of the drawing), RO: pair of ropes (one in front and the other behind the cylinder), CW: pair of coupled cart wheels (behind each other), as mounted firmly on their common axle, RU: rung connecting the wheels, W: adjustable weight [10]. Courtesy of Springer Verlag

which can be heated and cooled properly. Glass plates are preferably used because of their transparency. A light beam can pass through the glasses in every position. So the optical retardation can be determined during flow and afterwards. In Fig. 3.20 a drawing of this machine is presented.

The mentioned mechanism (see the cart wheels, the yoke and the ropes) modifies the force on the upper glass slide in the following way:

$$F_{\text{red}} = P \cdot A \, - \, Mg \, \sin(\alpha), \tag{3.17}$$

where P is the gas pressure, A is the area of the piston in the pneumatic cylinder, M is the adjustable mass of the weight, g is acceleration of gravity and α is the angle, by which the rung is turned away from its lowest starting position. If the radii of the cart wheels is large enough, one has approximately $\sin(\alpha) \approx \alpha$. This means that the required linear dependence of the counter force on the applied shear is readily realized. Smaller total shears than the maximum shear of 50 can be realized, if the starting position of the piston is chosen more closely to the shear unit, where the piston is stopped in any case.

The shear stress can readily be determined with the aid of (3.17). If this shear stress is multiplied by the obtained total shear, one obtains the reduced mechanical work applied. In Fig. 3.21 some results, as obtained with this machine, are shown. One notices the extremely short shearing times, which are realized for total shears of 20, 30, 40 and 50.
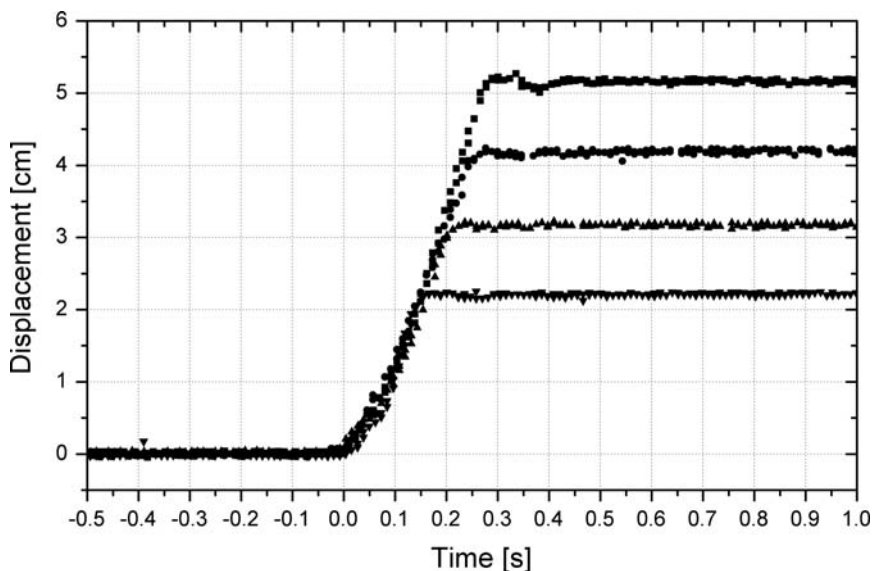
Fig. 3.21 Piston displacements vs. shearing times for the melt of an industrial PP at a shear stress of 84 kPa, for increasing total shears between 20 and 50 units and at a temperature of 145°C. The shear rate common to all curves can be estimated to be 150 s^{-1} [10]. Courtesy of Springer Verlag

Avoiding the influence of friction one can also calculate the applied specific work. For the rate of specific work one has $\eta \cdot q^2$, where q is the shear rate, which can be read from the graph (see Fig. 3.21) and $\eta(T,q)$ is the viscosity of the melt at the temperature and the shear rate of the experiment. Mostly one can rest content by multiplying the mentioned rate of specific work by the time of shearing in order to obtain the total specific work applied. If the shear rate should change too much, one could introduce an integral over the time.

After the shearing process the sample is kept at the temperature of shearing, until total depolarization is reached. This depolarization is indicated by the fact that the reduced intensities, which are obtained through parallel and crossed polars, both reach a value of one half. At the same time the total intensity goes nearly to zero. When the shearing time at 145°C was 0.25 s, the waiting time to total depolarization took about 100 s. This is a remarkable difference. After this stage was reached, the samples were quenched to room temperature and removed from the apparatus. Cross-sections were made parallel and perpendicular to the flow direction (in the 1,2 and in the 2,3 planes). With this machine no highly oriented structures could be achieved. The number of spherulites, which were cut per unit surface, was raised to the power 3/2 for an estimate of the number densities of nuclei, in analogy to the method applied on samples solidified from quiescent melts. In this way the data were obtained, which led to the right side of Fig. 1.1, where the logarithms of the number densities were plotted against the specific work. Remarkably, at relatively high temperatures these number densities reached the same level as the number densities, which were obtained after quenches of quiescent melts at much lower

temperatures. By the way, shearing at those low temperatures was not useful because of the badly defined initial conditions. In fact, a complex machine as the one shown in Fig. 3.20, cannot be quenched fast enough.

Before the results, as obtained in these shearing experiments, will be discussed in more detail, a particularly interesting feature of this shearing experiment will be demonstrated in Fig. 3.22 [11]. In this figure two diagrams are shown. The upper
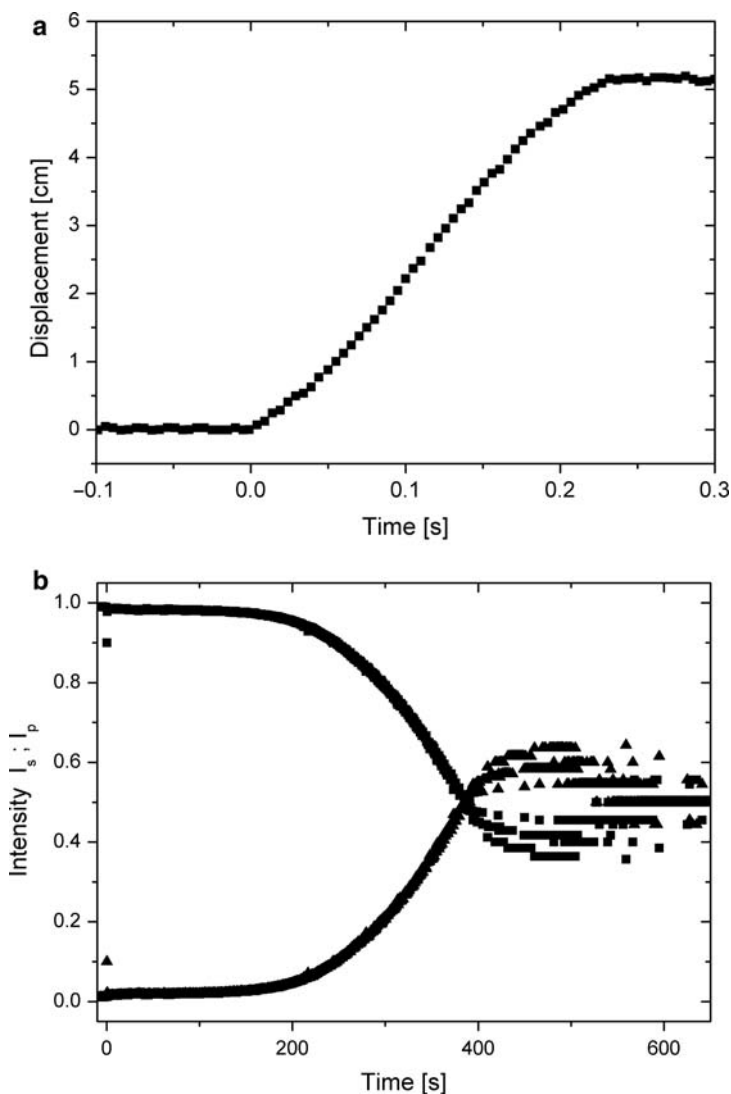
Fig. 3.22 A special shear treatment of the PP of Fig. 3.19 [11]. The conditions were: a temperature of 150°C and a shear stress of 106 kPa. In the *upper part* one finds the displacement of the upper glass plate with time. The *lower graph* gives the courses of the reduced intensities through parallel and crossed polars, after cessation of flow. Courtesy of Elsevier

graph shows the course of the displacement of the upper plate with time, as occurring on the polymer of Fig. 3.19 with a shear stress of 106 kPa at 150°C. The total shear of 50 units was reached within 0.23 s. The lower graph shows the changes of the reduced intensities with time through parallel and crossed polars after cessation of flow. It took almost 200 s before any change could be observed. After about 400 s a cross-over occurred. It followed a maximum in the intensity through crossed polars and a corresponding minimum for parallel polars. The measurement finally became quite inaccurate because of the increased turbidity of the sample. Nevertheless, there is no doubt about the fact that intermediately an optical anisotropy was found. This happened regularly with this type of measurements. As no anisotropy was found shortly after cessation of flow, one has to conclude that the birefringence build up was the consequence of lateral overgrowth on tiny completely oriented anisotropic particles, which were formed during the short period of flow. And it was also clear that these anisotropic particle acted like "point-like" nuclei giving rise to ordinary spherulites. In fact, on the cross-sections not a bit of anisotropy could be found. Later in this section a more striking example will be given with the aid of a polymer, which produces a much lower number of nuclei. As a consequence the spherulites can grow out to a much bigger size permitting the observation of the footprints of their formation.

For the moment the results, as obtained with the PP of Fig. 3.19, will be considered more closely. For the purpose the results depicted on the right side of Fig. 1.1 will be plotted on double logarithmic scales. This plot is shown in Fig. 3.23. One immediately notices that the dependence of the number density on the specific work is highly nonlinear. For a polybutene-1 Wolkowicz [5] has shown the nonlinear dependence of the density of nuclei on the shearing time as early as 1978. Actually, also in the majority of the experiments leading to the present Fig. 3.23 a time dependence is shown. As a matter of fact, a constant shear stress was used for these experiments (84.6 kPa). Only the points at a specific work of about 25 MPa and the points below 0.2 MPa were obtained along different routes. For our PP and a temperature of 160°C a slope of about four is obtained. For 140°C this slope is still about three. The lines seem to converge with increasing specific work. They seem to meet at about 25 MPa. This high specific mechanical work had been achieved in duct flow. In this connection one has to look at Fig. 3.19 [36]. The pertinent data are taken from the boundary between the highly oriented layer and the fine grained layer and show, where the transition from a multiplication of nuclei to a creation of a highly oriented structure can be expected for this polymer. For very low specific works data from extensional flow are taken [45, 46].

The fact that the points outside the middle range of Fig. 3.23 are not taken at an invariable shear stress of 84.6 kPa and, nevertheless, fit on the line for – say – 145°C, gives a strong evidence for the usefulness of the specific work instead of the shearing time. Of course, the time dependence has always been accentuated because of the fact that a well-known theory has been predicting a linear time dependence on the basis of the entropy change for many years. In fact, this entropy change should cause an increase of the melting point and, as a consequence, an increase of the degree of undercooling (see Sect. 3.2). This circumstance would create a better milieu for the sporadic formation of nuclei and, consequently, an
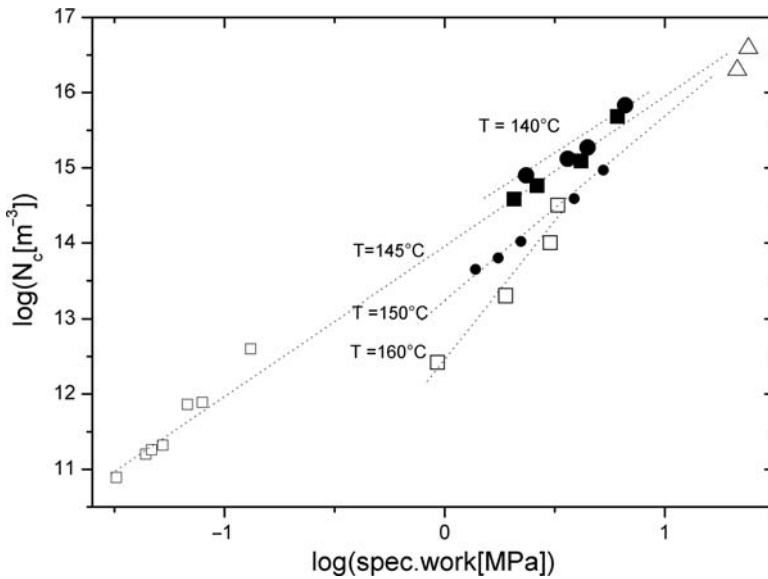
Fig. 3.23 Double logarithmic plot of the number density of nuclei versus the specific work applied on a PP of $M_w = 322{,}000$ and $M_n = 47{,}000$ at several temperatures. Except for the points at specific works below 0.2 MPa, where extensional flow was applied [45, 46], and for the points near 25 MPa, where duct flow was applied [36], all points were obtained at the same shear stress of 84.6 kPa. As a consequence, actually pure time dependences are shown in the middle range [10]. Courtesy of Springer Verlag

increased constant frequency for their occurrence. For their accumulation, a linear dependence on the shearing time would be evident.

As this subject is of such an importance, also another graph is shown. For the purpose, Fig. 3.24 has been prepared [11]. This figure shows for the same PP the increase of the said number density as a function of the applied specific work, if at 150°C a great variety of shear stresses is applied. These shear stresses varied from 25 to 250 kPa. Within the expected error margin all points fall on the same line. And also: this line coincides nicely with the line for 150°C in Fig. 3.23. The reader may notice that the shear stress and the specific work have the same physical dimension, i.e., Pascal. Only, the values of the applied shear stresses are at least one decade lower than those of the specific works.

3.3.2.2   Influence of Extensional Flow on the Number Density of Nuclei

Figure 3.23 also shows points below a specific work of 0.2 MPa. As already announced, these points were obtain in extensional flow. A sketch of the apparatus, which has been built for the purpose, is shown in Fig. 3.25 [45]. The main goal was a machine, where the samples had a considerable thickness also after their stretching, so that cross-sections could be prepared and the obtained morphology could be
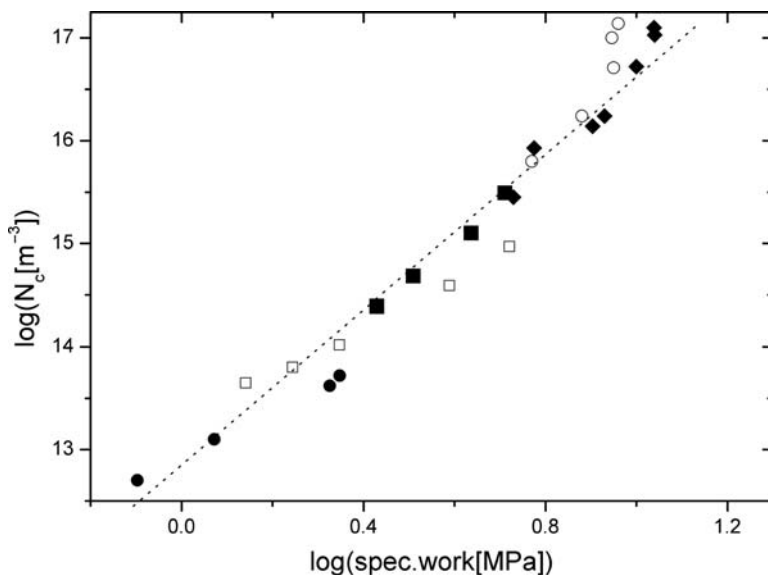
Fig. 3.24 Double logarithmic plot of the number density of nuclei versus specific work for the polymer of Fig. 3.23 at a temperature of 150°C. A variety of shear stresses has been applied: *full circles* 25 kPa, *full squares* 51 kPa, *open squares* 85 kPa, *open circles* 127–250 kPa, *full diamonds* 106–250 kPa [11]. Courtesy of Elsevier

observed. The machine was called the windbix (after the Dutch word "windbuks" for air-gun). In fact, the force, which must adequately decline during the extension for keeping the tensile stress constant, is created by gas pressure in the cylinder shown on the right side of the picture. The pressure in the chamber above the piston is continuously reduced during its downwards movement by the fact that during this movement more and more air can escape through a vertical slit in the pneumatic cylinder. On the left side the cylindrical sample is shown in its initial position inside a heating cylinder. This cylinder is drawn downwards just before stretching is started. The sample is extended in a heated glass cylinder with the aid of a thin wire. This wire connects the sample with the piston in the pneumatic tube. For the purpose it moves over two pulleys. Further details can be found in the caption of the figure.

The notorious necking of the sample was avoided by the use of flexible "clamps." From thin silk fabrics circular specks were cut. In the centers of these specks little ringlets were mounted. These specks were pressed on (glued to) the warmed-up end surfaces of the sample. The wire was tied to the ringlet on the upper side. At the lower side the ringlet was fixed in the center of the bottom plate. When the extension was started, the silk specks folded up like little umbrellas. In this way the circumferences of the end-surfaces were reduced properly.

Two pictures are of particular interest [46]: In Fig. 3.26 the morphologies of two samples of a high molar mass PP are shown. On one sample a very small amount of specific work of 0.01 MPa was applied. On the other sample a ten times higher
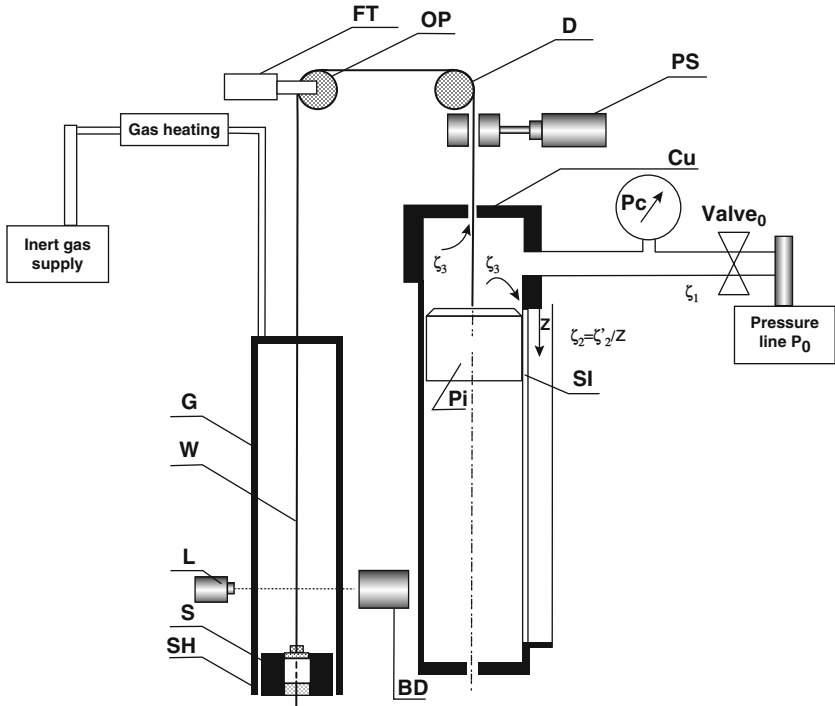
Fig. 3.25 Windbix extensional rheometer. *Left side*: SH: sample holder, S: sample, L: Laser, W: wire, G: glass tube, OP: overhead pulley, FT: force transducer, D: sample length transducer, PS: pneumatic brake, Cu: cover, Pi: piston, Si: slit, ζ_3: friction coefficient for gas flow through the leaks, $\zeta_2 = \zeta'_2/z$: friction coefficient for gas flow, decreasing with increasing length z of the slit [45]. Courtesy of the Society of Rheology
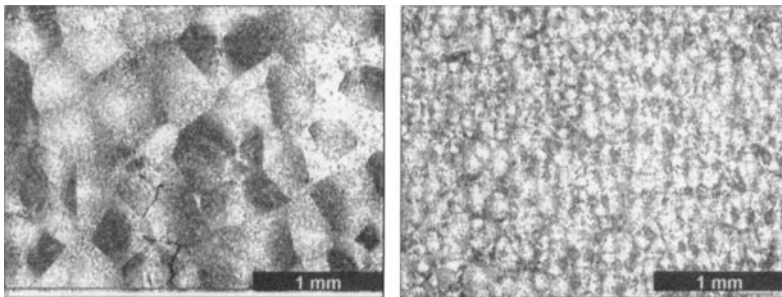
Fig. 3.26 Morphologies after extensional flows for a sample of PP, characterized by $M_w = 492,000$ and $M_n = 97,000$ [46]. The *left picture* was obtained at 145°C after the application of 0.01 MPa, the right picture after 0.1 MPa. Courtesy of the Society of Rheology
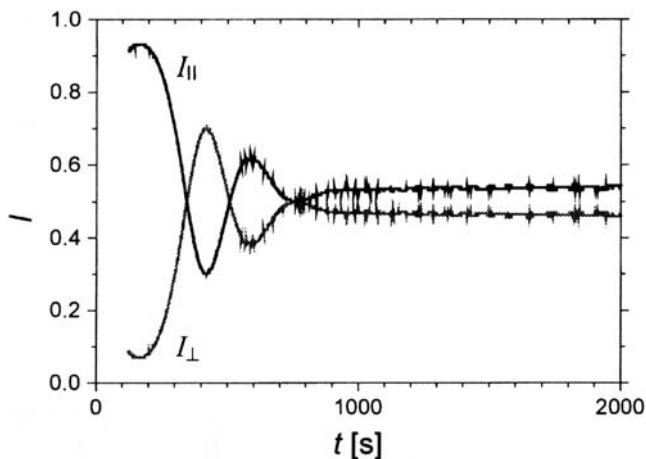
Fig. 3.27 Courses of the reduced light intensities, as obtained through parallel and crossed polars after the application of a tensile stress of 10 kPa for 3.5 s at a temperature of 145°C to the polymer of Fig. 3.26 [46]. Courtesy of the Society of Rheology

specific work of 0.1 MPa was applied. These treatments caused very different morphologies. The reader may have his own judgment. With respect to the left picture the number density of nuclei on the right picture is increased by a factor of one hundred. In spite of the application of a stretch no thread-like precursors were found with these low loads. These pictures resemble very much those, which have been obtained after the application of various specific works in shearing.

In connection with the fact that in the morphologies only spherulites have been found, a reproduction of the course of the optical properties, as monitored after the cessation of the flow, is of particular interest. In Fig. 3.27 the reduced intensities through parallel and crossed polars are shown as functions of the waiting time. To the polymer of Fig. 3.26 a tensile stress of 10 kPa was applied during 3.5 s at 145°C. Even after this low load a considerable temporary birefringence was registered during the formation of spherulites. Again, one must conclude that tiny anisotropic nuclei, as coming up during the short period of flow, were the basis for the final growth of spherical crystalline entities. One fact is clear in this connection: At the end of the flow treatment the lengths of these nuclei must still be small compared with the mutual distances between these nuclei. Otherwise there would be no space for the growth of spherulites.

3.3.2.3   Results Obtained with a Peroxide Degraded Polypropylene

The present author cannot abstain from presenting a more direct proof for the correctness of the conclusion just taken. For the purpose, however, a polymer is needed, which under all circumstances contains a much lower number of nuclei

than the polypropylenes used so far. With such a polymer the spherulites can grow out to a much bigger size. If by chance a cross-section goes exactly through the heart of such a spherulite, traces of the origin of this spherulite will be visible. It turned out that such a polymer was a peroxide degraded polypropylene. Apparently, the chemical structure is damaged by this treatment to such an extent that the association of molecules becomes much more difficult. Such a polymer was investigated in the Linz laboratory in the course of a routine investigation of a greater number of industrial polypropylenes.

First of all, a three dimensional picture is shown in Fig. 3.28, which is similar to the picture shown in Fig. 1.1. However, when looking at the scales one notices quite large differences in the orders of magnitude. In fact, for the virgin polymer of Fig. 1.1 one finds a number density of nuclei of $10^{16} m^{-3}$ at 100°C. For the degraded polymer this density is almost three decades lower.

For this polymer a picture, which has already been published, is shown as Fig. 3.29 [47]. On this figure the effects of short term shearing are shown for a temperature of 150°C. This figure consists of three parts. On the uppermost part the shear treatment is demonstrated. Shearing took less than 0.1 s for a total shear of 45 units at a shear stress of 210 kPa. On the middle part one can follow the courses of the reduced intensities, as obtained through parallel and crossed polars after cessation of flow. An indication for the occurrence of a crystallization process is found at about 500 s of waiting time (compared with 0.1 s shearing
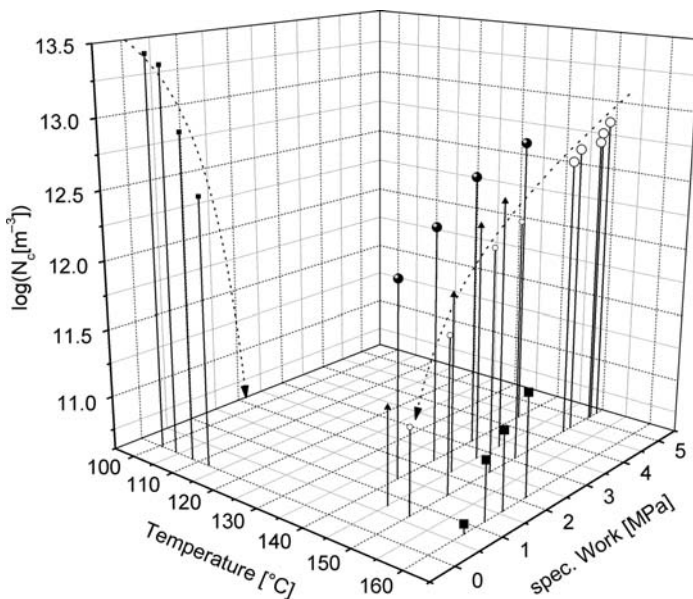
Fig. 3.28 Three dimensional plot of the logarithm of the number densities of nuclei against temperature after fast quenches (*left horizontal axis*) and specific work (*right horizontal axis*) for a peroxide degraded PP ($M_w = 160{,}000$ and $M_w/M_n \approx 2$). Unpublished work by E. Ratajski
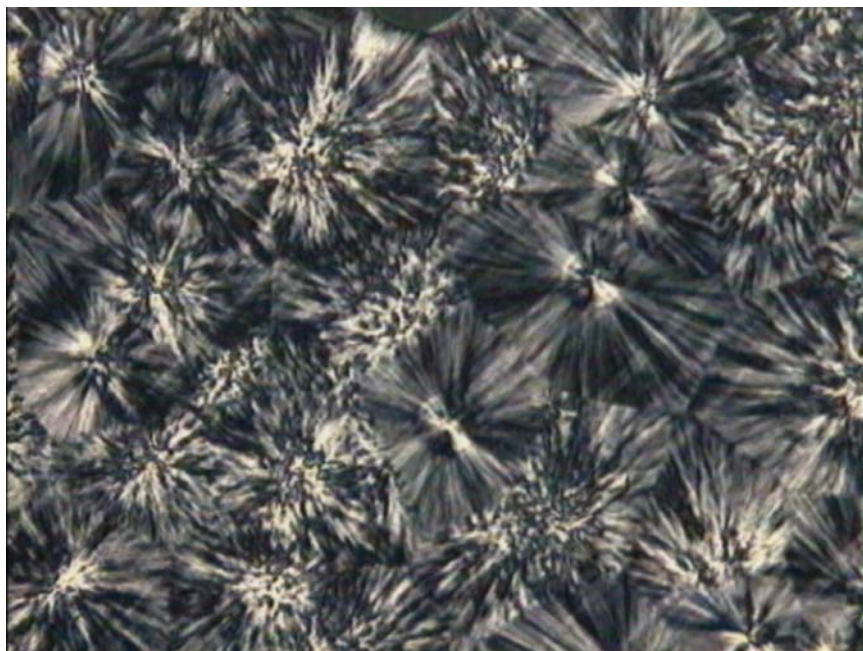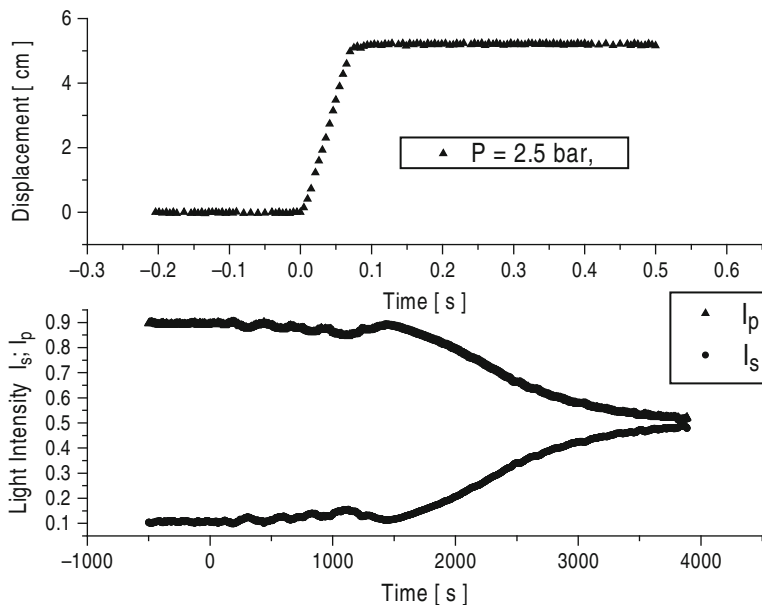
Fig. 3.29 Displacement profile of a short term shearing experiment on the peroxide degraded PP of Fig. 3.28 and the pertinent intensity curves, as obtained through parallel and crossed polars. Also the corresponding morphology of the crystallized sample is shown. Temperature and shear stress were 150°C and 210 kPa, respectively [47]. Courtesy of Hanser Verlag

time!). After about 1,200 s the curve for crossed polars shows a slight maximum, whereas the curve for parallel polars shows the corresponding slight minimum. As these extrema are not very distinct, one must conclude that only a small portion has been transformed into anisotropic nuclei. But this fact is in agreement with our conception. Complete depolarization was found only after about 4,000 s. The lowest picture shows a cross-section through the solidified sample. The direction of previous shearing is under 45° with the frame of the picture (lower left corner to upper right corner). In the middle of the picture two spherulites can be seen, which obviously were cut through their centers. At these centers one notices pairs of little bright and fan-like formations, which are oriented in a direction perpendicular to the previous flow direction. Obviously, these formations have their origin at short anisotropic nuclei oriented in the flow direction. With more rigorous flow treatments these short nuclei obviously grow out into shishs. In fact, one finds with this polymer rows of spherulites, which have their origins at sometimes clearly visible and seemingly endless strings oriented in the previous flow direction.

Quite recently I detected a paper, which clearly supports the view presented here (Kanaya et al. [48]). These authors performed depolarized light scattering (DPLS) measurements during the annealing of a melt of isotactic polystyrene after a pulse shear treatment. The melt was sheared at several temperatures and at a shear rate of 30 s^{-1} for some 6.7 min. At the lowest temperature of 210°C the scattering pattern showed the occurrence of elongated particles after 10 min. These particles were oriented in the direction of the previous flow. After 30 min, however, this pattern was covered over with a pattern typical for spherulites. At higher temperatures no visible pattern were obtained.

At this point it is time for a final conclusion. Apparently, nuclei grow in the direction of flow during the application of this flow. This fact leads to the establishment of a novel mechanism of flow induced nucleation in polymer melts. The assumption is that in quiescent melts, at temperatures below the melting temperature of the spherulites, there is a huge reservoir of dormant athermal nuclei. These nuclei are local alignments, which are stabilized during the process of cooling. Necessarily these nuclei have the shape of fringe micelles. Their length determines the temperature, where they become active as athermal nuclei: the longer (the more orderly) they are, the higher is the temperature, where they become active. In fact, as has been explained already in Sect. 2.3.2.3, the height of the barrier, which is built up at the beginning of lamellar growth, depends on the length (the orderliness) of the body of the micelle because of the dependence of the negative internal free energy on this length. This means that the said barrier becomes always lower, if the micelles become more orderly ("longer"). By the action of flow these micelles are oriented and their tangling ends are "ironed." Their length also increases by the association of other molecules, as has been explained in the last sections. However, before this idea will be worked out more accurately, the stability of the said nuclei will be discussed. In fact, if they are not stable enough, also the phenomena shown in the present section will stand on shaky ground.

3.3.3   Relaxation Phenomena

3.3.3.1   A Historical Review

In the course of duct flow experiments, which were carried out at Linz University with the aid of a single screw extruder, the research group at this university came across the phenomenon of the relaxation of flow induced nuclei. This happened at a surprisingly early date, i.e., before 1987 [20, 27, 33, 49]. As these results are very instructive even nowadays, they will be given here in detail. In fact, except for very recent measurements, which will be discussed below, these measurements of shear induced crystallization are the only ones, which have been carried out in a critical range of temperature, which has been characterized only in the present monograph by Fig. 1.3. This is the range between the equilibrium melting point and the temperature, where the spherulites melt. The overwhelming majority of the pertinent measurements were carried out below the temperature, where spherulites melt, because this latter temperature was erroneously considered as the true melting point. In all experiments, which have been carried out in Linz, samples of an industrial PP ($M_w = 290,000$, $M_n = 50,000$) were extruded through ducts of rectangular cross-section of large aspect ratio (1:10 in mm).

In one of these experiment [49] the arrangement was used, which is depicted in Fig. 3.30. The head of the extruder is at E. Between the end of the extruder screw and head E there is a zone of rest, in which the melt can relax from the maltreatment in the screw channel. In part D ducts of varying lengths can be inserted. The duct exit is invariably above the endless conveyor belt F, which is manufactured of a very thin steel band. The upper side of this conveyor belt moves in extrusion direction over two rolls R_1 and R_2. R_1 is a chill roll, which is driven by a motor. U is a heated pad and T is a heated tunnel, which consists of four segments. Normally the tunnel and the pad are heated to the extrusion temperature, so that
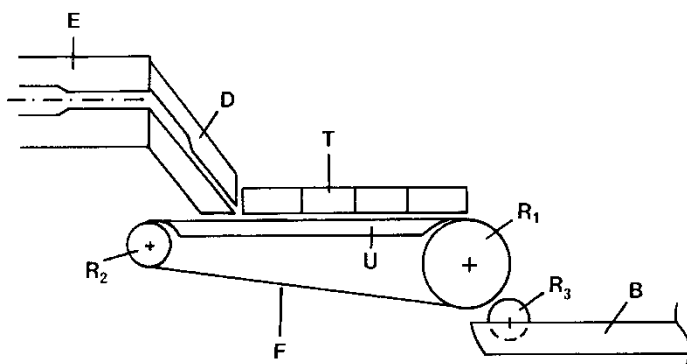
Fig. 3.30 Apparatus for the measurement of the relaxation of (lengthy) structure elements contained in the extruded strip. E extruder, D exchangeable slit die, T tunnel in segments, U heated pad, F conveyor belt, R_1, R_2, R_3 rolls of varying use, B bath (Janeschitz-Kriegl et al. [27, 49]). Courtesy of Alfred Hüthig Verlag

the extrudate, which is deposited on the belt during extrusion, can be tempered
during its movement through the tunnel, before it is quenched on the chill roll. The
quench is perfected, when the extruded strip is immersed in ice water, as contained
in the vessel B. R_3 is just a roll guiding the strip. In order to uncouple the residence
time in the tunnel from the extrusion speed, the length of the tunnel can be varied
by the use of a varying number of segments. Otherwise the residence time in the
tunnel would just be inversely proportional to the extrusion speed.

If various duct lengths were used at 200°C and the chill occurred directly after
the exit of the duct (no tempering), the following picture was obtained. It is
reproduced in Fig. 3.31 and shows that almost always oriented surface layers are
produced by the quench. The thickness of these layers depends on the extrusion
speed and on the duct length. Only at very low extrusion speeds no surface layers
are found. Apparently, the duct length is important. This means that the shearing
time is decisive. Interestingly enough, however, the precursors, which apparently
cause the oriented structure, are so tiny at 200°C, that they cannot be traced back in
the flow birefringence. This is shown in Fig. 3.32.

This flow birefringence was observed through an adapter mounted to the ends
of the ducts. This adapter contained windows in the large side walls. The lengths
of the ducts were increased in this way by 7 mm. But even with the shortest duct
no influence of the duct length on the flow birefringence could be observed at the
extrusion temperature. This was true even for the lower extrusion temperature of
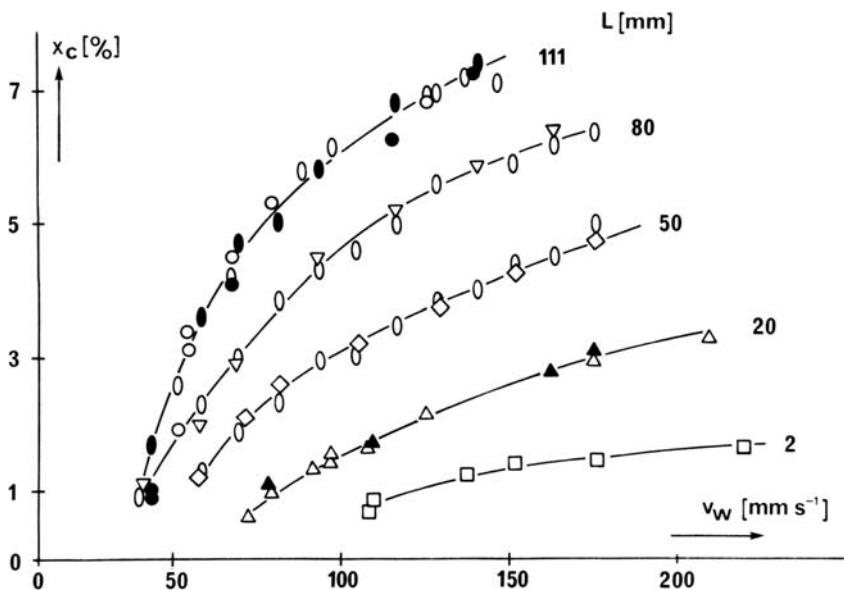
Fig. 3.31 Thickness of highly oriented surface layers as functions of the extrusion speed ($\approx$ roller
surface speed) for various duct lengths given near the curves, as obtained after quenches from
200°C to chill roll temperatures of 100°C (*open circles*), 50°C (*closed circles*) 10°C (*other
symbols*) [20, 49]. Courtesy of Alfred Hüthig Verlag
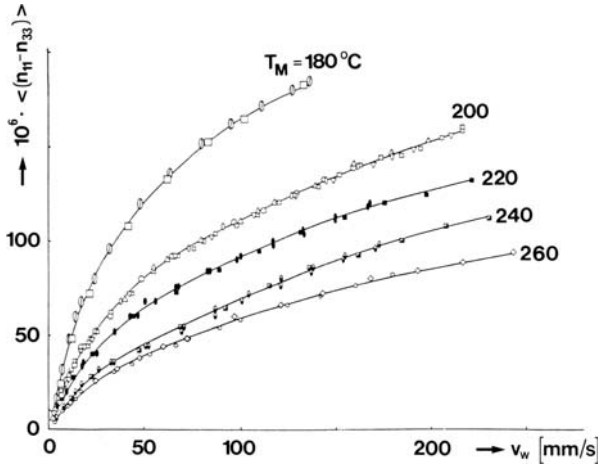
Fig. 3.32 Flow birefringence, as measured at the duct ends in the 1,3-plane (light beam normal to the large duct walls), for duct lengths quoted in Fig. 3.31. These duct lengths are increased only by 7 mm. The positions of the various symbols standing for this spectrum of lengths have no influence on the course of the curves. The extrusion temperatures are given near the curves [20, 33]. Courtesy of Steinkopff Verlag

180°C, where the polymer melt should be much more sensitive to crystallization tendencies. By the way, the fact that the flow birefringence as such is not influenced by the duct length even with the shortest duct shows that the steady state flow profile is already adjusted after a short distance from the duct entrance. This is in huge contrast to the formation of (invisible) precursors, which become effective only after the quench. In fact, as Fig. 3.31 shows, this formation of precursors is tremendously influenced by the duct length. By the way, from Fig. 3.31 one can also learn that the temperature of the chill role has no influence on the formation of the oriented layers. This puzzle, however, can be solved, when Fig. 3.33 is observed. This figure shows the relaxation of the precursors of PP, if the quench is postponed for several time spans of tempering in the tunnel. Except for the two uppermost curves, which were obtained, when the tunnel temperature was lowered to 170 and 130°C, all curves present results, which were obtained, when the tempering temperature agreed with the extrusion temperature of 200°C. For the highest extrusion speed of 150 mm s^{-1} temper temperatures of 130, 170 and 200°C were applied. For all the other curves the temperature was kept at 200°C, but the extrusion speeds were reduced step by step. The consequence of this stepwise reduction is clearly seen at time zero, were a stepwise reduction of the layer thickness is found. It can clearly be seen that after less than four seconds no traces of previous flow treatments can be found at 200°C, irrespective of the previous extrusion speed. This seems to show that the relaxation time is not very much influences by the prehistory. Enormous differences, however, are shown if the temper temperature is reduced. In fact, at 130°C the layer thickness is no longer influenced by the temper time of 4 s. This fact
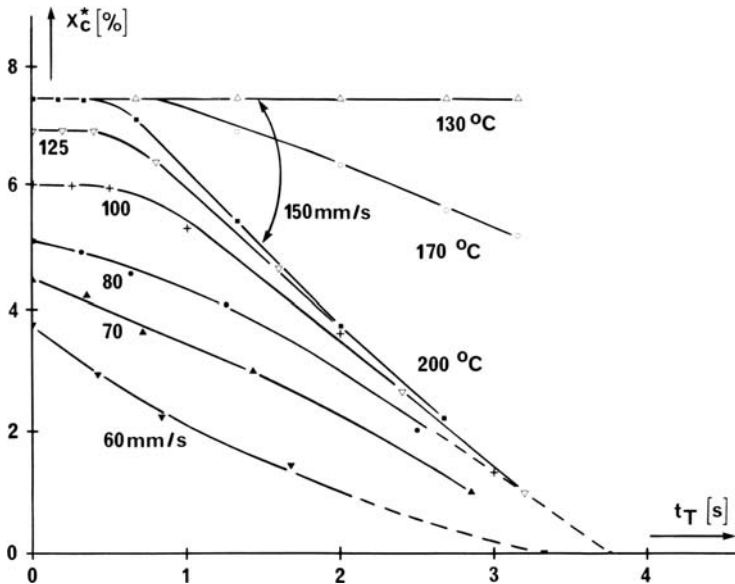
Fig. 3.33 Relaxing thickness of the surface layer as percentage of the final strip thickness, when the residence time t_T in the tunnel was varied [49]. Extrusion occurred at 200°C through a duct of 111 mm length. Extrusion speeds and temper temperatures are given near the curves. Chill-roll temperature was 10°C. Courtesy of Alfred Hüthig Verlag

explains, why the chill role temperatures, which were varied between 90°C and 10°C had no influence.

What can be learnt from these measurements? Apparently, flow produces a sufficient number of stretched molecules, which can associate sporadically in the temperature range between 212°C and – say – 170°C, where a metastable situation can be expected (see Fig. 1.3). However, normally the metastable range is characterized by a living equilibrium, where already formed associates disintegrate again voluntarily, but are replaced by other newly formed ones. Such an equilibrium can be expected without any doubt also for continued shearing. But, apparently, this equilibrium could not be reached in the present experiments because of insufficient shearing times. On the other hand one must realize that after cessation of flow relaxation of the formed structures is inevitable. The reason for this process is the fact that those molecules, which separate sporadically from the precursor, immediately coil up in the quieted down melt and are, therefore, no longer available for the formation of new stretched nuclei. Because of the fact, however, that the stability of the formed precursors increases rapidly with decreasing temperature, one deviates rapidly from the usual concepts of nucleation. For secondary nucleation, were only local rearrangements are required, this deviation is not so obvious, as has been posed in the second chapter of this monograph (see Sect. 2.3.1).

As has been mentioned in the original papers, one cannot derive from Fig. 3.31, whether with increasing shearing time the thickness of the layers tend to a final

value or not. Such a judgment is rendered difficult also by the fact that at a given extrusion speed the shear rates (and the shear stresses) decrease with the distance from the duct wall. This means that thick layers finally grow with a reduced speed. Another point is that the fluid layers change their shape, when the extruded material is deposited on the conveyor belt. The speed of the conveyor belt is chosen, so that the thickness of the extruded strip is lower than the duct height. This is the reason, why the thickness of the oriented surface layer is given in percentage of the thickness of the strip. Fluid layers, which have been close to the duct wall, are considerably stretched and, as a consequence, become much thinner. In the center of the strip layers are reduced in length and become thicker.

As reported in ref. [20], Wippel tried to obtain some better insight into the kinetics of the formation of oriented surface layers in the said high temperature range. For the purpose he had to get rid of the uncertainties, which arose in connection with the deposition of the extruded fluid strip on the conveyor belt. The only possibility was to quench the duct as a whole and to extract the solidified content. For the purpose the walls of the duct were equipped with channels, through which cooling water could be pumped as close to the duct surface as possible. Also, the duct was slightly tapered for lightening the extraction. Cross-sections were cut in the 1,2-plane. The boundaries of the highly oriented layers, as obtained for various throughputs, were plotted against the distance from the duct entrance. For one of the series of measurements these results are given in Fig. 3.34.
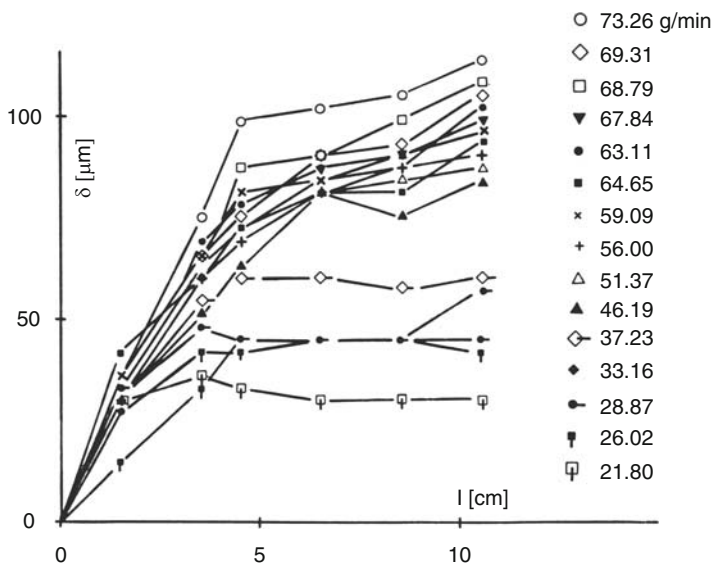
Fig. 3.34 Boundary layer thickness vs. distance from the entrance to the duct, as obtained by quenches immediately after the cessation of flows at 200°C for the PP of Fig. 3.28 [20]. The output rates are given on the right side of the figure. Courtesy of Pergamon Press

The flow profiles were calculated for the still unimpaired melt. In this way the residence times as functions of the distance from the entrance could be calculated for all kinds of fluid layers, which were found at varying distances from the duct surface and at corresponding shear rates. If at a certain distance from the duct wall a line is drawn parallel to this wall on a drawing like the one shown in Fig. 3.34, one obtains points of intersection with the diverse boundaries of oriented layers. From the distances between the entrance and these points of intersection the pertinent residence times can be obtained. At those residence times the layers were ready to form oriented structures after the quench.

On the next graph (Fig. 3.35) a double logarithmic plot of the obtained critical residence times against the corresponding shear rates is given for all throughputs of the series of Fig. 3.34. In spite of the scatter, as caused by the complicated method, one can clearly see that the critical residence times decrease rapidly with increasing shear rates. A line of slope minus two is inserted. It must only be said that below a shear rate of 400 s^{-1} no surface layers were found. One has approximately

$$t_v \approx C\,q^{-2},\tag{3.18}$$

where t_v is the critical residence time and q is the corresponding shear rate. Of course, one can rearrange this equation into $t_v q^2 = C$ and one can also take the
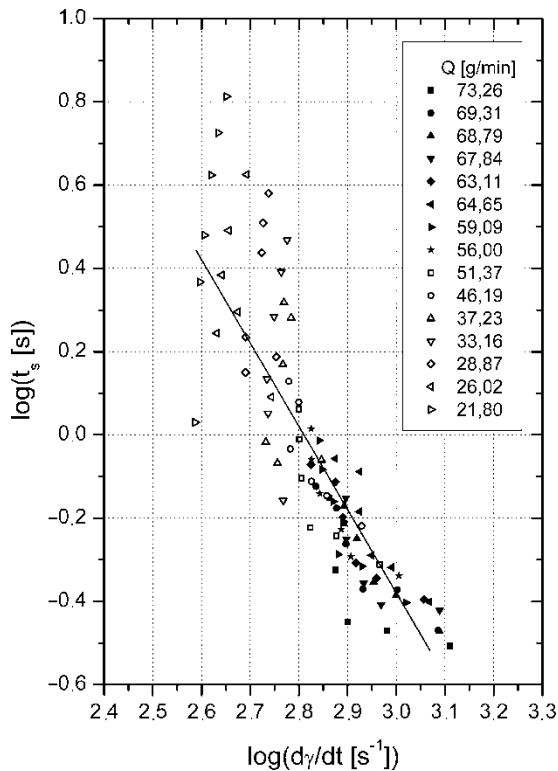
Fig. 3.35 A double logarithmic plot of the critical residence time against the corresponding shear rate for the PP of Fig. 3.28. at a temperature of 200°C. Unpublished graph, as prepared by Dr. Herbert Wippel

square of this equation: $t_v^2 q^4 = C^2$. In the present experiment one cannot discern between these options. But the conclusion is that the given results are not in contradiction to the results described in (3.6) of Sect. 3.3.1.1. For the moment it is of great interest that even at the high temperature of 200°C, where the precursors relax quite rapidly (see Fig. 3.33), their growth mechanism cannot be very different from the growth mechanism observed at much lower temperatures, where the precursors are practically stable.

A calculation of the specific mechanical work seems of interest. If one takes the point $t_v = 0.44$ s, $q = 1,000$ s^{-1}, one obtains $w \approx 44$ MPa, if the viscosity for this very high shear rate is estimated from the data given in ref. [50] ($\eta(0$ s$^{-1}) \approx$ 5,600 Pa.s, $\eta(1,000$ s$^{-1}) \approx 100$ Pa.s). This value of 44 MPa is certainly not completely unrealistic. In fact, for the transition from the fine grained layer to the highly oriented layer, as shown in Fig. 3.19 for the same polymer at a temperature of 150°C, a value for the specific work of about 25 MPa has been calculated. Admittedly, the slope in Fig. 3.35 does not seem too realistic, if the specific work is claimed to be the same for any transition to the highly oriented layer (as occurring after the quench), irrespective of the details of the previous flow condition. In fact, one has $w = \eta q.qt$, where $q^2 t = $ const for the chosen slope of two. But the viscosity η varies with the shear rate, which means that at the point $t_v = 2.5$ s and $q = 460$ s^{-1}, with $\eta \approx 166$ Pa.s, the specific work should be $w \approx 66$ MPa. This example shows up the uncertainties. Nevertheless, the orders of magnitude should be instructive. In fact, one cannot learn very much, if – say – shear rates of the order of 1 s^{-1} or less are applied (see the majority of recently published papers).

At this point a discussion of the said "uncertainty" becomes over-due. It is conspicuous that the concept of the specific work becomes less convincing just with experiments, which are carried out at high values of the shear rate. In fact, with Liedauer's experiments [16] an interpretation of the results was almost possible, if the influence of the viscosity was disregarded. (See our "law," as given in (3.6) and (3.13)). If one reconsiders the train of thoughts, which has led to the introduction of the concept of the specific work, one finds that the shear stress stands for the orientation and the shear rate for the frequency of encounter. Their product forms the rate of the specific work. However, what happens, if orientation is more or less saturated? If this is the case, the shear stress looses its function, and, with it, the viscosity. Under this condition one ends up with pure kinematics. And in this picture fit several facts: The parameter of (3.13a) appears to be almost independent of temperature. Also, the convergence of the lines of Fig. 3.23 points in this direction. The higher the specific work is, the less dependent on temperature is the number density of nuclei. So, we can notice a situation of transition. Thus, one can also see, how difficult the theoretical description of flow induced crystallization can be in principle.

3.3.3.2   Other Ways of Observing the Relaxation of Precursors

Wippel used the decay of the birefringence of surface layers. The pertinent values of the birefringence were obtained on the quenched samples after increasing

Table 3.1 Relaxation times
of the precursors responsible
for the oriented
crystallization, as found at
various flow temperatures for
the iPP of Fig. 3.19

Temperature(°C)	Relaxation time(s)
190	57.8
195	15.88
200	7.27
205	3.67
210	0.83

waiting times as applied at the still high temperatures. In these experiments Wippel made use of a series of extrusion temperatures between 210°C and 190°C. At temperatures above 210°C relaxation could not be observed. It would have been too fast, anyway. By the way: 212°C is the equilibrium melting point of iPP [51]. Below 190°C problems arose with the stability of the flow with the throughput rate of 75 gmin^{-1}, which was chosen throughout this series of experiments. The shear rate at the duct wall, corresponding with this throughput, was nearly 2,000 s^{-1}. In contrast to the findings of Krobath [33], the thickness of the boundary layer did not decrease during the relaxation of the precursors. Only the birefringence of the quenched layers decreased. Apparently, Wippels mechanical treatment was more rigorous. Wippels results are shown in Table 3.1. Importantly enough, a single temperature dependent relaxation time was found: The curve of log Δn vs. t_{rel} was found to be a straight line of negative slope within the error margin. A slight correction had to be carried out for an underground birefringence, which apparently was the consequence of a cooling process between rigid walls. A similar, more distinct experience was made later with PB-1, which clearly sticks to the wall [52].

The results of Table 3.1 were used for the preparation of Fig. 2.20 of the previous chapter because of the value of this figure in providing evidence for athermal nuclei as stable nuclei already at temperatures somewhat higher than the melting temperature of the spherulites. By the present Fig. 3.36 a comparison is rendered possible between the zero shear viscosity η_0 and the said relaxation time τ of the precursors. For the purpose a double logarithmic plot is prepared. If the temperature dependencies of both functions would be equal, a straight line under 45° should be expected. In reality, however, a very low slope is obtained. The temperature dependence of the relaxation time τ of the precursors is much higher, pointing to the fact that a supermolecular structure is relaxing. This fact is in contrast to the relaxation of the orientation of free or entangled molecules, which is responsible for the viscosity. In Fig. 3.36 the experimental points stand from left to right for the decreasing temperatures of the table. From an Arrhenius plot one obtains an activation energy of 334 kJ mol^{-1}. [53]. This activation energy is almost ten times the activation energy of 44 kJ mol^{-1}, which is obtained for viscous flow [54].

An analogical behavior was more recently found for the melt of a PB-1 [52, 53]. For this polymer it was found that under the influence of shear flow the stable crystal modification Form I immediately showed up. This fact was documented by an infrared study [52]. The difficulty with this polymer is that it attaches to the duct wall during the quench, if crystallization does not occur thoroughly enough. Apparently this is the case, if shearing is applied at too high a temperature.
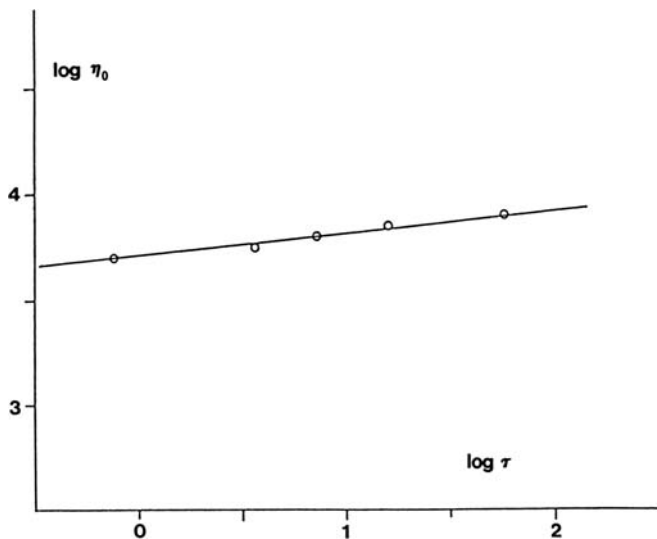
Fig. 3.36 The logarithm of the zero shear viscosity versus the logarithm of the relaxation time of the precursors for oriented crystallization for the PP of Fig. 3.19 [20]. The temperatures, as applied during shearing, were from *left to right* 210, 205, 200, 195, 190°C. Courtesy of Pergamon Press

As a consequence, cooling stresses and a corresponding birefringence come up because the polymer can contract only in a direction perpendicular the wall. (This is a well-known effect with the manufacture of compact disks [55]). Nevertheless, the impression was that precursors for Form I are formed at a temperature as high as 170°C. This is remarkable, if one realizes that the melting temperature of spherulites of Form I is between 124°C (for the Shell copolymer used in the cited research) and 134°C. Unfortunately, the equilibrium melting point of Form I seems to be unknown. The data for the investigated PB-1 are given in Table 3.2, which corresponds to Table 3.1 for PP.

For the precursors of this polymer an activation energy of 224 kJ mol^{-1} could be derived from the data of Table 3.2. For PB-1 the activation energy of viscous flow is about 44 kJ mol^{-1}, as with PP [54]. Again, one finds this enormous discrepancy.

On the basis of experiments, where a glass fiber was pulled through the undercooled melt, Alfonso and Azzurri of Genova [56–58] documented the relaxation of precursors in the melt of a high molar mass PB-1. These authors observed the

Table 3.2 Relaxation times of the precursors responsible for the oriented crystallization, as found at various flow temperatures for an PB-1 with the code name PB0110 of Shell [53]

Temperature(°C)	Relaxation time(s)
150	14.3
155	4.5
160	3.2
170	<0.9

disappearance of the track, which such a fiber left behind. This track consisted of a transcrystalline layer, which apparently had grown on the said precursors. Apparently, these precursors were oriented in the direction of the fiber. The impressive results of these authors are shown in Fig. 3.37, which is similar to our Fig. 2.20. There are a few differences, however. Our measurements on PB-1 were carried out in a temperature range between 150 and 170°C, whereas the measurements in Genova were carried out between 125 and 140°C. Also, our figures give the relative decay whereas the holding times of Genova give the times of the total disappearance of traces. In fact, the activation energy, as calculated from our results on a similar PB-1 (see our Table 2) is 224 kJ mol^{-1}, whereas about 500 kJ mol^{-1} can be derived from the results shown in Fig. 3.37. Nevertheless, the conclusions can be very similar. During cooling relaxation times of the said precursors reach enormously high values, before the temperature is reached, where the spherulites of the stable modification (Form I) melt in a quiescent melt. According to the manufacturer, this temperature is 124°C. It looks, as if the measurements, which are reported in Fig. 3.37, are less representative, because the temperature range of these measurements is more close to the melting temperature of the spherulites. However, this fact is only a consequence of the technique of the measurements: at 125°C a holding time of 56,000 s was found: This time corresponds with more than 15 h. At best one minute could be observed at 190°C in our measurements on PP (Fig. 2.20).
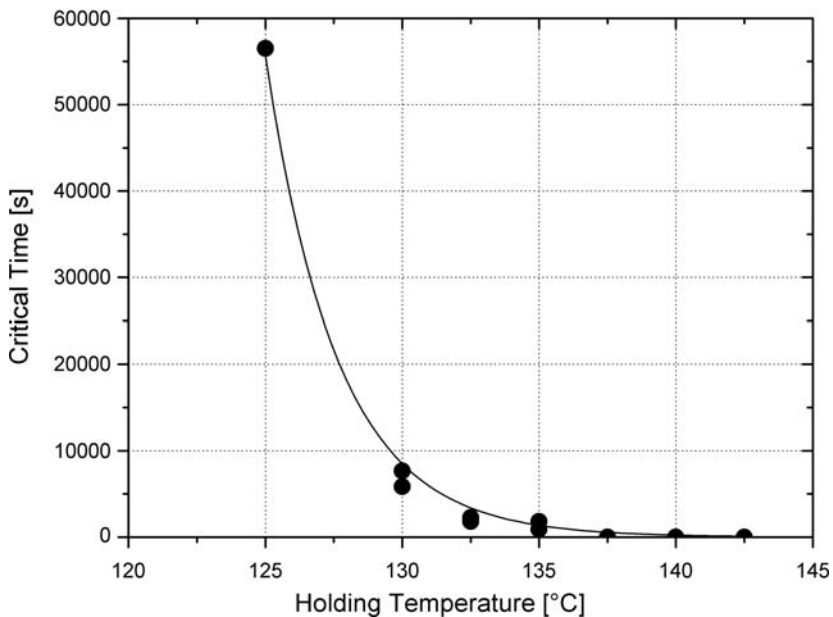
Fig. 3.37 Holding time versus temperature for the disappearance of traces of a track, produced by a glass fiber, when drawn through the undercooled melt of a PB-1 [56]. Courtesy of American Chemical Society

Table 3.3 Molar mass		M_n(kD)	M_w(kD)	M_z(kD)	M_w/M_n	M_z/M_w
characteristics of the PB-1	PB0400	31	176	368	5.7	2.1
samples of Shell Comp	PB0300	35	305	744	8.7	2.4
	BR200	39	762	2460	19.6	3.2

Alfonso and Azzurri [57, 58] also looked after the dependence of the said holding times on the molar masses of their PB-1 polymers. The molar mass characteristics of these polymers are given in Table 3.3.

The authors observed that the lifetimes increased with the 3.4th power of the molar mass. The fiber pulling conditions remained the same for this series of measurements, namely 5 mm in 1 s at 150°C. But this means that the only parameter, which remains of changing influence on the specific work, is the viscosity, which in fact increases with the 3.4th power of the weight average molar mass. Viewing this result from another corner of the eye one arrives at the conclusion that this result furnishes another example for the usefulness of the specific mechanical work as a decisive parameter in the field of flow induced crystallization. Having mentioned the conditions of fiber pulling one is inclined to quote an equation, which describes the shear rates near the fiber surface. This equation has been derived by Monasse [12] some time ago. It reads:

$$q(r) = \frac{1-n}{n} \frac{1}{r^{1/n}} \left[\frac{1}{r_f^{1-1/n} - R^{1-1/n}} \right] V_f, \qquad (3.19)$$

where r is the distance from the fiber axis, R is the theoretical radius of a cylindrical vessel, which stands here for half the thickness of the polymer sample, in which the fiber is embedded, r_f is the radius of the fiber and n is the power law index, describing the non Newtonian flow behavior of the unimpaired melt and V_f is the speed of the fiber.

Supplementally it should be mentioned that a few years after ref. [33] had appeared, Varga and Karger-Kocsis [59] reported a relaxation phenomenon, which occurred, when a glass fiber was pulled through undercooled melts of PP and its copolymers. In this connection it must be said that quite high shear rates of the order of 100 s^{-1} can be achieved close to the fiber surface. For the homopolymer of PP a critical temperature of about 140°C was found. Above this temperature only precursors for the α-crystal modification were formed. This fact was in accord with our earlier findings [16, 20, 33]. In fact, for this reason our experiments were carried out at temperatures between 140 and 200°C. When in the experiments of Varga and Karger-Kocsis the temperature of the experiment was increased step by step, relaxation became faster and faster. Also this finding was in accord with our results from 1987 [49]. (see also Fig. 2.20). These facts, however, should not diminish the merits of the said authors, who reported on a host of experiences with copolymers, and on experiments at lower temperatures, where the transition to the β-crystal modification could be studied.

Very recently interesting investigations were carried out on isotactic polystyrenes [48, 60]. The research group of Genova carried out micro-SAXS-WAXD measurements on the tracks of a fiber pulled through a melt of iPS at 260°C. Reportedly, similar measurements were carried out by Kanaya et al. [48]. Of particular interest is in this connection that Al-Hussein and Strobl [61] have improved the determination of the equilibrium melting point of iPS. According to the linear Hoffman–Weeks extrapolation this equilibrium melting temperature should be 242°C. But this would mean that some of the above shearing experiments were carried out above the equilibrium melting point. However, according to our experience a success of such a measurement is very improbable. So we are very glad with the finding of Al-Hussein and Strobl. These authors followed the melting and crystallization lines with the help of modern techniques in a similar way as Marand et al. [51] did for polypropylene. They arrived at the conclusion that the equilibrium melting point of isotactic polystyrene is 289 ± 5°C. But this means that all shearing experiments were carried out also for this polymer within the temperature range given by our Fig. 1.3. (The melting temperature of the spherulites is 230°C).

Very recently Azzurri and Alfonso reported on the relaxation behavior of shear induced nucleation precursors in samples of isotactic polystyrenes of narrow molar mass distributions [62]. In Table 3.4 the molecular characteristics of a sample of a broad molar mass distribution is given together with the characteristics of four samples of narrow molar mass distributions of increasing weight average molar masses. Because the samples of narrow molar mass distribution were very small, only the fiber pulling method could be applied to these samples (These samples were donated by H. Marand of Virginia Tech. University). The Linkam parallel plate apparatus was applied only to the unfractionated sample.

Fiber pulling was mostly applied at a temperature $T_p = 250$°C after a heating procedure erasing residues of previous crystallization. In a standard experiment the fiber was pulled with a constant speed of 5 mm s^{-1} over a distance of 5 mm. According to (3.19) this fiber speed corresponds with a shear rate of about 103 s^{-1} at the surface of the fiber of a diameter of $17 \pm 1 \mu$m. A total shear of $\gamma = 1,000$ was obtained in this way in five seconds. After the arrest of the fiber the sample was transferred to one of three temperatures T_R (260, 250 and 240°C) for relaxation at various holding times. After having done this the sample was transferred to a temperature of 180°C for the process of final crystallization. This temperature was chosen because growth speed has a maximum at this temperature. Several hot stages were successively engaged for the purpose. As crystallization is very

Table 3.4 Molecular characteristics of the investigated iPS samples [62]

Sample code	$\overline{M}_n$(kg mol^{-1})	$\overline{M}_w$(kg mol^{-1})	$\overline{M}_w/\overline{M}_n(-)$	Isotacticity index(%)
w		939	6.4	97
F1	234	291	1.24	96 ± 2
F2	563	605	1.07	96 ± 2
F3	989	1,022	1.03	96 ± 2
F4	1,540	1,700	1.10	96 ± 2

slow with iPS, there have been no quenching problems. For morphological investigation with the aid of a scanning electron microscope the sample surface was etched with amyl acetate at room temperature. At this temperature this fluid readily dissolves the amorphous phase. The etched surface was shaded with a thin layer of gold.

With the Linkam machine a gap width of $70\,\mu m$ was always used. A step shear rate of $q = 30\,\text{s}^{-1}$ was imposed for $t_s = 10$ s. A temperature $T_s = 250°C$ was chosen for the shearing. Various holding times were applied at several temperatures, before the samples were cooled at $30°C\,\text{min}^{-1}$ to $180°C$. Seemingly point-like nucleation centers were counted on a known area with known sample thickness. The reliability of those counts was improved by a repeated application. The number density, as obtained in permanently quiescent melts, was subtracted. In Fig. 3.38 the logarithm of N/N_0, as obtained in these experiments, is plotted against the holding time for the holding temperatures of 240, 250 and 260°C. It can be observed that the speed of the decline increases rapidly with increasing temperature. Straight lines can be drawn through the points. This means that single relaxation times are characteristic for the pertinent relaxation processes. This is of great interest, as with this iPS the relaxation of so-called point-like nuclei is described. Previously only the relaxation of thread-like precursors (highly oriented layers) could be described for an iPP [20, 33, 49]. The fact that also so-called point-like nuclei relax according to this scheme, is important for the validity of our Fig. 1.3, which shows that with decreasing temperature one arrives at practically stable nuclei already above the temperature, where spherulites melt.

If, as in the case of PB-1, only the complete disappearance of the track of the glass fiber was considered, the authors could only find the total holding time (the "life time"), but not the course of the decay of the number density of nuclei. If the reciprocal value of this life time, which is proportional to the rate of disappearance, is plotted against the reciprocal absolute temperature ($1,000/T$), one obtains an Arrhenius plot. For the samples of different molar masses these
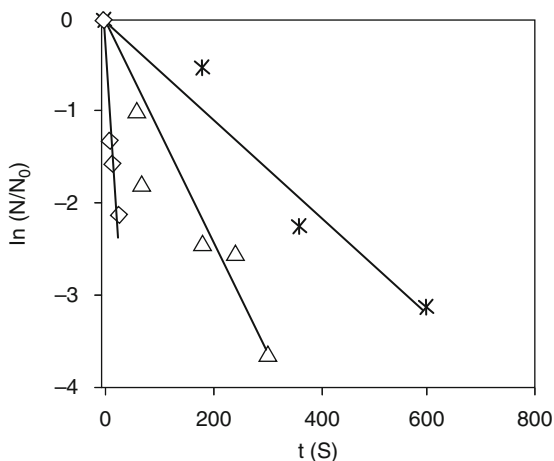
Fig. 3.38 Fractions of surviving (point-like) nucleation precursors as functions of holding times, where several temperatures T_R were applied (after the shearing of a sample of iPS) [62]. *Diamonds*: 260°C, *triangles*: 250°C, *stars*: 240°C. Courtesy of the American Chemical Society

Fig. 3.39 Temperature dependence of the rates of relaxation of the precursors of the investigated samples of iPS, as formed along the moving glass fiber [62]. *Full triangles*: F4, *open squares*: F3, *full diamonds*: W, *open circles*: F2, *full circles*: F1. Courtesy of the American Chemical Society
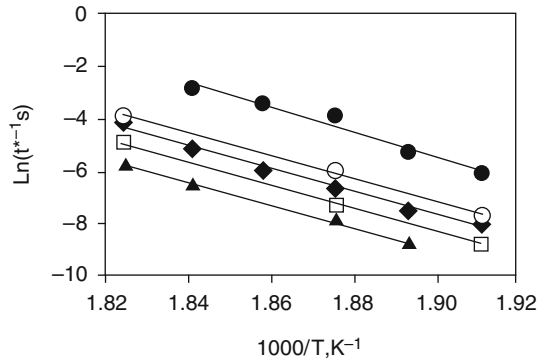
Arrhenius plots are given in Fig. 3.39. One immediately notices that the line for the polydisperse iPS (full diamonds) has the same slope and lies in the midst of the other lines. From the common slope one can calculate the activation energy, which is about 400 kJ mol^{-1}. This activation energy is of the same order of magnitude as with the other investigated polymers.

If on a double logarithmic plot the life times of the fractionated samples were plotted against their molar masses, a straight line was found. For a shearing temperature of 260°C life times were found in this way, which were proportional to a power 2.2 of the molar masses. This result seems in contrast to the finding that for PB-1 samples a power 3.4 has been found. However, the commercial samples of PB-1 were polydisperse, whereas the samples of iPS were practically monodisperse. In this respect a drastic difference in the behavior of the non Newtonian viscosity must be mentioned. With polydisperse samples the transition from the plateau at low shear rates to the power law behavior at high shear rates covers several decades in the shear rate and ends with a power law index of the order of 1/3. Also, the molar mass is still of influence in the high shear rate range. In contrast, with narrow fractions the mentioned transition from the plateau region to the power law region covers less than one decade in the shear rate and ends with a much higher power law index. Whereas the level of the plateau still obeys Flory's power 3.4 in the molar masses, the steep curves in the high shear rate range join in a common line independent of the molar masses. This fact has been shown for the first time by Stratton [63] in 1966 on monodisperse fractions of atactic polystyrenes, as obtained by ionic polymerization. This fact means that the molar mass dependence of the viscosity of monodisperse polymers decreases rather fast with increasing shear rates. This fact may be a valid explanation for the lower power 2.2. In fact, shear induced crystallization is certainly not evoked in the low shear rate range. As the reader may notice, the present author is defending his idea of the predominating influence of the specific mechanical work (see the explanation given above for the 3.4th power of the molar mass in the case of the PB-1 samples). In fact, if at some time in the future numerical simulations of processes will indeed become feasible, the most simple parameters will be the most successful ones. And the specific

mechanical work will include also the influence of the molar masses. Exceptions will be presented mainly by samples with exotic, artificial molar mass distributions, as obtained for instance by the addition of small fractions of an extraordinarily high molar mass, as Kornfield at al. did [41] for scientific reasons. Probably, the usefulness of the specific work will also be limited at very high shear rates. A pertinent discussion has already been tried at the end of Sect. 3.3.3.1.

The recent paper by Azzurri and Alfonso [62] contains even more fascinating results. After rinsing their glass fiber with amyl acetate and shading it with gold they obtained two pictures with the aid of SEM. These pictures are reproduced here as Fig. 3.40. For the upper picture the axis of the glass fiber was in a vertical direction. The glass fiber was moved according to the recipe given above (5 mm in 5 s) at 250°C and cooled afterwards immediately to 180°C. On the upper picture one sees ribbed formations, which look like rolls of money. The diameter of the single coins is about 400 nm. Their thickness is about 30 nm. Probably, the molecules are oriented in tangential directions within the coins. This would mean that their average direction is
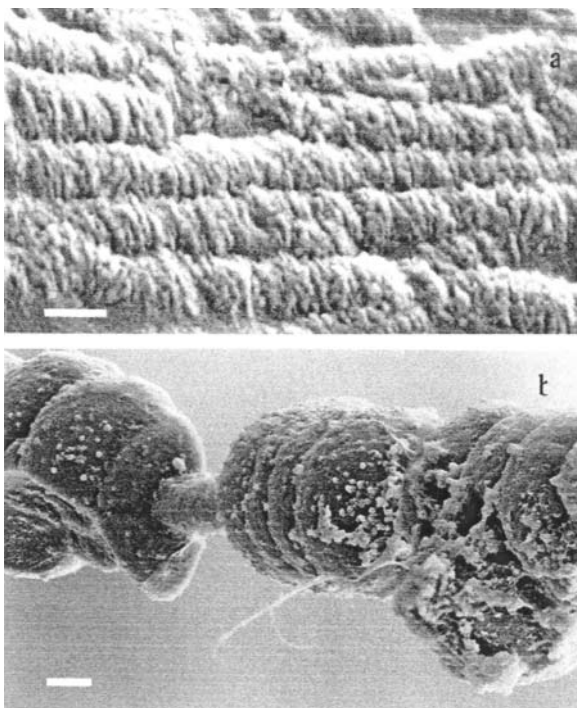
Fig. 3.40 (**a**) SEM micrograph of the transcrystalline layer, as formed on a glass fiber during 15 min at 180°C in a sample of "monodisperse" iPS being quenched immediately after cessation of flow at 250°C. The *scale bar* corresponds with 400 nm. (**b**) SEM micrograph of a macro shish-kebab, as formed during 2 h at 180°C on a sample of iPS being quenched 1 min after cessation of flow at 250°C. The *scale bar* corresponds with 20 μm [62]. Courtesy of the American Chemical Society

in the direction of the axis of the glass fiber. The appearance of the coins reminds us of the "spokes" seen in Fig. 3.10. In this figure a cross-section perpendicular to previous flow direction is shown. These spokes may be projections of coin-like formations. The coins of Fig. 3.40 were formed after the arrest of the fiber as spherulites, which were spatially restricted in their lateral growth.

It goes without saying that the formations shown in Fig. 3.40 are the result of overgrowth on a two-dimensional periodic pattern. There is one period of about 400 nm in the previous flow direction and another period in the transverse direction of only about 30 nm. Certainly this pattern was formed during the movement of the fiber at 250°C. The overgrowth, however, was formed only after the cessation of flow and a quench to 180°C. If in the already quiescent melt the quench was postponed for another minute, the lower picture of Fig. 3.40 was obtained. The magnification of this lower picture is much less. Part of the fiber is seen. One can see that the glass surface has not been active in nucleation. Apparently, the above two-dimensional pattern has largely disappeared during the rather short time of tempering at 250°C. Probably, the character of the – practically – two-dimensional pattern has to do with the fact that with fiber pulling the shear rate decreases extremely fast with increasing distance from the fiber surface. There is only a narrow zone of sufficient shearing. The decrease of the shear rate at the wall of a duct of rectangular cross-section must be seen as very mild compared with this rapid decrease at the fiber surface.

Furthermore, the great regularity of the said pattern cannot be the result of a process governed by statistics. It seems typical for a crystallization process. But, how can it occur? Unintentionally the reader is reminded of the occurrence of the so-called long period in melt-spun synthetic fibers. This long period comes up during a second stretching of the fiber at a temperature not too far below the melting temperature. By this second stretching the modulus of the synthetic fiber is improved. One should say that the period in the direction of the glass fiber of the above experiment would point to the existence of a similar crystallization process proceeding inside the precursors along the fiber. In fact, during the initial association process of macromolecules many irregularities are unavoidably built in. In a phase of improvement these irregularities may be pushed forward and herded, until their concentration becomes so large that they form a separate phase. This development should start at the primary nucleus, where the thread started growing in two opposite directions. As there is no reason for variations in the orderliness of the primary thread, the critical length of the ordered sections must be uniform. This fact would explain the periodicity in the direction of the glass fiber. Apparently, the lateral growth of the precursor is coupled with the growth in the flow direction. As growth in the direction of the thread must be much faster because of the anisotropy of the associated long molecules, the lateral dimension must be much smaller. This fact seems reflected by the much smaller period of only 30 nm in the transverse direction. A lateral coupling may be the reason for the fact that all precursors are in phase with their neighbors. Such an apparent lateral coupling had already been discovered some time ago by Monasse for a high density polyethylene [64], which was sheared between parallel glass plates. Sporadically, also in an investigation at

Linz University the transverse extension of a formation has been found for a polypropylene [50].

But this means that the monodispersity of the samples of iPS must not necessarily be the reason for the nice periodicity shown in Fig. 3.40. In fact, the well known row nucleation, which has frequently been found in the past, also points to a periodicity in the direction of the thread-like precursor. However, if the precursor does not exactly lie in the plain of the cross-section, one cannot see it on the picture.

Azzurri and Alfonso [62] concluded that the value of the activation energy, which was found to be the same for all samples of iPS, irrespective of their molar masses, forms a clue to the mechanism of the discussed relaxation. In this connection they quoted an interesting investigation, as carried out at Eindhoven University by Lippits et al. [65, 66]. These authors investigated the melting behavior of ultra high molecular weight polyethylenes (UHMW-PE) of molar masses above 106 Da. If such a polymer is polymerized with the aid of a single site catalyst at a low temperature, its nascent molecules directly crystallize during the process of polymerization. Apparently, these crystals do not contain amorphous regions, in which entanglements have been formed. The authors called this type of polymers "disentangled" nascent polymers. The crystals of those polyethylenes melt at a temperature of 141°C, which is close to the equilibrium melting point. In a temperature range above 135°C these crystals disintegrate rather fast. Below 135°C, however, the rate of disintegration slows down considerably. If in Arrhenius plots the logarithms of the pertinent relaxation times are plotted against the reciprocal values of the absolute temperature, one obtains very different activation energies above and below 135°C. Above 135°C one finds $5,000 \pm 1,000$ kJ mol^{-1}. Below 135°C two activation energies of $2,100 \pm 150$ kJ mol^{-1} and 600 ± 59 kJ mol^{-1}, respectively, were obtained. Apparently, above 135°C the crystal lattice collapses as a whole, whereas below 135°C two more subtle processes play a role. The lowest activation energy is interpreted as referring to the separation of single molecular segments bit for bit from the surface of the crystals. There is no doubt that the separation of a single mol of a repeating unit from the surface costs much less energy than the removal of an equal mol from the interior of the crystal. If recrystallization is carried out after complete melting, one finds for the newly formed crystals melting temperatures near 135°C. The above mentioned diversity of activation energies can no longer be observed.

Azzurri and Alfonso were intrigued by the relatively low activation energies of the order of 500 kJ mol^{-1}, which were found for several polymers of usual molar masses, if their precursors relaxed after the cessation of heavy flow treatments. In fact, for the precursors of the samples of iPS an activation energy of about 400 kJ mol^{-1} was found. As one can assume that no entanglements are present in those highly oriented structures, a comparison with the behavior of disentangled nascent samples of UHMW-PE seems justified. This means that one can assume that single segments of long molecules are dispatched bit by bit during the relaxation of oriented precursors. From the point of view of the position of the equilibrium melting point, this relaxation happens always in the temperature range of the metastable states. However, in contrast to the occurrences in the metastable regions

of low molar mass compounds, where new nuclei are permanently formed in a living equilibrium, until one is big enough for growth, no reassociation can occur in the melt of macromolecules because of the fact that those freed macromolecules directly coil up in the quieted down melt. The probability that new extended conformations are formed sporadically, is imperceptible, if there is no action of flow. Nevertheless, it is incorrect to speak of the entering into a new equilibrium, as many authors claim. In fact, even for a quiescent melt the temperature range between the high equilibrium melting point and the temperature, where spherulites melt, is and remains the metastable range of temperatures (see our Fig. 1.3). And the relatively low activation energy of the samples of iPS of about $400\,kJ\,mol^{-1}$ shows that Al-Hussein and Strobl must be right with their high melting point of iPS of $289 \pm 5°C$.

3.3.4   Adherence to the Growth Mechanism

3.3.4.1   Transformation of Dormant Nuclei by the Action of Flow [11]

In previous sections it has been emphasized that the orientation of macromolecules is a necessary but not a sufficient condition for the formation of oriented structures. This view is confirmed, if one looks at Fig. 3.10. On this figure one observes about 15 widely separated points, where thread-like precursors thrust through the plain of a cross-section, which has been cut perpendicular to the previous flow direction. And if one looks at Fig. 3.15, one learns, why such a separation is feasible and why the parameter of the specific work can be so useful. The conclusion must be that those treads are formed in a growth process. But every growth process must have a starting point. Corresponding spots must be envisaged. In this respect local alignments, which form dormant athermal nuclei below the temperature, where spherulites melt, are of particular interest. But also particles of nucleation agents can be active. In fact, the number of thread-like precursors increases tremendously, if a nucleation agent is used [50].

The question has been, why local alignments can form dormant athermal nuclei in a quiescent melt. In fact, the tensions, as caused by the tangling ends of those fringe micelles, depend on the thickness of these micelles. As long as such a micelle is very thin, these tangling ends enjoy a lot of freedom in their conformations (see Fig. 2.21). But this means that the "surface" tension at both ends of the body of the micelle remains rather small. But such a positive surface tension is always in balance with the negative difference of the free energies of the body with respect to the fluid. And the longer (the better organized) a micelle is, the larger is the value of this difference per unit cross-section of the micelle. If this negative free energy dominates, the micelle is stabilized: The local alignment can serve as a nucleus for the lateral growth of a micelle. However, during such a growth the tangling ends get into a squeeze. Their need of space will become larger than inside the ordered body. The growth of the lamella can be stopped, if the barrier in the tangling ends becomes too large. In this case the

said alignment will remain a dormant nucleus. The hypothesis is now that flow orients the lengthy alignments and irons their fringes. In this way the length of the body increases, This greater length (orderliness) causes a better stability of the alignment, so that it can become effective at a higher temperature. At the same time, this ironing paves the way for further growth. Such a micelle will still act as a point-like nucleus, as long as its length remains smaller than the distance to the centers of neighboring nuclei. But this distance decreases because of the increasing number of activated nuclei. This means that a critical configuration is reached during the growth of all those alignments. At this configuration the length surpasses the decreasing mutual distance. This fact may be the reason for the relatively sharp boundary normally found in duct flow experiments between the oriented surface layer and the core. It must also be emphasized that Fig. 1.1 is in favor of our hypothesis. Apparently, after various shear treatments at relatively high temperatures number densities of "point-like" nuclei are found, which correspond to equal number densities found in permanently quiescent melts at much lower temperatures.

For the present purpose Fig. 3.23 is redrawn, as shown in Fig. 3.41. In this latter figure a double logarithmic plot is given, in which the number density of "point-like" nuclei is drawn against the degree of undercooling $\Delta T = T_m - T_k$, where T_m is the equilibrium melting point and T_k is the temperature of the crystallization. For the purpose vertical lines have been drawn in Fig. 3.23 at various values of the specific work. The points of intersection of these vertical lines with the curves for constant temperatures are used in Fig. 3.41. For each chosen value of the specific work these points are connected. These new lines were called "isoergons." Also the isoergon for zero work is shown. It translates the course of the line on the left side of Fig. 1.1. In the present Fig. 3.41 this special isoergon is practically a straight line of the enormous slope of 30. Increasing undercooling is plotted in the negative direction in order to emphasize the decrease of the crystallization temperature. These crystallization temperatures are quoted for convenience at the upper ends of the corresponding vertical lines. The number density N is given per cubic meter m^{-3} and ΔT in K.

It must now be realized that the given number densities contain all nuclei, which are activated during the quench in the whole temperature range from the temperature of the stable melt to the intended temperature of crystallization. However, the number density of only those nuclei are required, which are activated in a small temperature interval – say of 1 K – near the temperature of their activation T_a. For the purpose the curves of Fig. 3.41 must be differentiated with respect to ΔT. By this differentiation one obtains a differential number density N' in $m^{-3}K^{-1}$. However, not only the number densities, which are obtained by a quench of the quiescent melt, must be differentiated in this way. Also for the isoergons, which hold for nonzero values of the specific work, the same differentiation must be carried out. In fact, all nuclei, which are located on the same isoergon at higher temperatures, can be activated already at these higher temperature by the specific work chosen.

It goes without saying that the said differentiation must be carried out in a correct way. This means that (for instance) $N \propto (\Delta T)^n$ – with $n = +30$ – has first to be
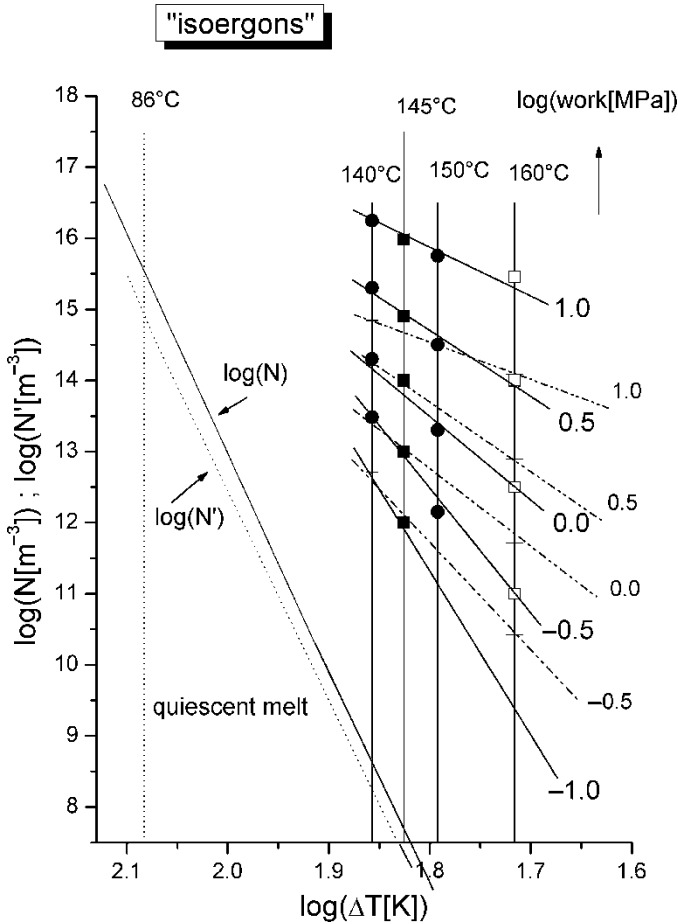
Fig. 3.41 Double logarithmic plots of isoergons, i.e., densities of "point-like" nuclei $N(m^{-3})$ and their differentiated versions $N'(m^{-3}K^{-1})$ vs. the degree of undercooling $\Delta T = T_m - T_k$. ΔT is plotted in the inverse direction. The differentiated isoergons are given as *dotted lines*. The logarithms of the specific works applied are given at the *right side*, big ciphers for the original isoergons and small ciphers for the differentiated isoergons [11]. Courtesy of Elsevier

transformed into a dimensionless expression, which is then differentiated, before being transformed back. In Fig. 3.41 the differentiated values N' are inserted as dotted lines. The logarithms of the specific works belonging to the original isoergons are given by bigger ciphers than those for the differentiated isoergons. Interestingly enough, all differentiated isoergons seem to converge at some temperature below 86°C. The corresponding value of N' is about $10^{16}m^{-3}K^{-1}$.

With the aid of the N's Fig. 3.41 is now transformed back into a figure, which is analogous to Fig. 3.23. However, in contrast to Fig. 3.23 in this new Fig. 3.42 the differentiated number densities are plotted against the specific work for the
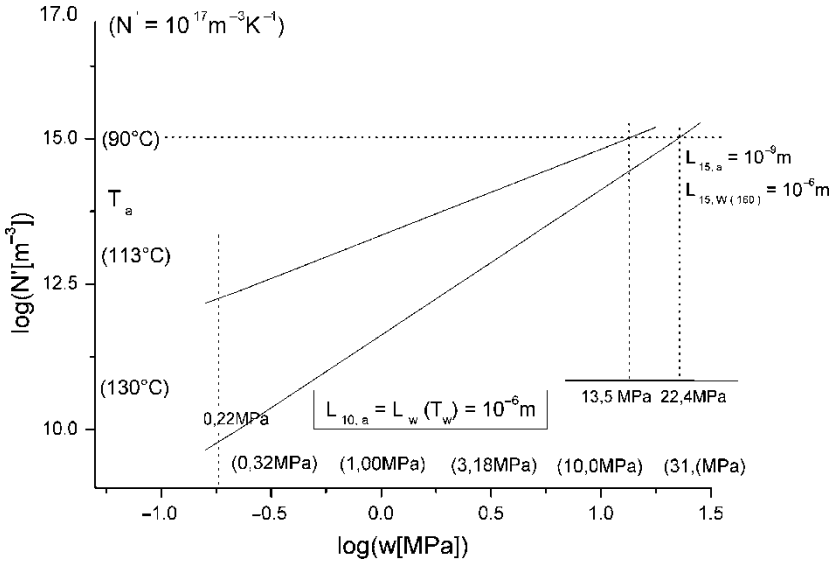
Fig. 3.42 Double logarithmic plots of the differentiated number densities N' against the specific works for the PP of Fig. 3.23 at two temperatures. On the ordinate axis also the corresponding activation temperatures are given between *brackets* [11]. Courtesy of Elsevier

industrial PP of Fig. 3.23. The advantage of this plot is that there is now a unique reciprocal relation between the logarithm of this differentiated number density N' and the temperature of activation T_a. Both parameters are given at the ordinate axis of Fig. 3.42. However, by all these redrawings the accuracy has suffered. So this figure must be considered as highly schematized. As a consequence only the lines for the limiting shearing temperatures $T_w = 160°C$ and $T_w = 140°C$ have been drawn.

Unfortunately, nothing is known explicitly about the size or the orderliness of the nuclei. Only the flow conditions and some numbers of nuclei are given. So it will be unavoidable that some assumptions must be made. For the purpose, however, the required symbols must be introduced first. Capital L is chosen for the effective length, i.e., for the orderliness of a nucleus. A first subscript gives the logarithm of the differentiated number density N'. (As "log N'" needs too much space in the subscript, the log-symbol is omitted, if log N' is meant in a general formulation. Explicitly, however, the value of the logarithm is given). A second subscript indicates, whether the temperature T_a of activation in the quiescent melt or the temperature T_w, at which the shearing has occurred, is meant. After the symbol the temperature T_w will always be given between brackets. Only occasionally T_a will be given, as this temperature is always coupled with log N'. For the specific work the symbol $w_{N'}(T_w)$ is used, where the subscript gives the logarithm of N', whereas the temperature between the brackets is the temperature, at which this specific work is applied. An example is now given: $L_{15,w}(160)$ means the effective length of a nucleus, which is activated in the quiescent melt at 90°C (log $N' = 15.0$),

but has undergone a shear treatment $w_{15}(160)$ at $T_w = 160°C$. For the effective length of a pristine nucleus at its activation temperature of 90°C, this activation temperature is only exceptionally given: $L_{15,a}(90)$. The specific work $w_{15}(160)$, which is responsible for $L_{15,w}(160)$, must be read from the graph. It is determined by the place on the log N' scale. In the present case this place is log $N' = 15$. Its amount is 22.4 MPa.

In a next step the insight is gained that along the lines in Fig. 3.42 the effective lengths do not change. It is assumed that a nucleus, which originates at some value of T_a (with a frequency N'), becomes an effective nucleus at the chosen shearing temperature T_w only, if it has just gotten an effective length corresponding to this T_w. This length must be independent of log N'. At zero specific work this length must be the one for $T_w = T_a$.

Before an effective length can be assigned to $T_a = 160°C$, the corresponding log N' must be found for $T_a = 160°C$. This is a precarious venture, however, as in Fig. 3.41 the intersection must be found of the vertical line at 160°C with the line of log N', which holds for the quiescent melt. This line must be lengthened to lower values. In this way one obtains for 160°C a value log $N' = 4.4$. Fortunately, the low accuracy of this value does not matter because of the extremely low value of the specific work of only 0.22 MPa, which is found at the lower end of the line drawn in Fig. 3.42 for $T_w = 160°C$. (The logarithmic scale for the specific work inflates at low arguments). At a higher temperature of the quiescent melt a lower number of nuclei reaches the characteristic length. But this occurs after a smaller specific work, as the original length is already larger.

Now the necessary assumptions must be made. These assumptions are:

$$L_{4.4,a}(160) = 10^{-7}m \quad \text{and} \quad L_{15,a}(90) = 10^{-8}m. \tag{3.20}$$

In the original publications [11] a much larger distance between these values was chosen, namely 10^{-6}m versus 10^{-9}m. This choice had the advantage that all contrasts where rather clear. However, according to more recent experiences the present choice is much more realistic. First of all, one must assume that a local alignment is longer than a single low molar mass molecule or a repeating unit of length 10^{-9}m. Secondly, the importance of the mutual distance between the centers of effective nuclei has been discovered meanwhile. But this distance refers to all effective nuclei, irrespective of their history. But this means that one has to go back to the unwrought Fig. 3.23. At a specific work of 25 MPa one has found a number density of nuclei of about $10^{16.5}$m^{-3}. But this corresponds to a mutual distance of about 3×10^{-6}m. Previously in this report the opinion has been expressed that a nucleus, which reaches a length comparable with the mutual distance between nuclei, can no longer grow out into a spherulite, but must be the starting point for an oriented structure. As a nucleus with such a length undoubtedly must be the result of a shear treatment – it actually has emerged only after such a treatment –, a mechanically untreated nucleus must have a shorter effective length. This fact explains the choice made on the left side of (3.20). Another argument for the choice of a lower upper bound for the effective length of a nucleus can also be given. It has to do with the more recent experience about the

considerable effect of pressurization on the number density of nuclei in a quiescent melt (see Fig. 3.2). However, one cannot assume that the tangling ends of a fringe micelle can be ironed by pressure so effectively that the effective length increases by a factor ten, a factor, which is assumed above for the influence of flow. Anyway, it must be admitted that virtually nothing is known a priori about the thermodynamics of a nucleus, and in particular about the dependence of a possible barrier height on the effective length of a nucleus.

At this stage of the consideration a choice must be made also for the growth mechanism. Reminding the reader of Fig. 3.15 one must opt for an exponential growth. In fact, Fig. 3.15 suggests that

$$\frac{dL}{dt} \propto L, \tag{3.21}$$

because of the fact that a bigger obstacle catches more passing molecules. (A bigger value of L does not only mean a higher orderliness but also a bigger size). According to our insights time t can be replaced by the specific work w. As a consequence one finds:

$$L_{N',w}(T_w) = L_{N',a}(T_a) \ \exp\left(A(T_w) \, w_{N'}(T_w)\right). \tag{3.22}$$

For the special case of log $N' = 15$ and $T_w = 160°\text{C}$ one gets:

$$L_{15,w}(160) \left(= L_{4.4,a}(160)\right) = L_{15,a}(90) \ \exp\left(A(160) \, w_{15}(160)\right), \tag{3.23}$$

with $L_{4.4,a}(160)$ and $L_{15,a}(90)$ from (3.20) and $w_{15}(160) = 22.4$ MPa. The only unknown in (3.23) is A(160). One obtains:

$$A(160) = 0.103 \ \text{MPa}^{-1} \tag{3.24}$$

This factor must be the same as long as $T_w(160)$ is the same. As a consequence one can now invert (3.22) for a calculation of intermediate values of $L_{N',a}$. For the purpose use is made of the values of $w_{N'}(160)$, which can be read from Fig. 3.42 for the diverse values of log N'. One has for instance:

$$L_{12.5,w}(160) \left(= L_{4.4,a}(160)\right) = L_{12.5,a}(113) \ \exp\left(A(160) \, w_{12.5}(160)\right) \tag{3.25}$$

Or

$$10^{-7} = L_{12.5}(113) \ \exp\left(0.103 \times 2.14\right). \tag{3.25a}$$

The solution of this equation is: $L_{12.5,a}(113) = 0.87 \times 10^{-7}$. Along the same route one obtains $L_{10,a}(130) = 0.96 \times 10^{-7}$. Table 3.5 contains a compilation of the relevant data for the primary nuclei together with the specific works applied at 160°C, which served for their calculation.

Table 3.5 Characteristics of activated nuclei, as calculated for quiescent melts of the PP of Fig. 3.23, with the specific works $w_{N'}(160)$

$L_{N',a}(m)$	$\log(N')(m^{-3}T^{-1})$	$T_a(°C)$	$w_{N'}(160)(MPa)$
1.00×10^{-7}	4.4	160	0.0
0.98×10^{-7}	10.0	130	0.22
0.87×10^{-7}	12.5	113	2.14
0.10×10^{-7}	15.0	90	22.4

These values of $L_{N',a}(T_a)$ have nothing to do with the working temperature $T_w = 160°C$ of an equation of the type of (3.25). They must be useful also for calculations at the lower working temperature of $T_w = 140°C$. In this connection the factor A(140) is of special interest. However, this factor cannot be calculated like A (160). In fact, $L_{N',w}(140)$, which must be a constant along the line for $T_w = 140°C$, can no longer be chosen independently, as it occurred for $L_{N',w}(160)$ in (3.23). Instead, use must be made just of this constancy of $L_{N',w}(140)$. So one has:

$$L_{12.5,w}(140) = L_{15,w}(140).\tag{3.26}$$

If the values of $L_{12.5,a}(113)$ and $L_{15,a}(90)$ are taken from Table 3.5, one obtains in more detail:

$$0.87\ \exp[A(140) \times 0.27] = 0.10\ \exp[A(140) \times 13.2].\tag{3.26a}$$

The solution of this equation reads:

$$A(140) = 0.168\ \text{MPa}^{-1}\tag{3.27}$$

This value is a little higher than the value of (3.24). But this is all right, as the sensitivity to the specific work must increase with decreasing working temperature. The next goal must be a calculation of the extra effective lengths, which are created, if with the growth of the nuclei the lines for the chosen values of T_w of Fig. 3.42 are surpassed. This happens, if instead of the values of $w_{N'}$, which just lead to the said lines, are replaced by the difference between 22.4 MPa and these values. In this way one obtains the over-lengths, which are obtained, when the transition to the oriented structure is observed for the nuclei, which are active already at 160°C (or at 140°C). One has for the lowest point on the line for $T_w = 160°C$:

$$L_{10,22.4}(160) = 0.98 \times 10^{-7}\text{m} \times e^{0.103 \times (22.4 - 0.2)} \cong 1 \times 10^{-6}\text{m}.\tag{3.28}$$

For the lowest point on the line for $T_w = 140°C$ one obtains:

$$L_{12.5,22.4}(140) = 0.87 \times 10^{-7}\text{m} \times e^{0.168 \times (22.4 - 0.3)} \cong 3.6 \times 10^{-6}\text{m}.\tag{3.29}$$

One observes that in both cases an over-length is obtained, which is close to the mutual distance between the nuclei, which is found in Fig. 3.23 for 25 MPa. Also the temperature dependence has become rather low. This result is in favor of our

hypothesis that the transition to the highly oriented structure starts, when the effective lengths of special nuclei becomes comparable with the mutual distances between all kinds of nuclei, irrespective of their history. In this case these special nuclei can no longer grow out into spherulites. In fact, during the action of flow two processes act in opposite directions: Nuclei grow in length, whereas the space around them decreases. But these nuclei would need this space for their development into spherulites after cessation of flow.

This fact seems to explain, why in duct flow experiments almost always a sharp boundary is observed between the highly oriented surface layer and the spherulitic core. Clearly, in these experiments the shear rate and – with it – the specific work decreases with increasing distance from the wall. So far no explanation has ever been tried for this conspicuous phenomenon. This phenomenon is also in favor of the hypothesis that the number of effective nuclei increases because by the growth in the flow field the effectiveness of otherwise dormant nuclei increases.

3.3.4.2 A Reassessment of the Model of Section 3.3.1.2

The result of Sect. 3.3.1.2 was achieved with the aid of very simple assumptions. The rate of formation of primary nuclei was assumed to be independent of the shearing time. It should depend only on the shear rate. A corresponding assumption was made for the rate of growth of thread-like precursors. Two proportionality factors were required in this way. The only condition was that the said factors were multiplied by even functions of the shear rate. In fact, the result should not depend on the direction of shearing. And the most simple even function is the square of the shear rate. By colleagues, who are possessed by the idea of numerical simulation, this approach has been criticized because of the fact that it contains two adjustable parameters. The said authors did not want adjustable parameters but a molecular theory without adjustable parameters. However, the results of the experimental investigations, which were described in the preceding sections, should convince the reader that such a molecular theory can not have any chance. There were only those foreseeing experiments, which enabled us to discern between different critical regions of temperature and of mechanical loads. In this respect the reader is reminded of the distinction between the role of the temperature range stretching down from the thermodynamic equilibrium melting point to the melting temperature of the spherulites and the role of temperatures below the melting temperature of spherulites. And also: three ranges of mechanical treatments could be discerned. There is the range of low mechanical loads characteristic for ordinary rotation viscometers, the range of intermediate loads covered by the measurements with the sandwich apparatus [10] and the range of high mechanical loads, as realized with the aid of duct flow experiments [16, 17, 20, 27, 37, 38] and with glass fiber pulling [12, 57–59]. In the latter experiments very high shear rates can be achieved. A necessary quantitative interpretation, however, is very difficult because of the very steep descent of the shear rate with increasing distance from the fiber. One should not forget that the shear rate at the

fiber surface goes to infinity, if the diameter of the fiber goes to zero. As a consequence only those fiber pulling measurements were useful, in which a comparison at constant pulling conditions was made. As a consequence, the duct flow experiments remained for a more advanced evaluation. And this fact throws a special light on the experiments discussed in Sects. 3.3.1.1 through 3.3.1.3. The obtained results can still be considered as extraordinary, even if later experiences raise new questions. With this hesitation in mind the following deliberation must be considered.

For example the line for 160°C in Fig. 3.42 is envisaged. With the aid of (3.28) one learns that for its lower end at $\log N' = 10$ the critical effective length of nuclei for the formation of shishs (of – say – 10^{-6} m length) is just reached after the application of a specific work of 22.4 MPa. However, if one takes the upper end of the curve for 160°C at $\log N' = 15$, the amount of specific work of 22.4 MPa is only sufficient to create an effective length of 10^{-7} m. But this length is only one tenth of the mutual distance between the average nuclei. If the growth mechanism remains unmodified, another amount of work of the order of 22.4 MPa will be needed to make these nuclei active for the formation of shishs.

However, can continued exponential growth occur also above $L = 10^{-6}$ m? In fact, it has been observed that thread-like nuclei form the scaffold for shish-kebabs, as soon as their increasing length becomes comparable with the decreasing distance between the centers of all kinds of activated nuclei. Whereas for the low density of activated nuclei, as shown in Fig. 1.1, an independent growth mechanism can be assumed, such an assumption will not necessarily be feasible, if the mutual distances between the nuclei become comparable with the lengths of the thread-like nuclei. As soon as this happens, an interference of growth mechanisms must occur. In fact, those lengthy nuclei become neighbors. They will move in flow direction with different speeds. This difference in speed, however, leads to the fact that their centers draw away from each other without limit. As a consequence also a disruptive effect will be manifest. So far, such a disruptive effect has always been neglected by model builders. But it will be most important in the high shear rate range. The present author became convinced of the inevitableness of such a disruptive mechanism, when trying to interpret results obtained with continued shearing. It cannot be excluded even with low shear rates, as will be explained in Sect. 3.3.5.2. And at high shear rates also a transition to a purely kinematical mechanism may be expected.

The conclusion must be that the exponential growth according to (3.22), which certainly is characteristic for the independent growth, must not necessarily be valid, if interactions play a role. But the described disruptive mechanism can only reduce the effective growth speed of threadlike precursors. In fact, these threads can also break. This conclusion is in favor of the mechanism described in Sect. 3.3.1.2, which – remarkably – excludes the influence of the viscosity. Apparently, nucleation and growth occur on a slower pace. Also, there do not exist other experimental results, which are capable of contesting a law like the one given in (3. 6) or (3. 13).

With the sandwich construction one would need longer glass slides. From Fig. 3.23 one knows that the points at 25 MPa cannot be obtained with the sandwich

apparatus. The highest point for the sandwich machine is at about 8 MPa. This means that with the sandwich apparatus the total shear must be increased by at least a factor three. In the present machine the slide length is 20 cm. Shear must be stopped, when a length of 5 cm is left between the slides. This means that with twofold length of the slides just a threefold shear can be reached. But a glass slide of a thickness of 1 mm and a length of 400 mm (instead of the previous 200 mm) is not a nice part. But a plate and plate rheometer cannot replace such a sandwich machine because of secondary flow. This flow causes radial displacement of fluid volumes and, with higher rotation speeds, leads to catastrophic situations.

Duct flow experiments suffer to some extent of a similar problem as fiber pulling experiments. If the duct is not long enough, only a zone close to the wall reaches high enough total shears. At a larger distance from the duct wall the finite residence time causes a limitation of the shear. But, if the zone near the wall becomes too narrow, an interpretation will be difficult. In principle also transcrystallization, which starts at the duct wall during cooling of the still quiescent melt, can be of influence. In fact, every metal wall is crystalline and provides nuclei, which can be active already at higher temperatures. Because of the restricted length of the duct one arrives at a similar conclusion as with the sandwich machine: the duct should be lengthened. But a rather long duct requires high extrusion pressures. Unfortunately, even short time pressurization can cause a considerable increase of the number density of effective nuclei (see Fig. 3.2).

Only recently the present author recalled old experiences from the time, when he was research leader in polymer melt extrusion about forty years ago in Holland at TNO. There is a well-known technique for coating an electric cable with a layer of insulating plastic. For the purpose, the blank cable is drawn through the orifice of the die head of an extruder. Probably, it will be possible to draw a thin steel band through a long duct of large aspect ratio. A linear flow profile on both sides of the moving steel band corresponds to a certain output. Exactly this output can be provided by the feed section. In such a case the extrusion pressure is practically zero. As a consequence the walls of the duct can be made of thin plates, so that cooling to the crystallization temperature or down to room temperature can be very fast. Also, no problem will arise with transcrystallization. There will be enough space in the interior of the duct because of the uniform shear rate. There will be no strong gradient of the shear rate near the walls. Of course, practical problems must be solved first. Dismantling of the apparatus must be easy. The duct must be filled, before the steel band is introduced. The amount of material must not be too large. A piston, which is moved in a properly heated cylinder, will be favored with respect to a screw extruder. A series of equidistant windows may be placed in the duct walls for following the movement of the band. For the purpose a little hole is drilled into the band, so that light can pass at corresponding moments. If the hole is at the first window, when flow is started, flow can be arrested at one of the later windows, so that certain amounts of shear can be administered at the chosen shear rate. The corresponding viscosities as functions of temperature and shear rate must be determined with the aid of standard equipment.

The reader may feel that a whole research program is introduced here. But the chances for a realization are not so good for an emeritus. As a consequence he wants to save these ideas for some future investigators.

3.3.5   Uninterrupted Flow Treatments

3.3.5.1   Continuous Shearing

Shearing of an undercooled polymer melt up to the rapid increase of its viscosity has been the eldest method for the characterization of flow induced crystallization. In this respect the papers by the school of Maxwell [1, 67] have to be mentioned. Very recently, a painstaking study has been published in this field by Hadinata et al. [68, 69], which will serve as a basis for the present discussion. The authors investigated three samples of industrial PB-1 of differing molar masses. These are the samples PB200, PB0300 and PB0400 of Table 3.3. Remarkably, the viscosities of these samples at 150°C are extremely different, namely 230 kPas, 11 kPas and 1.8 kPas, respectively. The melting temperature of Form II of 109.6°C was used, when the degree of undercooling was given. The melting temperature (of the spherulites) of Form I has been reported as 121°C.

A parallel plate rotational viscometer ("Advanced Rheometric Expansion System, ARES") was used for the mechanical measurements and the Linkam CSS450 hot stage, as developed by Mackley et al. [70], was used for the optical measurements on the microscope. After the usual annealing treatment (for PB-1 at 180°C), which aimed at an erasion of remains of previous crystallization, the hot samples were squeezed in the shearing units to the proper thickness. For the rheometer a thickness of 1 mm was appropriate. For the Linkam stage a thickness of only 0.07 mm had to be reached. The samples were permitted to relax, before they were cooled down to the temperatures, where the measurements should take place. At the lowest temperature of 99°C it took about one hour, before the quiescent sample started crystallizing. For the cooling procedure only about 300 s were required.

Results, as obtained for the sample of the lowest molar mass (PB0400), are shown in Fig. 3.43 for the three temperatures of 99, 103 and 107°C. The shear rates applied are given near the diagrams. They range from $10^{-4} \mathrm{s}^{-1}$ to $3 \times 10^{-1} \mathrm{s}^{-1}$. The normalized viscosity $\eta(t)/\eta(t=0)$ is plotted in all graphs against the logarithm of the time t of shearing. One observes that the time of the upturn is highest for the lowest shear rates. For the temperatures of 99 and 103°C there is almost no difference in these times for the lowest three shear rates. The conclusion by the authors has been that the averaged common time corresponds with the time of the upturn in a quiescent melt. For a more quantitative treatment times were chosen, where the reduced viscosity reached its doubled value. (See the dashed horizontal lines). One can see that with increasing shear rates the times of the upturn decrease tremendously. By the authors these times were called the times of the onset t_{on} of the crystallization.
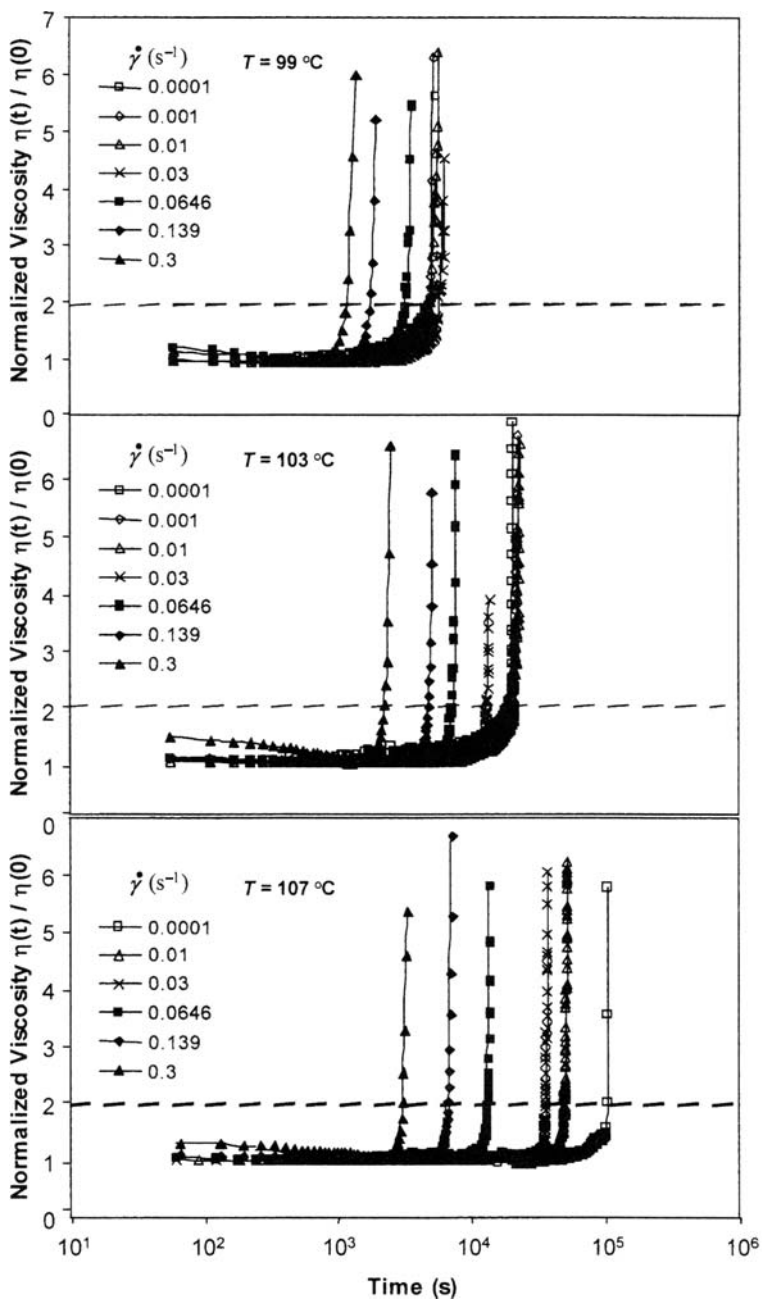
Fig. 3.43 Normalized viscosity development at crystallization temperatures of 99, 103 and 107°C and shear rates from 10^{-4} to $3 \times 10^{-1}\,\mathrm{s}^{-1}$ for sample PB0400, according to [68]. Courtesy of The Society of Rheology
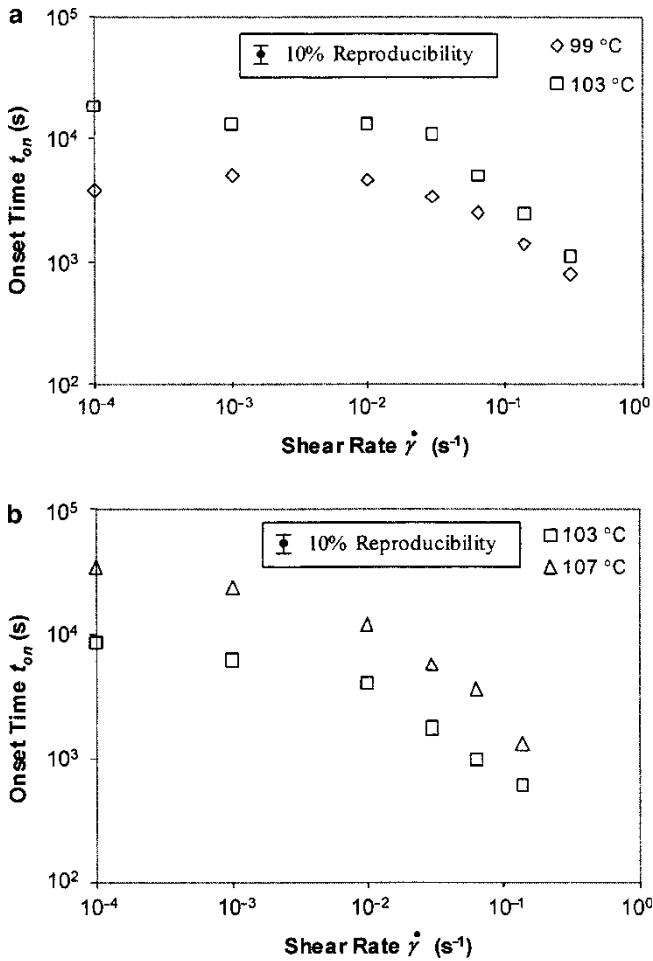
Fig. 3.44 The dependence of the onset time on temperature and shear rate for PB0300 (*upper picture*) and PB200 (*lower picture*) according to [68]. Courtesy of The Society of Rheology

In Fig. 3.44 the logarithms of these onset times are plotted against the logarithms of the shear rates for the two samples of the higher molar masses and, in each case, for two temperatures. The authors may excuse the comment that for the sample PB200 (lower picture) the onset time for the quiescent melt does not seem to be reached at the lowest shear rate of 10^{-4}s^{-1}. Later in this section there will be an explanation for this doubt, when the morphology is considered. In fact, a look on Fig. 3.23 shows that, avowedly, for another polymer, the number density of nuclei increases at 145°C with the third power of the specific work applied. Wolkowicz [5] has shown that also for a PB-1 the number density of nuclei increases very fast in a nonlinear way with the shear rate. In that year nobody expected that the specific work was the decisive parameter. But a strong dependence on the specific work

means that at equal shear rate the number density of the sample with the by far highest viscosity will be many times higher than that of the samples of much lower viscosities. In fact, at equal shear rate the specific work is proportional to the viscosity. So one can expect that the process of crystallization will be obvious much earlier in PB200. This means that one has to go to still lower shear rates for the determination of the onset time $t_{on,q}$ in the quiescent melt.

Another feature of these double logarithmic graphs is that at the high end of the shear rate range the slope of the curves is minus one. This fact is particularly clear in the graph for PB0400, which is omitted here because of space economy. Beautiful curves of this type have quite recently also been published by Chen et al. [71] for an industrial polypropylene ($M_w = 3.3 \times 10^5$). These authors used also the onset time of the normal force, as measured in their cone-and-plate rheometer (Bohlin instruments), as an indicator of the onset of crystallization. Interestingly enough, in their high shear rate range (0.07–1 s^{-1}) the onset times obtained with the aid of the normal force were a factor one half of those obtained with the aid of the shearing force (viscosity). Only at low shear rates equal values were obtained.

Hadinata et al. [69] succeeded in extending the shear rate range to values of the shear rate relevant for processing conditions. With their parallel plate machine flow became unstable at about 1 s^{-1}. In replacing this apparatus they used a concentric cylinder device and also a normal capillary rheometer. During extrusion through the undercooled capillary the effective radius of the capillary decreases with the distance from the entrance and with time. The initial extrusion pressure was calculated from the melt rheology at a higher temperature, using the time temperature shift factor. The ratio of the measured pressure and the initial pressure is shown as a function of the extrusion time in Fig. 3.45 for two apparent initial shear rates at the capillary wall, if sample PB0400 is used.
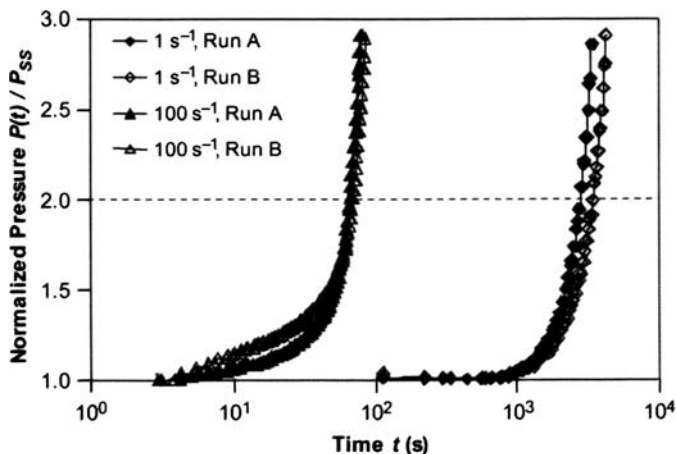
Fig. 3.45 Development of normalized extrusion pressure in capillary rheometer, as caused by the onset of crystallization at the wall. Apparent initial shear rates at the wall were 1 s^{-1} and 100 s^{-1} for PB0400 at 107°C. Measurements were possible up to 500 s^{-1}. According to [69], courtesy of Springer Verlag
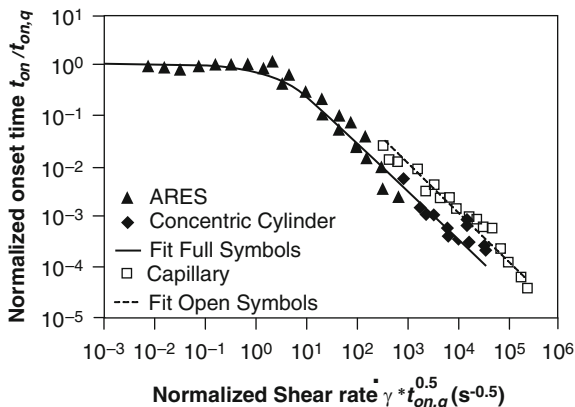
Fig. 3.46 Temperature invariant curves for PB0400, combining onset time data from "ARES," concentric cylinder apparatus and capillary rheometer as functions of reduced shear rate, according to [69], courtesy of Springer Verlag

In Fig. 3.46 a double logarithmic plot is given. It shows the normalized signals, as obtained with parallel plate rheometer, concentric cylinder apparatus and capillary, as functions of the normalized shear rate. The range of slope minus one is extended here over almost four decades. The response of the capillary occurs almost one decade later than that of the rotational viscometers. But it should be clear that always new uncrystallized melt entered the capillary. The residence times at several distances from the capillary axis take over the role of the onset times, as measured in the rotational devices. But the capillary measurements are of particular interest. They show that the highly oriented surface layers, as observed, e.g., in injection molded samples, can already solidify during injection.

The reduced shear rate $q t_{\text{on},q}^{0.5} (s^{-0.5})$ must still be explained. The authors found that by multiplying the shear rate q by the square root of the temperature dependent onset time $t_{\text{on},q}$ of the quiescent melt, they obtained a temperature independent plot, as shown in Fig. 3.46 (with the normalized onset time $t_{\text{on}}/t_{\text{on},q}$ on the ordinate axis). The authors also mentioned in ref. [68] that one would have got an equivalent plot, if as an abscissa the square of the said reduced shear rate would have been used, in accord with the findings of the research group in Linz [16]. In fact, the normalized onset time remains unchanged up to the moment of the upturn of the viscosity. So far this held only for the considered special polymer, which has, as a consequence of its low molar mass, a practically shear rate independent viscosity. But the authors also tried to find a plot, which was of a more general validity independent of the molar mass of the sample. For the purpose they multiplied the above reduced shear rate by the square root of characteristic retardation time Λ. This retardation time also includes the influence of the breadth of the molar mass distribution and is defined as:

$$\Lambda = \eta_0 J_e^0, \tag{3.30}$$

where η_0 is the zero shear viscosity and J_e^0 is the equilibrium shear compliance, which does not depend very much on temperature. In this way one obtains a normalized shear rate, which reads:

$$q t_{\text{on},q}^{0.5} \Lambda^{0.5}. \tag{3.31}$$

This normalized shear rate is dimensionless. If it is used on the abscissa, one obtains for all the three samples of PB-1 the same value of the normalized shear rate of about unity, where the deviation from the horizontal line of Fig. 3.46 starts. In (3.30) the Newtonian zero shear viscosity η_0 is used. But this means that the square of the normalized shear rate is proportional to the specific work only at low values of q (with J_e^0 as the proportionality factor). At normalized shear rates beyond unity the points for the diverse samples deviate to varying degrees from the lengthened horizontal line. The most pronounced decrease is found for the lowest molar mass. This decrease becomes less pronounced with increasing molar mass. However, proper shifts to the left of the logarithms of normalized shear rates could make points of the higher molar mass samples coincide with those of the lowest molar mass. In fact the factor $q^2 t \eta_0$ is no longer a proper measure for the specific work, if the shear rate is increased. With increasing molar mass the phenomenon of the non Newtonian viscosity becomes more and more pronounced. The viscosity decreases with increasing shear rate. Making this correction in the concept of Hadinata et al. [68] one would probably get an almost perfect reduction not only with respect to temperature, but also with respect to the molar mass.

There is still another point of great interest in the work by Hadinata et al. [68]. This interest has to do with the morphologies obtained. For two situations these morphologies are shown in Fig. 3.47 for the sample PB200 of the highest molar mass. At a temperature of 103°C the melt of this sample was sheared for an onset
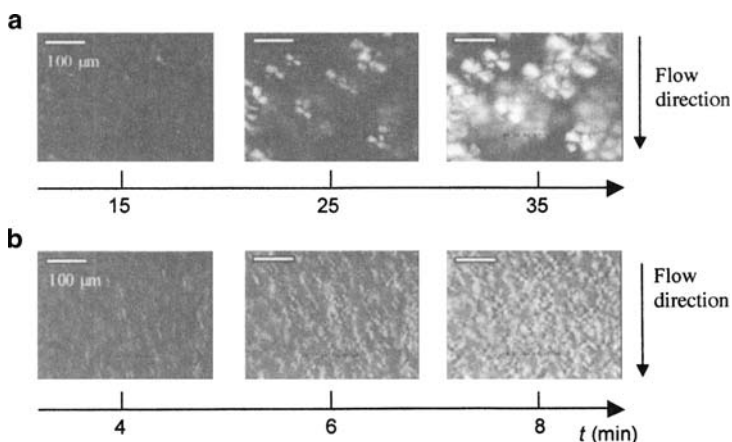
Fig. 3.47 Morphology development of PB200 after two shear treatments at 103°C: 0.139 s^{-1} for 420 s and 1 s^{-1} for 100 s, according to [68], courtesy of The Society of Rheology

time of 420 s at a shear rate of 0.139 s^{-1} (upper picture) and for a time of 100 s at a shear rate of 1 s^{-1} (lower picture). For the first mentioned treatment one finds the corresponding point in the lower graph of Fig. 3.44. It is the last point given by an open square. If a slope of minus one is drawn through this point, the corresponding straight line passes almost exactly the lower right corner of the graph. But this means that this corner should be considered as the corresponding point of the lower picture of Fig. 3.47. Rheology did not furnish this point for mechanical reasons. But the Linkam machine was able to reach the required deformation, but without permitting a viscosity measurement.

In both cases the formed morphologies could not be observed immediately after the cessation of flow. Waiting times were required for the development of these morphologies. These times are given in minutes below the photographs. Scaling bars indicating 100 μm are shown in the upper left corners of the photographs. In the waiting times the shearing times are included (7 min for the upper picture and 1.7 min for the lower picture). As also emphasized by the authors, only spherulites were found after the treatment characterized by the last point (open square – not in the corner!) in the lower graph of Fig. 3.44. But this point already lies within the range of slope minus one. Surprisingly, the upturn in the viscosity occurred, before any morphology could be observed. This means that the spherulites grow and impinge only later, after flow has been stopped. One is reminded of the unexplained mechanism prevailing in Winter's gelation (see Sect. 2.3.3). Can it be that this mechanism plays a role, if the distance between primary nuclei is reduced so much? This consideration may remain also worth of a deliberation for the harsher treatment, which has led to the lower picture of Fig. 3.47. But there is another important aspect of the lower row of pictures. On these photographs one can see lengthy structure elements. But the average distance between these structure elements is of the same order of magnitude as their length. This finding is in agreement with a crucial assumption of Sect. 3.3.4.1. According to this assumption the transition from nuclei, which give rise to the formation of spherulites, to nuclei, which form the back bone of thread-like precursors, occurs, when the length of the growing fringe micelles surpasses the decreasing distance between their centers. Also very satisfying is the fact that the number density between the upper and the lower row of photograph has increased tremendously. If one calculates the corresponding specific works, one arrives at a factor of about 13, if the non Newtonian behavior of the viscosity is ignored. A comparison with Fig. 3.23 gives an increase of the number density by about three decades for iPP. But here we have to do with another polymer. If the non Newtonian viscosity were taken into account for PB200, the said factor would become smaller. Nevertheless, the increase of the number density of nuclei would still be enormous, in agreement with Fig. 3.47.

3.3.5.2   A Tentative Model Consideration

The reader may feel that it must be quite difficult to understand the processes occurring in a sample during its continued deformation, if this deformation

practically ends, when a considerable change occurs in the mechanical properties (gelation, kind of solidification). In fact, understanding the behavior of formation of one dimensional structure elements like long fringe micelles, thread-like precursors or shishs is comparatively easy. These elements grow in the direction of the flow lines, whereas the formation of a three-dimensional structure always involves transverse growth. But transverse growth must not always be promoted by shear flow. One mostly thinks only of the positive effect of orientation. However, transverse expansion of structures will also be disturbed. As a reason for this fact it must be mentioned that the distances between the centers of gravity of already formed aggregates increase sometimes after short approaches unboundedly during steady shear flow. This fact can only lead to rupture of short living contacts, a process, which certainly is governed by some characteristic time. If the mentioned approaches occur in a too rapid succession, no aggregation will even be possible. For the first, however, these "secondary" influences will be disregarded.

With the use of the parallel plate rheometer the measurements have been carried out only in a range of specific works, where without exception only the number of effective nuclei can have been increased. These works were too low for the formation of thread-like precursors. So, one can make use of the experiences gathered in Sect. 3.3.2. There we found that the number density of effective nuclei increased with the specific work as follows:

$$N = A \left(\eta \, q^2 \right)^n t^n, \tag{3.32}$$

where A is a factor, η is the viscosity of the melt, q is the shear rate, t is the time of shearing and n is a number varying according to our experiments on iPP between three and four. In this equation time t is separated out because of the intended use of (3.32) in a time integral. (The specific work is $\eta q^2 t$.)

For the intended calculation Kolmogoroff's equation is used in the form given by (1.2). The situation with shear flow is treated here as an example. If for the virtual space covering ξ_g^* an upper limit of one is assumed, this means that the real degree of space covering has reached a value of 0.63. This value seems sufficient for the assumption that the viscosity has become large enough. An overall growth speed of $G(q)$ is assumed. In fact, the nuclei still behave like point-like nuclei and grow in all directions even if there is flow. We only aim at a degree of space filling. We have seen that spherulites actually become noticeable only some time after the cessation of (short term) flow. So we are inclined to assume that in a first process rather diffuse spheres of (mechanical) influence extend around the nuclei. Only later ready-built spherulites are growing. Those spherulites should grow within the said spheres of influence. So the discovery of Winter can gain an unforeseen importance. Because of the fact that the viscosity of the melt does not change considerably before its up-swing, one can assume that $G(q)$ remains practically unchanged up to this moment and depends only on the constant shear rate applied. In principle, also the contribution to the space covering, which would be caused by crystallization in the quiescent melt, should be included. So one has:

$$\xi_g^* = \frac{4\pi}{3} G^3 \left\{ N_0 t^3 + nA (\eta q^2)^n \int_0^t du \, u^{n-1} (t-u)^3 \right\}. \qquad (3.33)$$

In this equation N_0 is the number density of nuclei in the quiescent melt. In the second term between the accolades (3.32) is used in differentiated form in obtaining the rate of the appearance of effective shear induced nuclei. The time dependent radius of the spherical entities is given by $G(q)(t-u)$. The most relevant case of $n = 3$ is now treated. One obtains:

$$\xi_g^* = \frac{4\pi}{3} G^3 \left\{ N_0 t^3 + 0.05 (\eta q^2)^3 A t^6 \right\}. \qquad (3.34)$$

In this equation A has the dimension $(\text{mPa})^{-3}$. As the term containing the sixth power in time should rise later than the term with the third power, this equation would have the right form for our purpose. In this picture the more or less sudden rise of the viscosity with shearing time t will be assumed to be due to the sixth power of time in the second term between the accolades of (3.34). At shorter times, where the third power term dominates, one obtains a practically constant viscosity anyway because of the fact that the uninfluenced melt has already a finite viscosity, which is considerably surpassed only, if the volume of the crystalline phase becomes large enough. Unfortunately, our knowledge of the growth speed G is quite insufficient for a direct use of (3.34) at nonzero shear rate. In contrast, the shear rates themselves and the corresponding shearing times t_{on}, where the up-turn of the viscosity occurs, can readily be determined. These facts suggest a conversion of (3.34), so that the growth speed can now be determined indirectly. At the moment of "solidification" (3.34) becomes:

$$1 = \frac{4\pi}{3} G^3 \left\{ N_0 t_{on}^3 + 0.05 (\eta q^2)^3 A t_{on}^6 \right\}. \qquad (3.35)$$

First of all we are interested in the value of the factor A for our PP at 145°C. If in (3.32) the exponent n is put equal to three, one has:

$$N = A w^3 \quad \text{with} \quad w = \eta q \gamma. \qquad (3.36)$$

In this equation w is the specific work and $\gamma = qt$ is the total shear obtained at time t. Shear rate $q = 1 \text{ s}^{-1}$ is now chosen for practical reasons. For this shear rate Jerschow [50] found at 200°C a viscosity of $\eta = 3.140$ kPas. Using the known activation energy for viscous flow of PP of 44 kJ mol^{-1} one obtains for 145°C a value $\eta = 13.5$ kPas. A look on a figure in the paper by Chen et al. [71] is quite informative. This figure is of the same character as Fig. 3.44 of the present script. The Chinese authors inform the reader that for their PP, which is similar to our PP, a slope of minus one is found on a double logarithmic plot of t_{on} vs. q at $q = 1 \text{ s}^{-1}$ and a temperature of 145°C. Apparently $qt = \gamma$ is constant

with the said slope of –1. A value of $\gamma_{tot} \approx 1{,}000$ can be deduced from the said graph at $q = 1 \text{ s}^{-1}$. (For the polybutenes only a value of $\gamma_{tot} \approx 100$ was found by Hadinata at al. [68]). Using the values of γ_{tot} and η one obtains for the PP a value of $w = 13.5$ MPa. (By the way: only at 25 MPa we found the transition to the shish formation!) From Fig. 3.23 one learns that at the value $w = 13.5$ MPa the number density of effective nuclei is $2.0 \times 10^{16} \text{m}^{-3}$. So, one obtains:

$$A(\text{PP}, 145°\text{C}) = 0.815 \times 10^{-5} (\text{mPa})^{-3}. \tag{3.37}$$

In a next step one can now calculate the shearing time, where according to (3.35) the terms of the third and the sixth power in t become equal, and where they cross each other. In fact, from that moment the sixth's power term will dominate. One has:

$$t^3_{cross} = \frac{N_0}{0.05\,A\,(\eta q^2)^3}, \tag{3.38}$$

Or

$$t_{cross} = \left(\frac{N_0}{0.05\,A}\right)^{1/3} \frac{1}{\eta q^2}. \tag{3.38a}$$

The next parameter we need is N_0. From Fig. 3.41 one can learn that N_0 is of the order of 10^7m^{-3}. A more accurate value cannot be deduced from the extrapolation made. However, as only the third root of N_0 will be needed, there will be no serious problem. Another point is the viscosity. The above value of 13.5 kPas holds for $q = 1 \text{ s}^{-1}$. As also lower values of the shear rate are of interest, this viscosity will be higher in this range of shear rates. As a consequence, the values of t_{cross}, as calculated with the above constant viscosity, will be too large. A factor (1/6)th will for t_{cross} correspond with the zero shear viscosity. If nevertheless the constant viscosity $\eta = 13.5$ kPas is used, one obtains with (3.38a):

$$q = 1 \text{ s}^{-1} : \quad t_{cross} = 2.14 \text{ s}$$

$$q = 0.1 \text{ s}^{-1} : \quad t_{cross} = 214 \text{ s}$$

$$q = 0.01 \text{ s}^{-1} : \quad t_{cross} = 21400 \text{ s}. \tag{3.39}$$

At first sight these values seem realistic. However, a look at (3.38a) teaches us that according to this equation $t_{on}q^2$ is expected to be constant. However, from experiments it is well-known that in the critical range of higher shear rates the product $t_{on}q$ is constant. If the non Newtonian viscosity is taken into account, this discrepancy is mitigated. The calculated longest times will become shorter, as the viscosity is actually higher at the low shear rates. In this respect one must not forget that the

decrease of the viscosity with increasing shear rate is ascribed to the disentangle-
ment process. But this process is a kind of wrecking a structure. If some provisional
crystalline structure is in the make, such a wrecking can be destructive for such a
structure. If this (partial) wreckage is not ignored, the shortest times, as predicted by
(3.38a), will become longer. So, the demand that $t_{on} \cdot q$ must be constant, will be
approached. (See also the first paragraph of this section). A supplemental discussion
will be given below. It seems that for the polybutenes lower values are expected for
t_{on}. But no pertinent estimates can be made because of a lack of data, as presented in
Fig. 3.23 for our PP.

At sufficiently low values of time the first term between the accolades of (3.35) will
dominate. One obtains the quasi-quiescent situation. For this situation the value of G is
known from direct measurements. This means that t_{on} can be calculated. This is in
contrast to the situation at long times, where the second term between the accolades
dominates. As mentioned above, for this advanced situation we have only the possi-
bility to calculate G from the quite accurate experimental values of t_{on} and q. However,
let us remain for the moment at the low values of time, where $t_{on} = (3/4\pi)^{1/3} N_0^{1/3} G^{-1}$.

For 145°C a value of $G = 4 \times 10^{-9}$m s^{-1} has been found [27, 72] for the
quiescent melt. With this value a t_{on} of 0.724×10^6s is obtained. At first sight this
value seems too high. Probably, G is too low. In fact, at those high temperatures the
polymer does not like to crystallize in a quiescent melt, so that one can get great
experimental difficulties. For PB0300 we know the growth speed at 100°C [73] but
no value for A. In fact, we have no graph like Fig. 3.23 for this polymer. But the
growth speed of the spherulites of PB0300 is a factor ten higher at 100°C than that
of the PP at 145°C. There is a tinge of reality anyway in this comparison. In the
work of Chen et al. [71] the onset time of their PP for the quasi-quiescent situation
is more than a factor ten higher at 145°C than with PB0400 at 107°C [68], but not
high enough for a correspondence with the value calculated in the second paragraph
after (3.39).

A calculation of the growth speed for $t \geq t_{cross}$ will be a necessary task. If the first
term between the accolades of (3.35) can be neglected, on has:

$$ G = \left(\frac{15}{\pi}\right)^{1/3} \frac{1}{A^{1/3} \, \eta \, \gamma_{tot}^2}. \tag{3.40} $$

Actually, in the denominator of this equation the product of $q t_{on}$ should show up
instead of γ_{tot}. However, because of the fact that according to the experiments this
product is independent of q at $q \geq 1$ s^{-1}, this replacement is permitted. As a
consequence, however, G becomes explicitly independent of the shear rate, which
seems surprising. Because γ_{tot} is constant, also G must be constant according to
(3.40). One reads from this result that at high shear rates, where in a short time t the
density of effective nuclei becomes quite high (with t^3), a short shearing time
suffices for a solidification by lateral growth over small distances. At low shear
rates, where the density of effective nuclei is still relatively small even at longer
shearing times, these longer shearing times suffice for a solidification by growth

over much longer distances, even if the growth speed G remains the same. The interesting fact is that this growth speed apparently does not depend on the shear rate. Using the parameters showing up in (3.40), which have all together been determined, one obtains.

$$G(\text{PP, 1 s}^{-1}, 145°\text{C}) = 3.66 \times 10^{-9}\,\text{m} \cdot \text{s}^{-1}. \tag{3.41}$$

Within the errors involved γ_{tot} is the most uncertain factor. Surprisingly, this value of G almost agrees with its value in the quiescent melt. But this means that flow has no great influence on G. And this should mean that the upturns in the viscosity would exclusively be a consequence of the increase in the number density of effective nuclei. In fact, it has been found that this increase with increasing shearing time (increasing specific work) is so strong with iPP.

Interestingly, at 160°C a higher value of the exponent n of (3.32) has been found, i.e., $n = 4$ (see Fig 3.23). Of course, one can carry out the described calculations also for this value of n. One finds in this way that G actually decreases (slightly) with increasing $q^{1/3}$. However, as at such a relatively high temperature no measurements of γ_{tot} have ever been carried out, a further discussion is of no avail.

3.3.5.3   Continuous Stretching

Also this subject has been treated in a superb way by Hadinata et al. [74]. For the purpose the "extensional viscosity fixture (EVF)" of the ARES machine was used. Between two vertically positioned cylinders rotating in opposite directions a sample of the dimensions $18 \times 10 \times 1\,\text{mm}^3$ is stretched until after one revolution of the cylinders the ends of the sample meet. As the fluid sample has to be tempered and cooled, before the stretching procedure can be started, sagging is a serious problem. In the EVF-unit this problem is minimized by the fact that the large surface of the sample is in the vertical position. (The width of 10 mm reduces the tendency of bending). Nevertheless, only a polymer of a sufficiently high molar mass can be investigated. Only such a polymer has a sufficiently high viscosity. As a consequence, only PB200, as characterized in Sect. 3.3.5.1 and in Table 3.3, could be used.

There is still another experimental problem with the EVF-unit. With the parallel plate geometry, where the metal plates are in direct contact with the sample, the sample temperature can easily be controlled because of the fact that the temperature of the plates can quickly be adjusted. However, the situation with the EVF-unit is quite different. During the required cooling process the temperature of the sample can be controlled only with the aid of a stream of a gas having the desired end-temperature. This means that the adjustment of the sample temperature takes much more time. In addition, the said cylinders are heat sinks because of their axles having contact with the environment. The authors managed to overcome all these problems. For comparison with measurements in the parallel plate unit an artificial temperature protocol was constructed for these plates. This protocol mimicked the course of the

slow temperature change in the sample, which was suspended in a gas stream. In this way it could be shown that for both types of samples the upturn in the viscosity occurred at the same time, when a flow was applied. This experiment showed that also in the slow cooling process premature crystallization did not occur to any extent. However, the stretching process must be carried out close enough to the melting temperature, so that crystallization is extremely slow, before flow is applied.

Additional problems can best be explained by a look on Fig. 3.48, which is taken from the paper by Hadinata et al. [74]. This figure contains two pictures. The upper one is for 101°C, the lower one for 97°C. In this figure the courses of the so-called elongational viscosities are plotted against the time of stretching for various constant stretching rates. Three times the shear viscosity $\eta(t)$ was calculated from dynamic mechanical measurements at 150°C. The obtained curve was "shifted" to the lower measurement temperatures with the aid of the activation energy of the melt. The ordinates of the obtained curves (for 101°C and 97°C) were multiplied by three. In this way one obtains the courses of the elongational viscosity, if no crystallization (and no so-called strain hardening) occurs. The courses of the shifted
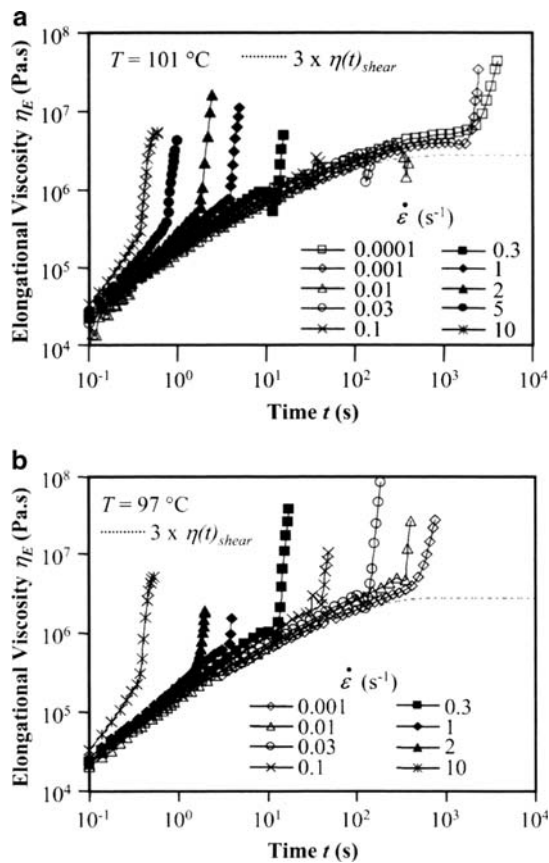
Fig. 3.48 Transient elongational viscosity versus stretching time for BP200 for various strain rates at 101°C (**a**) and 97°C (**b**), according to [74], Courtesy of The Society of Rheology

curves were inserted as dotted lines in both pictures. They should save as basic lines. At 101°C stretching rates between 10^{-4} and $10^{+1}s^{-1}$ were applied. A lower range from 10^{-3} to $10^{+1}s^{-1}$ was used at 97°C. It is obvious that with increasing stretching rates the upturns occurred at decreasing stretching times. At 101°C this method failed at the stretching rates of 0.01, 0.03 and 0.1 s^{-1}. The reason is that at these stretching rates the cylinders completed a whole revolution, before the upturn of the torque occurred. One notices that the experimental curves deviate from the line of $3 \times \eta(t)$ in an upwards direction, before the actual upturns occur. This deviation is ascribed by the authors to strain hardening as a consequence of entanglements. The influence of entanglements on the flow behavior in elongational flow has been treated theoretically. For the present discussion, however, it suffices, if it is mentioned that the line for the doubled value of the elongational viscosity is not drawn at proper distances above the line of $3 \times \eta(t)$, in analogy to the shear experiments, but above the sharp bents of the present experimental lines. As the onset times the times were used, where the adjusted lines for the doubled elongational viscosities cut the lines after the upturns.

For the present author it seems of importance to point to the fact that with elongational flow all upturns occurred at times, for which the steady state of flow had not yet been reached. This is in contrast to the results on the same polymer, if shear flow is applied. With shear flow the upturns occurred much later, so that the steady state was reached before the upturns occurred [68].

The onset times, which have been obtained with BP200 according to the procedure described above, are shown in Fig. 3.49 for the two temperatures of 101°C and 97°C. For the higher temperature one finds a larger quasi-quiescent onset time. Above an extension rate of about $10^{-2}s^{-1}$ the influence of the temperature is no longer noticeable. In this range of strain rates the double logarithmic plot shows a slope of minus one.

If these curves are compared with the curves obtained by shearing, one observes that in the range of very low deformation rates ($10^{-4}s^{-1}$ to $10^{-3}s^{-1}$) corresponding points coincide. However, in the range, where the double logarithmic plots show a slope of minus one, the points from shearing lie about one decade higher. This
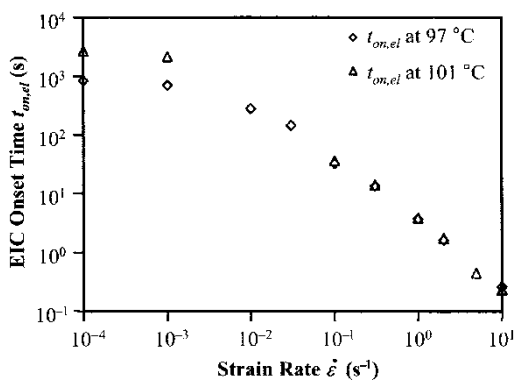
Fig. 3.49 Onset times of BP200 vs. extension rates at 101°C (*upper curve*) and 97°C (*lower curve*), according to [74], Courtesy of The Society of Rheology

effect becomes unmistakable, if the measurements with the coaxial cylinder apparatus [69] are included.

A temperature invariant plot similar to the one shown in Fig. 3.46 has finally been given in [74]. In contrast to Fig. 3.46 this plot, which is reproduced here as Fig. 3.50, shows the normalized onset times vs. the reduced extension rates. The reduced extension rate is defined in the same way as the one for shearing. For comparison the temperature invariant results from shearing experiments are inserted. This picture clearly shows the contrast between the results in shearing and in stretching.

Nevertheless, the present author feels that he must add a supplemental discussion. The first point will be the integration of the strain rate over the time. According to Hencky one has:

$$\frac{1}{\lambda(t)} \frac{d\lambda}{dt} = \frac{d\varepsilon}{dt}, \tag{3.42}$$

where λ is the relative extension with respect to the original length and ε is the strain named after Hencky. Its advantage is that it does not depend on the original length.
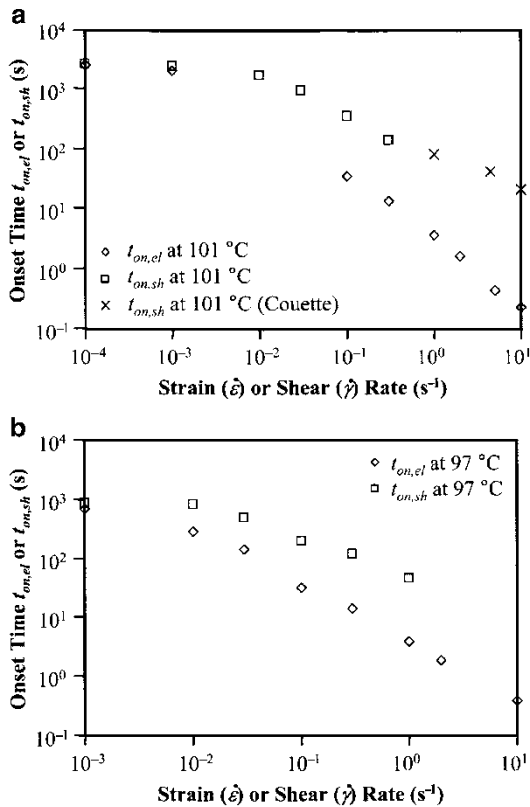
Fig. 3.50 Temperature invariant presentation of onset times vs. deformation rates for extension experiments on PB200. For comparison the results of corresponding shear experiments are also given according to [74]. Courtesy of The Society of Rheology

A constant value of the rate $d\varepsilon/dt$ is realized in the "extensional viscosity fixture EVF" of the ARES apparatus. However, the integration over the time gives a value for the Hencky strain ε, which is independent of the path. One has:

$$\varepsilon = \int_0^t \frac{d\varepsilon}{dt'}\, dt' = \int_1^\lambda d\,\ln \lambda' = \ln \lambda. \tag{3.43}$$

If $d\varepsilon/dt$ is constant, one has a special case of this integration, where the product $(d\varepsilon/dt) \cdot t$ is also $\varepsilon = \ln \lambda$.

As a next step the nature of shear flow must be scrutinized. As Zülle et al. [75] have emphasized, shear flow can be considered as a planar extension, where in one direction no change of the dimension of the sample takes place (i.e., in the 3-direction, if the 1-direction is the direction of flow and the 2-direction is the direction of the velocity gradient). With this planar extension, however, the extension rate decreases continuously with increasing total shear. For shearing the relation between the total shear γ and the relative extension λ is [21]:

$$\gamma = \lambda - \frac{1}{\lambda}. \tag{3.44}$$

For $\gamma = 0$ one has $\lambda = 1$, as it should be. For large values of γ, however, one has $\gamma \cong \lambda$. But according to (3.43) this means that $\varepsilon_{sh} \cong \ln \gamma$. (In fact, the differential equation (3.42) also holds for the Hencky measure ε_{sh} in planar extension). If one finds $\gamma_{\text{tot}} \cong 100$, as Hadinata et al. [68] did for the polybutene samples in the range of slope minus one of their double logarithmic plots, one has a Hencky strain $\varepsilon_{sh.\text{tot}} = \ln 100 = 4.6$ for shearing. This value is not so much higher than the value $\varepsilon_{\text{tot}} = 4$, which is directly derived from the high strain rate range in Fig. 3.49 for the stretch experiments. And these values are certainly comparable, because the integration of (3.43) is independent of the path. A decrease of the extension rate during the shearing process does not show up in the result of the integral and has no considerable influence on the final result. In fact, a look on various figures of the section shows that in the high deformation rate ranges (slope minus one in the double logarithmic plots) a decrease of the deformation rates has no direct influence on the total deformation (at the moment of the solidification) because the shearing time increases adequately.

At this point the work of Okamoto et al. [76] has to be mentioned. These authors carried out an extensive study on structure development during stretching of under-cooled melts of poly(ethylene naphthalates). There is one result of this work, which is of particular interest for the view of the present author. The elongational flow was realized in the elongational rheometer developed by Meissner and Hostettler [77]. Okamoto et al. succeeded to measure also the small angle light scattering, which was released by their samples. Only the polymer, which was polymerized with a Germanium catalyst, showed useful results for our purpose. For this polymer the measurements

were in the range of slope minus one in a double logarithmic plot of onset time vs. extension rate. Shortly before the upturn of the viscosity always a symmetric pattern was found. Such a pattern points to the occurrence of an isotropic structure. This is exactly what has been assumed in Sect. 3.3.5.2 (A tentative model consideration). Only after the upturn a highly asymmetric pattern was found. This pattern showed a much larger extension in the direction perpendicular to the stretch direction, indicating a larger extension of structure elements in the direction of this stretch.

In the last but one paragraph the opinion is expressed that in principle there is not such a large difference between the consequences of shearing and stretching. If this is true, a comparison with the previous Fig. 3.47 is justified. This figure holds for BP200 at 107°C. In the upper part of this figure spherulites just come up at the moment of the upturn of the viscosity, if a shear rate of about $10^{-1}s^{-1}$ has been applied. For the lower part a higher shear rate of $100~s^{-1}$ has been applied under otherwise identical conditions. Here one finds a much higher density of nuclei, which just start growing out into lengthy particles. In fact, according to our experience the number density of nuclei increases rapidly with the shear rate and the shearing time. Only, if the average distance between the nuclei is comparable with their length, shishs can be formed. So one finds a qualitative agreement with the measurements of Okamoto et al.

There are still a few additional points, which have to be included in the discussion. It is quite clear that up to the moment, when with increasing deformation the upturn of the viscosity occurs, spherulites are formed in the melt. The transformation into anisotropic structure elements only occurs after the upturn, if flow is continued. But this certainly means that solidification is not perfect at the upturn of the viscosity. This also means that the idea of a massive coil-stretch transition must be rejected. In such a case the sample should become so rigid that flow would be stopped immediately. In reality one finds that after the first coagulation of melt spun synthetic fibers these fibers can additionally be stretched considerably in a separate process, which is known to be essential for the improvement of the mechanical strength of these fibers.

Finally, a note by Samon, Schultz and Hsiao should be mentioned [78]. In this note the authors report that the total deformation of a melt spun fiber is responsible for the solidification, irrespective of the type of polymer. In fact, chemically very different polymers were investigated, as there are: HDPE, PVDE, PA6 and POM. With all of these polymers a double logarithmic plot of crystallization onset time vs. take-up speed showed a slope of practically minus one. So we can hope that an explanation of this fact can be given soon.

References

1. Haas TW, Maxwell B (1969) Effects of shear stress on the crystallization of linear polyethylene and polybutene-1. Polym Eng Sci 9:225–241
2. Mackley MR, Keller A (1973) Flow induced crystallization of polyethylene melts. Polymer 14:16–20

3. Sherwood CH, Price FP, Stein RS (1978) Effect of shear on the crystallization kinetics of poly (ethylene oxide) and poly(ε-caprolactone) melts. J Polym Sci Polym Symp 63:77–94

4. Ulrich RD, Price FP (1976) Morphology development during shearing of poly(ethylene oxide) melts. J Appl Polym Sci 20:1077–1093

5. Wolkowicz MD (1978) Nucleation and crystal growth in sheared poly(1-butene) melts. J Polym Sci Polym Symp 63:365–382

6. Van der Vegt AK, Smit PPA (1967) Crystallization phenomena in flowing polymers. Soc Chem Ind Lond Mongr 26:313–326

7. Devaux N, Monasse B, Haudin JM, Moldenaers P, Vermant J (2004) Rheooptical study of the early stages of flow enhanced crystallization in isotactic polypropylene. Rheol Acta 43:210–222

8. Pogodina NV, Lavrenko VP, Srinivas S, Winter HH (2001) Rheology and structure of isotactic polypropylene near the gel point: quiescent and shear induced crystallization. Polymer 42:9031–9043

9. Wereta A, Gogos CG (1971) Crystallization studies on deformed polybutene-1 melts. Polym Eng Sci 11:19–27

10. Janeschitz-Kriegl H, Ratajski E, Stadlbauer M (2003) Flow as an effective promotor of nucleation in polymer melts: a quantitative evaluation. Rheol Acta 42:355–364

11. Janeschitz-Kriegl H, Ratajski E (2005) Kinetics of polymer crystallization under processing conditions: transformation of dormant nuclei by the action of flow. Polymer 46:3856–3870

12. Monasse B (1992) Polypropylene nucleation on a glass fiber after melt shearing. Mater Sci 27:6047–6052

13. Kantz MR, Newman HD, Stigale FH (1972) The skin-core morphology and structure properties relationship in injection molded polypropylene. J Appl Polym Sci 16:1249–1260

14. Mencik Z, Fitchmun DR (1973) Texture in injection molded polypropylene. J Polym Sci Polym Phys Ed 11:973–989

15. Tadmor Z (1974) Molecular orientation in injection molding. J Appl Polym Sci 18:1753–1772

16. Liedauer S, Eder G, Janeschitz-Kriegl H, Jerschow P, Geymayer W, Ingolic E (1993) On the kinetics of shear induced crystallization in polypropylene. Int Polym Proc 8:236–244

17. Kumaraswamy G, Verma RK, Kornfield JA (1999) A novel flow apparatus for investigating shear-enhanced crystallization and structure development in semicrystalline polymers. Rev Sci Instrum 70:2097–2104

18. Flory PJ (1947) Thermodynamics of crystallization in high polymers. J Chem Phys 15:397–408

19. Gaylord RJ, Lohse DJ (1976) Morphological changes during oriented polymer crystallization. Polym Eng Sci 16:163–167

20. Eder G, Janeschitz-Kriegl H, Liedauer S (1990) Crystallization processes in quiescent and moving polymer melts under heat transfer conditions. Progr Polym Sci 15(629–714):678

21. Janeschitz-Kriegl H (1983) Polymer melt rheology and flow birefringence. Springer, Berlin, pp 46, 63, 113, 146, 175

22. Wales JLS, Philippoff W (1973) Anisotropy of simple shearing flow. Rheol Acta 12:25–34

23. Bandrup J, Immergut EH (eds) (1975) Polymer Handbook, 2nd edn. Wiley, New York, p V-16

24. Münstedt H, Laun HM (1979) Elongational behavior of a low density polyethylene melt. II. Transient behavior in constant stretching rate and tensile creep experiments. Comparison with shear data. Temperature dependence of the elongational properties. Rheol Acta 18:492–504

25. Wales JLS (1976) The application of flow birefringence to rheological studies of polymer melts. Doctoral thesis, Delft University Press

26. Brochard-Wyart F, de Gennes PG (1988) Ségrègration par traction dans un homopolymere. CR Acad Sci Paris II 306:699–702

27. Eder G, Janeschitz-Kriegl H (1997) Processing of polymers 5: Crystallization. Mater Sci Technol 18:269–342

28. Boon J, Challa G, Van Krevelen DW (1968) Crystallization kinetics of isotactic polystyrene II: influence of thermal history on number of nuclei. J Polym Sci A-2 6:1835–1851

29. Van Krevelen DW (1978) Crystallinity of polymers and the means to influence the crystallization process. Chimia 32:279–294
30. Van Krevelen DW (1990) Properties of polymers, 3rd edn. Elsevier, Amsterdam, p 592
31. Keller A, Kolnaar HWH (1997) Processing of polymers 4: flow-induced orientation and structure formation. Mater Sci Technol 18:189–268
32. Mandelkern L (2004) Crystallization of Polymers, vol 2, 2nd edn. Cambridge University Press, Cambridge, p 372
33. Eder G, Janeschitz-Kriegl H, Krobath G (1989) Shear induced crystallization, a relaxation phenomenon in polymer melts. Progr Colloid Polym Sci 80:1–7
34. De Gennes PG (1982) Kinetics of diffusion controlled processes in dense polymer systems. II Effect of entanglements. J Chem Phys 76:3322–3326
35. Doi M, Edwards SF (1986) The theory of polymer dynamics. Claredon, Oxford
36. Liedauer S, Eder G, Janeschitz-Kriegl H (1995) On the limitations of shear induced crystallization in polypropylene melts. Int Polym Proc 10:243–250
37. Kumaraswamy G, Verma RK, Issian AM, Wang P, Kornfield JA, Yeh F, Hsiao BS, Olley RH (2000) Shear-enhanced crystallization in isotactic polypropylene part 2. Analysis of the formation of the oriented "skin". Polymer 41:8931–8940
38. Kumaraswamy G, Issian AM, Kornfield JA (1999) Shear enhanced crystallization in isotactic polypropylene. 1. Correspondence between in situ rheo-optics and ex situ structure determination. Macromolecules 32:7537–7547
39. Williams ML, Landel RF, Ferry JD (1955) Temperature dependence of relaxation mechanisms in amorphous polymers and other glass forming liquids. J Am Chem Soc 77:3701–3707
40. Kumaraswamy G, Kornfield JA, Yeh F, Hsiao BS (2002) Shear-enhanced crystallization in isotactic polypropylene. 3. Evidence of a kinetic pathway to nucleation. Macromolecules 35:1762–1769
41. Seki M, Thurman DW, Oberhauser JP, Kornfield JA (2002) Shear-mediated crystallization of isotactic polypropylene: The role of long-chain chain overlap. Macromolecules 35:2583–2594
42. De Gennes PG (1979) Scaling concepts in polymer physics. Cornell University Press, Ithaca
43. Jeffrey GB (1922) The motion of ellipsoidal particles immersed in a viscous fluid. Proc R Soc Lond 102:161–179
44. Bird RB, Armstrong RC, Hassager O (1987) Dynamics of polymeric liquids, vol 1, 2nd edn. Wiley, New York, p 171
45. Stadlbauer M, Janeschitz-Kriegl H, Lipp M, Eder G, Forstner R (2004) Extensional rheometer for creep flow at high tensile stress. Part I. Description and validation. J Rheol 48:611–629
46. Stadlbauer M, Janeschitz-Kriegl H, Eder G, Ratajski E (2004) New extensional rheometer for creep flow at high tensile stress. Part II. Flow induced nucleation for the crystallization of iPP. J Rheol 48:631–639
47. Eder G, Janeschitz-Kriegl H, Ratajski E (2006) Towards the prediction of structure development in injection molded semicrystalline polymers. In: Greener J, Wimberger-Friedl R (eds) Precision injection molding. Carl Hanser, Munich, pp 137–152
48. Kanaya T, Takayama Y, Ogino Y, Matsuba G, Nishida K (2007) In: Reiter G, Strobl G (eds) Progress in understanding of polymer crystallization. Springer, Berlin, pp 87–96
49. Janeschitz-Kriegl H, Wimberger-Friedl R, Krobath G, Liedauer S (1987) On the formation of layer structures in plastic parts (in German). Kautschuk+Gummi Kunststoffe 40:301–307
50. Jerschow P, Janeschitz-Kriegl H (1997) The role of long molecules and nucleation agents in shear induced crystallization of isotactic polypropylenes. Int Polym Proc 12:72–77
51. Marand H, Xu J, Srinivas S (1998) Determination of the equilibrium melting temperature of polymer crystals: Linear and non-linear Hoffman-Weeks extrapolation. Macromolecules 31:8219–8229
52. Braun J, Wippel H, Eder G, Janeschitz-Kriegl H (2003) Industrial solidification processes in polybutene-1. Part II-Influence of shear flow. Polym Eng Sci 43:188–203
53. Janeschitz-Kriegl H, Eder G (2007) Shear induced crystallization, a relaxation phenomenon in polymer melts: a recollection. J Macromol Sci B 46:1–11

54. Van Krevelen DW (1990) Properties of polymers, 3rd edn. Elsevier, Amsterdam, p 469
55. Wimberger-Friedl R (1996) Molecular orientation in polycarbonate induced by cooling stress. Int Polym Proc 11:373–382
56. Alfonso GC (1999) Formation of cylindritic morphology in melt-sheared it-polybutene-1. Polym Mater Sci Eng 81:330–331
57. Alfonso GC, Azzurri F (2001) Shear enhanced polymer crystal nucleation: interaction between molecular characteristics and flow. Conference on flow induced crystallization of polymers, Salerno
58. Azzurri F, Alfonso GC (2005) Lifetime of shear-induced crystal nucleation precursors. Macromolecules 38:1723–1728
59. Varga J, Karger-Kocsis J (1996) Rules of supermolecular structure formation in sheared isotactic polypropylene melts. J Polym Sci B Polym Phys 34:657–670
60. Garcia Gutierrez MC, Alfonso GC, Rickel C, Azzurri F (2004) Spatially resolved flow-induced crystallization precursors in isotactic polystyrene by simultaneous small- and wide-angle X-ray microdiffraction. Macromolecules 37:478–485
61. Al-Hussein M, Strobl G (2002) The melting line, the crystallization line and the equilibrium melting temperature of isotactic polystyrene. Macromolecules 35:1672–1676
62. Azzurri F, Alfonso GC (2008) Insights on formation and relaxation of shear-induced nucleation precursors in isotactic polystyrene. Macromolecules 41:1377–1383
63. Stratton RA (1966) The dependence of non-Newtonian viscosity on molecular weight for 'monodisperse' polystyrenes. J Colloid Interf Sci 22:517–530
64. Monasse B (1995) Nucleation and anisotropic crystalline growth of polyethylene under shear. J Mater Sci 30:5002–5012
65. Lippits DR, Rastogi S, Höhne GWH (2006) Melting kinetics of polymers. Phys Rev Lett 96:218303-1–218303-4
66. Lippits DR, Rastogi S, Höhne GWH, Mezari B, Magusin PCMM (2007) Heterogeneous distribution of entanglements in the polymer melt and its influence on crystallization. Macromolecules 40:1004–1010
67. Lagasse RR, Maxwell B (1976) An experimental study of the kinetics of polymer crystallization during shear flow. Polym Eng Sci 16:189–199
68. Hadinata C, Gabriel C, Ruellmann M, Laun HM (2005) Comparison of shear-induced crystallization behavior of PB-1 samples with different molecular weight distribution. J Rheol 49:327–349
69. Hadinata C, Gabriel C, Ruellmann M, Kao N, Laun HM (2006) Shear-induced crystallization of PB-1 up to processing relevant shear rates. Rheol Acta 45:539–546
70. Mackley MR, Wannaborworn S, Gao P, Zhan F (1999) The optical microscopy of sheared liquids using a newly developed optical stage. J Microsc Anal 69:25–27
71. Chen Q, Fan Y, Zheng Q (2006) Rheological scaling and modeling of shear-enhanced crystallization rate of polypropylene. Rheol Acta 46:305–316
72. Janeschitz-Kriegl H, Eder G, Stadlbauer M, Ratajski E (2005) A thermodynamic frame for the kinetics of polymer crystallization under processing conditions (in English). Monatshefte für Chemie 136:1119–1137
73. Braun J, Pillichshammer D, Eder G, Janeschitz-Kriegl H (2003) Industrial solidification processes in polybutene-1. Part I – Quiescent melts. Polym Eng Sci 43:180–187
74. Hadinata C, Boos D, Gabriel C, Wassner E, Rüllmann M, Laun HM (2007) Elongation-induced crystallization of high molecular weight isotactic polybutene-1 melt compared to shear-induced crystallization. J Rheol 51:195–215
75. Zülle B, Linster JJ, Meissner J, Hürlimann HP (1987) Deformation hardening and thinning in both elongation and shear of a low density polyethylene melt. J Rheol 31:583–598
76. Okamoto M, Kubo H, Kotaka T (1998) Elongational flow-induced crystallization and structure development in supercooled poly(ethylene naphthalate). Macromolecules 31:4223–4231
77. Meissner J, Hostettler J (1994) A new elongational rheometer for polymer melts and other highly viscoelastic liquids. Rheol Acta 33:1–21

78. Samon JM, Schultz JM, Hsiao BS (2002) Structure development in the early stages of crystallization during melt spinning. Polymer 43:1873–1875
79. Kimata S, Sakurai T, Nozue Y, Kasahara T, Yamaguchi N, Karino T, Shibayama M, Kornfield JA (2007) Molecular basis of the Shish-Kebab morphology in polymer crystallization. Science 316:1014–1017

Chapter 4
Closing Remarks

4.1 General Aspects

The field of polymer crystallization is already an old field and, as such, a very extended one. As a consequence, one unfortunately cannot feel competent in all aspects. In fact, one can be impressed by the amount of special work, which has been presented so far. But this is the reason, why one can still feel as a newcomer, even if one has entered the field already 25 years ago for an investigation of structure formation during processing of semicrystalline polymers. Before the author had been engaged by virtue of life in several other areas of polymer science, as there were: regenerated cellulose, flow birefringence of polymers in solution (development of a flawless apparatus as a starting point), single screw extrusion and polymer melt rheology (heat transfer and flow, inauguration of the flow birefringence of polymer melts). This information must serve as an excuse, if he has overlooked some contributions in the field of polymer crystallization. But this is the risk if at almost sixty one gets the idea to start with a new subject. In such a case there remains only one option, namely to promote own ideas without much delay. Of course, an incontestable condition is the conviction that these ideas are essential, original and not yet promoted by others.

One example is the allusion to the strange temperature dependence of the crystallization kinetics of quiescent melts. Nobody has ever expressed openly his surprise about the enormous difference between the equilibrium melting point and the temperature, where the spherulites of such a polymer are melting. Chen et al. [1] have friendly spoken recently of the "demarcation," as discovered by the present author. This demarcation is illustrated in Fig. 1.3 for iPP. The difference between the equilibrium melting point of the α-crystal-modification and the temperature range, where the spherulites of this modification melt, is more than $40°C$. A similar difference has recently been found for iPS by Al-Hussein and Strobl [2]. Also for Form I of iPB-1 such a considerable difference can be expected, as will be shown in the next section. In fact, there is practically no sporadic formation of nuclei within the range of temperatures between the equilibrium melting point and the

temperature, where the spherulites melt. The explanation of this fact is quite simple. At the equilibrium melting point the crystals contain the molecules in stretched conformation. This means that also the pertinent nuclei must contain the molecules in their stretched conformation. But this condition is rarely fulfilled in the melt, where the molecules are coiled up. As a consequence, the activation energy for those nuclei is extremely high.

This means that the usual equations for sporadic primary nucleation, as formulated for the first time by Becker and Döring [3], will not be applicable. Anyway, at an undercooling of about 40°C they will no longer hold. A look on Fig. 1.3 will help us further. In this figure a hatched area is shown. This area indicates the presence of stable nuclei already above the temperature range, where spherulites melt. These nuclei have their origin in self-nucleation or in a flow induced process. The pertinent events have been described in previous sections. The stability of these nuclei and of other ones, which are present also at temperatures below the melting temperature of the spherulites, has been explained in these sections. For these nuclei, which have the shape of fringe micelles, their thickness determines the value of the tension at the ends of their body. In fact, in very thin micelles the tangling ends possess a large degree of conformational freedom, which is reduced, if the micelles become thicker. As a consequence, the so-called surface tension at the ends of the micelles increases up to a limiting value characteristic for the fully grown lamellae. The said nuclei are assumed to be descendants of local alignments. The stability of those alignments depends on the balance between their slenderness and their length. Both properties are distributed in the melt by virtue of statistical rules. The growth of a lamella can only set in, if the undercooling is sufficient for a supremacy of the negative free energy difference per unit cross-section, which is proportional to the length of the micelle. This negative free energy difference must be larger than the positive tensions at the ends of the micelle. This mechanism also explains, why spherulites can melt and leave sufficiently slender and – therefore – stable micelles behind (self-nucleation).

In this way one can also explain, why the number density of effective (apparently pre-formed) nuclei increases so tremendously with decreasing crystallization temperature. With iPP and with iPS enormous increases of these numbers could be observed. Factors around one hundred thousand were found, if the melts were quickly undercooled to temperatures 130–160°K below the equilibrium melting points. This has been described in previous sections. Also the large influence of pressurization on the number density of effective nuclei could be explained along this route. In fact, the lengths of the micelles must increase by "ironing" of the tangling ends.

Also the so-called heterogeneous nucleation of HDPE can now be understood. Enormous number densities of seemingly heterogeneous nuclei have regularly been found. But it cannot be assumed that so many more heterogeneous particles are brought into the body of the polymer during the polymerization. This polymerization is certainly as clean as with, say, PP. However, the molecules of HDPE are extremely flexible, when compared with those of other polymers. But this means that the assimilation of the shapes of neighboring molecules is

particularly easy. This fact can explain why one has so many more effective local alignments.

It should also be emphasized that the large influence of flow on the number density of effective nuclei can be explained by the presence of fringe micelles. Without any doubt these micelles are oriented and "ironed" by the action of flow. A closer look on this subject will be preserved for the next section. This comment is only made here for showing that there is enough reason to believe in this concept. Fortunately, the CALTECH group [50] has given a direct proof for the correctness of our assumptions with respect to the nature of the said nuclei. This work has gratefully been quoted in Sect. 2.3.2.3 of this monograph. Probably, the mesomorphic initial states of lamellar growth, as found by Strobl [4] and by Lotz [5], can be harmonized with this view.

Another aspect deserves the attention of the reader. As a starting point for the description of growth speeds the validity of an equation of the type of (2.12) was proposed in Sect. 2.3.1. At this occasion it has been told to the reader that for primary nucleation at small degrees of undercooling such an equation cannot be used. In fact, sporadic primary nucleation for ideal crystals does practically not take place in polymers. Unacceptably long waiting times would be required because spontaneously stretched conformations should be so extremely rare (Flow may alleviate this situation). And with lowering the temperature one quickly arrives in a range of temperatures, where kinetic barriers become smaller than kT. But this should mean that spinodal decomposition would become due [6]. However, such a decomposition does not occur within realistic time spans. This certainly has to do with the fact that the two well-known steps of crystallization, namely (a) the formation of primary nuclei and (b) the growth on these nuclei, is governed for polymers by very different laws. In fact, if one only thinks of sporadic nucleation, one must assume two different melting points for these two steps: the melting point of ideal crystals for step (a) and the melting temperature of spherulites for step (b).

Except for very short molecules, the growth speed of spherulites has been shown to be practically independent of the molar mass [7,8]. From this result one can conclude that local rearrangements are sufficient for the growth mechanism. But this also means that only rather short parts of molecules must spontaneously be remodeled for the purpose. The probability for such a process is very large when compared with the extremely low probability for a spontaneous stretching of a whole molecule.

Notwithstanding the fact that very often the same crystal modification is present in the spherulites and in the ideal crystals, in the lamellae one nevertheless has to do with another type of crystals with a much lower melting temperature. In fact, the kinks and the tangling ends at the surfaces of the lamellae belong to the characteristic features of these crystals. As soon as the surface of the lamella is large enough for a constant surface tension (see Fig. 2.21), one has only a small degree of undercooling, if as a reference the melting temperature of the spherulites is considered. At the same time for the sporadic nucleation of ideal crystals the undercooling is so high that one is tempted to expect spinodal decomposition. This is another reason why primary nuclei can only be "heterogeneous" in the temperature range below the melting temperature of the spherulites.

Some readers of the old school may find this reasoning too digressive. In this respect it is important to have some more formal arguments. As is well-known, Ziabicki [9] proposed an equation, which is based on the classical work by Turnbull and Fisher [10]. This equation reads in the form used, e.g., by Chen et al. [1]:

$$\frac{dN}{dt} = C \, kT \, \Delta G \, \exp\left(-\frac{E_a}{kT}\right) \exp\left[-\frac{K_n}{T(\Delta G)^n}\right]. \tag{4.1}$$

In this equation dN/dt is the rate of nucleation, which refers to the formation of primary nuclei in the homogeneous melt (exponent $n = 2$) or to the formation of secondary nuclei on the surface of already existing crystallites or on primary nuclei (exponent $n = 1$). The symbol ΔG gives the positive difference of bulk free energies between the melt and the body of the nucleus. For small degrees of undercooling one has:

$$\Delta G = \Delta H \frac{\Delta T}{T_m}, \tag{4.2}$$

where ΔH is the latent heat of melting, ΔT is the undercooling and T_m is the equilibrium melting point. In addition one has in (4.1) with E_a the activation energy and with K_n a constant of rather complicated structure, namely:

$$K_n = \frac{v_0}{nk} \left[\frac{n \, c_{n+1} \, \sigma_{n+1}}{(n+1) \, v_0^{1/2}}\right]^{n+1}. \tag{4.3}$$

In this equation v_0 is the volume of a kinetic element, c is a shape factor and $\sigma_{n+1} = (\sigma_e \sigma_s^n)^{1/(n+1)}$ is the average surface tension, with subscript e standing for the end surfaces and subscript s for the side surface. Obviously K_n stands for the energy barrier (see the surface tensions included). Except for the fact that in K_n the required parameters cannot be determined readily, there is also the principal objection against the use of this equation for the exponent $n = 2$. In fact, this exponent is reserved for the primary nucleation in the homogeneous melt, which does not happen according to our reasoning. In the contrary, (4.1) can be useful for secondary crystallization, if as the melting point the melting temperature of the spherulites is used. This has been done by Van Krevelen [11], as explained in Sect. 2.3.1.

Unfortunately, (4.1) is not very useful in the case of the influence of flow. This will be explained in detail in the next section. For the moment it seems sufficient, if it is stated that most experiments on flow induced crystallization have been carried out at temperatures, which are too low for the validity of this equation. And with the aid of flow birefringence etc. it has also been shown in Sect. 3.2 that mostly also the entropy change, as caused during flow by orientation, has been too small for a noticeable increase of ΔG. So the degree of undercooling

has not been decreased to any noticeable extent. This conclusion must be a bitter pill for those, who have based their theory on the entropy concept.

We have emphasized from the beginning of our research that the progress of crystallization is proportional to the momentary total surface (the "inner" surface) of the already formed crystalline volume elements. And with isothermal crystallization this growth occurs from the very first moment on the surfaces of the seemingly heterogeneous nuclei, which are there already. But usually such a momentary inner surface very much depends on the thermal history. With fast cooling many more nuclei are involved than with slow cooling. In fact, with slow cooling nuclei, which are activated already at higher temperatures, get the time to grow over space, where otherwise at lower temperatures more nuclei can be activated.

However, there were proposals that the volume fraction itself should be responsible for the progress of crystallization (see, e.g., Malkin [12]). These authors argue (correctly) that crystallization is a self accelerating process, which is stopped only by space filling. Nevertheless, the simplifications made are too rigorous.

If inside the newly formed spherulites secondary crystallization follows with some unexplored delay on primary crystallization, there will be a problem with the delayed or incomplete release of latent heat, being responsible for the course of local temperatures. However, for the morphology, as observed on cross-sections, secondary crystallization is of no direct influence. In fact, this morphology is determined by the original number of activated nuclei and by the corresponding number density of spherulites or, in the case of flow, also by structure elements, which are created during this flow. These features do not change any more, if secondary crystallization sets in later.

Notwithstanding all these facts the final degree of secondary crystallization can have a large influence on the properties of the product, in particular on its density and its elasticity modulus. With respect to the fracture mechanics one cannot be so sure of a positive effect. Anyway, under processing conditions the progress of secondary crystallization cannot easily be followed. For instance, a quench can preserve the morphology, but certainly cannot stop secondary crystallization. It can even promote it. And thermal or X-ray methods will often be too sluggish. Curiously enough, a simple method, as proposed by Magill [13] a long time ago, may be helpful in this respect. This author claimed the usefulness of the depolarization effect, which comes up, when crossed polars are used. It should be indicative for the onset of crystallization. During later investigations on shear induced crystallization also light scattering experiments were used. These investigations will be dealt with in the next section. It turned out that Magill's assumption is not completely true. The said depolarization effect becomes of importance only during secondary crystallization, as soon as the anisotropy of the scattering units becomes fully developed.

4.2   Views on Flow Induced Processes

To be square with this subject will not be so easy. In fact, as indicated previously in this monograph, there were approaches, which the present author considered as

doubtful. However, if he did not realize the importance of those papers, he should apologize for his possible failure. But the seriousness of his fault is certainly alleviated by the fact that so many papers have suddenly appeared on this subject in the last decade, whereas the pertinent work at Linz university dates back to 1985. It seemed as if suddenly so many people had discovered this field as promising. But understanding is sometimes a very difficult mental process. In this connection the author should admit that he himself was unable to understand the implications of some of his own findings immediately. But this fact shows, how low the appreciation for a foreign paper can be, if this paper is studied only once and in a hurry. The author's most impressive retarded ignition for own work must be described here: As early as 1985 the conspicuous relaxation behavior of shear induced crystallization was discovered in Linz, when a sample of PP was investigated (see Sect. 3.3.3.1). But also in our own group the importance of this discovery escaped notice for almost 5 years. Finally, however, this scientific adventure formed the starting point for all of our ideas about flow induced crystallization. The pertinent facts were published twice in original papers [14,15] and later in two reviews of 1990 and 1997 [16,17]. But, does it wonder, if other authors ignored our finding completely? This explains, why the present author cannot be too angry about this ignorance. However, he was very happy, when Alfonso and his people finally grasped the door-latch around 2000 (see, e.g., [18]).

Thread-like precursors, which were formed under high shear loads at rather high temperatures (not too far below the equilibrium melting point) relaxed in the quieted down melt at unchanged temperatures. However, the pertinent relaxation times showed an enormous temperature dependence. These relaxation times increased with decreasing temperature much faster than the relaxation times of the spectrum of free or entangled molecules. At the melting temperature of the spherulites, the relaxation time of the said threads had increased tremendously. It had reached a practically infinite value. But this fact has set us thinking.

As a first step, the method of short term shearing (or stretching) was invented by us on this basis (By the way, nowadays already several authors use this method without quoting us. Sometimes the term "shear pulse" is used). This method can be successful only because of the extremely slow relaxation of the primary structures created during the flow. In fact, because of this extremely slow relaxation the consequences (e.g., the growth of shish-kebabs) can be followed comfortably. The relatively fast dynamics of free or entangled molecules cannot have a noticeable (negative) influence on these processes.

Also, it was evident that we had obtained threads. After proper quenches the traces of these threads could be seen by TEM in cross-sections parallel to the previous flow direction. The mutual distances of these traces could nicely be seen in cross-sections perpendicular to the previous flow direction. The number of points of star-like appearance, where the threads pierced the cross-section, could easily be counted. From these distances one could calculate the total length of the threads per cubic meter. Enormous macroscopic lengths were found. It was evident to us that these threads could not have been formed by spontaneous association of neighboring oriented molecules. Lateral self-diffusion would have taken much too long

times, when compared with the short shearing times. In fact, mutual distances as large as about $1\,\mu$m should have been bridged in a transverse direction during the period of flow. The conclusion was that the said threads grew from spots in the melt, where nuclei of some kind (activated fringe micelles etc.) were already present. This is illustrated by Fig. 3.15. By the way, any positive influence of lateral self-diffusion becomes questionable also by the fact that shear can act in a destructive way. This fact becomes evident, if already formed little aggregates, which seem ready for association, are a little too far from each other in a lateral direction. Those aggregates draw away from each other. The well-known process of disentanglement, which causes the non Newtonian viscosity, is a good example for this destructive action of flow (see also Sects. 3.3.5.2 and 3.3.5.3). These facts convince the present author that theoretical approaches, which take into account solely the degree of orientation of singled out molecules, cannot lead to a realistic description of the process of flow induced crystallization. To the regret of the author, pertinent papers by the research groups in Eindhoven and in Naples must be dismissed as unrealistic [19–21].

In fact, last year the present author found the remains of a plastic beaker in the mountains of Tyrol. The side-wall of this beaker had been corroded by the influence of the environment. A palisade of bristles (like very thin toothpicks) had survived after the oxidation of the less crystalline zones. These bristles all had the same length equal to the height of the beaker and were grounded in the rim of the bottom, which still existed. As long as the just mentioned theories cannot explain this phenomenon, the present author cannot succumb to these ideas. The said authors should not overlook the many peculiar features of flow induced crystallization, as described in the previous sections.

The Genova group was able to elucidate the nature and the relaxation behavior of the thread-like precursors. This work was discussed in Sect. 3.3.3.2. Apparently, the said threads contain crystalline prestages, in which the macromolecules are arranged without being impaired by entanglements. It seems that during the formation of such an arrangement the macromolecules are lined out by the flow. Other arrangements, which are also bare of entanglements, are found in HDPE crystals, which are directly formed during polymerization. Conclusions were drawn from the typical activation energies. These activation energies, which are a factor ten higher than those of free or entangled molecules in viscous flow, are observed for melting processes, if these processes occur at temperatures of small but increasing distances from the equilibrium melting point. In such a process molecules are separated bit for bit from the outer surface of the crystalline aggregates. Very close to the equilibrium melting point the said crystals of HDPE (and apparently also our threads) decompose practically at once (with an extremely high activation energy) (See Sect. 3.3.3.2). Probably, this kind of prestages has been characterized for iPP by Li and de Jeu [22] in their X-ray studies.

With respect to our view on the specific work as a useful parameter some additional remarks may be of interest. In Sect. 3.3.1.4 a kinetic interpretation of the action of the rate of specific work was given. In this interpretation the role of the rate of shear is that of a probability for encounter. This is not an energetic

view. In their calculations Zuidema et al. [23] replace the specific work by the stored free energy (or the equivalent recoverable strain). Unfortunately, the present author cannot agree with this replacement. Admittedly, in a transitional situation shortly after the onset of flow, such a calculation may lead to a realistic result. During this transition specific work is successively accumulated in the melt. However, the stored free energy reaches a limiting value in steady flow. But our interpretation is independent of this condition. In fact, it turns out that the creation of precursors for crystalline structures is continued after the fluid has reached its steady flow behavior. One has only to look on Fig. 3.43. In fact, for this PB-1 of rather low molar mass steady shear viscosity was reached long before the upturn of viscosity occurred. Even for the investigated PB-1 of the highest molar mass steady state was reached just before the said upturns occurred. Only with extensional flow the upturns occurred for this polymer already during the transitional situation (see Fig. 3.48). Also Elmoumni and Winter [24] reported that "steady shearing conditions were amply reached during preshearing" in all experiments on their three PP samples. In fact, the Deborah numbers $De = \tau/t_s$ were always very small (with τ being a relaxation time representative for the melt and t_s the shearing time). It is only that these authors gave a different interpretation to their results. They claimed that the strain requirements for shear induced crystallization were higher than those for the steady state flow. We cannot agree with this interpretation. Surprisingly, Pogodina et al. [25] had found also for themselves that shishs relaxed very slowly. The present author is afraid that the authors of ref. [24] are too much impressed by their Weissenberg number, which is defined as $We = q\tau$. In fact, following them many authors did not spare their energy in looking for the best value of the relaxation time τ, trying hard to use the arguments of Doi and Edwards [26] and their successors. However, in our opinion any relaxation time of the fluid is inadequate for the just mentioned problem. In fact, here we have to do with the relaxation of the formed structure elements and not with the relaxation of the fluid. And we have learnt that in most cases the relaxation time of the structure elements is by far larger than the relaxation times of the spectrum of the fluid at the temperatures chosen. And if the relaxation time of the structure elements is by far larger than any shearing time t_s, one can add up in principle the effects of prolonged shearing. The total amount of the specific work, as we have defined it, will be essential. The Weissenberg number can only be a measure for the readiness of association, even if in nonlinear cases the relaxation time of the fluid is not exactly equal to the time needed for the establishment of a molecular orientation. And in steady flow the degree of orientation is constant anyway.

So far it has silently been assumed that between the rate of applied specific work and – say – the rate of activation of nuclei a correlation exists, which is specific for the type of polymer chosen. The position of the line in Fig. 3.24 represents this correlation for iPP. We were able to show this with the aid of another, high molar mass industrial iPP (see Stadlbauer et al. [27]). In a plot of the number density of nuclei vs. the specific work the points for the high molar mass PP coincided readily with those of the general purpose PP.

However, it will be shown immediately that this consideration must be refined, if polymers of unusual molar mass distributions are investigated. With industrial polymers the molar mass distribution has always a similar shape. This means that the experiences gathered so far can be used for industrial polypropylenes without large modifications. The effect of varying average molar masses is then almost automatically taken into account. However, Kumaraswamy, Kornfield, Yeh and Hsiao [28] used also mixtures of polypropylenes, in which small portions of a fraction of very high molar mass were contained. They also investigated the behavior of the pure high molar mass fraction. They found that in the mixtures the presence of the high molar mass fraction accelerated the growth of shishs considerably. This fact can easily be understood qualitatively with the aid of our conception. Surprisingly however, the pure fraction of high molar mass did not produce shishs at all at similar shear stresses. According to the well-known behavior of elastic liquids, for which external stress and birefringence are proportional, if the stress is not exceptionally high, there is no doubt that at a certain usual shear stress the average orientation is the same in a sharp fraction of high molar mass and in a polydisperse polymer, which is characterized by a molar mass distribution with a high molar mass tail. However, in the sharp fraction orientation will evenly be distributed over all molecules, so that each molecule is only slightly oriented. In the polymer, which contains a high molar mass tail, however, mainly the longest molecules are oriented. They are stretched extraordinarily and contribute a major part to the shear stress. So, they also preferentially further the growth of the shishs (according to Fig. 3.15). But what about the corresponding shear rate? It must not necessarily be much different. So, it can happen that the same specific work is applied to both polymers, but with very different consequences. This would mean that a theory for the said correlation should be developed. Will the above Weissenberg number play a role in such a development as a measure for the readiness of association?

This comment, however, does not mean that we can return to the oversimplified description in which only the degree of molecular orientation plays a role. The usual calculations in this type of theories make use of an equation of the type of (4.1). In such an equation the undercooling is reflected by ΔG. In principle, this ΔG is increased by the decrease of the entropy, as caused by the orientation of the free or entangled molecules. However, in Sect. 3.2 it has been shown that the corresponding increase of ΔG will not be large enough. In fact, it can be measured with the aid of flow birefringence. However, even at the highest attainable shear rates it remains insufficient for a considerable increase of the melting point. Evidently, this judgment is based on the assumption that stresses in polymeric fluids are of a purely entropic nature (no energetic contribution by – say – hindered rotations etc.). But this is a very common feature of elastic liquid models (polymer melts). Naturally, also the more detailed model calculations adhere to the entropic nature of the stresses. However, these theoretical models are based on additional simplifications (use of dumb-bells or of the reptation model). The measured flow birefringence, however, is free of this ballast. The claim that with those theoretical models adjustable parameters are not required, must be dismissed.

Admittedly, close to the equilibrium melting point strong shearing actually produces shishs, as has been shown already in our early experiments. Probably, however, one should seek the explanation for this formation of shishs rather in the fact that the molecules are uncoiled, so that they are ready for the necessary association (in a reduction of the activation energy E_a). This is in contrast to the quiescent melts, where one cannot find molecules of stretched conformation. As even with such a strong shearing the equilibrium melting point is hardly increased, one can draw conclusions about the position of this equilibrium melting point. Two examples have been discussed in previous sections, namely for isotactic polypropylene and for isotactic polystyrene. In fact, for both polymers the relaxation time of the shishs approached the value zero, when the known equilibrium melting point was approached. For the stable Form I of i-PB-1 this equilibrium melting point was never determined to our knowledge. However, as the relaxation time of the shishs approaches zero near 170°C [29], one can assume that in the vicinity of this rather high temperature the equilibrium melting point of Form I of this polymer will lie. The melting temperature of the spherulites of Form I lies at about 130°C. So one finds the usual undercooling of about 40°C, as depicted in Fig. 1.3 for iPP. Unfortunately, a detailed determination of the crystallization kinetics under the influence of flow at the high temperatures near the equilibrium melting point has not yet been possible.

It should be emphasized that in the first experiments of other authors, which were reviewed in Eder, Janeschitz-Kriegl and Liedauer in 1990 [16], only mild conditions of shearing were applied. In these investigations the samples were sheared up to the moment, when signs of crystallization were obtained (viscosity upturn, light scattering etc.). Also, part of the work by Hadinata et al. [30] was carried out at those mild conditions. Compared with these conditions a series of conditions applied in Linz [17] must be considered as very harsh. In particular, shishs occurred only at comparatively high mechanical loads (see, e.g., Janeschitz-Kriegl, Ratajski and Stadlbauer [31]). But this means that the observer remains with the puzzle, why those mild conditions lead to solidification, whereas the harsh conditions are not successful in this respect. The present author tried hard to solve this puzzle in Sect. 3.3.5.2. It can also be that at high shear rates molecular orientation becomes saturated. This means that the concept of the specific work must be replaced by a kinematical approach, where the number density of created nuclei becomes independent of temperature (see the end of Sect. 3.3.3.1).

So far the influence of nucleation agents has hardly been mentioned in the present monograph. At the time Binsbergen [32] was seriously engaged in this matter. In particular, if a sorbitol derivative is used in iPP, one finds quite intriguing results, as also very recent work by Balzano [33] shows (At Linz we are very much indebted for quickly receiving this doctoral thesis from Eindhoven university). The interaction of a compound like bis(dimethyldibenzylidene)sorbitol (BDMDBS) with iPP has previously been discussed by Thierry et al. [34], Alcazar et al. [35] and Kristiansen et al. [36]. BDMDBS is used as a clarifier in PP, which means that it normally produces an enormous amount of tiny spherulites with diameters below the wave length of the light. The central part of the quite flat molecules of

BDMDBS is polar, whereas the fringes are apolar. This compound dissolves in the melt of iPP above 250°C. Concentrations below one percent are usual. With cooling BDMDBS crystallizes from such a solution at a temperature, which depends on the concentration, but always lies above the equilibrium melting point of iPP (See also [37]). With this phase separation fibrils are formed, which become part of a network. In the fibrils the molecules of BDMDBS are piled up. The necessary cohesion is caused by hydrogen bonds between the central parts. The outside of the fibrils is apolar. The distance between the molecular layers corresponds with the 3_1 helix of iPP. With short term flow the network is destroyed. At the same time, the fibrils should be oriented and act like thread-like precursors for lateral growth of lamellae of iPP. As always, this type of growth happens after cessation of flow. In the mentioned thesis by Balzano many details are explored by small angle X-ray Synchrotron scattering, dynamic mechanical measurements and differential scanning calorimetry.

Nevertheless, some question marks will be unavoidable. In fact, only one selected shearing condition was applied, namely a standard short term shearing for 3 s at a shear rate of $60°s^{-1}$. This choice is certainly insufficient. Our experience is that the mechanical load is one of the most important parameters. In Region I, at temperatures above the phase separation of BDMDBS, only isotropic structures were found after the quench to room temperature. There is nothing against this finding. However, at suitable thermal and mechanical conditions similar effects can be found also in the absence of BDMDBS. In this connection one should look at our Figs. 1.1, 3.23, 3.24. In all these cases seemingly point-like nuclei were caused by the influence of flow. In reality, however, these nuclei were not point-like. They only had an average length smaller than their mutual average distance. As a consequence, spherulites could grow on them after cessation of flow. As a consequence isotropic morphologies were created. An important additional information is that the number density of these activated nuclei is growing tremendously with increasing shearing load. (See also Tribout et al. [38]). Such an investigation is missing in the thesis by Balzano. Probably, one will find a similar effect in the presence of BDMDBS. This effect can even be more pronounced with BDMDBS. It can also give disclosure on the stability of the fibrils in the flow field. In fact, it may be that these fibrils are broken in stronger flows because of the relative weakness of the hydrogen bonds and the comparative thickness, as compared with polymer molecules. Because of this thickness these fibrils will be particularly prone to the forces exerted by the flow. In fact, these fibrils possess a relatively large surface per unit of length. By the fracture of fibrils the number density of effective nuclei can be increased enormously. Unfortunately, a count of nuclei or of corresponding spherulites has not been carried out.

In pure polymer melts, the formation of thread-like precursors, which are built of polymer molecules only, is furthered by increasing shearing loads (see the two open triangles in the upper right corner of Fig. 3.23). Those thread-like precursors can grow even close to the equilibrium melting point of i-PP. They relax quickly at these high temperatures after cessation of flow. Only a fast quench can preserve them (see Sect. 3.3.3 and Fig. 2.20). In fact, according to Balzano [33] also the

influence of BDMDBS vanishes in all his experiments, if they are carried out close to the equilibrium melting point of i-PP near 212°C [39].

As Haas and Maxwell [40] reported already a long time ago, no textural details could be seen under the microscope in their experiments, if the upturn in the viscosity was surpassed. Apparently, the spherulitic morphology, which was found by Hadinata et al. [30] for a similar PB-1 just before the viscosity upturn, was smoothed out by continued shearing (apparently at increased stress). This fact may serve as an excuse for those theoreticians, who still use the Nakamura approach [41], which has been criticized in Sect. 1.2.1 for being inadequate for the prediction of morphology.

In this respect, the simulation of melt spinning must be mentioned. Obviously, melt spinning is a very complicated process. All kinds of influences have to be taken into account, as there are the influences of: rapid stretching, heat transfer (stabilizing the process), lateral shrinkage, air drag, inertia, gravity. According to Spruiell and White [42], very often there is an abrupt uphold in the fiber temperature at the distance from the spinneret, where crystallization starts. This effect shows that crystallization occurs quite rapidly. Probably it does not matter too much for the course of such a fast process, if the details of crystallization are ignored. With so-called high-temperature polymers amorphous regions can be retained in a crude description, as will be discussed below. In this connection the present author has to admit that it cannot be his task to review those intricate papers. And if it is only because of his lacking experience with numerical simulations. As a consequence only the last paper of the school of McHugh [43] is quoted. Previous papers of this group can be found in the quoted paper. A similar comment also holds for a recent paper by Tanner [44], even if this author claims that he can describe a slow isothermal process reported by Wassner and Maier [51], for which more details have been made available by Hadinata et al. [30]. The applied Nakamura process is unable to describe these details (creation of spherulites, which – by the way – are smoothed out subsequently).

A special subject deals with polymers, which crystallize very slowly. An explanation for such a slow process has been given by Van Krevelen (see Fig. 2.18 of the present monograph). In those polymers the distance between the glass transition temperature and the melting point is rather small. Mostly one has to do with so-called high temperature polymers. As a consequence one finds with cooling amorphous glassy areas in the samples. Numerical simulations on the basis of Nakamura's equation can furnish boundaries between amorphous and crystalline areas, which look realistic. The only necessary assumption is that the glass transition temperature, as known a priori, is much less influenced by the cooling speed and by the rate of deformation than the crystallization kinetics. But this means that nobody knows the position of the said boundary exactly. Fortunately very often, the exact position of such a boundary is not so relevant.

However, there is still another feature of these special polymers. Mostly the chain lengths of their molecules are rather small compared with those of – say – the polyolefins. Amongst others this means that the growth speed of the spherulites is no longer independent of the molar mass, as has been shown by Van Krevelen [11]

(See also Sect. 2.2.2.2). As a consequence the "demarcation" (see Fig. 1.3), which is so characteristic for long chain polymers, does no longer exist. In fact, this demarcation is based on the fact that in a quiescent melt sufficiently long molecules will never reorganize spontaneously into a stretched conformation. But such a conformation is much more probable for the mentioned short and mostly stiff molecules. So, one must conclude that the crystallization kinetics of the short chain polymers differs in many respects considerably from that of the polyolefins and much less from that of ordinary low molar mass materials. Only the slowness of the process reminds us of the fact that one has still to do with macromolecules. It may be instructive to mention that in the corresponding temperature ranges the growth speeds of the spherulites of PET are about two decades lower than those of PB-1 (see Fig. 2.15), and that a comparison of the characteristics of flow induced crystallization has not yet been carried out.

Returning to the problem of crystallization in the spin line one has to state that also the cross-sections through melt spun fibers do show details of structure. This has been shown by White and Cakmak [45] in a monumental study quite a long time ago. For the moment, however, the question remains still unanswered, whether those structures can be understood completely. The reports of Linz university have features of a detective story, whereas the just mentioned paper confronts us with solid facts, as obtained in a complex process. We always tried to find simple situations, which are interpretable, but still realistic enough for an industrial process. So the character of research differs very much, and the present author does not feel competent to review papers like the one cited above, which does not mean that an extended synopsis of those results cannot lead to important insights. Meanwhile Cakmak has published a great number of papers, in which structures are shown in fibers and in injection molded parts, mostly obtained with high temperature polymers, as characterized above. Obviously, the activities of Cakmak were strongly dictated by problems, which came up during the industrial processing of special purpose polymers or their mixtures. Nowadays it is easy to find papers of M. Cakmak, and also – say – of Avraam I. Isayev – in the internet. And if the present author does not feel prepared for a review, it may be sufficient, if he quotes the names in reminding the reader of the merits of these authors.

At the end of this last chapter 1 feel the necessity to mention two contributions of the school in Sophia Antipolis. In the first contribution by Haudin et al. [8] an advance has been made to determine the growth speed as a function of the shear rate. As the reader may remember, this subject has not been treated extensively in this book. Only once an attempt has been made to get an impression of this function in Sect. 3.3.5.2 (see (3.40)). There it has been concluded that this growth speed cannot be very dependent on the deformation rate. This deficiency was attributed to the destructive action of flow, which should be particularly pronounced in shear flow. From this point the contribution by Haudin et al. deserves particular interest. These authors have observed that the apparent thickness of a glass fiber increases continuously, if it is drawn with constant speed through an undercooled crystallizing polymer melt. Obviously, this growth must have to do with the growth of a

crystalline zone on the surface of the glass fiber under the influence of flow. This should be a particular simple experiment.

From (3.19) we learn that the shear rate in the fluid must decrease rapidly with the distance r from the hart of the glass fiber. The radius r_f of the fiber is now replaced by the growing apparent radius of the fiber, which for simplicity is now called $r_f(t)$. At various fixed distances r from the heart of the fiber (outside $r_f(t)$) one obtains now an estimate of the flow rates in the fluid, as it varies with time t. Steady state conditions, as reflected by (3.19), are no longer guaranteed! Anyway, if one observes a point at a fixed distance r in the fluid, one finds a continuous increase of the shear rate up to the moment, when this point is reached by the growth front. But this encounter causes the end of this development. In contrast, this final shear rate, as reached at the arrival of the growth front, decreases with the distance r. If now the observed rate of the apparent radius of the fiber at the growth front would be seen as the required growth rate of the crystalline zone as a function of the local shear rate, one should expect a decreasing function with increasing $r_f(t)$. But this has not been found. Instead, a practically constant apparent growth rate was found.

Correctly, the authors concluded that the fluid was pretreated, before the growth front arrived. One reads: "Crystallization occurs under a complex shear rate and shear stress history and nevertheless the growth rate is constant." In fact, in the beginning of the experiment, when the apparent radius $r_f(t)$ is still small, the polymer melt passes through high shear rates acting only for a short time span. Later, when the radius $r_f(t)$ has become relatively large, one has much lower shear rates, but acting over a much longer time.

As the reader may remember, these ideas are not unfamiliar to us. But these experiments show that it is almost impossible to get reliable values of the growth rate as a function of the local shear rate. In this respect we cannot agree with the second part of the above sentence, as quoted from the original paper. But we can be thankful to the authors for demonstrating their results so clearly. With a large number of polypropylene samples of widely varying parameters they found for the sensitivity to shear the following equation:

$$S = 0.65 \ \exp(7.7 \times 10^6 \ M_w), \qquad (4.4)$$

where S is the ratio of the growth speed under shear over the growth speed in the quiescent melt. This equation holds for a temperature of $126°C$ and does not contain the shear rate as a parameter. For us the role of the molar mass M_w remains unclear. We know that the number density of nuclei always increases rapidly even with low shear rates (with low specific mechanical works). But the rate of this increase depends on the viscosity, which – on its part – is a function of the molar mass. If those nuclei are already in the fluid, when the growth front at the fiber arrives, one must not be surprised, if that growth rate is influenced by M_w.

Finally, however, there is a message, which will be much more in favor of the group at Sophia Antipolis. Together with a group at the Katholieke Universiteit Leuven an investigation was carried out with the aid of optical means (Devaux et al.

[46]). In this context the use of small angle light scattering (SALS) is of interest, in particular for isotropic samples. According to the theory by Stein and Wilson [47] one has to measure the total scattered intensity I_{Vv}, which is obtained, when parallel polars are used, and the total scattering intensity I_{Hv}, when crossed polars are used. Scattering invariants were defined, which are given by:

$$Q_\eta = \int_0^\infty \left(I_{Vv} - \frac{4}{3} I_{Hv} \right) q^2 \, dq \qquad (4.5)$$

and

$$Q_\delta = \int_0^\infty I_{Hv} \, q^2 \, dq. \qquad (4.6)$$

In these equations q is the scattering vector defined as:

$$|q| = \frac{4\pi}{\lambda} \sin \frac{\theta}{2}, \qquad (4.7)$$

where λ is the wave length of the light and θ is the polar scattering angle. Invariant Q_η is proportional to the mean-square density fluctuation $<\eta^2>$ and invariant Q_δ is proportional to the mean of the squared anisotropy $<\delta^2>$.

Measurements with home made optics, as combined with the Linkam unit (see Mackley et al. [48] and also Sect. 3.3.5.1), furnished a clear picture of the development of crystallization in the undercooled quiescent melt of an industrial PP. This picture is shown in Fig. 4.1.

The most important result of this picture seems to be that the invariant Q_η for the density fluctuations reaches already its maximum, when the invariant Q_δ for the internal anisotropies just starts to grow. Without any doubt the course of this latter invariant indicates the ripening of the structure. On the other hand, at the time, when the maximum of Q_η is reached, about half of the volume is already occupied by the embryonic phase. And the true depolarization starts even later than Q_δ (notice the logarithmic time scale!).

Certainly, we may assume that the upcoming of strong unoriented anisotropies has to do with the secondary crystallization. This has already been emphasized at the end of Sect. 4.1. If a series of shear flows of increasing shear rates is applied, the time scale shrinks tremendously. The authors found that with an unchanged shearing time of 30 s and increasing shear rates up to $1.4°s^{-1}$ the location of the maximum in Q_η shifted from about 2,000 s at zero shear rate to about 400 s at $1.4°s^{-1}$. But a shear rate of 1.4 s^{-1} must still be considered as a very low shear rate. Spherulites still grow and the above theory remains valid. However, the present author (Janeschitz-Kriegl [49]) has been able to show that an interpolation leads to results, which fit quite well with those obtained in Linz at much higher shear rates.
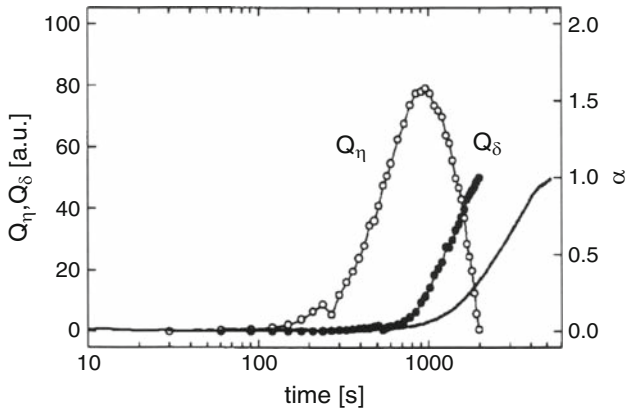
Fig. 4.1 Evolution of the scattering invariants Q_η and Q_δ in a mildly sheared melt of an i-PP at a temperature of 136°C according to [47]. The *full line* gives the course of the degree of depolarization. Courtesy of Springer

Figure 4.1 is explicitly shown here as a hint for future research, even if one must not forget in this connection that (4.5) and (4.6) only hold for the isotropic case. For the present presentation, however, this does not matter. In fact, the crystallization of ref. [46] occurred after the cessation of a flow, which was mild enough for the occurrence of spherulites. If one would aim at an investigation of the course of secondary crystallization, as occurring already during flow, one should start with a systematic investigation of light scattering and depolarization. For the purpose these measurements should be carried out at a series of temperatures, pressures and deformation rates for all kinds of interesting polymers. Because of the application of deformation rates calorimetric measurements will not be feasible. With respect to the optics one will have to be content with simpler concepts.

The course of secondary crystallization is of interest in connection with the release of latent heat in processes, in which heat transfer is involved. In particular, the course of this release can be important, if numerical simulations are to be carried out. So far numerical simulations of – say – injection molding were carried out without this knowledge. But inadequately calculated local temperatures can give a wrong picture. Sometimes one can be lucky, if secondary crystallization sets in only after the form giving process is finished. But in such a case the puzzle remains about the part of the latent heat, which is relevant already to the primary ("embryonic") crystallization. However, the present book should not have been written, if this primary crystallization would not be so relevant for the formation of decisive structures.

Unfortunately, crystallization kinetics in equibiaxial extension has not yet been investigated. It can be very different from the kinetics in uniaxial extension.

References

1. Chen Q, Fan Y, Zheng Q (2006) Rheological scaling and modeling of shear-enhanced crystallization rate of polypropylene. Rheol Acta 46:305–316
2. Al-Hussein M, Strobl G (2002) The melting line, the crystallization line and the equilibrium melting temperature of isotactic polystyrene. Macromolecules 35:1672–1676
3. Becker R, Döring W (1935) Kinetic treatment of the formation of nuclei in over-saturated steam (in German). Ann Phys 5(24):719–752
4. Strobl G (2000) From the melt via mesomorphic and granular layers to lamellar crystallites: a major route followed in polymer crystallization? Eur Phys J E 3:165–183
5. Lotz B (2000) What can polymer crystal structure tell about polymer crystallization processes? Eur Phys J E 3:185–194
6. Terrill NJ, Fairclough PA, Town-Andrews E, Komanschek BU, Young RJ, Ryan AJ (1998) Density fluctuations: nucleation event in isotactic polypropylene crystallization. Polymer 39:2381–2385
7. Magill JH (1967) Crystallization of poly (tetra-p-silphenylene) siloxane. J Polym Sci A-2 5:89–99
8. Haudin JM, Duplay C, Monasse B, Costa JL (2002) Shear induced crystallization of polypropylene. Growth enhancement and rheology in crystallization range. Macromol Symp 185:119–133
9. Ziabicki A (1996) Crystallization of polymers in variable external conditions. 1. General equations. Colloid Polym Sci 274:209–217
10. Turnbull D, Fisher JC (1949) Rate of nucleation in condensed systems. J Chem Phys 17:71–73
11. Van Krevelen DW (1990) Properties of polymers, 3rd edn. Elsevier, Amsterdam, pp 594–603
12. Malkin AYa, Beghishev VP, Keapin IA, Andreyanova ZS (1984) General treatment of polymer crystallization kinetics – Part 2: The kinetics of nonisothermal crystallization. Polym Eng Sci 24:1402–1408
13. Magill JH (1962) A new technique for following rapid rates of crystallization, II Isotactic polypropylene. Polymer 3:35–42
14. Janeschitz-Kriegl H, Wimberger-Friedl R, Krobath G, Liedauer S (1987) On the formation of layer structures in plastic parts (in German). Kautschuk + Gummi Kunststoffe 40:301–307
15. Eder G, Janeschitz-Kriegl H, Krobath G (1989) Shear induced crystallization, a relaxation phenomenon in polymer melts. Progr Polym Sci 80:1–7; Janeschitz-Kriegl H, Eder G (2007) Shear induced crystallization, a relaxation phenomenon in polymer melts: a recollection. J Macromol Sci B 46:1
16. Eder G, Janeschitz-Kriegl H, Liedauer S (1990) Crystallization processes in quiescent and moving polymer melts under heat transfer conditions. Progr Polym Sci 15:629–714
17. Eder G, Janeschitz-Kriegl H (1997) Processing of polymers 5: Crystallization. Mater Sci Technol 18:269–342
18. Azzurri F, Alfonso GC (2005) Lifetime of shear-induced crystal nucleation precursors. Macromolecules 38:1723–1728
19. Peters GWM, Swartjes FHM, Meijer HEH (2002) A recoverable strain-based model for flow-induced crystallization. Macromol Symp 185:277–292
20. Van Meerveld J, Peters GWM, Hütter M (2004) Towards a rheological classification of flow induced crystallization experiments of polymer melts. Rheol Acta 44:119–134
21. Coppola S, Balzano L, Gioffredi E, Maffettone PL, Grizzuti N (2004) Effects of the degree of undercooling on flow induced crystallization in polymer melts. Polymer 45:3249–3256
22. Li L, de Jeu WH (2003) Shear-induced ordering as a precursor of crystallization in isotactic polypropylene. Macromolecules 36:4862–4867
23. Zuidema HG, Peters GWM, Meijer HEH (2001) Development and validation of recoverable strain based model for flow-induced crystallization of polymers. Macromol Theory Simul 10:447–460

24. Elmoumni A, Winter HH (2006) Large strain requirements for shear-induced crystallization of isotactic polypropylene. Rheol Acta 45:793–801
25. Pogodina NV, Lavrenko VP, Srinivas S, Winter HH (2004) Rheology and structure of isotactic polypropylene near the gel point: quiescent and shear-induced crystallization. Polymer 42:9031–9043
26. Doi M, Edwards SF (1986) The theory of polymer dynamics. Clarendon, Oxford
27. Stadlbauer M, Janeschitz-Kriegl H, Eder G, Ratajski E (2004) New extensional rheometer for creep flow at high tensile stress. Part II. Flow induced nucleation for the crystallization of PP. J Rheol 48:631–639
28. Kumaraswamy G, Kornfield JA, Yeh F, Hsiao B (2002) Shear-enhanced crystallization in isotactic polypropylene. 3. Evidence for a kinetic pathway of nucleation. Macromolecules 35:1762–1769
29. Braun J, Wippel H, Eder G, Janeschitz-Kriegl H (2003) Industrial solidification processes in polybutene-1. Part II – Influence of shear flow. Polym Eng Sci 43:188–203
30. Hadinata C, Gabriel C, Ruellmann M, Laun HM (2005) Comparison of shear-induced crystallization behavior of PB-1 samples with different molecular weight distribution. J Rheol 49:327–349
31. Janeschitz-Kriegl H, Ratajski E, Stadlbauer M (2003) Flow as an effective promotor of nucleation in polymer melts: a quantitative evaluation. Rheol Acta 42:355–364
32. Binsbergen FL (1970) Heterogeneous nucleation in the crystallization of polyolefins: Part I Chemical and physical nature of nucleation agents. Polymer 11:253–267
33. Balzano L (2008) Flow induced crystallization of polyolefins. Doctoral Thesis. Eindhoven University of Technology
34. Thierry A, Fillon B, Straupé C, Lotz B, Wittmann JC (1992) Polymer nucleation agents: Efficiency scale and impact of physical gelation. Progr Colloid Polym Sci 87:28–31
35. Alcazar D, Ruan J, Thierry A, Lotz B (2006) Structural matching between the polymeric nucleating agent isotactic poly(vinylcyclohexane) and isotactic polypropylene. Macromolecules 39:2832–2840
36. Kristiansen M, Werner M, Tervoort T, Smith P, Blomenhofer M, Schmidt HW (2003) The binary system isotactic polypropylene/bis (3, 4-dimethyl benzylidene) sorbitol: phase behavior, nucleation and optical properties. Macromolecules 36:5150–5156
37. Jerschow P, Janeschitz-Kriegl H (1997) The role of long molecules and nucleation agents in shear induced crystallization of isotactic polypropylene. Int Polym Proc 12:72–77
38. Tribout C, Monasse B, Haudin JM (1996) Experimental study of shear-induced crystallization of an impact polypropylene copolymer. Colloid Polym Sci 274:197–208
39. Marand H, Xu J, Srinivas S (1998) Determination of the equilibrium melting temperature of polymer crystals: linear and nonlinear Hoffman-Weeks extrapolation. Macromolecules 31:8219–8229
40. Haas TW, Maxwell B (1969) Effects of shear stress on the crystallization of linear polyethylene and polybutene-1. Polym Eng Sci 9:225–241
41. Nakamura K, Watanabe T, Katayama K, Amano T (1972) Some aspects of non-isothermal crystallization of polymers. I Relationship between crystallization temperature, crystallinity and cooling conditions. J Appl Polym Sci 16:1077–1091
42. Spruiell JE, White JL (1975) Structure development during the melt spinning of fibers. Appl Polym Symp 27:121–157
43. Kohler WH, McHugh AJ (2007) 2D modeling of high-speed fiber spinning with flow-enhanced crystallization. J Rheol 51:721–733
44. Tanner RI (2003) On the flow of crystallizing polymers I. Linear regime. J Non-Newtonian Fluid Mech 112:251–268
45. White JL, Cakmak M (1986) Orientation development and crystallization in melt spinning of fibers. Adv Polym Technol 6:295–338
46. Devaux N, Monasse B, Haudin JM, Moldenaers P, Vermant J (2004) Rheological study of flow enhanced crystallization in isotactic polypropylene. Rheol Acta 43:210–222

47. Stein RS, Wilson PR (1962) Scattering of light by polymer films possessing correlated orientation functions. J Appl Phys 33:1914–1922
48. Mackley MR, Wannaborworn S, Gao P, Zhan F (1999) The optical microscopy of sheared liquids using a newly developed optical stage. J Microsc Anal 69:25–27
49. Janeschitz-Kriegl H (2006) Phases of flow-induced crystallization of iPP: How remote pieces of the puzzle appear to fit. Macromolecules 39:4448–4454
50. Olsen AP, Flagan RC, Kornfield JA (2006) Manipulation of athermal nuclei in aqueous poly (ethylene oxide) by scanning activity gravimetric analysis. Macromolecules 39(17):5946–5951
51. Wassner E, Maier RD (2000) In: Binding DM et al. (eds) Shear-induced crystallization of polypropylene melts. Proceedings of the XIII International Congress on Rheology, Cambridge, pp 183–185

Subject Index

Author Index